Progress of Theoretical Physics, Vol. 85, No. 3, March 1991

Octupole Vibrations with $K=1$ and 2 in Superconducting, Superdeformed Nuclei

Shoujirou MIZUTORI, Yoshifumi R. SHIMIZU*
and Kenichi MATSUYANAGI

Department of Physics, Kyoto University, Kyoto 606
**Department of Physics, Kyushu University, Fukuoka 812*

(Received October 22, 1990)

We calculate the response functions for octupole vibrations in superdeformed nuclei by means of the RPA using a large configuration space composed of 9 major shells. The strongly collective octupole vibrations with $K=1$ and 2 are predicted to appear very low in excitation energy, as well as those with $K=0$, if an appreciable amount of pairing correlation is present in superdeformed nuclei. Numerical examples are presented for ^{192}Hg and ^{144}Gd.

Last year, a new region of superdeformed nuclei was found in $^{191-194}$Hg.[1),2)] Moreover, many excited configurations of the superdeformed shape have been identified[3)] both in the Hg region and the previously known[4)] Gd-Dy region. Thus a new field of yrast spectroscopy for nuclear structure, called "superdeformed spectroscopy" is just opening.[5)]

As is well known, properties of nuclear vibrations are intimately connected to the shell structure. Because of the new shell structure called "the 2:1 shell structure" in superdeformed nuclei, which is drastically different from that of ordinary deformed nuclei, we expect that new properties emerge for the collective vibrations about the superdeformed equilibrium shape.

In a previous paper,[6)] we suggested that strongly collective octupole vibrations with $K=0$ appear very low in excitation energy in superdeformed nuclei that have magic numbers for the 2 : 1 shell structure. In the previous calculation we neglected the pairing correlations, since the static pairing gap Δ for ^{152}Dy discussed there is expected to be negligibly small because of the pronounced 2:1 shell gap. In this paper, we consider superdeformed nuclei which have relatively small shell gaps and, consequently, have finite value of Δ. The superdeformed bands in Hg region are suggested to have such properties.[14),18)] The result of calculation predicts that collective octupole vibrations with $K=1$ and 2 also appear below about 2 MeV in excitation energy in such superconducting superdeformed nuclei. In this paper, we report the result of calculation for the case that the rotational frequency $\omega_{\rm rot}$ is zero. The case of finite $\omega_{\rm rot}$ is deferred to a future publication.

We start from the familiar Nilsson plus BCS Hamiltonian,

$$h=h_{\rm Nilsson}-\Delta\sum_i(c_i^\dagger c_{\bar{i}}^\dagger+c_i c_{\bar{i}}) \tag{1}$$

with Δ being the pairing gap, and use the doubly-stretched octupole-octupole interactions as residual interactions:

$$H=h-\frac{1}{2}\sum_K \chi_{3K} Q''^{\dagger}_{3K} Q''_{3K}\,, \tag{2}$$

where Q''_{3K} are the octupole operators defined in terms of the doubly-stretched coordinates $x_i''=(\omega_i/\omega_0)x_i$ with $i=1$, 2 and 3. Here (ω_i/ω_0) denotes the ratios of the frequencies of the deformed harmonic-oscillator potential to that of the spherical one. The importance of the doubly-stretched multipole-multipole interactions for deformed nuclei was first pointed out by Kishimoto[7] in connection with the deformation splitting of the giant quadrupole resonances. The force-strengths χ_{3K} can be determined from the selfconsistency conditions between the potential and the density, once the single-particle potential at the equilibrium is given. They are given, for the deformed harmonic oscillator potential, by

$$\chi_{3K}=\frac{4\pi}{7}M\omega_0{}^2\left\{\langle(r^4)''\rangle_0+\frac{2}{7}(4-K^2)\langle(r^4P_2)''\rangle_0+\frac{1}{84}(K^2(7K^2-67)+72)\langle(r^4P_4)''\rangle_0\right\}^{-1}, \tag{3}$$

where P_l denotes the Legendre polynomial. The detailed derivation can be found in a recent paper by Sakamoto and Kishimoto.[8] We evaluate the expectation values appearing on the r.h.s. by using the calculated ground-state configurations for the Nilsson plus BCS Hamiltonian h. We then treat the residual interactions in the RPA, and calculate the strength functions for the doubly stretched octupole operators Q''_{3K}

$$S(Q''_{3K};\,\omega)=\sum_n \delta(\omega_n-\omega)|\langle n|Q''_{3K}|0\rangle|^2\,, \tag{4}$$

where the $|n\rangle$ are the excited states obtained in the RPA. It should be noted that, although we call the modes associated with the $Q''_{3K}\equiv(r^3Y_{3K})''$ operators "octupole modes" for brevity, they are in fact linear combinations of the ordinary octupole fields $Q_{3K}\equiv r^3Y_{3K}$ and the compressional dipole fields r^3Y_{1K}. It should also be mentioned that the spurious center of mass motions associated with the rY_{1K} operators are also separated out in the same way as in Ref. 9). In order to calculate, for example, the $B(E3)$ values, we need the transition amplitudes $\langle n|Q_{3K}|0\rangle$ for the true octupole operators Q_{3K}. These quantities are easily obtained from those for the doubly stretched operators, $(r^3Y_{3K})''$ and $(r^3Y_{1K})''$, by means of a linear transformation.

The procedure of numerical calculation is essentially the same as in Ref. 10). The parameters v_{ls} and v_{ll} of the Nilsson Hamiltonian are the same as in Ref. 11), except that we use the doubly-stretched coordinates also for the $(l\cdot s)$- and l^2-terms, and neglect the hexadecupole deformation. For the RPA calculation with the use of the theoretical equation, Eq. (3), a large model space is needed for treating octupole correlations. Thus, we use 9 major shells; $N_{\rm osc}=2-10$ for neutrons and $N_{\rm osc}=1-9$ for protons. The equilibrium deformation $\delta_{\rm osc}$ and the pairing gap Δ are determined by means of the conventional procedure of the Strutinsky method,[12] except that, following Ref. 13) we use $\tilde{\Delta}=14.0A^{-1/2}$ MeV instead of $\tilde{\Delta}=12.0A^{-1/2}$ MeV for the smoothed pairing gap parameter. The pairing gaps Δ determined in this way are 0.8~1.0 MeV for ^{192}Hg and ^{144}Gd presented below. The values of Δ_p, Δ_n and $\delta_{\rm osc}$ for individual nuclei are given in figure captions. The calculated value of $\delta_{\rm osc}$ for ^{144}Gd seems somewhat small in comparison with those evaluated by Åberg for nuclei in this region. This is because we have used a different single particle potential, namely, the

doubly stretched $(l\cdot s)$- and l^2- terms and neglect of the hexadecupole deformation. However, we believe that this difference is not important for the consideration on the properties of collective vibrations presented below. Also, modification of the pairing gap Δ of the order 10~20% will not change the essential point of this paper.

Figure 1 shows the strength functions for the doubly stretched octupole operators with $K=0$, 1, 2 and 3, calculated for ^{192}Hg which is a closed-shell nucleus for the superdeformed shape. The upper columns display the RPA strength functions, while the lower columns the unperturbed ones without the octupole-octupole interactions. We see prominent peaks below 2.5 MeV for all the K components, which correspond to the collective octupole vibrations. The calculated $B(E3)$ values for these peaks are written in the figure in units of the Weisskopf unit. These values indicate that they are strongly collective in character. In fact, the calculated $B(E3)$ values are much larger than the largest known value $B(E3;\ 3^-\rightarrow 0^+)\approx 40$ w.u. of the 3^- state in ^{208}Pb.

The $K=0$ octupole vibration splits into two peaks. This is due to the two quasiparticle poles at about 2.2 MeV in the unperturbed response functions. Aside from such datails, the major character of the $K=0$ components is the same as that discussed for ^{152}Dy in our previous paper.[6] Namely, they are mainly composed of one-particle-one-hole excitations across the closed shells associated with the 2:1 shell structure, which transfer the asymptotic quantum numbers (n_3, Λ) of the Nilsson diagram by $\Delta n_3=1$ and $\Delta\Lambda=0$, and the shell quantum number N_{shell} defined as $N_{\text{shell}}=2n_\perp+n_3$ by $\Delta N_{\text{shell}}=1$.

A remarkable new feature of these strength functions, which is absent in the case of ^{152}Dy, is the existence of the $K=1$ octupole vibrations below 2 MeV. Comparing the RPA strength function with the unperturbed one, we see that it emerges from many two-quasiparticle excitations distributing above 2 MeV. The octupole strengths of the individual two-quasiparticle excitations are rather small, but they coherently contribute to form the strongly collective $K=1$ octupole vibration. To understand the microscopic structure of this vibration, we show in Fig. 2 the major part of the unperturbed particle-hole configurations in the Nilsson potential, which correnpond to the two-quasiparticle excitations with $K=1$. We see that they transfer the quantum numbers $(N_{\text{shell}}, n_3, \Lambda)$ by $\Delta N_{\text{shell}}=0$, $\Delta n_3=2$ and $\Delta\Lambda=1$. In the limit of the deformed harmonic-oscillator potential, they correspond to those within the same N_{shell} shell of the 2:1 shell structure, and are therefore forbidden at the closed shell nucleus. This feature persists also for the Nilsson potential, and thus the low-lying $K=1$ octupole vibration is absent in the closed shell nuclei, as we have examined[6] for ^{152}Dy. However, if the pairing gap Δ is finite as is the case for ^{192}Hg, nucleon distribution over the 2:1 shell closure becomes smooth and the two-quasiparticle excitations corresponding to such $0\hbar\omega_z$ excitations are allowed. Their unperturbed excitation energies distribute starting just above the pairing gap $2\Delta\approx 2$ MeV, since their excitation energies in the Nilsson potential are very small. Due to the attractive octupole-octupole residual interactions, their energies are lowered, and coherently contribute to form the collective vibrations at about 1.6 MeV. Thus, the existence of a finite pairing gap seems essential for the appearance of the low-lying $K=1$ octupole vibrations.

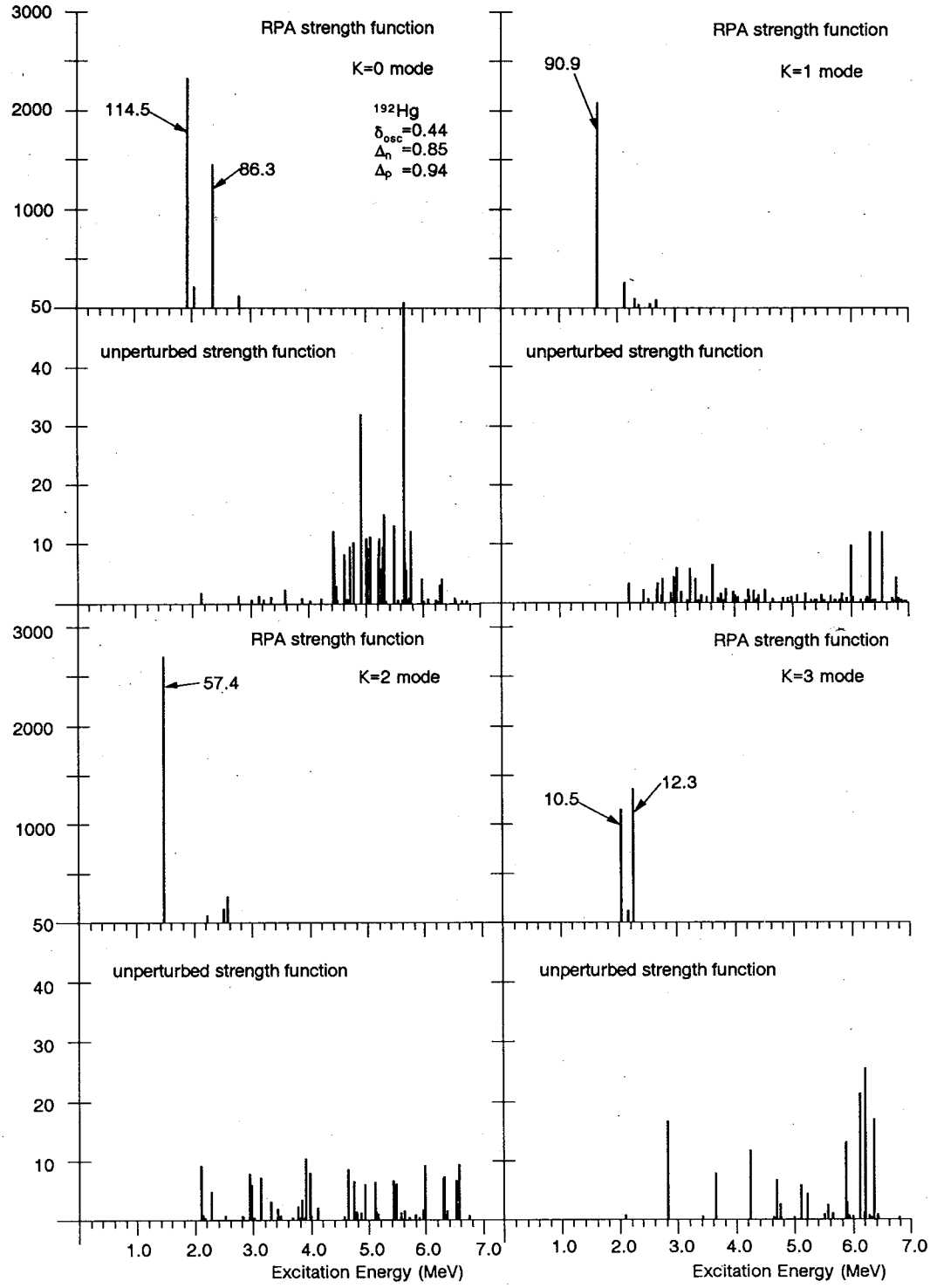

Fig. 1. Strength functions for the doubly stretched octupole operators Q'_{3K} with $K=0$, 1, 2 and 3 calculated for ^{192}Hg. The upper columns display the RPA strength functions for the energy range below 3.0 MeV, while the lower columns the unperturbed ones up to 7.0 MeV. The equilibrium deformation δ_{osc} and the pairing gaps Δ_p and Δ_n for protons and neutrons are evaluated by means of the Strutinsky method: They are $\delta_{osc}=0.44$, $\Delta_p=0.94$ MeV and $\Delta_n=0.85$ MeV. The unit is $(\hbar/M\omega_0)^3$. The calculated $B(E3)$ values for the main peaks are written in units of the Weisskopf unit.

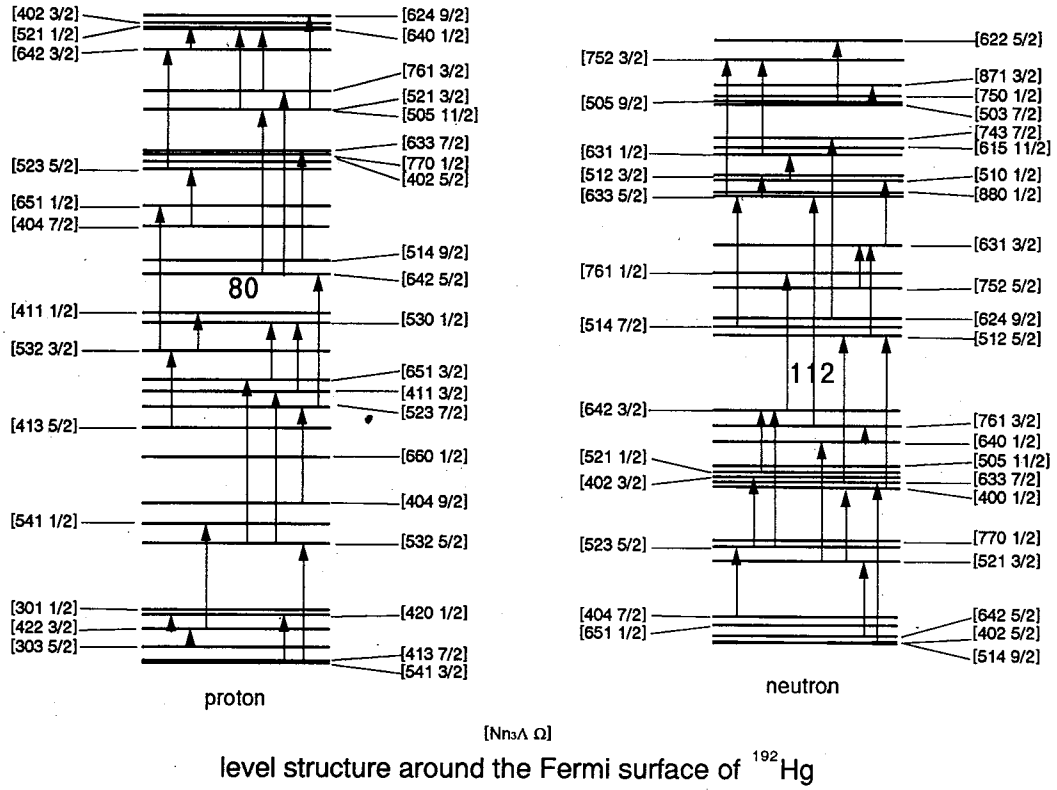

Fig. 2. Particle-hole configurations of the Nilsson potential, which correspond to the two-quasiparticle excitations constituting the collective $K=1$ octupole vibrations in ^{192}Hg. The set of numbers indicated for each level is the familiar asymptotic quantum numbers $[N_{\rm osc}, n_3, \Lambda, \Omega]$ of the Nilsson diagram. Note that $N_{\rm osc}$ are different from the shell quantum number $N_{\rm shell}$ discussed in the text.

It should be emphasized that this mode of excitation exhibits truly a new feature of the 2:1 shell structure in which the major shell is evenly composed of both positive and negative-parity single-particle orbits. It is also worth emphasizing that this mode is the first example of the isoscalar shape vibrations with $K=1$, since the isoscalar dipole and quadrupole modes correspond to the zero-frequency Nambu-Goldstone modes, i.e., translations and rotations, respectively.

In Fig. 1 we see that the octupole strength for the low-lying $K=2$ vibration is also very strong. In the previous calculation[6] for ^{152}Dy, we obtained a low-lying $K=2$ vibration composed mainly of the $\Delta N_{\rm shell}=1$ particle-hole excitations across the closed shell. Its excitation energy was about the same with that of the $K=0$ vibrations, but its octupole strength was much weaker than the latter. In the present calculation for ^{192}Hg, due to the presence of the finite pairing gap Δ, we have appreciable contributions from the two-quasiparticle excitations within the same major shell, in addition to these across the magic numbers. In contrast with the $K=1$ octupole vibration discussed above, there is no $\Delta N_{\rm shell}=0$ excitation for the $K=2$ mode. However, due to the $(l\cdot s)$- and l^2-terms, there exists many $\Delta N_{\rm shell}=1$ excitations within the same major shell for the Nilsson potential corresponding to the superdeformed shape. These excitations are allowed for the closed shell nuclei when $\Delta\neq 0$. Both types of

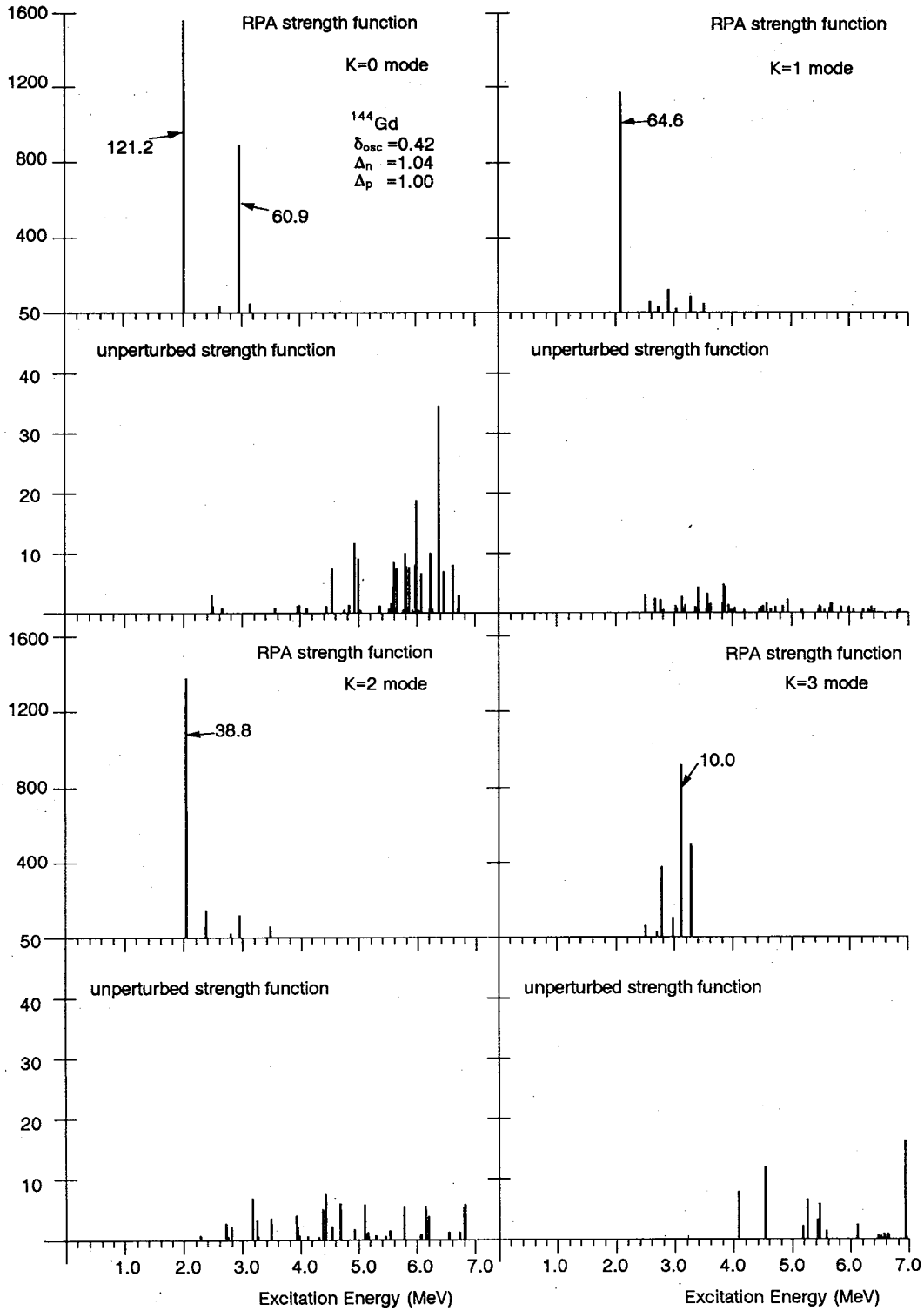

Fig. 3. Same as Fig. 1, but for ^{144}Gd. The RPA strength functions are drawn for the energy range below 3.5 MeV, while the unperturbed ones are shown up to 7.0 MeV. Calculated values for δ_{osc}, Δ_p and Δ_n are 0.42, 1.00 MeV, and 1.04 MeV, respectively.

two-quasiparticle configurations, i.e., those across the major shells and those within the major shells, correlate coherently due to the octupole-octupole interaction. Thus, the strongly collective $K=2$ octupole vibration is formed.

Concerning the $K=3$ octupole vibrations, their collectivities are relatively weak in comparison with the $K=0$, 1 and 2 modes discussed above, when they are measured in terms of the octupole strength functions. It should be noted here that, although the transition amplitudes $|\langle n|Q''_{3K}|0\rangle|$ with the doubly-stretched coordinates are of the same order of magnitude for all K values, those for the true octupole operators are considerably scaled down especially for the $K=3$ components relatively to the other components. Thus, as the $B(E3)$ values indicate, those for the true octupole operators, $|\langle n|Q_{3K}|0\rangle|$, are in fact smaller, for the $K=3$ component, than they look in Fig. 1. It should also be noted that the number of low-lying two-quasiparticle $K=3$ configurations are relatively smaller than those of the other modes, since both the $\Delta N_{\text{shell}}=0$ and 1 excitations are absent for the case $K=3$.

As an example of the calculation for superdeformed nuclei away from the closed shell, we show in Fig. 3 the octupole strength functions calculated for ^{144}Gd. We again see the existence of the low-lying collective octupole vibrations for all the K components. Their characteristics are very similar to those discussed above for ^{192}Hg. We have carried out the same calculation for a number of nuclei both in the Hg region and in the Gd-Dy region, and found similar results as long as the calculated pairing gaps are not negligibly small. Thus, we expect that the statements made above for ^{192}Hg apply also for other superdeformed nuclei.

In this paper, we have reported the result of calculation for the case that the rotational frequency ω_{rot} is zero. It is an interesting subject to investigate how the characteristics of the low-lying octupole vibrations discussed here change when the pairing gap Δ becomes small with increasing ω_{rot}. We plan to discuss this problem in a future publication.

Finally, we mention that the octupole softness of the superdeformed nuclei is also suggested in the potential-energy calculation in Refs. 14) and 15). Quite recently, the first experimental evidence supporting the prediction for strong octupole correlation in superdeformed nuclei is reported for ^{193}Hg[16] and for ^{147}Gd.[17]

The computer calculation has been financially supported in part by the Grant-in-Aid for Scientific Research of the Japan Ministry of Education, Science and Culture (No. 01540245), and in part by Research Center for Nuclear Physics, Osaka University, and done partly by using the computer center of Institute for Nuclear Study, University of Tokyo.

References

1) D. Ye et al., Phys. Rev. **C41** (1990), R13.
2) F. S. Stephen et al., Phys. Rev. Lett. **64** (1990), 2623.
3) P. J. Twin, Nucl. Phys. **A520** (1990), 17C.
4) P. J. Nolan and P. J. Twin, Ann. Rev. Nucl. Part. Sci. **38** (1988), 533.
5) *Slide Report of the Workshop and Symposia on Nuclear Structure in the Era of New Spectroscopy, Copenhagen, Sept. 11-Nov. 24, 1989.*
6) S. Mizutori, Y. R. Shimizu and K. Matsuyanagi, Prog. Theor. Phys. **83** (1990), 666.
7) T. Kishimoto et al., Phys. Rev. Lett. **35** (1975), 552.
T. Kishimoto, *Proc. Int. Symp. on Highly-Excited States in Nuclear Reaction, RCNP, Osaka, 1980,*

p. 145.
8) H. Sakamoto and T. Kishimoto, Nucl. Phys. **A501** (1989), 205.
9) J. L. Egido and H. Weidenmüller, Phys. Rev. **C39** (1989), 2398.
10) Y. R. Shimizu and K. Matsuyanagi, Prog. Theor. Phys. **72** (1984), 1087; **75** (1986), 1161.
11) T. Bengtsson and I. Ragnarsson, Nucl. Phys. **A436** (1985), 14.
12) M. Brack, J. Damgaard, A. S. Jensen, H. C. Pauli, V. M. Strutinsky and C. Y. Wong, Rev. Mod. Phys. **44** (1972), 320.
13) R. Bengtsson, Y.-S. Chen, J.-Y. Zhang and S. Åberg, Nucl. Phys. **A405** (1983), 221.
14) S. Åberg, Nucl. Phys. **A520** (1990), 35C.
15) J. Dudek, *The Variety of Nuclear Shapes*, ed. J. D. Garrett et al. (World Scientific, Singapore, 1987), p. 195.
16) D. M. Cullen et al., Phys. Rev. Lett. **65** (1990), 1547.
17) K. Zuber et al., Nucl. Phys. **A520** (1990), 195C.
18) Y. R. Shimizu, Nucl. Phys. **A520** (1990), 477C.

Progress of Theoretical Physics, Vol. 86, No. 1, July 1991

Soft Octupole Vibrations with $K=0$ and $K\neq 0$ Built on Superdeformed Rotational Bands and Static Pairing Correlations

Shoujirou MIZUTORI,*) Yoshifumi R. SHIMIZU* and Kenichi MATSUYANAGI

Department of Physics, Kyoto University, Kyoto 606
**Department of Physics, Kyushu University, Fukuoka 812*

(Received January 21, 1991)

Properties of low-lying octupole vibrations (with $K=0$, 1, 2 and 3) built on superdeformed rotational bands are investigated by means of the RPA in a uniformly rotating frame. Large configuration space composed of 9 major shells is used. Numerical examples are presented for the superdeformed band in ^{192}Hg as a typical case where appreciable amount of static pairing correlations remains at finite values of the rotational frequency. We obtain strongly collective low-frequency octupole vibrations with $K=0$, 1 and 2. It is shown that the properties of the $K=1$ octupole vibrations are especially sensitive to the static pairing correlations. The Coriolis-mixings among these soft octupole vibrations are shown to become important when the rotational frequency $\omega_{\rm rot} \gtrsim 0.2$ MeV/$\hbar$.

§ 1. Introduction

Quite recently, many excited configurations as well as yrast states of superdeformed rotational bands have been found in both the Hg region and the Gd-Dy region.[1)~5)] Their microscopic structures are now lively discussed mainly in terms of the particle-hole excitations from the yrast configurations for rotating deformed potentials. Thus, a new field of yrast spectroscopy for nuclear structure, called "superdeformed spectroscopy" is just opening.[5)]

We are interested in the question which kind of collective vibrations could be built on such superdeformed rotational bands. As is well known, properties of nuclear vibrations are intimately connected to the shell structure. Because of the new shell structure called "the 2 : 1 shell structure" in superdeformed nuclei, which is drastically different from that of ordinary deformed nuclei, we expect that new properties emerge for the collective vibrations about the superdeformed equilibrium shape.

In Refs. 6) and 7), we suggested that strongly collective octupole vibrations with $K=0$ could appear very low in excitation energy in superdeformed nuclei that have magic numbers for the 2 : 1 shell structure. In Ref. 8), we also suggested that octupole vibrations with $K=1$ and 2 could appear below about 2 MeV in excitation energy, in addition to the $K=0$ modes, if appreciable amount of static pairing correlations is present in superdeformed nuclei. This work was, however, restricted to the case that the rotational frequency $\omega_{\rm rot}$ was zero.

In this paper, we extend our previous calculation[8)] to finite values of $\omega_{\rm rot}$, and investigate how the characteristics of these low-lying octupole vibrations change when the pairing gaps Δ decrease with increasing $\omega_{\rm rot}$. Since the superdeformed

*) Present address: Institute for Nuclear Study, University of Tokyo, Tanashi 188.

bands in the Hg region are considered to have finite values of Δ,[9] we shall discuss the case of ^{192}Hg as a typical example.

For this purpose, we solve the RPA equations based on the cranked Nilsson plus BCS potential, using a large configuration space composed of 9 major shells (for both protons and neutrons). The calculational procedure is summarized in § 2. To get a rough idea about the properties of different K components of the octupole vibrations built on the superdeformed shape, we consider in § 3 the simple case of the deformed harmonic-oscillator potential with axis ratio 2 : 1. Results of the large-scale numerical calculation are presented and discussed in § 4. In § 5, conclusions are given and some future problems are mentioned.

§ 2. Method of calculation

Basic framework of our calculation is the RPA based on the cranked Nilsson plus BCS potential, which has been extensively used in order to investigate the properties of the gamma vibrations at high spin.[10] This framework is easily applicable also to the octupole vibrations built on the superdeformed rotational bands.

We start from the cranked Nilsson plus BCS Hamiltonian,

$$h'=h_{\text{Nilsson}}-\Delta\sum_i(c_i^\dagger c_{\bar{i}}^\dagger+c_{\bar{i}}c_i)-\lambda\hat{N}-\omega_{\text{rot}}\hat{J}_x \tag{2·1}$$

with Δ and λ being the pairing gap and the chemical potential, respectively, and use the doubly-stretched octupole-octupole interactions as residual interactions:

$$H=h'-\frac{1}{2}\sum_K\chi_{3K}Q_{3K}''^\dagger Q_{3K}'' , \tag{2·2}$$

where Q_{3K}'' are the octupole operators defined in terms of the doubly-stretched coordinates $x_i''=(\omega_i/\omega_0)x_i$ with $i=1$, 2 and 3. Here (ω_i/ω_0) denote the ratios of the frequencies of the deformed harmonic-oscillator potential to that of the spherical one. We use K to denote the components of angular momentum on the symmetry axis of the potential. The force-strengths χ_{3K} can be determined from the self-consistency conditions between the potential and the density,[11] once the single-particle potential at the equilibrium is given. They are given,[11] for the deformed harmonic oscillator potential, by

$$\chi_{3K}=\frac{4\pi}{7}M\omega_0^2\Big\{\langle(r^4)''\rangle_0+\frac{2}{7}(4-K^2)\langle(r^4P_2)''\rangle_0 +\frac{1}{84}(K^2(7K^2-67)+72)\langle(r^4P_4)''\rangle_0\Big\}^{-1} , \tag{2·3}$$

where P_l denotes the Legendre polynomial. We assume that the above expression can be used also for the cranked Nilsson plus BCS Hamiltonian h', and evaluate the expectation values appearing on the r. h. s. by using the calculated ground-state configurations for h'. Thus, the values of χ_{3K} are determined as functions of ω_{rot}. In fact, however, the dependence of χ_{3K} on ω_{rot} is very weak. We then treat the residual interactions in the RPA, and calculate the strength functions in the rotating frame for

the doubly stretched octupole operators Q''_{3K}

$$S(Q''_{3K};\ \omega)=\sum_n \delta(\omega_n-\omega)|\langle n|Q''_{3K}|0\rangle|^2\,, \tag{2·4}$$

where the $|n\rangle$ and $|0\rangle$ are respectively the one-phonon excited states and the vacuum state obtained in the RPA, and ω_n are the RPA excitation energies. It should be noted that, although we call the modes associated with the $Q''_{3K}\equiv(r^3Y_{3K})''$ operators "octupole modes" for brevity, they are in fact linear combinations of the ordinary octupole fields $Q_{3K}\equiv r^3Y_{3K}$ and the compressional dipole fields r^3Y_{1K}. In order to calculate, for example, the $B(E3)$ values, we need the transition amplitudes $\langle n|Q_{3K}|0\rangle$ for the true octupole operators Q_{3K}. These quantities are easily obtained from those for the doubly stretched operators, $(r^3Y_{3K})''$ and $(r^3Y_{1K})''$, by means of a linear transformation. In the case of deformed harmonic-oscillator potential, the spurious motion of center of mass is exactly decoupled by the use of the doubly-stretched octupole-octupole interactions.[11] Because of the $\boldsymbol{l}^2$ and $\boldsymbol{l}\cdot\boldsymbol{s}$ terms, however, this decoupling is not exactly guaranteed in realistic calculations. We found in fact the effect of the spurious mode on the octupole strength function is less than few percent, so that it is not important.

Procedure of numerical calculation is essentially the same as described in Ref. 10). The parameters v_{ls} and v_{ll} of the Nilsson Hamiltonian are the same as those given in Ref. 12), except that we use the doubly-stretched coordinates also for the $(\boldsymbol{l}\cdot\boldsymbol{s})$- and $\boldsymbol{l}^2$-terms, and neglect the hexadecupole deformation. For the RPA calculation with the use of the theoretical force-strength, Eq. (2·3), a large model space is needed for treating octupole correlations. Thus, we use 9 major shells; $N_{\rm osc}=2$–10 for neutrons and $N_{\rm osc}=1$–9 for protons. The equilibrium deformation $\delta_{\rm osc}$ is determined at $\omega_{\rm rot}=0$ by means of the conventional procedure of the Strutinsky method,[13] and assumed to be constant at finite $\omega_{\rm rot}$. The $\Delta N_{\rm osc}=2$ parts of the cranking term are neglected for simplicity. The pairing-force strengths for protons and neutrons, G_p and G_n, are determined by means of the smoothed gap equation method. For the smoothed pairing gap parameter $\tilde{\Delta}$ appearing in this method, we use, following Ref. 14), the value $14.0\,A^{-1/2}$ MeV instead of $12.0\,A^{-1/2}$ MeV adopted in Ref. 13). The actual values of the pairing gaps for protons and neutrons, Δ_p and Δ_n, for individual nuclei are calculated as functions of $\omega_{\rm rot}$ by solving the gap equations with the force-strength G determined above. In fact, these values cannot be precisely determined by comparison with the experimental data available for the superdeformed states in ^{192}Hg, so that there are 10~20 % ambiguities in the calculated gap parameters. Therefore, we aim in § 4 at drawing qualitative conclusions from the result of numerical calculations, which will be unaffected by small modifications of Δ_p and Δ_n.

§ 3. Qualitative considerations

Before discussing the result of large-scale numerical calculations, it is instructive to consider at $\omega_{\rm rot}=0$ the simple case of the deformed harmonic-oscillator potential with axis ratio 2 : 1. By writing the octupole operators $Q_{3K}\equiv r^3Y_{3K}$ in terms of the

creation and annihilation operators of the oscillator quanta, we can classify the particle-hole excitations associated with these operators in the following way. The particle-hole excitation energies for the $K=0$ modes are classified into four cases: ω_z, $2\omega_\perp-\omega_z$, $3\omega_z$ or $2\omega_\perp+\omega_z$, where $\omega_\perp$ and ω_z denote the harmonic-oscillator frequencies perpendicular and parallel to the symmetry axis, respectively, and where we put $\hbar=1$. In a similar manner, those for the $K=1$ modes are classified into four cases: $\omega_\perp-2\omega_z$, $\omega_\perp$, $\omega_\perp+2\omega_z$ and $3\omega_\perp$. Likewise, the $K=2$ modes are classified into ω_z, $2\omega_\perp-\omega_z$ and $2\omega_\perp+\omega_z$, and the $K=3$ modes are divided into $\omega_\perp$ and $3\omega_\perp$. Following Ref. 15), let us now define the shell quantum number $N_{\rm sh}$ by $N_{\rm sh}=an_\perp+bn_3$ and the spacing of the shells $\omega_{\rm sh}$ by $\omega_{\rm sh}=\omega_\perp/a=\omega_z/b$, for a deformed axially symmetric oscillator potential with a rational ratio $a:b$ between the frequencies $\omega_\perp$ and ω_z. In the case of axis ratio 2:1 under consideration, they are given by $N_{\rm sh}=2n_\perp+n_3=2N_{\rm osc}-n_3$ and $\omega_{\rm sh}=\omega_z$, respectively. Thus the $K=0$ octupole modes consist of $\omega_{\rm sh}$, two kinds of $3\omega_{\rm sh}$, and $5\omega_{\rm sh}$ excitations, which transfer the shell quantum number $N_{\rm sh}$ by $\Delta N_{\rm sh}=1$, 3 and 5, respectively. In a similar way, the $K=1$ octupole modes consist of 0, $2\omega_{\rm sh}$, $4\omega_{\rm sh}$ and $6\omega_{\rm sh}$ excitations which correspond to $\Delta N_{\rm sh}=0$, 2, 4 and 6, respectively. Likewise, the $K=2$ modes consist of $\Delta N_{\rm sh}=1$, 3 and 5 excitations, and the $K=3$ modes $\Delta N_{\rm sh}=2$ and 6 excitations. For a doubly closed shell nucleus where the single-particle levels are completely filled up to a certain number of $N_{\rm sh}$ (for both protons and neutrons), the $\Delta N_{\rm sh}=0$ excitations appearing in the $K=1$ octupole modes are forbidden by the Pauli principle. Thus, the lowest-energy particle-hole excitations are those with $\Delta N_{\rm sh}=1$ which occur for the octupole modes with $K=0$ and 2. Due to the attractive octupole-octupole residual interactions, collective octupole vibrations with $K=0$ and 2 constituted from coherent superpositions of the $\Delta N_{\rm sh}=1$ particle-hole excitations are shifted down in energy much below their unperturbed energies $\omega_{\rm sh}\approx 5$ MeV. This is the basic reason why we obtained in Ref. 7) very collective $K=0$ octupole vibrations below 2 MeV in ^{152}Dy. The reason why the collectivity measured by the octupole strength is much higher for the $K=0$ modes than for the $K=2$ modes is discussed below by means of the sum-rule consideration.

Next let us consider the case where appreciable amount of static pairing correlations is present even at the doubly closed-shell nucleus for the superdeformed shell structure with axis ratio 2:1. In this case, two-quasiparticle excitations within the same major shells (having the same shell quantum number $N_{\rm sh}$), which are characterized by $\Delta N_{\rm sh}=0$, are allowed near the Fermi surface. Therefore, possibility of producing a low-energy $K=1$ octupole vibration arises. This is just the point we intend to explore in § 4. Here, a striking characteristic of the 2:1 shell structure should be noticed. Namely, each major shell is composed of single-particle levels with both positive and negative parities in almost equal weights. This situation is quite different from the familiar harmonic-oscillator shell structure at the spherical shape, in which each major shell is entirely composed of single-particle levels with either positive or negative parities. Thus, once the $K=1$ octupole excitations within the same major shell are allowed, they tend to form a very collective vibration, since a large number of such degenerate two-quasiparticle configurations are correlated by attractive octupole-octupole interactions. In this respect, the low-lying $K=1$ octupole vibration is expected to have some similarities with the low-frequency

quadrupole vibrations in open-shell nuclei.

Superdeformed open-shell nuclei having valence particles (holes) outside (inside) of the magic numbers associated with the 2 : 1 shell structure are expected to have finite pairing gaps Δ. Therefore, we can apply the above consideration for the $K=1$ octupole modes also to such cases. On the other hand, the shell structure energy, which is responsible for the existence of the superdeformed equilibrium shape, is expected to decrease with increasing number of valence particles (holes). It is thus an interesting subject to investigate the region of existence of the $K=1$ octupole vibrations and to see how their properties change as the number of valence particles (holes) changes.

Lastly, let us evaluate the energy-weighted sum rule value

$$S_1(K)\equiv\sum_n \omega_n|\langle n|Q_{3K}|0\rangle|^2=\frac{1}{2}\langle 0|[Q_{3K},[H,Q_{3K}]]|0\rangle$$

for the octupole operators Q_{3K}. For doubly closed-shell nuclei with respect to the axially symmetric harmonic-oscillator potential, they are analytically calculable. Under the approximation that the density $\rho(\boldsymbol{r})$ is isotropic in the doubly stretched coordinates x_i'', they are given by[16]

$$S_1(K)=\frac{21\hbar^2}{8\pi M}\left(3\frac{\omega_0^4}{\omega_z^4}+2\frac{\omega_0^4}{\omega_\perp^4}\right)\langle x''^4\rangle \qquad \text{for} \quad K=0, \tag{3·1}$$

$$=\frac{7\hbar^2}{8\pi M}\left(6\frac{\omega_0^4}{\omega_z^4}+4\frac{\omega_0^4}{\omega_\perp^2\omega_z^2}+5\frac{\omega_0^4}{\omega_\perp^4}\right)\langle x''^4\rangle \qquad \text{for} \quad K=1, \tag{3·2}$$

$$=\frac{35\hbar^2}{8\pi M}\left(2\frac{\omega_0^4}{\omega_z^2\omega_\perp^2}+\frac{\omega_0^4}{\omega_\perp^4}\right)\langle x''^4\rangle \qquad \text{for} \quad K=2, \tag{3·3}$$

$$=\frac{105\hbar^2}{8\pi M}\left(\frac{\omega_0^4}{\omega_\perp^4}\right)\langle x''^4\rangle \qquad \text{for} \quad K=3, \tag{3·4}$$

where M is the nucleon mass. At the superdeformed shape with $\omega_\perp=2\omega_z$, their ratios are given by

$$S_1(K=0):S_1(K=1):S_1(K=2):S_1(K=3)=50:39:15:5. \tag{3·5}$$

Thus, the octupole strengths are appreciably concentrated on the modes with lower values of K. This is an important characteristic of the superdeformed states, which we should keep in mind when discussing collectivities of the vibrational modes built on them.

At finite ω_{rot}, these octupole vibrations with different values of K are mixed with each other by the Coriolis term $\omega_{\text{rot}}\hat{J}_x$. The mixing effects are discussed in the next section for the realistic case using the Nilsson potential.

§ 4. Results of calculation

We now discuss the results of calculation for ^{192}Hg based on the cranked Nilsson-plus-BCS potential.

The calculated pairing gaps are 0.94 and 0.85 MeV for protons and neutrons,

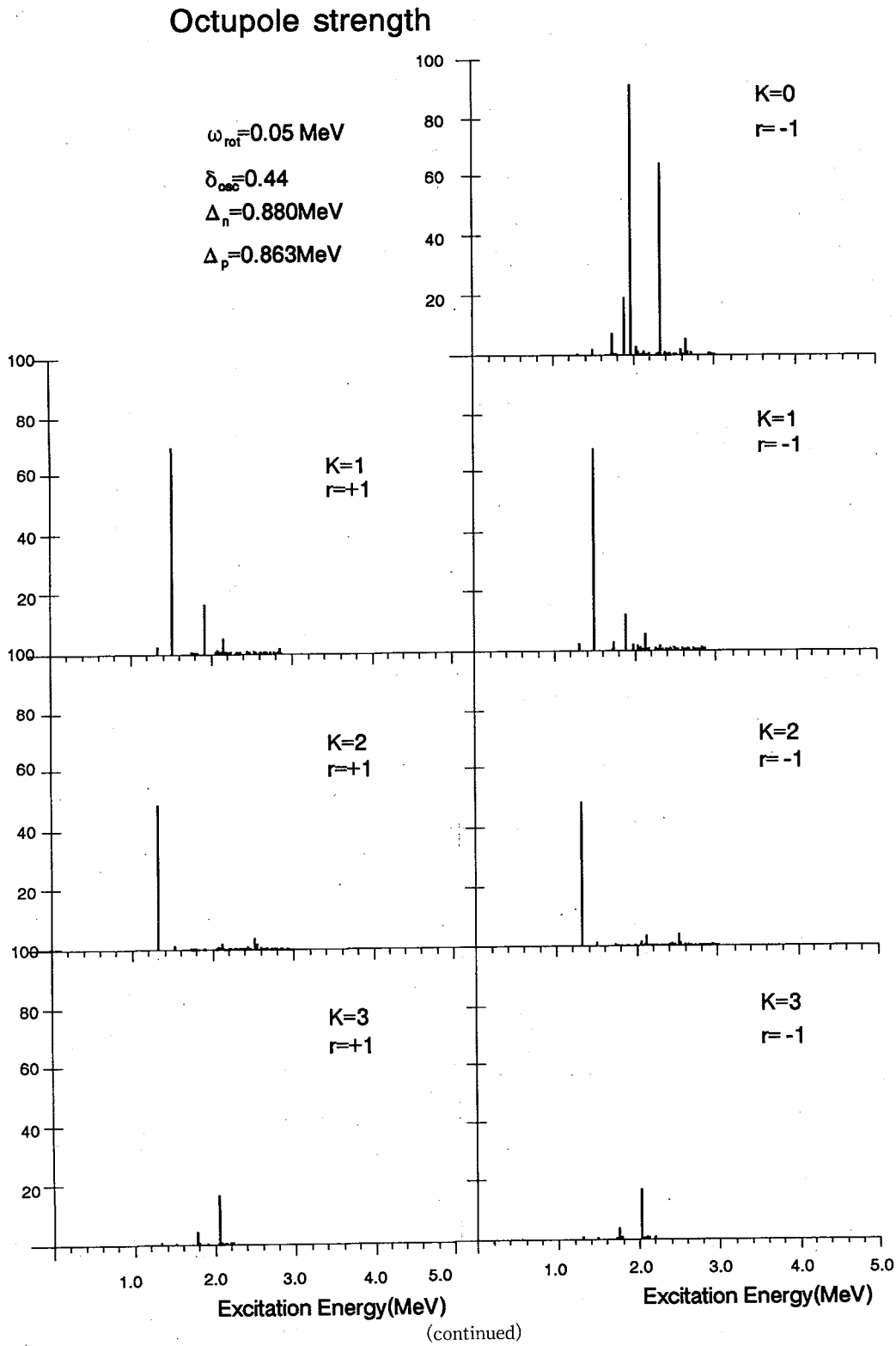
Octupole strength
ω_{rot}=0.05 MeV
δ_{osc}=0.44
Δ_n=0.880MeV
Δ_p=0.863MeV
K=0
r=-1
K=1
r=+1
K=1
r=-1
K=2
r=+1
K=2
r=-1
K=3
r=+1
K=3
r=-1
Excitation Energy(MeV)
Excitation Energy(MeV)

(continued)

Fig. 1. The RPA strength functions for the electric octupole operators $Q_{3K}^{(E)}$ with $K=0$, 1, 2 and 3 calculated at $\hbar\omega_{\rm rot}=0.05$ MeV for ^{192}Hg. Only the low-energy parts below 3 MeV are shown. These are normalized so that the abscissas indicate the octupole strength $|\langle n|Q_{3K}^{(E)}|0\rangle|^2$ in Weisskopf units. Note that they are defined in the intrinsic frame. The left-hand side shows the positive-signature sector, while the right-hand side the negative-signature sector. The equilibrium deformation $\delta_{\rm osc}$ and the pairing gaps Δ_p and Δ_n for protons and neutrons are evaluated by means of the Strutinsky method.

respectively, at $\omega_{\rm rot}=0$. They diminishes at $\omega_{\rm rot}\lesssim 0.4$ MeV. As we mentioned in § 2, this result should be taken in a qualitative sense. The calculated deformation parameter $\delta_{\rm osc}=0.44$ is almost the same with the values usually adopted,[17] and is fairly smaller than 0.6 which corresponds to the axis ratio 2 : 1. Thus, together with the effects of the $\boldsymbol{l}^2$ and $\boldsymbol{l}\cdot\boldsymbol{s}$ terms in the Nilsson potential, we should expect some deviations of the actual shell structure from that discussed in § 3 for the harmonic-oscillator potential with axis ratio exactly 2 : 1.

Figures 1~6 display the octupole strength functions calculated in RPA at $\omega_{\rm rot}=0.05$, 0.10, 0.15, 0.20, 0.30, 0.40, respectively. These strength functions are normalized so that abscissas indicate the $|\langle n|Q_{3K}^{(E)}|0\rangle|^2$ values in Weisskopf units, where $Q_{3K}^{(E)}$ denote the electric octupole operators. Together with the K-value, the strength functions are classified in Figs. 1~6 in terms of the signature quantum number which represents the transformation property with respect to the rotation of π about the rotation axis. The left (right)-hand sides of these figures show those with signature $r=+1$ (-1). As is well known, the signature remains as a good quantum number although the K-values are mixed in the RPA eigenmodes at finite $\omega_{\rm rot}$. Thus the $K=1$, 2, 3 parts of the left-hand sides show the properties with respect to the operators $Q_{3K=1,2,3}^{(E)}$ of the same RPA modes belonging to the $r=+1$ sector, although poles of non-collective RPA modes that have little octupole strengths are not always visible. In the same manner, the $K=0$, 1, 2, 3 parts of the right-hand sides show those belonging to the $r=-1$ sector. At finite $\omega_{\rm rot}$, properties of the RPA modes are expected to depend on the signature quantum number. In fact, we can see some differences, for instance, between the $K=1$ octupole strength functions with $r=+1$ and -1. However, generally speaking, such signature dependence is not very strong in the range of rotational frequency under consideration.

Let us first discuss the case of relatively small values of the rotational frequency, i.e., $\omega_{\rm rot}\lesssim 0.15$ MeV, displayed in Figs. 1~3. These are extensions of the calculation at $\omega_{\rm rot}=0$ reported in Ref. 8). We see prominent peaks below 2.5 MeV for all the K components, which correspond to the collective octupole vibrations. The octupole strengths of many of these peaks are much larger than the largest known value $B(E3;\ 3^-\rightarrow 0^+)\approx 40$ w.u. of the 3^- state in ^{208}Pb. Thus, they are strongly collective in character. It is seen that the octupole strength functions are gradually modified by the effects of the Coriolis term. However, the effects are rather weak, and the octupole vibrations may still be approximately characterized by the K values (in spite of the K-mixings). Thus, essentially the same considerations as in the case $\omega_{\rm rot}=0$[8] apply also to Figs. 1~3.

There appear prominent peaks at about 2 MeV for the $K=0$ strength functions. They are associated with the octupole vibrations that have approximate quantum

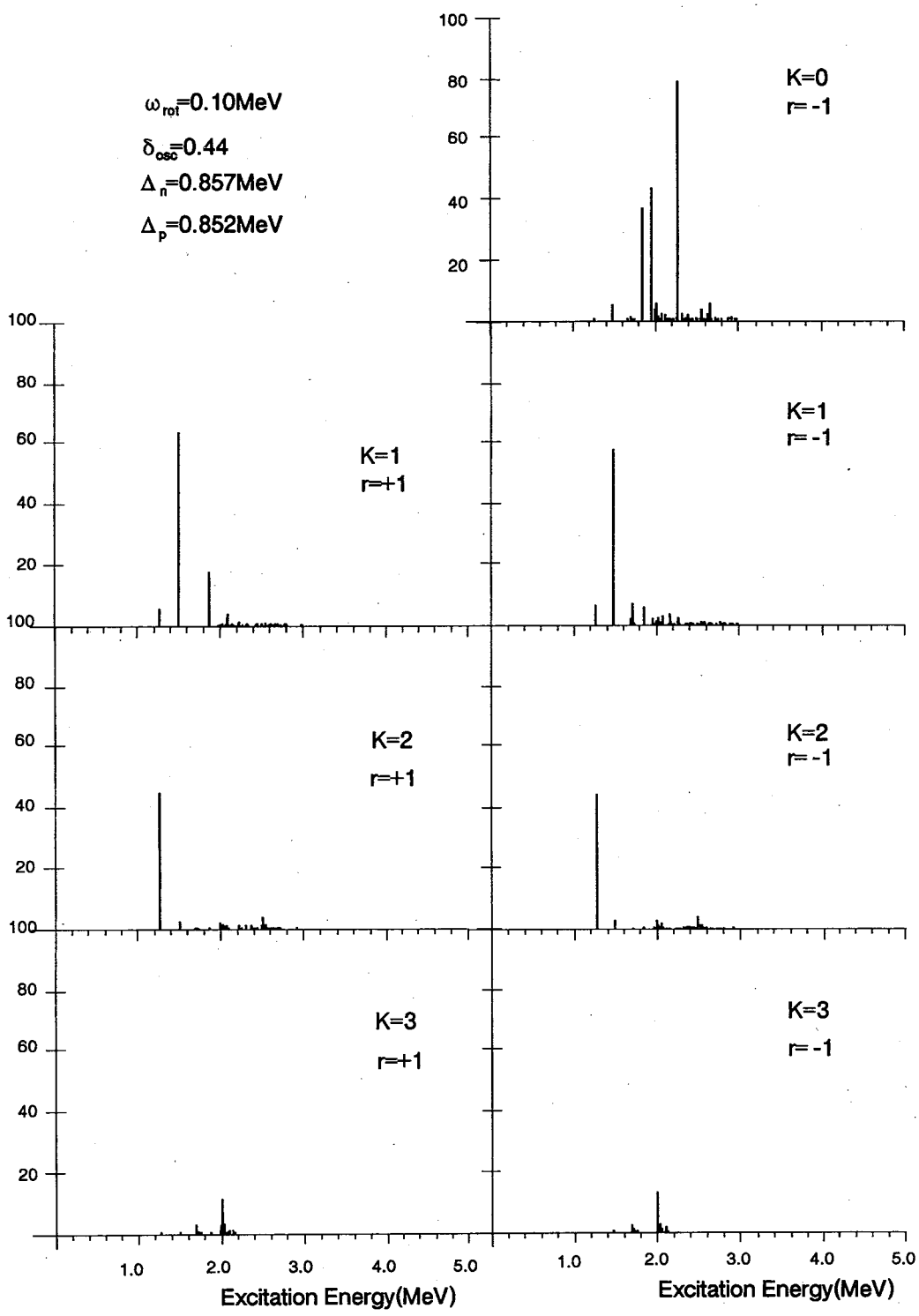

Fig. 2. The same as Fig. 1 but for $\hbar\omega_{\rm rot}=0.10$ MeV.

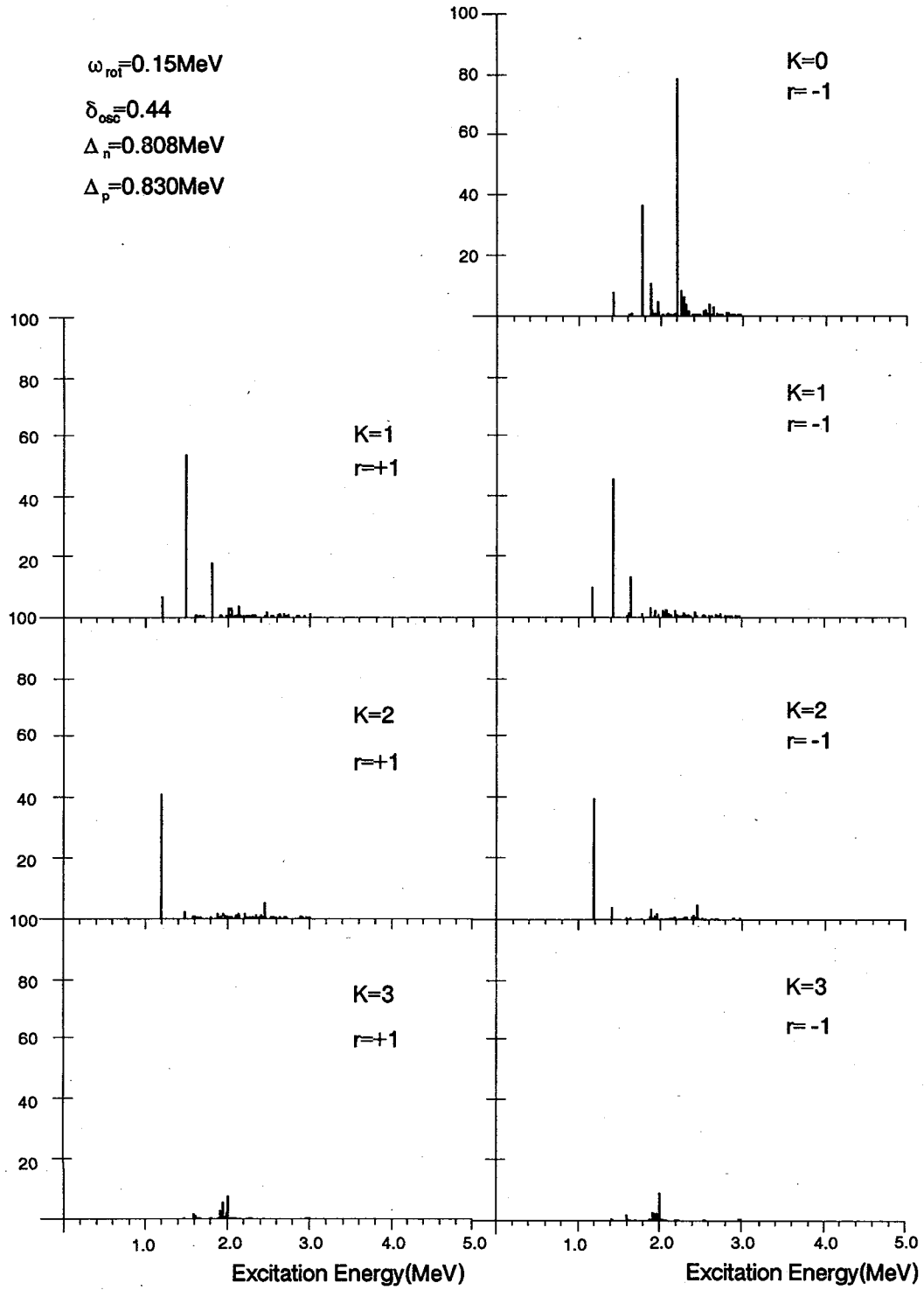

Fig. 3. The same as Fig. 1 but for $\hbar\omega_{\mathrm{rot}}=0.15$ MeV.

number $K=0$. Aside from such splittings of the "$K=0$" mode into two or three peaks, which sensitively depend on the details of the two-quasiparticle poles in the unperturbed response functions, the major character of the $K=0$ components is the same as that discussed for ^{152}Dy in Ref. 6). Namely they are mainly composed of one-particle-one-hole excitations across the superdeformed shells which transfer the shell quantum number $N_{\rm sh}$ by $\Delta N_{\rm sh}=1$, and the asymptotic quantum numbers (n_3, Λ) of the Nilsson diagram by $\Delta n_3=1$ and $\Delta\Lambda=0$.

The unperturbed energies of such excitations constituting the "$K=0$" modes are clustered at about 5 MeV, i.e., at almost the same energy expected for the case of harmonic-oscillator potential discussed in § 3. This is because relative single-particle energies for the particle-hole configurations with $\Delta n_3=1$ and $\Delta\Lambda=0$ are rather unaffected in spite of the large shifts in individual energies due to the $\boldsymbol{l}^2$ and $(\boldsymbol{l}\cdot\boldsymbol{s})$ terms in the Nilsson potential. For example, the relative energy between the Nilsson levels $[770\frac{1}{2}]$ and $[880\frac{1}{2}]$ remains approximately constant although their energies are both considerably affected by the $\boldsymbol{l}^2$ and $(\boldsymbol{l}\cdot\boldsymbol{s})$ terms. Owing to the attractive octupole-octupole interactions, these particle-hole excitations coherently contribute to generate the "$K=0$" collective vibrations at about 2 MeV.

A remarkable new feature of these strength functions, which is absent in the case of ^{152}Dy, is the existence of the octupole vibrations having the approximate quantum number $K=1$ below 2 MeV. Comparing the RPA strength function with the unperturbed one, we see that it emerges from many two-quasiparticle excitations distributing above 2 MeV which transfer the quantum numbers ($N_{\rm sh}$, n_3, Λ) by $\Delta N_{\rm sh}=0$, $\Delta n_3=2$ and $\Delta\Lambda=\pm1$. The octupole strengths of these individual two-quasiparticle configurations are rather small, but they coherently contribute to generate the strongly collective $K=1$ octupole vibration. In the limit of the deformed harmonic-oscillator potential, these excitations correspond to those within the same $N_{\rm sh}$ shell of the 2 : 1 shell structure, and are therefore forbidden at the closed shell nucleus. This feature persists also for the Nilsson potential, and thus the low-lying "soft $K=1$ octupole" vibration is absent in the closed shell nuclei, as we have examined[7] for ^{152}Dy. However, if the pairing gap Δ is finite as is the case for ^{192}Hg, nucleon distributions over the superdeformed closed shells become smooth and the two-quasiparticle excitations corresponding to such $0\hbar\omega_{\rm sh}$ excitations are allowed. Their unperturbed excitation energies distribute starting just above the pairing gap $2\Delta\approx2$ MeV, since their excitation energies in the Nilsson potential are very small. Due to the attractive octupole-octupole residual interactions, their energies are lowered, and coherently contribute to form the collective vibrations at about 1.5 MeV. Thus, the existence of a finite pairing gap seems essential for the appearance of the low-lying "soft $K=1$" octupole vibrations.

It should be emphasized that this mode of excitation exhibits truly a new feature of the superdeformed shell structure in which the major shell is evenly composed of both positive and negative-parity single-particle orbits. It is also worth emphasizing that this mode is the first example of the isoscalar shape vibrations with $K=1$, since the isoscalar dipole and quadrupole modes correspond to the zero-frequency Nambu-Goldstone modes, i.e., translations and rotations, respectively.

In Figs. 1~3 we see that the octupole strengths for the low-lying "$K=2$" vibration

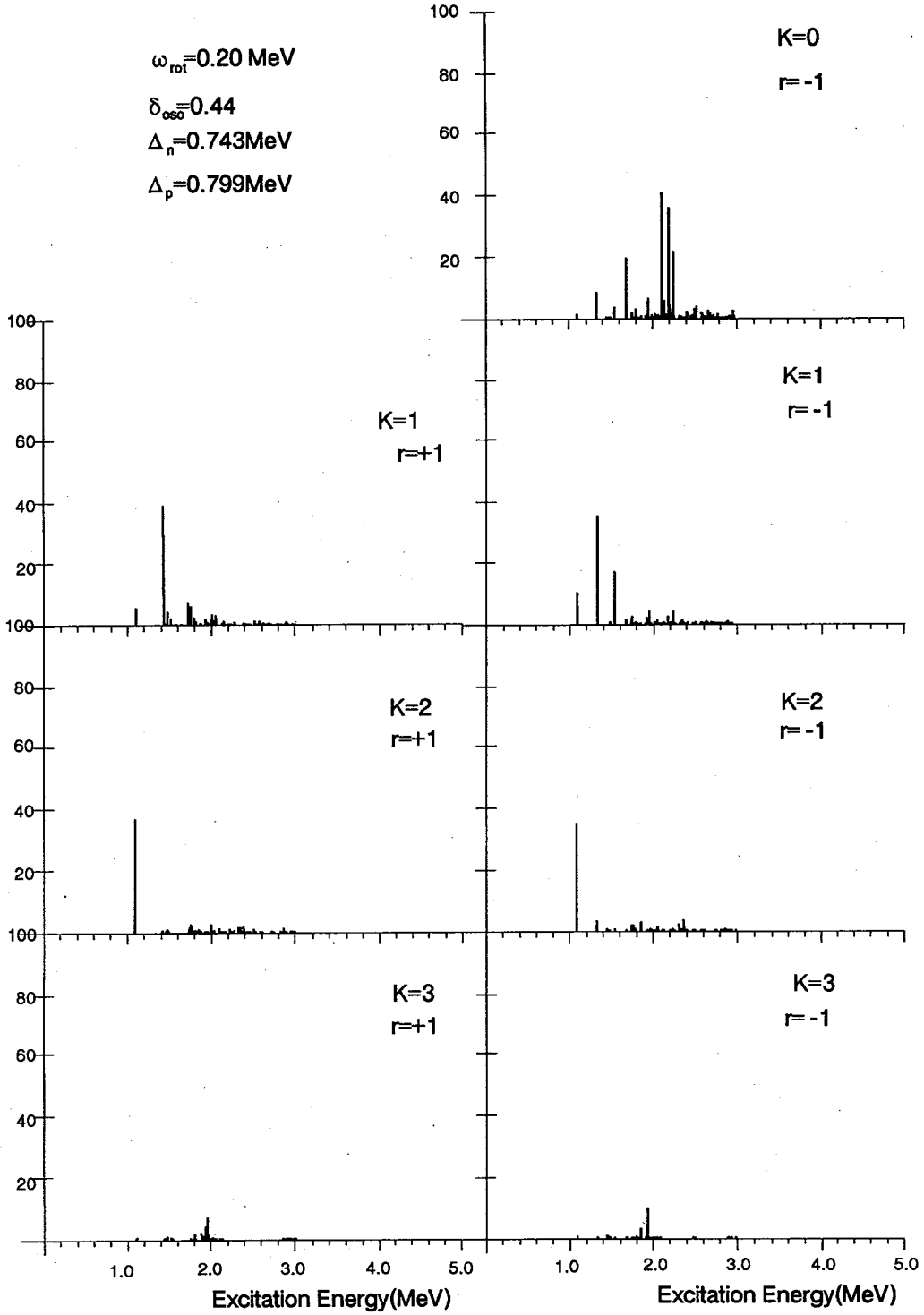

Fig. 4. The same as Fig. 1 but for $\hbar\omega_{\rm rot}=0.20$ MeV.

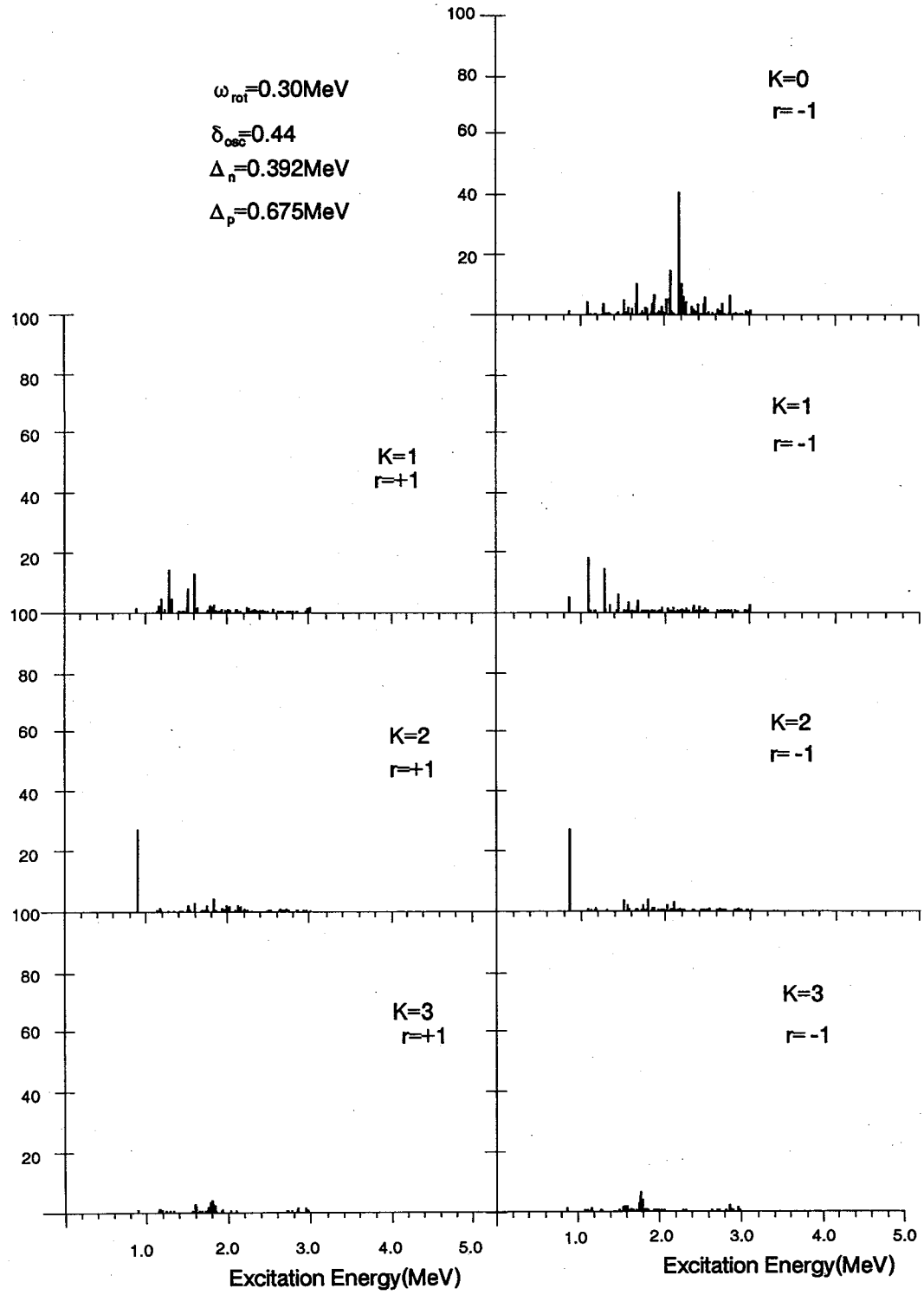

Fig. 5. The same as Fig. 1 but for $\hbar\omega_{\rm rot}=0.30$ MeV.

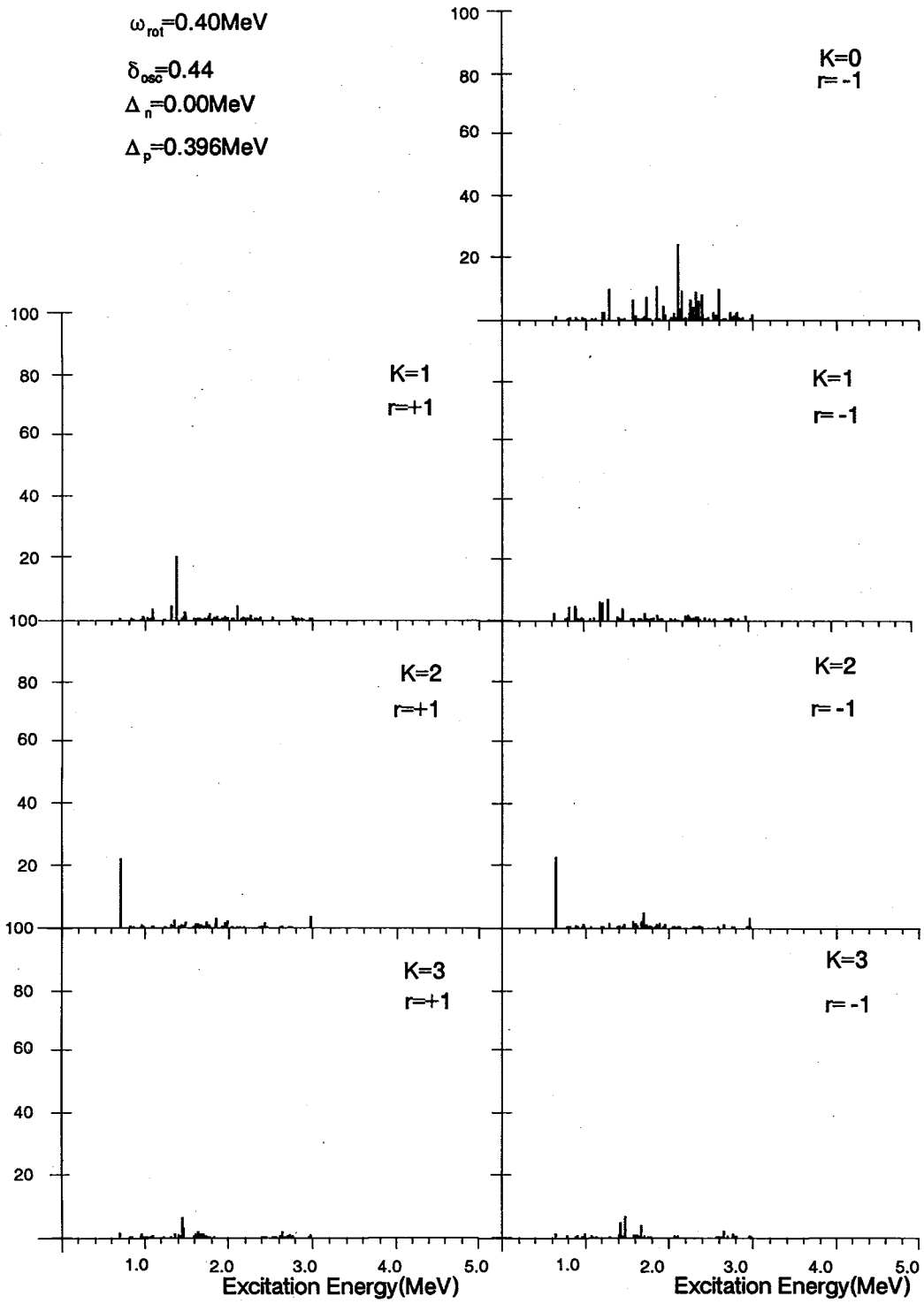

Fig. 6. The same as Fig. 1 but for $\hbar\omega_{\rm rot}=0.40$ MeV.

are also very strong. In the case of ^{152}Dy, we obtained in Ref. 7) a low-lying $K=2$ vibration composed mainly of the one-particle-one-hole excitations across the closed shell, which transfer the quantum numbers ($N_{\rm sh}$, n_3, Λ) by $\Delta N_{\rm sh}=1$, $\Delta n_3=1$ and $\Delta\Lambda=\pm 2$. Its excitation energy was about the same with that of the "$K=0$" vibrations, but its octupole strength was much weaker than the latter. In the present case of ^{192}Hg, due to the presence of the finite pairing gaps Δ_n and Δ_p, we have appreciable contributions from two-quasiparticle excitations within the same major shells, in addition to those across the magic numbers, both for protons and neutrons. In contrast with the "$K=1$" octupole vibration discussed above, there is no $\Delta N_{\rm sh}=0$ excitation for the "$K=2$" mode. However, due to the $(\boldsymbol{l}\cdot\boldsymbol{s})$- and $\boldsymbol{l}^2$-terms, there exist many $\Delta N_{\rm sh}=1$ configurations with low-energies, some of which come even within the same major shells for the Nilsson potential corresponding to the superdeformed shape. For example, the Nilsson level $[624\frac{9}{2}]$ goes down so that it comes close to the $[512\frac{5}{2}]$ level. Thus, there is no essential difference between both types of two-quasiparticle configuration with $K=2$, i.e., those across the major shells and those within the major shells, and they correlate coherently due to the octupole-octupole interactions. In this way, the strongly collective "$K=2$" octupole vibration is generated.

Concerning the "$K=3$" octupole vibrations, their collectivities are relatively weak in comparison with the $K=0$, 1 and 2 modes discussed above, when they are measured in terms of the octupole strength functions. The main reason is that the octupole strengths are considerably shifted from the high-K components to the low-K components, as is analytically shown in terms of the energy-weighted sum rule for the case of the harmonic-oscillator potential. In addition, the number of low-lying two-quasiparticle $K=3$ configurations are relatively smaller than those of the other modes, since both the $\Delta N_{\rm sh}=0$ and 1 excitations are absent in the case $K=3$.

Let us proceed to the case of larger values of $\omega_{\rm rot}$ displayed in Figs. 4~6. With increasing $\omega_{\rm rot}$, the mixing effects between different K components become stronger, and the classification of the RPA eigenmodes in terms of the approximate K quantum number gradually becomes inappropriate. For instance the peaks seen at about 1.1 MeV in both the $K=1$ and 2 components in the negative-signature sector (the right-hand side) of Fig. 4 are associated with the same RPA eigenmode, in which the $K=1$ and $K=2$ octupole vibrations discussed in connection with Figs. 1~3 are appreciably mixed with each other. In a similar manner, the peaks seen at about 1.3 MeV in both the $K=0$ and 1 components in the same figure are associated with the eigenmode in which the $K=0$ and 1 octupole vibrations are fairly mixed. Due to such K-mixing effects, the octupole strength for each component is shared among many different octupole vibrations. Thus, for example, the number of peaks below 2 MeV in the $K=0$ component in Fig. 5 (which is calculated at $\omega_{\rm rot}=0.3$ MeV) is appreciably increased in comparison with that in Fig. 1 at $\omega_{\rm rot}=0.05$ MeV. Apparently, many among these peaks are associated with those in the $K=1$ and 2 components. As a consequence of the K-mixing effects, the heights of individual peaks in each K-component tend to decrease. It remains to be more thoroughly investigated whether this decrease indicates an onset of fragmentation of collectivities or simply indicates that the octupole operators with definite K (whose quantization axis are taken along

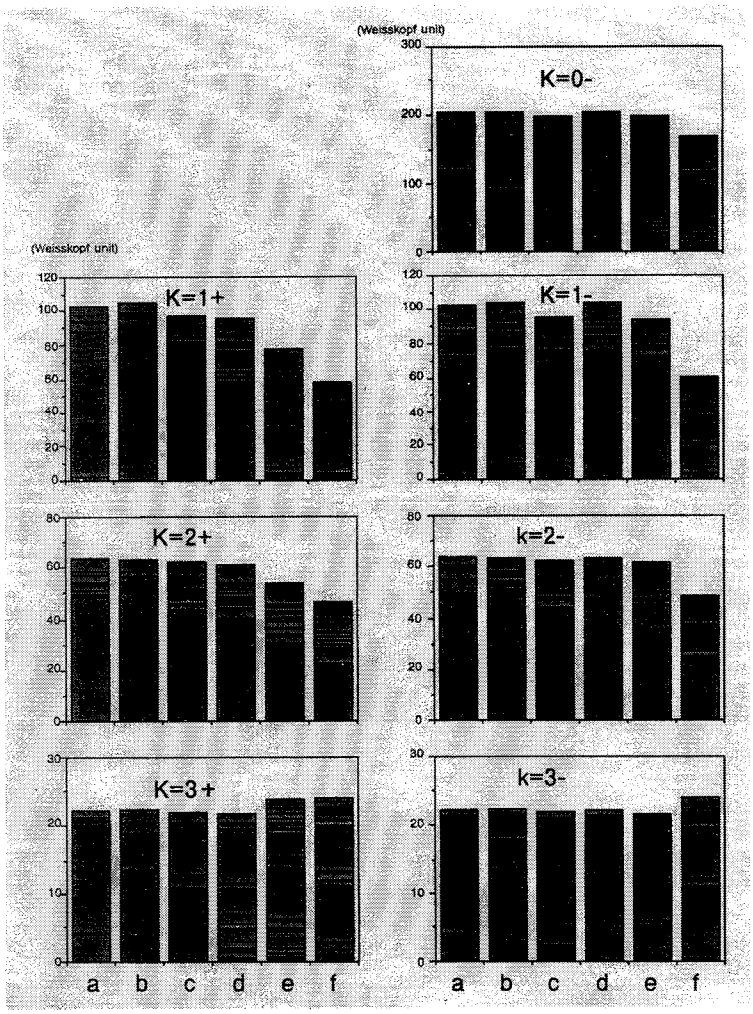

Fig. 7. The strengths $\Sigma_n|\langle n|Q_{3K}^{(E)}|0\rangle|^2$ in Weisskopf units for the electric octupole operators $Q_{3K}^{(E)}$, summed over the RPA eigenmodes lying below 3 MeV. The symbols a, b, c, d, e, f in the ordinates denote the calculations at $\hbar\omega_{\rm rot}=0.05$, 0.10, 0.15, 0.20, 0.30, 0.40, respectively. Parameters used in these calculations are the same as in Figs. 1~6. Vertical lines in each rectangle divide contributions from individual eigenmodes except for the uppermost parts where integrated values of a large number of modes with very small strengths are shown.

the symmetry axis of the Nilsson potential) are no longer the appropriate quantities to measure the collectivities of the RPA modes at high-spin, or both.

Above $\omega_{\rm rot}\approx 0.3$ MeV, the pairing gaps are considerably reduced. In Fig. 6 calculated at $\omega_{\rm rot}=0.4$ MeV, the neutron gap Δ_n is zero, and the proton gap Δ_p is only about 0.4 MeV. The decrease of the static pairing correlation affects most strongly on the $K=1$ component of the strength function. This is because, as discussed in § 3, the low-energy $K=1$ excitations are largely forbidden in the superdeformed closed-shell nuclei when the pairing gaps are diminished.

The dependence of the $K=1$ excitations on the pairing gaps is clearly seen in Fig. 7 which displays the sums of strengths $|\langle n|Q_{3K}^{(E)}|0\rangle|^2$ associated with the RPA eigenmodes lying below 3 MeV. Here $Q_{3K}^{(E)}$ denote the electric octupole operators.

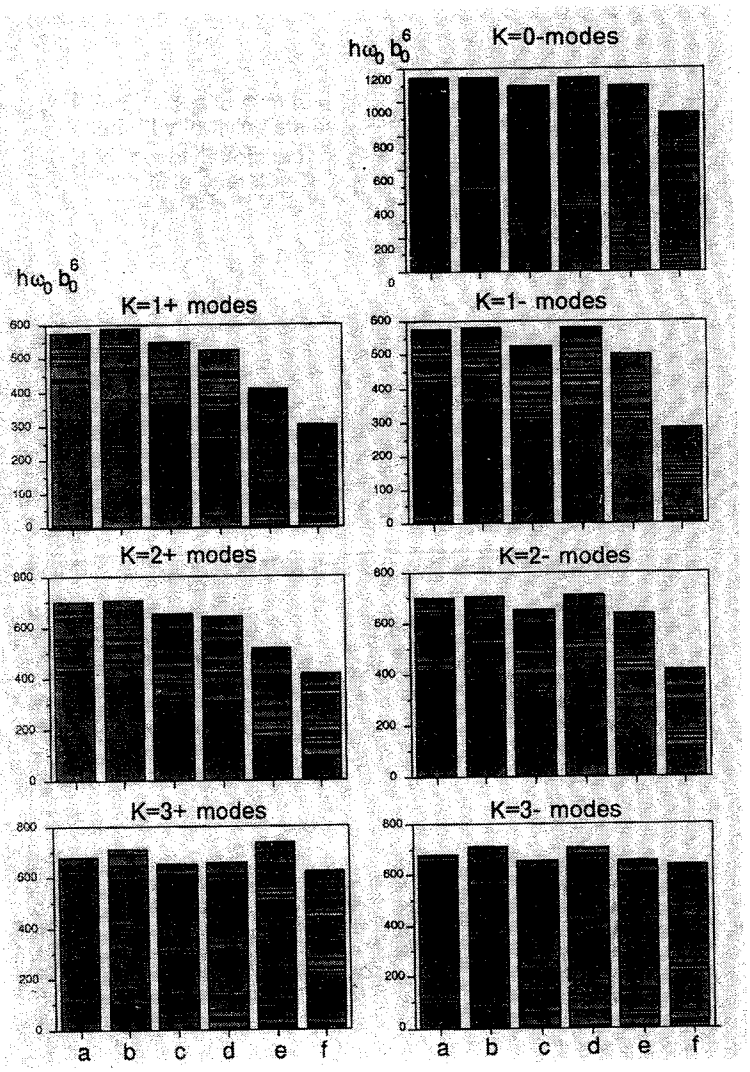

Fig. 8. The energy-weighted transition strength for the doubly-stretched octupole operators Q''_{3K}, $\sum_n \omega_n |\langle n|Q''_{3K}|0\rangle|^2$, summed over the RPA eigenvalues lying below 3 MeV. Notations and parameters used are the same as in Fig. 7.

Note that different scales are used in the abscissa for different K components. Thus, the sums are about 200, 100, 60 and 20 Weisskopf units for $K=0$, 1, 2 and 3, respectively. In this figure, the ordinates indicate the different values of $\omega_{\rm rot}$, i.e., the symbols a, b, c, d, e, f denote the cases $\omega_{\rm rot}=0.05$, 0.10, 0.15, 0.20, 0.30, 0.40 MeV, respectively. It is seen that the strength of the $K=1$ component in fact drops from about 100 to about 60 at $\omega_{\rm rot}=0.4$ MeV, where the neutron pairing gap vanishes and the proton pairing gap is also largely diminished. A similar phenomenon is seen also for the $K=2$ component, but with smaller extent. Figure 8 displays the energy-weighted transition strengths $\sum_n \omega_n |\langle n|Q''_{3K}|0\rangle|^2$ summed over the RPA eigenmodes lying below 3 MeV. They are found to carry about 24.4 %, 11.7 %, 11.9 %, 9.6 % of the total sum rule values given by Eqs. (3·1)~(3·4) for the harmonic-oscillator potential, for $K=0$, 1, 2 and 3, respectively. (It should be noted here that the total sum rule values

actually calculated in ^{192}Hg for the Nilsson plus BCS potential are about 105 % of those for the harmonic oscillator case.) These values are larger than the fraction of the energy-weighted sum rule value carried by the low-lying quadrupole vibrations, which are known to be less than about 10 %. Similarly to Fig. 7, we can see the decrease of these quantities mainly for $K=1$ and 2, at $\omega_{\rm rot}\approx 0.4$ MeV.

§ 5. Concluding remarks

We have suggested that strongly collective, low-frequency octupole vibrations with $K\neq 0$ could be built, in addition to those with $K=0$, on superdeformed high-spin states, provided that appreciable amount of the static pairing correlations exists. The octupole vibrations built on superdeformed shapes are expected to have different characteristics according to the approximate quantum number K. The low-lying $K=0$ octupole vibrations are composed mainly of one-particle-one-hole excitations with $\Delta N_{\rm sh}=1$ across the closed shells of the superdeformed shell structure. Therefore, they are expected to exist independent of the pairing correlations. In contrast, the low-lying $K=1$ octupole vibrations are composed mainly of two-quasiparticle excitations with $\Delta N_{\rm sh}=0$ within the major shells. This kind of excitations are allowed in doubly-closed shell configurations only when the superdeformed states have finite pairing gaps. In this paper, we have explored this possibility by considering the superdeformed rotational band in ^{192}Hg as a typical case. We have seen that they have large octupole strengths reflecting the fact that each major shell at the superdeformed shape consists of about equal numbers of positive- and negative-parity levels. The low-lying $K=2$ octupole vibrations are formed by superpositions of the particle-hole excitations across the closed shells and the two-quasiparticle excitations within the major shells. Thus, their characters are intermediate between the $K=0$ and 1 vibrations discussed above. The collectivity of the low-lying $K=3$ octupole vibrations measured by $B(E3)$ values is weaker than those with $K=0$, 1 and 2, because of the reasons discussed in § 3.

The above classification of the octupole vibrations in terms of the approximate K quantum number may be valid when the rotational frequency $\omega_{\rm rot}$ is small. With increasing $\omega_{\rm rot}$, the Coriolis effects in a rotating potential play increasingly important roles, and different K components will eventually be mixed with each other. In our calculation for ^{192}Hg, the K mixing effects are found to be very important for $\omega_{\rm rot}\gtrsim 0.2$ MeV.

Although we have reported the result of a large-scale numerical calculation for ^{192}Hg, quantitative details should not be taken too seriously, since we have not attempted any optimal choice of parameters appearing in our model Hamiltonian. For example, we have used the octupole-force strengths χ_{3K} that are theoretically derived for the case of the harmonic-oscillator potential. Details of the excitation energies of individual states could be sensitive to a slight modification of the χ_{3K} values.

The octupole strength functions calculated in this paper are those defined in the intrinsic frame associated with the uniformly rotating Nilsson plus BCS potential. In order to evaluate the $B(E3)$ values, we should of course carry out a transformation

into the laboratory frame. To do this on the basis of the cranking model, it is convenient to choose the quantization axis of the octupole operator along the rotation axis (instead of the symmetry axis of the potential). Such a representation is expected to be better suited to characterize the octupole vibrations at large values of $\omega_{\rm rot}$. This will be done in our next paper.

It is well known that the octupole vibrations in deformed nuclei decay mainly by electric dipole transitions (rather than octupole).[15] Since $B(E1)$ values in deformed nuclei are proportional to $\delta_{\rm osc}^2$ $B(E3)$, we expect that the dipole transitions associated with the octupole vibrations play important roles in superdeformed nuclei. According to our preliminary calculations,[18] the $B(E1)$ values are of the order 10^{-3} to 10^{-4} in Weisskopf units, and therefore the decay probability of the octupole vibrations by $E1$ is, of the order 10^3 to 10^4, larger than that by $E3$. The calculation of $B(E1)$ is in progress by taking into account the coupling effects with the giant dipole resonances.

The octupole softness of the superdeformed rotational bands has been suggested[17),19),22] also in the potential-energy calculations by means of the Strutinsky method. In these calculations, only the $K=0$ component of the octupole degrees of freedom has been taken into account. In view of the results discussed in this paper, it is strongly desired to extend such calculations to include the components with $K=1$ and 2.

Finally, we mention that the first experimental data suggesting strong octupole correlations in superdeformed rotational bands are recently reported for ^{193}Hg[20] and for ^{147}Gd.[21]

Acknowledgements

The computer calculation has been financially supported in part by the Grant-in-Aid for Scientific Research of the Japan Ministry of Education, Science and Culture (No. 01540245), and in part by Research Center for Nuclear Physics, Osaka University, and done partly by using the computer center of Institute for Nuclear Study, University of Tokyo.

References

1) D. Ye et al., Phys. Rev. **C41** (1990), R13.
2) F. S. Stephen et al., Phys. Rev. Lett. **64** (1990), 2623.
3) P. J. Twin, Nucl. Phys. **A520** (1990), 17c.
4) P. J. Nolan and P. J. Twin, Ann. Rev. Nucl. Part. Sci. **38** (1988), 533.
5) Slide Report of the Workshop and Symposia on "Nuclear Structure in the Era of New Spectroscopy", Copenhagen, Sept. 11~Nov. 24, 1989.
6) S. Mizutori, Y. R. Shimizu and K. Matsuyanagi, Prog. Theor. Phys. **83** (1990), 666.
7) S. Mizutori, Y. R. Shimizu and K. Matsuyanagi, *Proc. Symp. on "Nuclear Collective Motion and Nuclear Reaction Dynamics", Riken, Dec. 1989,* ed. K.-I. Kubo, M. Ichimura, M. Ishihara and S. Yamaji (World Scientific, Singapore), p. 119.
8) S. Mizutori, Y. R. Shimizu and K. Matsuyanagi, Prog. Theor. Phys. **85** (1991), 559.
9) Y. R. Shimizu, Nucl. Phys. **A520** (1990), 477c.
10) Y. R. Shimizu and K. Matsuyanagi, Prog. Theor. Phys. **72** (1984), 1087; **75** (1986), 1161.
11) H. Sakamoto and T. Kishimoto, Nucl. Phys. **A501** (1989), 205.
12) T. Bengtsson and I. Ragnarsson, Nucl. Phys. **A436** (1985), 14.
13) M. Brack, J. Damgaard, A. S. Jensen, H. C. Pauli, V. M. Strutinsky and C. Y. Wong, Rev. Mod. Phys. **44** (1972), 320.

14) R. Bengtsson, Y.-S. Chen, J.-Y. Zhang and S. Åberg, Nucl. Phys. **A405** (1983), 221.
15) A. Bohr and B. R. Mottelson, *Nuclear Structure* (Benjamin, New York 1975), vol. 2.
16) T. Nakatsukasa, S. Mizutori and K. Matsuyanagi, in preparation.
17) S. Åberg, Nucl. Phys. **A520** (1990), 35c.
18) S. Mizutori, Doctor Thesis, Kyoto University, 1990 (unpublished).
19) J. Dudek, *The Variety of Nuclear Shapes,* ed. J. D. Garrett et al. (World Scientific, Singapore, 1987), p. 195.
20) D. M. Cullen et al., Phys. Rev. Lett. **65** (1990), 1547.
21) K. Zuber et al., Nucl. Phys. **A520** (1990), 195c.
22) J. Dudek, T. R. Werner and Z. Szymansky, Phys. Lett. **B248** (1990), 235.

Progress of Theoretical Physics, Vol. 87, No. 3, March 1992

Octupole Vibrations in the Harmonic-Oscillator-Potential Model with Axis Ratio Two to One

Takashi NAKATSUKASA, Shoujirou MIZUTORI* and Kenichi MATSUYANAGI

Department of Physics, Kyoto University, Kyoto 606-01
**Institute for Nuclear Study, University of Tokyo, Tanashi 188*

(Received September 20, 1991)

Properties of the RPA solutions for the octupole vibrations (with $K=0, 1, 2, 3$) in the prolate harmonic-oscillator-potential model with the frequency ratio 2:2:1 are investigated. Special attention is directed to their dependence on the K-quantum number and on the shell-quantum number N_{sh} (characterizing the 2:1 shell structure). This analysis suggests that strongly collective, soft $K=1$ octupole vibrations exist in open-shell superdeformed configurations, and that they strongly couple with the quasiparticle modes in odd-A nuclei.

§ 1. Introduction

We have suggested[1),2)] in terms of the RPA calculation based on the cranked Nilsson model, that strongly collective octupole vibrations with $K=0, 1, 2, 3$ could be built on superdeformed rotational bands having prolate shapes with the axis ratio approximately 2:1. Recently, a similar suggestion has been obtained in the calculation[3)] in terms of the parity-projected generator-coordinate method (though this calculation has been restricted to the $K=0$ mode only). Octupole instability of some superdeformed rotational bands have also been suggested in the potential-energy calculations[4)~7)] utilizing the Strutinsky method. Thus, octupole correlations in superdeformed nuclei have become one of the current issues in superdeformed spectroscopy.[8)]

In this paper, we summarize the properties of the RPA solutions for the octupole vibrations in the superdeformed harmonic-oscillator-potential model which is characterized by the rational ratio 2:1 between the frequencies along the minor and the major axes. We shall also discuss the case where the frequency ratio slightly deviates from 2:1, and call the shell structure associated with the harmonic-oscillator potential whose frequency ratio is approximately 2:1 "superdeformed shell structure". Needless to say, the harmonic-oscillator-potential model is not very realistic. Still, we believe that some interesting properties of the octupole vibrations obtained in this model have relevance to realistic situations. In fact, we know, at least, some cases where the major characteristics of realistic calculations can be easily understood in connection with the properties of the harmonic-oscillator potential.[1),2)]

We use the doubly-stretched octupole interactions proposed by Sakamoto and Kishimoto[9)] as the residual interactions to be treated in the RPA. It is recapitulated in § 2. In § 3 we discuss the equilibrium deformations of the closed-shell configurations for the superdeformed shell structure, and analytically derive the RPA dispersion equations. In § 4 energy-weighted sum rules are given both for the ordinary and doubly-stretched octupole operators. In § 5 numerical examples of the RPA

octupole vibrations are presented. In § 6 we extend the discussion to the case where the superdeformed states are uniformly rotating with the rotational frequency $\omega_{\rm rot} \neq 0$. In § 7 we discuss the open-shell superdeformed configurations and suggest that soft $K=1$ octupole vibrations will appear. In § 8 the octupole vibration-quasiparticle couplings in odd-A superdeformed configurations having finite pairing gaps Δ are discussed. Main conclusions of this work is summarized in § 9.

§ 2. The doubly-stretched octupole interaction

We start from the harmonic-oscillator-potential model

$$h_{\rm HO}=\sum_{k=1}^{A}\left\{\frac{\boldsymbol{p}^2}{2M}+\frac{1}{2}M\sum_{i=1}^{3}\omega_i^2 x_i^2\right\}_k , \tag{2·1}$$

and introduce the doubly-stretched octupole interactions[9] as residual interactions. Namely, we consider a model Hamiltonian

$$H=h_{\rm HO}-\frac{1}{2}\sum_K \chi_{3K}\sum_{kl} Q''^{\dagger}_{3K}(k)Q''_{3K}(l) , \tag{2·2}$$

where the doubly-stretched octupole operators Q''_{3K} are obtained from the ordinary octupole operators Q_{3K} by replacing the coordinates x_i with $x_i''=(\omega_i/\omega_0)x_i$. The doubly-stretched multipole-multipole interactions are natural extensions of the familiar multipole-multipole interactions to the cases where equilibrium shapes of the single-particle potential have quadrupole deformations. Use of these interactions guarantees us to fulfill the selfconsistency between the shape of density distribution and that of the vibrating potential at any instant of time. Importance of this selfconsistency has been discussed in detail by Sakamoto and Kishimoto.[9] They have systematically investigated low-lying collective states and high-frequency giant resonances in spherical and ordinary deformed nuclei by the use of the doubly-stretched multipole interactions. These interactions were used also by Neergard and Vogel,[10] and by Marshalek.[11] In the following, we shall make use of the results obtained by Sakamoto and Kishimoto.[9] We shall call the vibrational modes associated with the $Q''^{\dagger}_{3K}Q''_{3K}$ interactions "octupole vibrations" for simplicity, although Q''_{3K} are in fact linear combinations of the ordinary octupole operators r^3Y_{3K} and the compressional dipole operators r^3Y_{1K}.

The RPA dispersion equations determining the frequency ω of the octupole vibrations about the quadrupole deformed shape can be written as

$$\frac{1}{2\chi_{3K}}=\sum_{\Delta E}\frac{\Delta E\Sigma(\Delta E;3K)}{(\Delta E)^2-(\hbar\omega)^2} \tag{2·3}$$

with

$$\Sigma(\Delta E;3K)=\sum_{i(\Delta E)}|\langle i|\sum_{k=1}^{A}(Q''_{3K})_k|0\rangle|^2 , \tag{2·4}$$

where $|0\rangle$ and $|i\rangle$ are the ground state and the particle-hole excited states of the single-particle Hamiltonian $h_{\rm HO}$. The quantity $\Sigma(\Delta E;3K)$ represents a partial sum of

particle-hole strengths with a definite excitation energy $\Delta E=E_i-E_0$. The force-strengths χ_{3K} are determined from the selfconsistency condition as

$$\chi_{3K}=\frac{4\pi}{7}M\omega_0^2\Big\{\langle(r^4)''\rangle_0+\frac{2}{7}(4-K^2)\langle(r^4P_2)''\rangle_0 + \frac{1}{84}(K^2(7K^2-67)+72)\langle(r^4P_4)''\rangle_0\Big\}^{-1} \tag{2·5}$$

with P_l being the Legendre polynomial. Here, the double primes denote the quantities written in terms of the doubly-stretched coordinates, and $\langle\ \rangle_0$ the expectation values with respect to the ground state $|0\rangle$, where the summation $\sum_{k=1}^{A}$ is implied although it is omitted for simplicity of notation.

The frequencies ω_i of the deformed harmonic-oscillator potential are to be determined such that they satisfy the well-known equilibrium condition[12]

$$\omega_1^2\langle\sum_{k=1}^{A}(x_1^2)_k\rangle_0=\omega_2^2\langle\sum_{k=1}^{A}(x_2^2)_k\rangle_0=\omega_3^2\langle\sum_{k=1}^{A}(x_3^2)_k\rangle_0\,. \tag{2·6}$$

§ 3. Closed-shell configurations with the axis ratio 2:1

For the axially-symmetric case, the equilibrium condition (2·6) can be written as

$$\omega_\perp\left\langle\sum_k\left(\hat{n}_+ +\frac{1}{2}\right)_k\right\rangle_0=\omega_\perp\left\langle\sum_k\left(\hat{n}_- +\frac{1}{2}\right)_k\right\rangle_0=\omega_3\left\langle\sum_k\left(\hat{n}_3+\frac{1}{2}\right)_k\right\rangle_0\,, \tag{3·1}$$

where $\omega_1=\omega_2=\omega_\perp$ and $(\sum_k(\hat{n}_+ +(1/2))_k\rangle_0$, etc. denote the expectation values of the oscillator quanta in the ground-state configuration (see the Appendix).

Let us consider the cases where $\omega_\perp\approx 2\omega_3$ and introduce the quantum number $N_{\rm sh}$ defined by[13]

$$N_{\rm sh}=2n_\perp+n_3\,, \tag{3·2}$$

where $n_\perp=n_1+n_2$ denotes the number of oscillator quanta perpendicular to the symmetry axis. When $\omega_\perp=2\omega_3$, the single-particle energies are given by $e=\hbar\omega_{\rm sh}(N_{\rm sh}+(5/2))$ with $\omega_{\rm sh}=\omega_3$, and the degenerate single-particle states having the same value of $N_{\rm sh}$ constitute a major shell. From the volume conservation condition $\omega_\perp^2\omega_3=\omega_0^3$, where ω_0 is the frequency of the spherical oscillator, we obtain $\omega_{\rm sh}\approx 0.63\ \omega_0$ when $\omega_\perp=2\omega_3$, which is about $4.8\,{\rm MeV}/\hbar$ for $N=Z=80$. Let us consider a closed-shell configuration in which all single-particle states are completely filled up to the major shell with $(N_{\rm sh})_{\max}\equiv N_{\rm F}$. The expectation values $\langle\sum_k(\hat{n}_+)_k\rangle_0$, etc. with respect to the closed-shell configuration are calculated in the Appendix and given by (A·11). Inserting these expressions in Eq. (3·1) we find that the equilibrium condition is in fact fulfilled at $\omega_\perp=2\omega_3$ when $N_{\rm F}$ is odd. Namely, the quadrupole shape with the axis ratio 2:1 is selfconsistent for the closed-shell configuration with odd-$N_{\rm F}$. On the other hand, we obtain

$$\frac{\omega_\perp}{\omega_3}=\frac{\left\langle\sum_k\left(\hat{n}_3+\frac{1}{2}\right)_k\right\rangle_0}{\left\langle\sum_k\left(\hat{n}_++\frac{1}{2}\right)_k\right\rangle_0}=2\frac{N_F^2+6N_F+6}{N_F^2+6N_F+12}, \tag{3·3}$$

when N_F is even. Namely, the equilibrium deformations for such closed-shell configuration somewhat deviate from the 2:1 shape. Accordingly, the single-particle energies belonging to the same N_{sh} shell somewhat split in this case, although the superdeformed shell structure remains and is well characterized by the shell quantum number N_{sh}.

The difference in equilibrium deformation noted above is related with the super-shell structure discussed by Bohr and Mottelson,[13] and recently by Nazarewicz et al.[14] (see also Refs. 15) and 16)). Namely, we can rewrite the shell quantum number N_{sh} as

$$N_{sh}=2n+p \quad (n=0, 1, 2, \cdots) \tag{3·4}$$

with $p=0$ or 1, and regard the shell structure in the case $\omega_\perp=2\omega_3$ as consisting of two kinds of spherical harmonic oscillator with the same frequency $2\omega_3$ but with different "internal" quantum number p. When N_F is odd, both families ($p=0$ and 1) are evenly occupied. In contrast, when N_F is even, one more major shell is filled in the $p=0$ family in comparison with the $p=1$ family. The magic numbers $(4, 16, 40, 80, \cdots)$ belong to the odd-N_F case, while $(2, 10, 28, 60, \cdots)$ to the even-N_F case (these numbers are multiplied by factor 2 taking the spin degree of freedom into account).

The partial sums of particle-hole strengths $\Sigma(\Delta E; 3K)$ appearing in the RPA dispersion equations (2·3), as well as the force-strengths χ_{3K} given by (2·5), can be analytically evaluated for the closed-shell configurations. When N_F is odd, using the relation $\omega_\perp=2\omega_3$ we obtain the following equations determining the RPA frequency ω for the octupole vibrations with $K=0, 1, 2$ and 3:

$$\begin{aligned}40(N_F^2+6N_F+10)=&12(N_F-1)(N_F+7)\frac{2\omega_3^2}{\omega_3^2-\omega^2}\\&+5(3N_F^2+18N_F+23)\frac{6\omega_3^2}{9\omega_3^2-\omega^2}\\&+15(N_F^2+6N_F+17)\frac{10\omega_3^2}{25\omega_3^2-\omega^2}\end{aligned} \tag{3·5a}$$

for the $K=0$ mode,

$$\begin{aligned}40(N_F^2+6N_F+11)=&2(11N_F^2+66N_F-37)\frac{4\omega_3^2}{4\omega_3^2-\omega^2}\\&+16(N_F^2+6N_F+13)\frac{8\omega_3^2}{16\omega_3^2-\omega^2}\\&+2(3N_F^2+18N_F+59)\frac{12\omega_3^2}{36\omega_3^2-\omega^2}\end{aligned} \tag{3·5b}$$

for the $K=1$ mode,

$$40(N_F^2+6N_F+13)=10(N_F-1)(N_F+7)\frac{2\omega_3^2}{\omega_3^2-\omega^2}$$
$$+5(3N_F^2+18N_F+19)\frac{6\omega_3^2}{9\omega_3^2-\omega^2}$$
$$+25(N_F^2+6N_F+17)\frac{10\omega_3^2}{25\omega_3^2-\omega^2} \qquad (3\cdot5c)$$

for the $K=2$ mode,

$$40(N_F^2+6N_F+13)=30(N_F-1)(N_F+7)\frac{4\omega_3^2}{4\omega_3^2-\omega^2}$$
$$+10(3N_F^2+18N_F+59)\frac{12\omega_3^2}{36\omega_3^2-\omega^2} \qquad (3\cdot5d)$$

for the $K=3$ mode.

Obviously, each term on the r.h.s. represents the contributions from the particle-hole configurations with the following excitation energies:

$$K=0 \text{ and } 2;\ \hbar\omega_3, 3\hbar\omega_3 \text{ and } 5\hbar\omega_3,$$
$$K=1;\ 2\hbar\omega_3, 4\hbar\omega_3 \text{ and } 6\hbar\omega_3,$$
$$K=3;\ 2\hbar\omega_3 \text{ and } 6\hbar\omega_3. \qquad (3\cdot6)$$

These are obtained by putting $\omega_\perp=2\omega_3$ in expression (A·9).

When N_F is even, the degeneracy of the single-particle energies in the major shell is slightly lifted so that the RPA dispersion equation becomes more complicated. Finally, we note that Eqs. (3·5a)~(3·5d) possess the $\omega=0$ solutions, except for the $K=1$ case, in the limit $N_F\to\infty$.

§ 4. Energy-weighted sum-rule values

Let us evaluate the energy-weighted sum-rule values

$$S(\hat{O})=\sum_n(E_n-E_0)|\langle n|\hat{O}|0\rangle|^2=\frac{1}{2}\langle 0|[\hat{O}^\dagger,[H,\hat{O}]]|0\rangle \qquad (4\cdot1)$$

for the operator $\hat{O}=\sum_{k=1}^{A}(Q_{3K})_k$ or $\sum_k(Q''_{3K})_k$, where $|0\rangle$ and $|n\rangle$ denote the ground state and the excited states, respectively, and where E_0 and E_n their energies. As is well known, the RPA approximation conserves these sum rules. Replacing $|0\rangle$ with the unperturbed ground state and assuming that its density distribution $\rho(\boldsymbol{x})$ depends only on the radial coordinate r'' defined in terms of the doubly-stretched coordinates, we can considerably simplify the expressions for S. Rigorously speaking, $\rho(\boldsymbol{x})$ is not isotropic even in the doubly-stretched coordinates and, accordingly, the expectation values $\langle(r^4P_2)''\rangle_0$ and $\langle(r^4P_4)''\rangle_0$ in Eq. (2·5) are not zero. However, their magnitudes are of the order N_F^{-2} in comparison with the main term $\langle r''^4\rangle_0$ so that we expect that the above assumption holds in a good approximation.

Under the approximation mentioned above, the energy-weighted sum-rule values

$S''(3K)$ for the doubly-stretched octupole operators Q''_{3K} are given in the axially-symmetric deformed harmonic-oscillator-potential model as follows:

$$S''(30)=\frac{1}{5}\left\{3\left(\frac{\omega_3}{\omega_0}\right)^2+2\left(\frac{\omega_\perp}{\omega_0}\right)^2\right\}\langle r''^4\rangle_0,$$

$$S''(31)=\frac{1}{15}\left\{8\left(\frac{\omega_3}{\omega_0}\right)^2+7\left(\frac{\omega_\perp}{\omega_0}\right)^2\right\}\langle r''^4\rangle_0,$$

$$S''(32)=\frac{1}{3}\left\{\left(\frac{\omega_3}{\omega_0}\right)^2+2\left(\frac{\omega_\perp}{\omega_0}\right)^2\right\}\langle r''^4\rangle_0,$$

$$S''(33)=\left(\frac{\omega_\perp}{\omega_0}\right)^2\langle r''^4\rangle_0, \tag{4·2}$$

in units of $(21\hbar^2/8\pi M)$. In the same way, the sum-rule values $S(3K)$ for the ordinary octupole operators Q_{3K} are given as

$$S(30)=\frac{1}{5}\left\{3\left(\frac{\omega_0}{\omega_3}\right)^4+2\left(\frac{\omega_0}{\omega_\perp}\right)^4\right\}\langle r''^4\rangle_0,$$

$$S(31)=\frac{1}{15}\left\{6\left(\frac{\omega_0}{\omega_3}\right)^4+4\left(\frac{\omega_0}{\omega_3}\right)^2\left(\frac{\omega_0}{\omega_\perp}\right)^2+5\left(\frac{\omega_0}{\omega_\perp}\right)^4\right\}\langle r''^4\rangle_0,$$

$$S(32)=\frac{1}{3}\left\{2\left(\frac{\omega_0}{\omega_3}\right)^2\left(\frac{\omega_0}{\omega_\perp}\right)^2+\left(\frac{\omega_0}{\omega_\perp}\right)^4\right\}\langle r''^4\rangle_0,$$

$$S(33)=\left(\frac{\omega_0}{\omega_\perp}\right)^4\langle r''^4\rangle_0, \tag{4·3}$$

in units of $(21\hbar^2/8\pi M)$, where the quantity $\langle r''^4\rangle_0$ is used for convenience of comparison with Eq. (4·2). When $\omega_\perp=2\omega_3$, their ratios for different K values are given by

$$S''(30):S''(31):S''(32):S''(33)=11:12:15:20,$$

$$S(30):S(31):S(32):S(33)=50:39:15:5. \tag{4·4}$$

We thus find an interesting property. Namely, the sum-rule values for the doubly-stretched operators are larger for larger values of K, while those for the ordinary octupole operators are larger for smaller values of K. This dependence on K apparently stems from the large equilibrium deformation and is very strong: In fact, we see that $S(30)$ is ten times larger than $S(33)$. Note also that $S(32)=S''(32)$.

The matrix elements of the doubly-stretched operators are related to the amplitudes of the RPA vibrations, while those of the ordinary octupole operators to the $E3$ transition strengths. Therefore, the above ratios indicate that the $E3$ transition strengths may be considerably shifted to the octupole modes with lower values of K, although the vibrational amplitudes of the modes with larger values of K may be large.

§ 5. Octupole vibrations in doubly-closed-shell configurations with $\omega_\perp\approx 2\omega_3$ at $\omega_{\rm rot}=0$

In this section, we discuss the properties of the RPA solutions for octupole

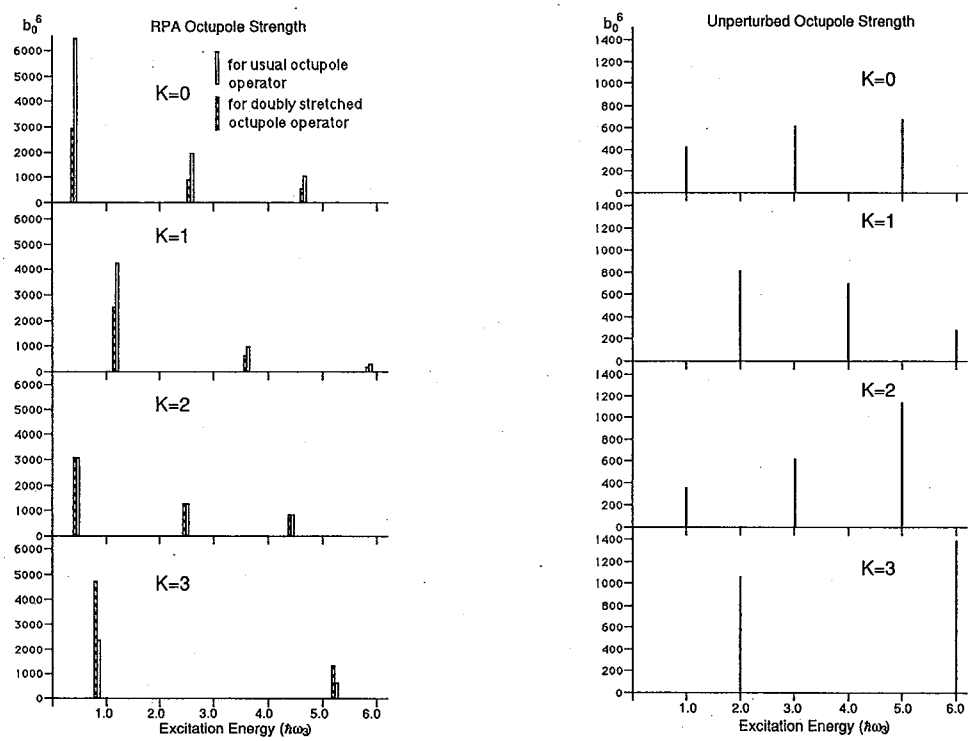

Fig. 1. (a) RPA octupole strength functions calculated at the doubly-closed-shell configurations with $N=Z=80$. The strengths $|\langle n|Q''_{3K}|0\rangle|^2$ for the doubly-stretched octupole operators Q''_{3K} are indicated by striped bars, while $|\langle n|Q_{3K}|0\rangle|^2$ for the ordinary octupole operators Q_{3K} by open bars. The unit is $b_0^6=(\hbar/M\omega_0)^3$.

(b) Unperturbed strength functions for the doubly-stretched octupole operators at the doubly-closed-shell configuration with $N=Z=80$. Compare with (a).

vibrations created on the doubly-closed-shell configurations with $\omega_\perp \approx 2\omega_3$ at $\omega_{\rm rot}=0$. In the following, we explicitly take into account the proton and neutron degrees of freedom. Also, the degeneracy of the single-particle states is multiplied by two considering the spin-degree of freedom. Since, these extensions are straightforward, we shall not write down the resulting expressions.

Figure 1(a) shows the RPA octupole strength functions calculated at the doubly-closed-shell configuration with the proton number $Z=80$ and the neutron number $N=80$ (which belongs to the odd-$N_{\rm F}$ case). For reference, we also show the unperturbed strength functions (obtained by setting $\chi_{3K}\to 0$) in Fig. 1(b). As is expected from the structure of the RPA dispersion equations (3·5a)~(3·5d) we obtain low-frequency, strongly collective octupole vibrations with $K=0$ and 2. Their excitation energies are lowered to about 40% of the unperturbed particle-hole energy $\hbar\omega_3$. If we measure the collectivity by the octupole strength $|\langle n|Q_{3K}|0\rangle|^2$, we find that it amounts to about 380 W.u. for the $K=0$ octupole vibration. Here, it is important to note that the octupole strengths take considerably different values whether they are measured in terms of the ordinary octupole operators Q_{3K} or the doubly-stretched operators Q''_{3K}. Thus, the octupole strength $|\langle n|Q_{33}|0\rangle|^2$ for the $K=3$ vibration is the smallest, although

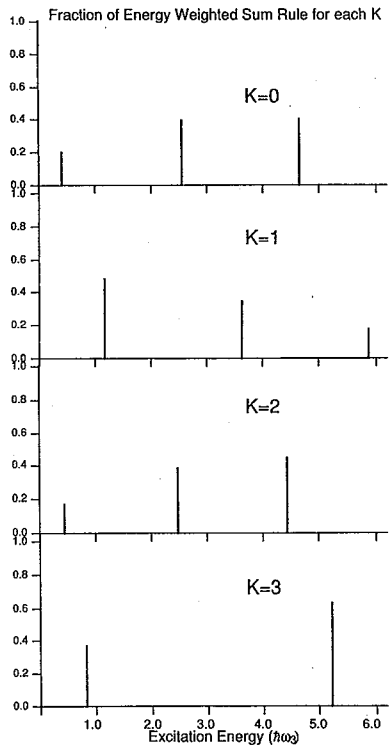

Fig. 2. Fractions of the energy-weighted sum-rule values carried by individual octupole modes, calculated at the doubly-closed-shell configurations with $N=Z=80$.

the doubly-stretched strength $|\langle n|Q''_{33}|0\rangle|^2$ is the largest, among the octupole vibrations with $K=0, 1, 2$ and 3. By the same reason, the octupole strength for $K=0$ is much stronger than that for $K=2$, although the doubly-stretched strengths are approximately the same for $K=0$ and 2. As shown in Fig. 2, these low-lying modes carry about 20% of the energy-weighted sum-rule values.

Next, let us discuss the dependence of the properties of the octupole vibrations on the maximum number N_F of the shell-quantum number N_{sh} (characterizing the closed shells). Figure 3 shows the excitation energies of the lowest octupole vibrations for individual K, calculated at the doubly-closed-shell configurations with $N=Z=16$, 28, 40, 60, 80, 110, 140 and 182 (which corresponds, respectively, to $N_F=3, 4, \cdots, 10$). We see that they exhibit a saw-tooth behavior, except for $K=2$, reflecting whether N_F is even or odd; i.e., their energies are lowered when N_F is even in comparison with the odd-N_F cases. This indicates that the closed-shell configurations with even-N_F are softer against the octupole deformations than those with odd-N_F. The difference between the even-N_F and the odd-N_F cases is clearly seen also in Fig. 4 which displays the strength functions for the doubly-stretched octupole operators calculated at the doubly-closed shell

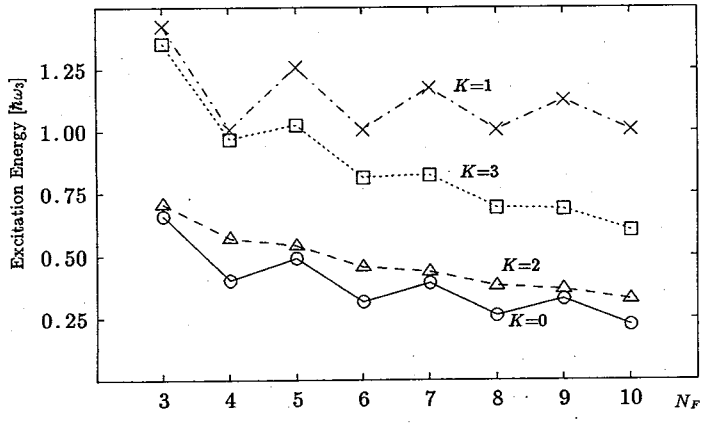

Fig. 3. Dependence on N_F(of the closed-shells) of the RPA excitation energies of the lowest octupole vibrations with $K=0, 1, 2$ and 3, created on the doubly-closed-shell configurations with $N=Z$. The energies are plotted in units of $\hbar\omega_3$.

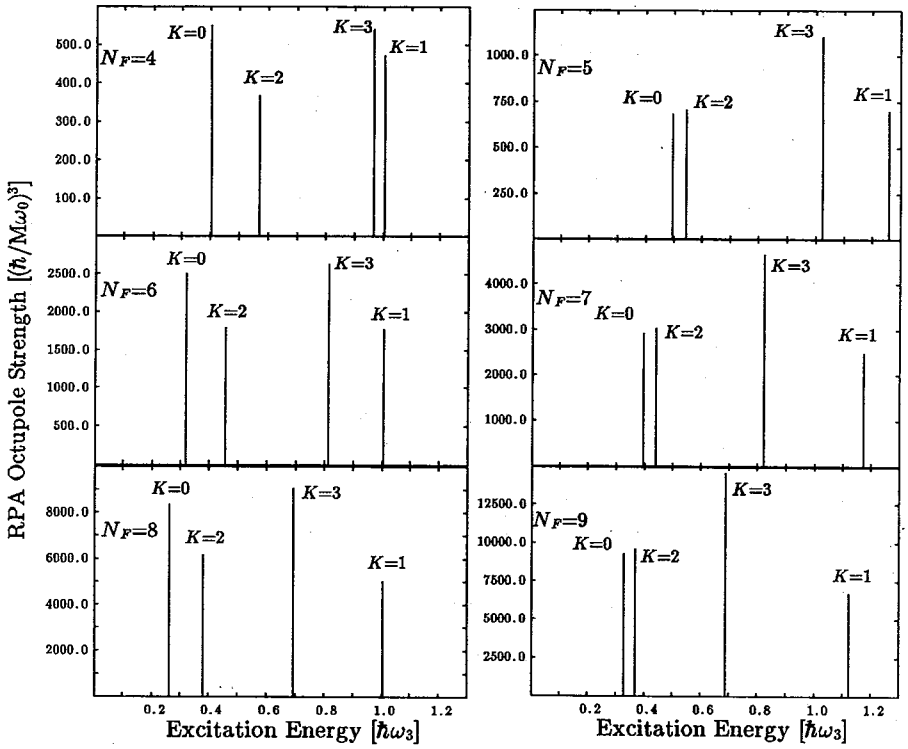

Fig. 4. The strengths $|\langle n|Q'_{3K}|0\rangle|^2$ carried by the lowest octupole vibrations with $K=0, 1, 2$ and 3, calculated in the RPA at various doubly-closed-shell configurations with $N_F=4, 5, \cdots, 9$. The unit is $(\hbar/M\omega_0)^3$. The excitation energies are measured in units of $\hbar\omega_3$.

configurations with $N_F=4, 5, \cdots, 9$.

§ 6. Octupole vibrations in doubly-closed-shell configurations with $\omega_\perp \approx 2\omega_3$ at finite ω_{rot}

In this section, we discuss how the properties of the RPA solutions presented in § 5 are modified when $\omega_{rot}\neq 0$. For this purpose, we replace the single-particle part h_{HO} in the total Hamiltonian (2·2) with the rotating harmonic-oscillator model Hamiltonian h'_{HO} defined by

$$h'_{HO}=h_{HO}-\omega_{rot}\sum_{k=1}^{A}\{l_1\}_k\,, \tag{6·1}$$

where $l_1=x_2p_3-x_3p_2$ denotes the component of the orbital angular momentum along the first axis (which is taken as the rotation axis). At finite ω_{rot}, the octupole vibrations with different K values couple with each other due to the Coriolis effects. Thus, instead of Eq. (2·3), we obtain coupled RPA dispersion equations. Although the K is no longer the good quantum number, the octupole vibrations can still be classified by the signature quantum number $r=\pm 1$ which represents the symmetry property with respect to the rotation 180° about the 1st axis (see the Appendix). We have numerically solved the coupled RPA equation for each signature sector.

Figure 5 shows eigenvalues of h'_{HO} with $\omega_\perp=2\omega_3$ as functions of ω_{rot} (here the

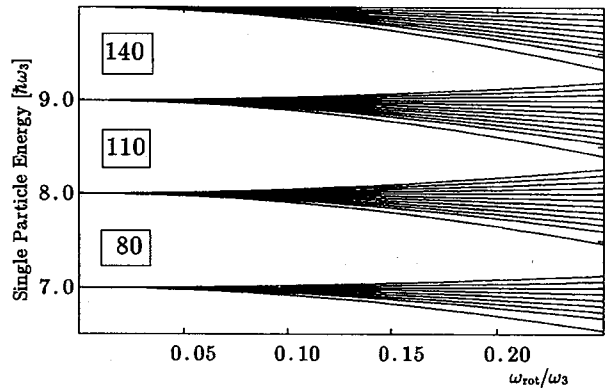

Fig. 5. Eigenvalues of the rotating harmonic-oscillator Hamiltonian $h'_{\rm HO}$ with $\omega_\perp=2\omega_3$, plotted as functions of $\omega_{\rm rot}/\omega_3$ and in units of $\hbar\omega_3$. Only eigenvalues belonging to the major shells with $N_{\rm sh}=7\sim10$ are shown.

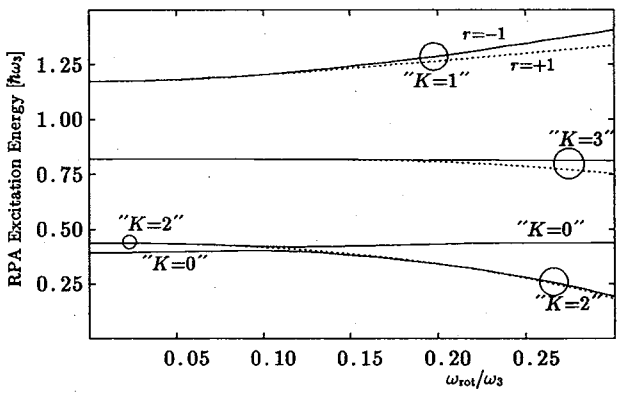

Fig. 6. Excitation energies (in units of $\hbar\omega_3$) of the low-frequency octupole vibrations, plotted as functions of $\omega_{\rm rot}/\omega_3$. The solid (dotted) lines indicate the solutions for the negative (positive) signature sector. The symbols like "$K=2$" indicate the main components of the solutions, although the K are mixed in every solution. These are obtained by solving the coupled RPA dispersion equations for the doubly-closed-shell configurations with $\omega_\perp=2\omega_3$ and with $N=Z=80$.

$\Delta N_{\rm osc}=2$ terms of the Coriolis force are neglected). We see that the major shell structure at $\omega_\perp=2\omega_3$ is not destroyed in the range $\omega_{\rm rot}\lesssim0.25\ \omega_3$ in spite of the Coriolis effects. Here, we should keep in mind the limitation of the harmonic-oscillator-potential model under consideration where the special effects of the unique-parity orbits like $j_{15/2}$ are not properly taken into account. It is known that such special orbits sensitively respond to the increase of $\omega_{\rm rot}$ in realistic situations.

Figure 6 displays excitation energies of the low-frequency octupole vibrations as functions of $\omega_{\rm rot}$, which are obtained by solving the coupled RPA dispersion equations for the doubly-closed shell configurations with $\omega_\perp=2\omega_3$ and with $N=Z=80$(odd-$N_{\rm F}$ case). Here the negative (positive) signature solutions are shown by solid (dotted) lines. We see that the signature-splittings (differences in energy between signature-partners), which are caused by the Coriolis effects, are rather small. It is interesting to note that there occurs a pseudo-level crossing between the lowest two solutions in

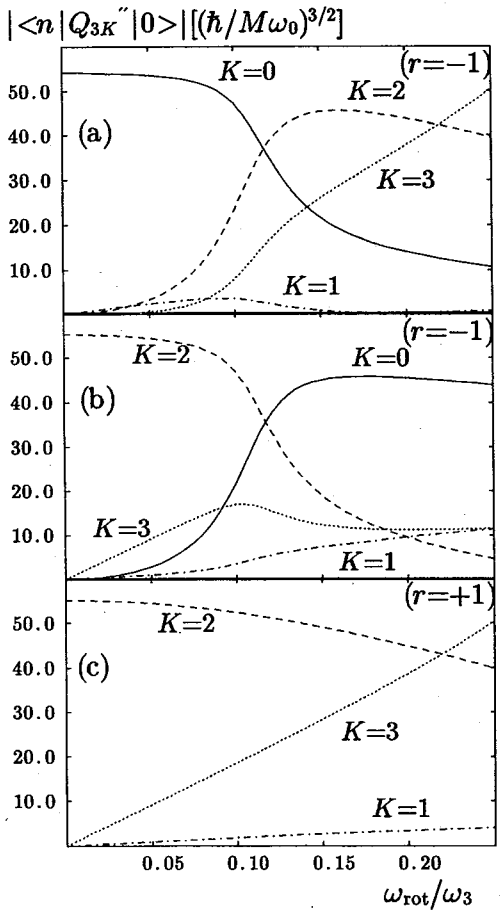

Fig. 7. Doubly-stretched octupole strengths $|\langle n|Q_{3K}''|0\rangle|$ in units of $(\hbar/M\omega_0)^{3/2}$ for the lowest two octupole modes with negative signature ((a) and (b)) and the lowest positive-signature mode (c), whose excitation energies are displayed in Fig. 6.

the negative-signature sector at about $\omega_{rot}\approx 0.1\,\omega_3$. As a result, the main K component of the lowest-energy solution changes from $K=0$ to $K=2$ after the pseudo-level crossing. This is clearly seen in Fig. 7 which shows the octupole strengths $|\langle n|Q_{3K}''|0\rangle|$ for the lowest three modes. This figure also indicates that the K-mixing due to the Coriolis force becomes increasingly important with increasing ω_{rot}. In particular, we see that the $K=3$ components rapidly increase in the modes whose main components are $K=2$, in accordance with the fact that the doubly-stretched octupole matrix elements with $K=3$ are large.

§ 7. Soft $K=1$ octupole vibrations in open-shell configurations

In this section we show that strongly collective, low-frequency $K=1$ octupole vibration will emerge in open-shell configurations having finite pairing gaps Δ.

The $K=1$ octupole operator $Q_{31}^{(\pm)}$ can create (annihilate) two quanta along the 3rd axis decreasing (increasing) at the same time one quantum along the axis perpendicular to it (see (A·5b) in the Appendix). The excitation energy of these transitions, $2\hbar\omega_3-\hbar\omega_\perp$, is zero when $\omega_\perp=2\omega_3$ meaning that they correspond to transitions within the same major shell. Such excitations are forbidden at the closed-shell configurations because of the Pauli principle. When several particles (holes) exist outside (inside) the closed shells, however, this type of excitations is allowed. Thus, we expect that such zero-frequency excitations will generate a new type of collective excitations in open-shell configurations. It may be worthy of emphasizing here that the degeneracy of the single-particle states with positive and negative parities within the same major shell is one of the important characteristics of the harmonic-oscillator potential with the axis ratio 2:1.

In open-shell configurations, the pairing correlations among valence particles (or holes) will play important roles. Thus, we expect that the $K=1$ collective octupole vibrations (suggested to arise from the zero-frequency excitations) are analogous to the familiar low-frequency quadrupole vibrations about the spherical shape whose

properties are strongly affected by the pairing correlations.

To examine the possibility mentioned above, we introduce the ordinary pairing force acting among the valence particles and treat it with the BCS approximation. The procedure to obtain the quasiparticle RPA equations is standard so that we shall not write down the resulting expressions. We here assume that $\omega_\perp/\omega_3=2$ for simplicity, although the ratio for the equilibrium deformation may be slightly smaller than 2. We also use the force strength χ_{3K} determined at the doubly-closed shell.

Figure 8 shows a typical result of the quasiparticle RPA calculation. Here the open-shell configurations (outside the magic number 80) with $Z=80+2$ and $N=80+N_{\rm val}$ are considered, and the excitation energies at $\omega_{\rm rot}=0$ of the lowest octupole vibrations for every K value are plotted as functions of the number of valence neutrons $N_{\rm val}$. It is clearly seen that the excitation energy of the $K=1$ mode drastically decreases with increasing $N_{\rm val}$, while those for the $K=0$ and 2 modes are approximately constant. This trend is just expected and is easily understood from the fact that the $K=1$ mode is generated from the correlations among the valence particles while the $K=0$ and 2 modes are created from the particle-hole excitations across the closed shells. The properties of the $K=1$ mode are sensitive to the magnitude of the pairing gap Δ. For example, when the pairing force G is decreased by 10% in the calculation, their excitation energies are lowered (compare Case (b) with Case (a) in Fig. 8) and we obtain an imaginary RPA solution at $N_{\rm val}=8$ indicating an instability toward the octupole deformation with $K=1$ (the "banana" shape[13]).

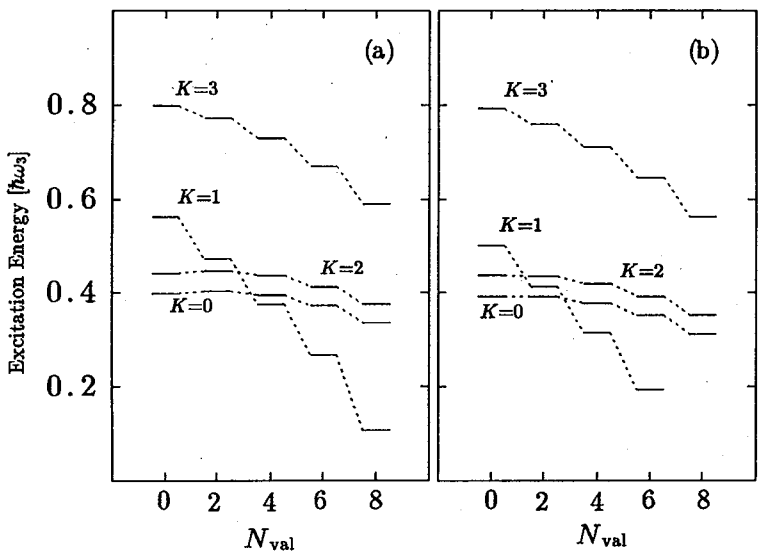

Fig. 8. Excitation energies (in units of $\hbar\omega_3$) of low frequency octupole vibrations, plotted as functions of the number of valence neutrons $N_{\rm val}$. This quasiparticle RPA calculation was done for open-shell configurations with $Z=80+2$ and $N=80, 80+2, \cdots, 80+8$, where 80 is the magic number (odd-$N_{\rm F}$ case). In Cases (a) and (b), slightly different values of the pairing-force strength G are adopted. In Case (a), the calculated proton gap $\Delta_p=0.17$ and the calculated neutron gap $\Delta_n=0.0$, 0.17, 0.22, 0.25 and 0.28 for $N_{\rm val}=0$, 2, 4, 6 and 8, respectively in units of $\hbar\omega_3$. In Case (b), the corresponding values are $\Delta_p=0.15$, $\Delta_n=0.0$, 0.15, 0.20, 0.23 and 0.25, respectively.

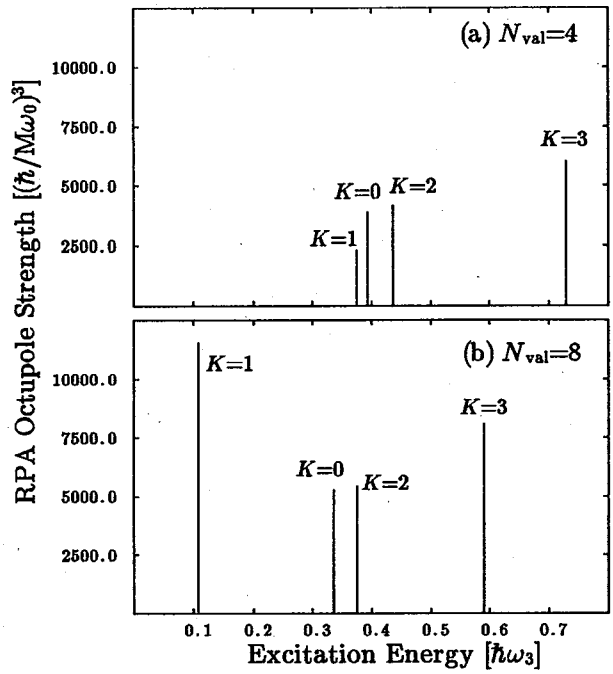

Fig. 9. The strengths $|\langle n|Q''_{3K}|0\rangle|^2$ carried by the lowest octupole vibrations with $K=0$, 1, 2 and 3 whose excitation energies are shown in Fig. 8(a). Only the cases $N_{val}=4$ and 8 are presented in (a) and (b), respectively. The unit is $(\hbar/M\omega_0)^3$.

This is analogous to the well-known quadrupole instability in transitional nuclei (between spherical and quadrupole shapes). Thus, the $K=1$ octupole vibrations may be regarded as a kind of soft modes associated with the octupole instability of the superdeformed configurations toward the "banana" shape.

Figure 9 shows the doubly-stretched octupole strengths $|\langle n|Q''_{3K}|0\rangle|^2$ for the octupole vibrations whose excitation energies are displayed in Fig. 8(a). We see that the strength for the $K=1$ mode is large and it increases with increasing N_{val} indicating the growth of its collectivity.

§ 8. Octupole vibration-quasiparticle couplings in odd-A systems

In this section we point out that the quasiparticle modes in open-shell odd-A configurations may be significantly modified by the coupling effects with the soft $K=1$ octupole vibrations discussed in the preceding section. For simplicity, we here consider only the case $\omega_{rot}=0$.

Following the conventional procedure,[12] we can easily derive the coupling Hamiltonian between the octupole vibrations and the quasiparticle modes in open-shell odd-A configurations having finite pairing gaps Δ_p and Δ_n from the doubly-stretched octupole interactions in Eq. (2·2). In the lowest-order approximation, it takes the following form:

$$\mathcal{H}_{coupl}=\sum_{n\mu\nu} f_n(\mu\nu)(X_n^\dagger+\tilde{X}_n)a_\mu^\dagger a_\nu\,, \tag{8·1}$$

where $X_n^\dagger$ and $\tilde{X}_n$ represent the creation and the (time-reversed) annihilation operators of the octupole vibrations defined in the RPA, and $(a_\mu^\dagger, a_\nu)$ are quasiparticle operators. The vertex functions $f_n(\mu\nu)$ can be expressed as functions of the doubly-stretched octupole matrix elements $Q''_{3K}(\mu\nu)$ between the quasiparticle states μ and ν, the RPA transition matrix elements $\langle n|Q''_{3K}|0\rangle$, associated with the octupole vibrations labeled by n, and the octupole-interaction strengths χ_{3K}. It is important here to note the selection rules of the octupole operator Q_{3K}, which is characteristic to the $\omega_\perp=2\omega_3$ case under consideration. Namely, if we restrict the quasiparticle transitions $(\mu\leftrightarrow\nu)$ only within a single major shell (having a definite shell-quantum number $N_{\rm sh}$), only the $K=1$ component of the octupole interactions contribute to the quasiparticle-vibration coupling Hamiltonian $\mathcal{H}_{\rm coupl}$. This is obvious from (A·5) and (A·9) in the Appendix. Needless to say, such quasiparticle transitions are energetically favored and expected to play major roles in determining near-yrast spectra of open-shell odd-A systems. As was emphasized in § 7, the degeneracy of approximately the same number of positive- and negative-parity single-particle states within the same major shell is one of the important characteristics of the harmonic-oscillator potential with the axis ratio 2:1. Therefore, there are many transitions (within the same major shell) connecting the quasiparticle states μ and ν having parities opposite to each other.

According to the above consideration, let us discuss the coupling effects between the soft $K=1$ octupole vibrations and the quasiparticles. We diagonalize the total Hamiltonian

$$\mathcal{H}=\sum_\mu E_\mu a_\mu^\dagger a_\mu+\sum_n \hbar\omega_n X_n^\dagger X_n+\mathcal{H}_{\rm coupl}\,, \tag{8·2}$$

regarding the $K=1$ vibrations as boson modes independent of quasiparticles and restricting the sum with respect to μ within one major shell. (At $\omega_{\rm rot}=0$, it is convenient to classify the $K=1$ vibrations by $K=\pm1$ instead of the signature $r=\pm1$. In this section, we adopt this convention.) We consider up to the double-vibrational excitations. Then, the eigenstates of $\mathcal{H}$ can be written as

$$|\phi\rangle=\sum_\mu C_0(\mu)a_\mu^\dagger|0\rangle+\sum_{\nu n}C_1(\nu n)a_\nu^\dagger X_n^\dagger|0\rangle$$

$$+\sum_{\nu'}\sum_{n'\le n''}C_2(\nu' n' n'')\frac{1}{\sqrt{1+\delta_{n'n''}}}a_{\nu'}^\dagger X_{n'}^\dagger X_{n''}^\dagger|0\rangle\,. \tag{8·3}$$

We note here that these states have definite K values. Thus, sums of the 3rd components of the quasiparticle and vibrational angular momenta are conserved, i.e., $\Lambda_\mu=\Lambda_\nu+K_n=\Lambda_{\nu'}+K_{n'}+K_{n''}$.

We present in Fig. 10 a typical result of the calculation. In this figure, the probabilities of the zero-, one- and two-phonon states in the eigenstate $|\phi\rangle$ are displayed, together with the excitation energies of the soft $K=1$ octupole vibrations, as functions of the pairing gap Δ (treating the pairing force strength G as a parameter). The probabilities of the 0, 1 and 2 phonon states are defined by $\sum_\mu|C_0(\mu)|^2$, $\sum_{\nu n}|C_1(\nu n)|^2$ and $\sum_{\nu' n' n''}|C_2(\nu' n' n'')|^2$, respectively. It is seen that the mixing of the one and two phonon states in the one-quasiparticle state is significant and becomes larger as the excitation energy $\hbar\omega_{K=1}$ of the soft $K=1$ octupole vibration decreases.

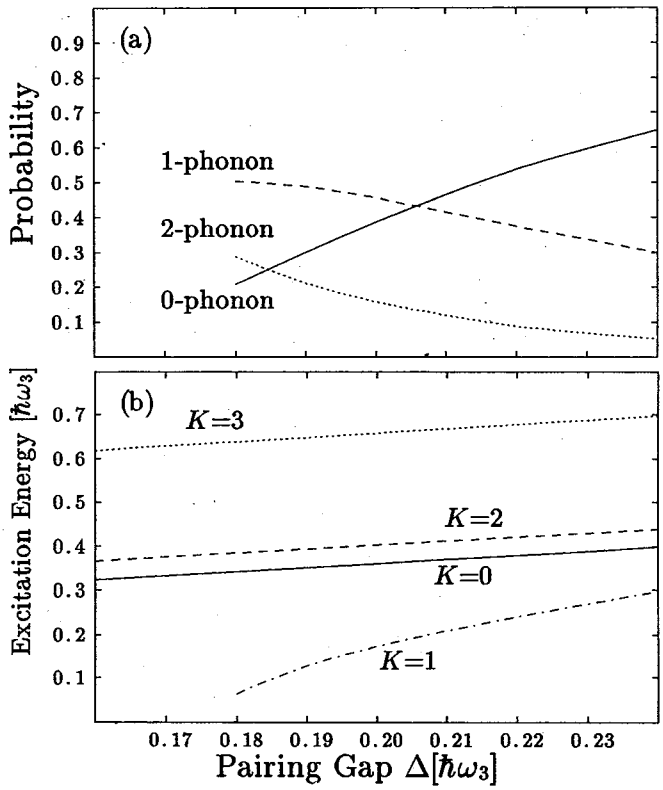

Fig. 10. (a) Dependence on the pairing gap Δ of the probabilities of the zero-, one- and two-phonon states in the eigenstates of the total Hamiltonian $\mathcal{H}$. They are shown by solid, broken and dotted lines, respectively. This is a result of calculation for an odd-A system consisting of the even-even core having 4 valence protons and 4 valence neutrons and the odd-quasiparticle in the $N_{sh}=8$ shell outside the $N=Z=80$ closed shell.

(b) Dependence on the pairing gap Δ of the excitation energy of the soft $K=1$ octupole vibration, which is calculated by the RPA for the $N=Z=84$ system treating the pairing gap $\Delta(=\Delta_p=\Delta_n)$ as a parameter. An instability occurs at about $\Delta\approx 0.17$ in units of $\hbar\omega_3$.

Thus, the probability of the one-quasiparticle state becomes less than 50% when $\hbar\omega_{K=1}\lesssim 0.2\hbar\omega_3(\approx 1\,\mathrm{MeV})$. This indicates that the properties of the one-quasiparticle modes in open-shell odd-A systems will be greatly modified by the coupling effects of the soft $K=1$ octupole vibrations. The mixing probabilities are sensitive to the magnitude of the pairing gap Δ because the excitation energy $\hbar\omega_{K=1}$ strongly depends on it. From this result, we suggest that the properties of the near-yrast spectra of open-shell odd-A superdeformed nuclei will be sensitive to the subtle interplay between the pairing correlations and the octupole correlations. Of course we should expect that this interplay strongly depends on details of the realistic superdeformed shell structure which are not taken into account in the harmonic-oscillator-potential model under consideration.

§ 9. Concluding remarks

Main results obtained in this work for the harmonic-oscillator-potential model may be summarized as follows:

1) At the closed-shell configuration of the superdeformed shell structure, the equilibrium deformation determined by the selfconsistency condition exactly satisfies the relation $\omega_\perp/\omega_3=2$ at $\omega_{\rm rot}=0$ when the shell-quantum number $N_{\rm sh}$ of the uppermost filled major shell, $N_{\rm F}$, is odd. On the other hand, the ratio $\omega_\perp/\omega_3$ is slightly smaller than 2 when $N_{\rm F}$ is even (§ 3).
2) The energy-weighted sum rules for the ordinary octupole operators Q_{3K} and those for the doubly-stretched operators Q'_{3K} possess quite different K-dependence: The former becomes larger for smaller K, while the latter takes larger values for larger K (§ 4).
3) We obtain strongly collective, low-frequency octupole vibrations with $K=0$ and 2 at the doubly-closed-shell configurations with $\omega_\perp\approx 2\omega_3$ (§ 5).
4) Excitation energies of the $K=0$ octupole vibrations exhibit a saw-tooth behavior depending on whether $N_{\rm F}$ is even or odd: They are lower in the even-$N_{\rm F}$ case compared to the odd-$N_{\rm F}$ case (§ 5).
5) Due to the Coriolis effects mixing octupole vibrations with different K, we obtain at $\omega_{\rm rot}\approx 0.1\omega_3$ a pseudo-crossing between the lowest two octupole vibrations with negative signature, whose main components are $K=0$ and 2 (§ 6).
6) We obtain soft octupole vibrational modes (the "banana" modes) generated by the $K=1$ octupole correlations among the valence nucleons in open-shell configurations with $\omega_\perp\approx 2\omega_3$ (§ 7).
7) Couplings between the soft $K=1$ octupole vibrations and the quasiparticles in open-shell odd-A configurations with $\omega_\perp\approx 2\omega_3$ are strong. The coupling effects as well as the properties of the $K=1$ modes are quite sensitive to the pairing correlations (§ 8).

Concerning point 7) above, we note that experimental data suggesting octupole effects have recently been reported for the superdeformed states in ^{193}Hg.[17] We are making realistic calculations for the octupole vibration-quasiparticle coupling effects in superdeformed, superconducting odd-A nuclei including ^{193}Hg, and the result will be reported in a forthcoming paper.

Quite recently, it has been pointed out by Nazarewicz et al.[14),18] that the octupole softness of the superdeformed states significantly depends on whether $N_{\rm F}$ is even or odd, and that it is related to the dynamical symmetry of the rational harmonic-oscillator potential. Their argument is consistent with our result mentioned as point 4) above. Nazarewicz[18] has furthermore shown that the closed-shell configurations with even-$N_{\rm F}$ become unstable against the octupole deformations with $K=0$, 1 and 3, if we extract only the shell-structure energy from the harmonic-oscillator-potential model and combine it with the macroscopic energy (described by the liquid-drop

model) by means of the Strutinsky procedure. Octupole instability of the superdeformed states, their relations to the supershell structure, and to the dynamical symmetry of rational harmonic oscillators are certainly very interesting open questions for the future.

Acknowledgements

One of the authors (K. M.) would like to thank Professor W. Nazarewicz for valuable discussions on octupole instability of superdeformed bands, especially for his suggestion of its possible relation to dynamical symmetries of rational harmonic oscillators. He also wishes to acknowledge stimulating discussions concerning microscopic structures of superdeformed states with Professors R. R. Chasman, D. H. Feng, J. Garrett, A. Klein, E. R. Marshalek and C. -L. Wu. This work was done as a part of the cooperative study with Dr. Y. R. Shimizu and we are indebted to him for his active participation in it. The computer calculation for this work has been financially supported in part by Research Center for Nuclear Physics, Osaka University.

Appendix

Let us consider the axially symmetric case with $\omega_1=\omega_2\equiv\omega_\perp$ and introduce the creation and annihilation operators of the harmonic-oscillator quanta by[13]

$$x_1=(-i)\sqrt{\frac{\hbar^2}{2M\omega_\perp}}(c_1^\dagger-c_1)\,,\qquad p_1=\sqrt{\frac{\hbar M\omega_\perp}{2}}(c_1^\dagger+c_1)\,,$$

$$x_2=\sqrt{\frac{\hbar^2}{2M\omega_\perp}}(c_2^\dagger+c_2)\,,\qquad p_2=i\sqrt{\frac{\hbar M\omega_\perp}{2}}(c_2^\dagger-c_2)\,,$$

$$x_3=(-i)\sqrt{\frac{\hbar^2}{2M\omega_3}}(c_3^\dagger-c_3)\,,\qquad p_3=\sqrt{\frac{\hbar M\omega_3}{2}}(c_3^\dagger+c_3)\,. \tag{A·1}$$

Let us also define

$$c_\pm^\dagger=\mp\frac{1}{\sqrt{2}}(c_1^\dagger\mp c_2^\dagger)\quad\text{and}\quad c_\pm=\mp\frac{1}{\sqrt{2}}(c_1\mp c_2)\,. \tag{A·2}$$

In terms of these operators, the axially-symmetric deformed harmonic-oscillator Hamiltonian is written as

$$h_{\rm HO}=\sum_{k=1}^{A}\left\{\hbar\omega_\perp(\hat{n}_++\hat{n}_-+1)+\hbar\omega_3\left(\hat{n}_3+\frac{1}{2}\right)\right\}_k\,, \tag{A·3}$$

where $\hat{n}_\pm=c_\pm^\dagger c_\pm$ and $\hat{n}_3=c_3^\dagger c_3$.

Expectation values of $h_{\rm HO}$ depend only on $N_{\rm osc}\equiv n_1+n_2+n_3$ and n_3, where n_i denote the numbers of oscillator quanta along the i axis. For a given set of $(N_{\rm osc}, n_3)$, there are degenerate states having different values of projection Λ of the orbital angular momentum on the symmetry axis. As is well known, the Λ is given by $\Lambda=\langle\hat{n}_+-\hat{n}_-\rangle$ and takes the following values:

$$\Lambda=\pm n_\perp, \pm(n_\perp-2), \cdots, \pm 1 \text{ or } 0, \tag{A·4}$$

where $n_\perp=n_1+n_2$.

The octupole operators $Q_{3K}\equiv r^3 Y_{3K}$ are written in terms of the creation and annihilation operators of the oscillator quanta as follows:

$$\begin{aligned} Q_{30}=&i\left(\frac{7}{32}\frac{\hbar^3}{M^3\omega_0{}^3}\right)^{1/2}\{3f_3c_+^\dagger c_-^\dagger c_3^\dagger+(f_1c_3^{\dagger 3}-3f_3c_+^\dagger c_-^\dagger c_3)\\ &+3(f_3(1+\hat{n}_++\hat{n}_-)-f_1\hat{n}_3)c_3^\dagger\}+(\text{Hermite conjugate}), \end{aligned} \tag{A·5a}$$

$$\begin{aligned} Q_{31}=&i\left(\frac{21}{64}\frac{\hbar^3}{M^3\omega_0{}^3}\right)^{1/2}\{f_4c_+^{\dagger 2}c_-^\dagger+2f_2c_+^\dagger c_3^{\dagger 2}\\ &+(f_4(1+\hat{n}_++2\hat{n}_-)-2f_2(1+2\hat{n}_3))c_+^\dagger+2f_2c_3^{\dagger 2}c_-\}\\ &-(\text{Hermite conjugate with the replacement } c_+\leftrightarrow c_-), \end{aligned} \tag{A·5b}$$

$$\begin{aligned} Q_{32}=&i\left(\frac{105}{64}\frac{\hbar^3}{M^3\omega_0{}^3}\right)^{1/2}f_3(c_+^{\dagger 2}c_3^\dagger-c_+^{\dagger 2}c_3+2c_+^\dagger c_3^\dagger c_-)\\ &+(\text{Hermite conjugate with the replacement } c_+\leftrightarrow c_-), \end{aligned} \tag{A·5c}$$

$$\begin{aligned} Q_{33}=&i\left(\frac{35}{64}\frac{\hbar^3}{M^3\omega_0{}^3}\right)^{1/2}f_4(c_+^{\dagger 3}+3c_+^{\dagger 2}c_-)\\ &-(\text{Hermite conjugate with the replacement } c_+\leftrightarrow c_-). \end{aligned} \tag{A·5d}$$

Here the coefficients f_1, f_2, f_3, f_4 are defined as

$$f_1=\left(\frac{\omega_0{}^3}{\omega_3{}^3}\right)^{1/2},\quad f_2=\left(\frac{\omega_0{}^3}{\omega_3{}^2\omega_\perp}\right)^{1/2},\quad f_3=\left(\frac{\omega_0{}^3}{\omega_3\omega_\perp{}^2}\right)^{1/2},\quad f_4=\left(\frac{\omega_0{}^3}{\omega_\perp{}^3}\right)^{1/2}. \tag{A·6}$$

The octupole operators can be classified according to the signature quantum number r with respect to the rotation 180° about the 1st axis, as well as the familiar K quantum number: Namely, the octupole operators which have the signature $r=\pm 1$ are defined by

$$Q_{3K}^{(\pm)}=\sqrt{\frac{1}{2(1+\delta_{K0})}}r^3(Y_{3K}\mp Y_{3-K}). \tag{A·7}$$

For convenience, we write here their explicit expressions in terms of the Cartesian coordinates:

$$Q_{30}^{(-)}=\left(\frac{7}{16\pi}\right)^{1/2}z(2z^2-3x^2-3y^2),$$

$$Q_{31}^{(+)}=-\left(\frac{21}{32\pi}\right)^{1/2}x(4z^2-x^2-y^2),$$

$$Q_{31}^{(-)}=-i\left(\frac{21}{32\pi}\right)^{1/2}y(4z^2-x^2-y^2),$$

$$Q_{32}^{(+)}=i\left(\frac{105}{16\pi}\right)^{1/2}2xyz,$$

$$Q_{32}^{(-)}=\left(\frac{105}{16\pi}\right)^{1/2}z(x^2-y^2)\,,$$

$$Q_{33}^{(+)}=-\left(\frac{35}{32\pi}\right)^{1/2}x(x^2-3y^2)\,,$$

$$Q_{33}^{(-)}=-i\left(\frac{35}{32\pi}\right)^{1/2}y(3x^2-y^2)\,, \qquad (A\cdot8)$$

where $(x, y, z)=(x_1, x_2, x_3)$. Note that there is no $r=+1$ operator for $K=0$.

From the above expressions (A·5)~(A·8), we see that each octupole operator can create particle-hole excitations with the following energies:

$$Q_{30}^{(-)};\ \hbar\omega_3,\ 2\hbar\omega_\perp-\hbar\omega_3,\ 3\hbar\omega_3 \quad \text{and} \quad 2\hbar\omega_\perp+\hbar\omega_3\,,$$

$$Q_{31}^{(\pm)};\ 2\hbar\omega_3-\hbar\omega_\perp,\ \hbar\omega_\perp,\ 2\hbar\omega_3+\hbar\omega_\perp \quad \text{and} \quad 3\hbar\omega_\perp\,,$$

$$Q_{32}^{(\pm)};\ \hbar\omega_3,\ 2\hbar\omega_\perp-\hbar\omega_3 \quad \text{and} \quad 2\hbar\omega_\perp+\hbar\omega_3\,,$$

$$Q_{33}^{(\pm)};\ \hbar\omega_\perp \quad \text{and} \quad 3\hbar\omega_\perp\,. \qquad (A\cdot9)$$

Using the above expressions and employing the technique developed by Sakamoto and Kishimoto,[9] we can easily evaluate the partial sums $\Sigma(\Delta E;\ 3K)$ appearing in the RPA dispersion equation (2·3): They are given in terms of the expectation values of the operators $\hat{n}_3$, $\hat{n}_\pm$, $\hat{n}_3^2$, $\hat{n}_\pm^2$, $\hat{n}_+\hat{n}_-$ and $\hat{n}_3\hat{n}_\pm$ (see Eqs. (B·30) ~(B·33) of the first paper of Ref. 9)).

Below, we consider the special case $\omega_\perp=2\omega_3$, where the eigenstates of $h_{\rm HO}$ having the same shell quantum number $N_{\rm sh}=2n_\perp+n_3$ are degenerate and constitute a major shell. The sums of expectation values of the operators $\hat{n}_3$, $\hat{n}_\perp$, etc. with respect to the single-particle states belonging to a major shell (having a definite value of $N_{\rm sh}=2n+p$) are given as follows:

$$\langle 1\rangle_{N_{\rm sh}}=\frac{1}{2}(n+1)(n+2)\,,$$

$$\langle \hat{n}_3\rangle_{N_{\rm sh}}=\frac{1}{6}(n+1)(n+2)(2n+3p)\,,$$

$$\langle \hat{n}_+\rangle_{N_{\rm sh}}=\frac{1}{6}n(n+1)(n+2)\,,$$

$$\langle \hat{n}_3^{\,2}\rangle_{N_{\rm sh}}=\frac{1}{6}(n+1)(n+2)\{2n(n+1)+p(4n+3)\}\,,$$

$$\langle \hat{n}_+^{\,2}\rangle_{N_{\rm sh}}=\frac{1}{12}n(n+1)^2(n+2)\,,$$

$$\langle \hat{n}_+\hat{n}_-\rangle_{N_{\rm sh}}=\frac{1}{24}(n-1)n(n+1)(n+2)\,,$$

$$\langle \hat{n}_+\hat{n}_3\rangle_{N_{\rm sh}}=\frac{1}{12}n(n+1)(n+2)(n-1+2p)\,. \quad (p=0 \text{ or } 1) \qquad (A\cdot10)$$

Summing up the above expressions, we obtain the expectation values with respect to

the closed-shell configurations where the major shells are filled up to $(N_{\rm sh})_{\rm max}=N_{\rm F}=2n+p$:

$$\langle 1\rangle_{N_{\rm F}}=\frac{1}{6}(n+1)(n+2)(2n+3+3p)\,,$$

$$\langle \hat{n}_3\rangle_{N_{\rm F}}=\frac{1}{6}(n+1)(n+2)\{n(n+2)+p(2n+3)\}\,,$$

$$\langle \hat{n}_+\rangle_{N_{\rm F}}=\frac{1}{12}n(n+1)(n+2)(n+1+2p)\,,$$

$$\langle \hat{n}_3{}^2\rangle_{N_{\rm F}}=\frac{1}{30}(n+1)(n+2)\{n(4n^2+13n+8)+5p(2n^2+6n+3)\}\,,$$

$$\langle \hat{n}_+{}^2\rangle_{N_{\rm F}}=\frac{1}{60}n(n+1)(n+2)\{2n^2+4n+4+5p(n+1)\}\,,$$

$$\langle \hat{n}_+\hat{n}_-\rangle_{N_{\rm F}}=\frac{1}{120}(n-1)n(n+1)(n+2)(2n+1+5p)\,,$$

$$\langle \hat{n}_+\hat{n}_3\rangle_{N_{\rm F}}=\frac{1}{120}n(n+1)(n+2)\{4n^2+3n-7+10p(n+1)\}\,.\quad (p=0 \text{ or } 1)\qquad (\text{A}\cdot 11)$$

References

1) S. Mizutori, Y. R. Shimizu and K. Matsuyanagi, Prog. Theor. Phys. **83** (1990), 666; **85** (1991), 559; **86** (1991), 131.
2) S. Mizutori, Y. R. Shimizu and K. Matsuyanagi, in *Nuclear Collective Motion and Nuclear Reaction Dynamics*, ed. K. I. Kubo, M. Ichimura, M. Ishihara and S. Yamaji (World Scientific, 1990), p. 119.
3) P. Bonche, S. J. Krieger, M. S. Weiss, J. Dobaczewski, H. Flocard and P. -H. Heenen, Phys. Rev. Lett. **66** (1991), 876.
4) J. Dudek, T. R. Werner and Z. Szymanski, Phys. Lett. **B248** (1990), 235.
5) S. Åberg, Nucl. Phys. **A520** (1990), 35c.
6) R. R. Chasman, Argonne Preprint PHY-6824-TH-91, to be published.
7) Xunjun Li and J. Dudek, private communication.
8) P. J. Nolan and P. J. Twin, Ann. Rev. Nucl. Part. Sci. **38** (1988), 533.
9) H. Sakamoto and T. Kishimoto, Nucl. Phys. **A501** (1989), 205; **A501** (1989), 242; **A486** (1988), 1; **A528** (1991), 73.
10) K. Neergard and P. Vogel, Nucl. Phys. **A145** (1970), 33.
11) E. R. Marshalek, Phys. Rev. **C29** (1984), 640.
12) See, for example, P. Ring and P. Schuck, *The Nuclear Many-Body Problem* (Springer-Verlag, 1980).
13) A. Bohr and B. R. Mottelson, *Nuclear Structure*, Vol. 2 (Benjamin, New York, 1975).
14) W. Nazarewicz, J. Dobaczewski and P. Van Isacker, to be published in the *Proceedings of the Workshop-Symposium on Future Directions in Nuclear Physics with* 4π *Gamma Detection Systems of the New Generation, Strasbourg 1991* (AIP Proc. Press, 1991).
15) T. Bengtsson, M. E. Faber, G. Leander, P. Möller, M. Ploszajczak, I. Ragnarsson and S. Åberg, Phys. Scripta **24** (1981), 200.
16) G. Rosensteel and J. P. Draayer, J. of Phys. **A22** (1989), 1323.
17) D. M. Cullen et al., Phys. Rev. Lett. **65** (1990), 1547.
18) W. Nazarewicz and J. Dobaczewski, Phys. Rev. Lett. **68** (1992), 154.

Progress of Theoretical Physics, Vol. 89, No. 2, February 1993

Octupole Instability of the Closed-Shell Configurations in the Superdeformed Oscillator Potential

Ken-ichiro ARITA and Kenichi MATSUYANAGI

Department of Physics, Kyoto University, Kyoto 606-01

(Received June 19, 1992)

We show that the closed-shell configurations in the axially-symmetric harmonic-oscillator potential with the frequency ratio $\omega_\perp/\omega_z=2$ are unstable against octupole deformation when their uppermost shell quantum numbers $N_{\rm sh}^{\rm F}$ are even, whereas they are stable when $N_{\rm sh}^{\rm F}$ are odd, in agreement with the recent suggestion by Nazarewicz and Dobaczewski. We also suggest a possible relationship between the octupole instability of the superdeformed shape and the supershell effect in reflection-asymmetric superdeformed potentials.

In recent years, octupole instability of some superdeformed nuclei has been suggested in shell-structure energy calculations by means of the Strutinsky method.[1)~6)] Concerning the physical condition for the occurrence of octupole instability, Nazarewicz et al.[7)~9)] have discussed dynamical symmetry of the harmonic-oscillator potential with frequencies in rational ratio, and suggested that the octupole instability might occur for closed-shell configurations in the axially-symmetric oscillator potential with frequency ratio $\omega_\perp/\omega_z=2$ (which we call "superdeformed oscillator" for brevity) when the single-particle levels are filled up to the major shells with $N_{\rm sh}$=even, $N_{\rm sh}$ being the shell quantum number defined by $N_{\rm sh}=2n_\perp+n_z$.[10)] The single-particle levels in the superdeformed oscillator potential can be divided into two classes according to whether $N_{\rm sh}$ are even or odd. Each class corresponds to the single-particle levels in a spherical oscillator potential having frequency $2\omega_z$.[8)] This dynamical symmetry was previously discussed by Bengtsson et al.[11)] For the closed-shell configurations whose uppermost shell-quantum number $N_{\rm sh}^{\rm F}$ are even, the particle numbers belonging to two spherical oscillator potentials are unequal so that one can expect a tendency toward a reflection-asymmetric shape under the assumption that each spherical oscillator corresponds to a spatial cluster. Evaluating octupole susceptibility of shell-structure energy by the second-order perturbation, they have shown[7),9)] that the shell-energy octupole-stiffness coefficient is negative (positive) when $N_{\rm sh}^{\rm F}$ is even (odd).

The purpose of this paper is twofold: Firstly, in order to examine the $N_{\rm sh}^{\rm F}$ dependence of the octupole instability, we evaluate the shell-structure energies of the closed-shell configurations in the superdeformed oscillator potential as functions of octupole-deformation parameters by means of the Strutinsky method. The calculation is done such that the volume-conservation condition is rigorously fulfilled. Secondly, we show that the supershell effect,[10)] which is intimately connected with the dynamical symmetry of the superdeformed oscillator potential, becomes more pronounced when the reflection symmetry is broken by the octupole deformation term. This result indicates that the octupole instability is related with the super-shell

structure in reflection-asymmetric superdeformed potential.

Let us evaluate shell-structure energies for the single-particle Hamiltonian

$$h=\frac{\boldsymbol{p}^2}{2M}+\frac{1}{2}M\{\omega_0(\lambda_{3K})\}^2\{r^2(1-2\lambda_{3K}\tilde{Y}_{3K})\}'', \quad (K=0, 1, 2 \text{ or } 3) \tag{1}$$

where

$$\tilde{Y}_{3K}=\frac{1}{\sqrt{2(1+\delta_{K0})}}(Y_{3K}+Y_{3K}^*). \tag{2}$$

Here λ_{3K} are octupole deformation parameters and the double primes indicate that the quantity in parenthesis is defined in terms of the doubly-stretched coordinates $x_i''=(\omega_i/\omega_0)x_i$.[12] For frequencies ω_i along the i axis, we assume $\omega_1=\omega_2=\omega_\perp$, $\omega_3=\omega_z$ and the ratio $\omega_\perp=2\omega_z$, so that the Hamiltonian (1) reduces to the superdeformed oscillator in the limit $\lambda_{3K}\to 0$. We determine the frequency $\omega_0(\lambda_{3K})$ so that the volume conservation condition is fulfilled at each value of λ_{3K}. Thus,

$$\omega_0(\lambda_{3K})=\mathring{\omega}_0\left[\frac{1}{4\pi}\int d\Omega(1-2\lambda_{3K}\tilde{Y}_{3K}(\Omega))^{-3/2}\right]^{1/3}, \tag{3}$$

where $\mathring{\omega}_0$ is the value of ω_0 at $\lambda_{3K}=0$. The reflection asymmetric term $(r^2Y_{3K})''$ in (1) is different in radial dependence from the $(r^3Y_{3K})''$ term used by Nazarewicz et al.[7] As is well known, a merit of using the r^2 dependence is that we can simultaneously conserve the volumes inside equipotential surfaces defined by $U(r, \Omega)=v$ for different values of the constant v.[13]

Figure 1 shows shell-structure energies of the ground-state configurations for the

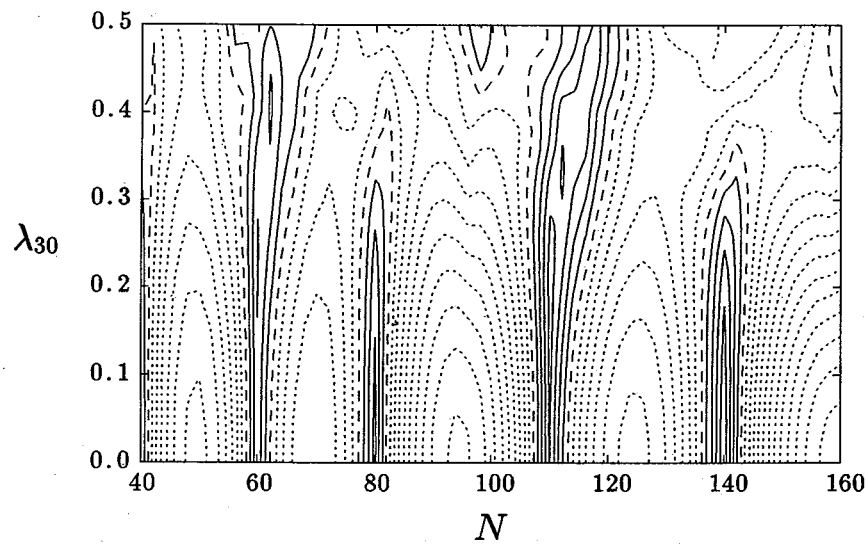

Fig. 1. Shell-structure energy $E_{\rm sh}$ for the axially-symmetric but reflection-asymmetric oscillator potential defined by (1) plotted as a function of the octupole-deformation parameter λ_{30} and the particle number N. The solid (dotted) lines are used for the area with negative (positive) values of $E_{\rm sh}$, and their distances correspond to values of $E_{\rm sh}$ differing by $0.2\hbar\omega_0$. The spin-degeneracy factor 2 is taken into account when counting the nucleon number N, which may be regarded as either proton or neutron number. The same applies for all calculations in this paper.

Hamiltonian (1) in the case $K=0$, which are calculated by the Strutinsky method.[14] The same energies are plotted in Fig. 2 as functions of the octupole-deformation parameter λ_{3K} for the closed-shell configurations. We can clearly see that the minima occurs at finite values of λ_{30} for $N=60$ and 110 which correspond to $N_{\rm sh}^{\rm F}=$even, in agreement with the suggestion by Nazarewicz et al.[7] In this figure, shell-structure energies are plotted also for the case $K\neq 0$, but we find pronounced minima only for $K=0$.

For the Hamiltonian (1), we have also calculated the quantity

$$C_{3K}=\sum_i e_i^{(2)}\delta n_i(\lambda_{3K}=0) \tag{4}$$

called "shell-energy octupole-stiffness coefficients" by Nazarewicz et al.[7)~9)] Here $\delta n_i(\lambda_{3K})$ are defined by subtracting the smoothed parts $\tilde{n}_i$ from the occupation numbers n_i as

$$\delta n_i(\lambda_{3K})=n_i(\lambda_{3K})-\tilde{n}_i(\lambda_{3K})\,, \tag{5}$$

and $e_i^{(2)}$ denote the second-order term of the single-particle energies $e_i(\lambda_{3K})$ expanded in λ_{3K} as $e_i(\lambda_{3K})=\sum_n e_i^{(n)}\lambda_{3K}^n$. The result is shown in Fig. 3. We find that this result

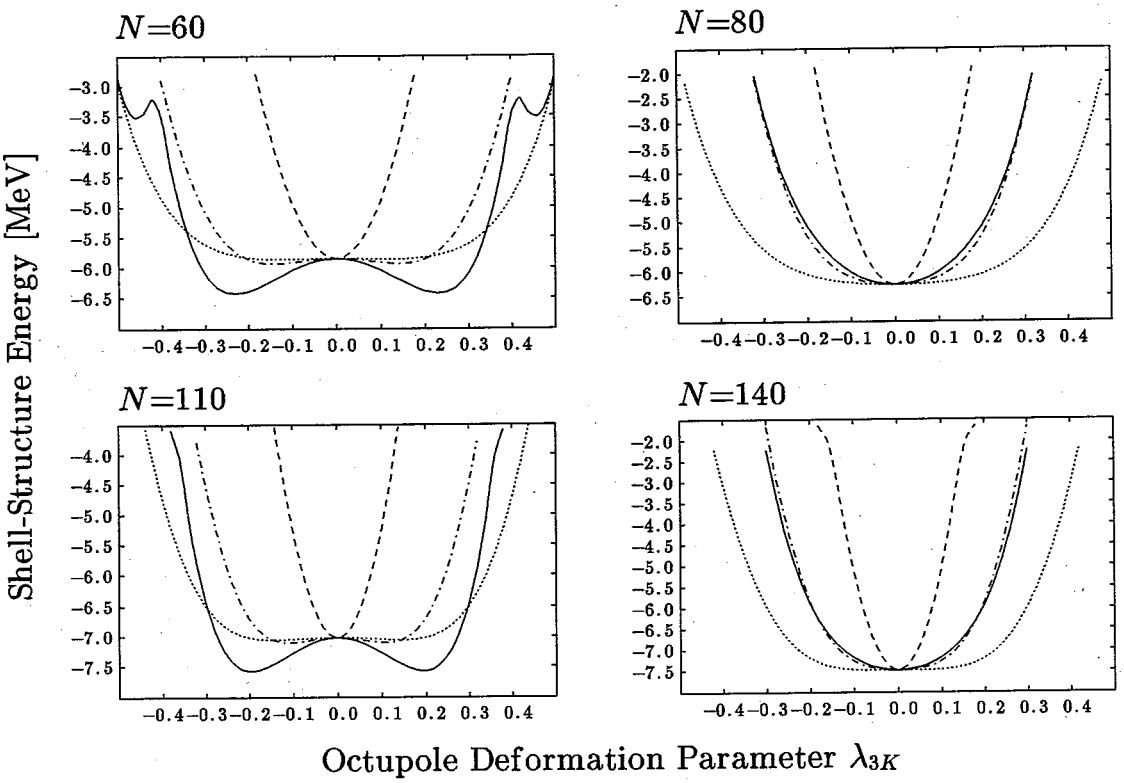

Fig. 2. Shell-structure energies of the closed-shell configurations with $N=60$, 80, 110 and 140 (which correspond to $N_{\rm sh}^{\rm F}=6$, 7, 8 and 9, respectively), plotted as functions of λ_{3K} with $K=0$ (solid lines), $K=1$ (broken lines), $K=2$ (dotted lines) and $K=3$ (dotted broken lines). The unit is MeV.

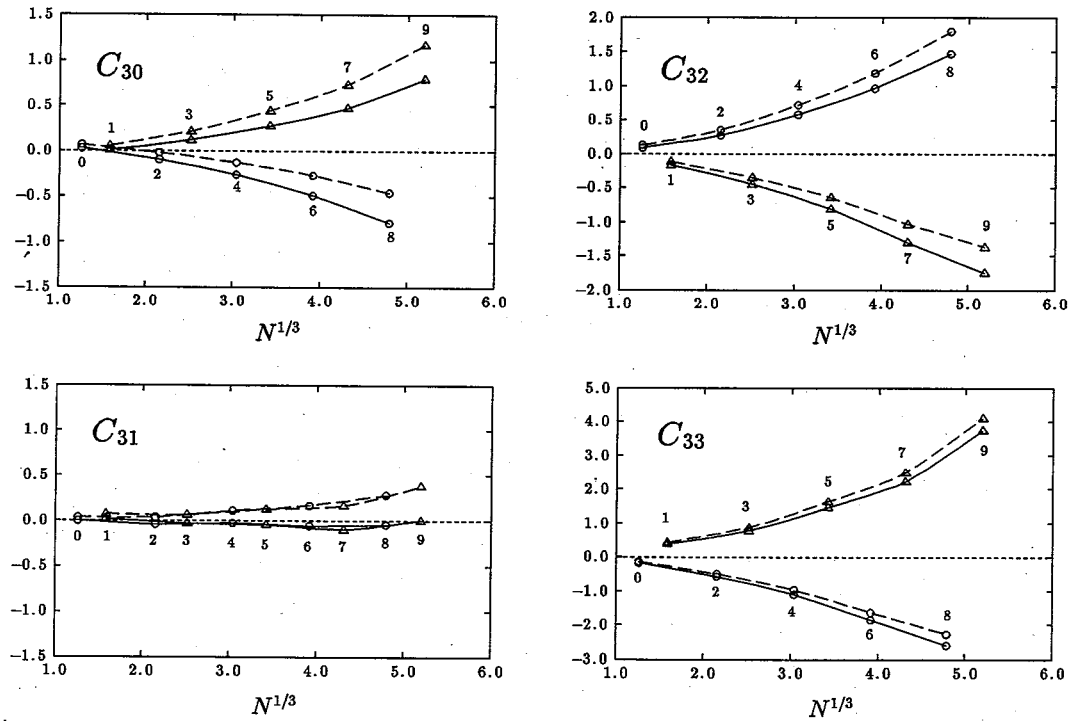

Fig. 3. Values of C_{3K} defined by (4) and calculated for the Hamiltonian (1). Open circles (triangles) indicate the values for the closed-shells with $N_{\rm sh}^{\rm F}$=even (odd). The values calculated with (without) imposing the volume-conservation condition are connected by solid (broken) lines. The unit is $\hbar\omega_0$. The integers beside these symbols denote the shell quantum numbers $N_{\rm sh}^{\rm F}$ specifying the closed-shell configurations.

(where the octupole field $(r^2 Y_{3K})''$ is used) is qualitatively the same with that of Ref. 9) for $K=0$ and 3, but is rather different for $K=1$ and 2. This indicates that the quantity C_{3K} may be sensitive to the chosen radial dependence of the octupole field.

It should be mentioned here that the C_{3K} defined above is different from the curvature $d^2E_{\rm sh}/d\lambda_{3K}^2$ of the shell energy $E_{\rm sh}$ at $\lambda_{3K}=0$, because the λ_{3K} dependence of the oscillating components of the occupation numbers, δn_i, is neglected in the definition (4). In fact, the curvatures of $E_{\rm sh}$ for various values of K estimated by Fig. 2 are considerably different from the C_{3K} values displayed in Fig. 3, so that, rigorously speaking, it is inappropriate to call C_{3K} "shell-energy octupole-stiffness coefficients".

Beside the minima at $\lambda_{30}\approx 0.25$ and 0.2 for $N=60$ and 110, respectively, mentioned above, we find in Fig. 1 other minima at $\lambda_{30}\simeq 0.4$ and 0.35 for $N=62$ and 112. These minima are associated with new magic numbers 62 and 112, which arise at larger values of λ_{30} in the single-particle spectrum for the Hamiltonian (1); see Fig. 4. Figure 5 represents, for the two cases $\lambda_{30}=0$ and 0.38, how the shell-structure energy varies with the nucleon number N. Comparing the two cases, we find an interesting fact: The minima at $N=80$ and 140 associated with the closed shells with $N_{\rm sh}^{\rm F}$=odd decline when one goes from $\lambda_{30}=0$ to 0.38. In contrast, as mentioned above, new minima emerge at $N=62$ and 112 for $\lambda_{30}=0.38$ replacing the minima at $N=60$ and 110 associated with the closed shells with $N_{\rm sh}^{\rm F}$=even for $\lambda_{30}=0$. It is worthy of note that

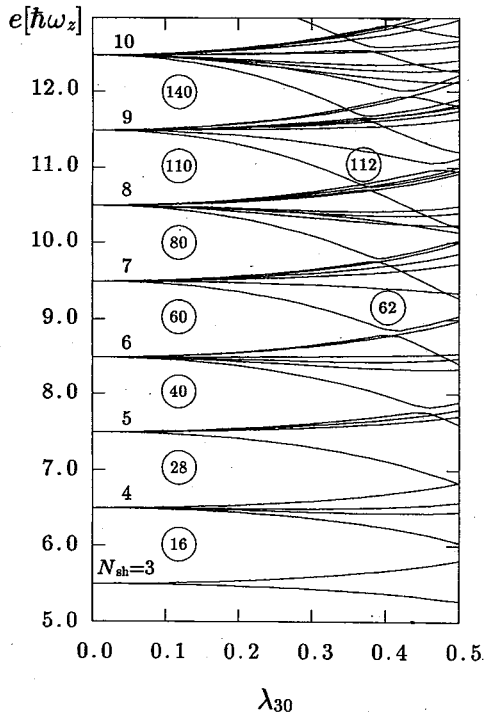

Fig. 4. Single-particle energy diagram in units of $\hbar\omega_{sh}=\hbar\omega_z$ for the potential (1) with $K=0$, plotted as a function of λ_{30}. The shell quantum numbers N_{sh} and the magic numbers of closed-shell configurations are indicated.

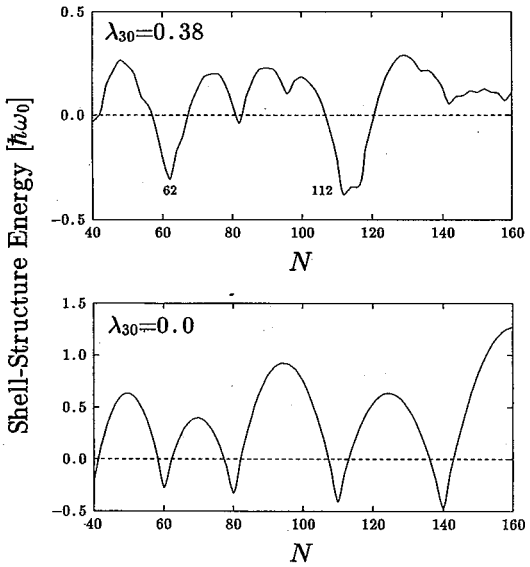

Fig. 5. Comparison between the shell-structure energies for the reflection-asymmetric case ($\lambda_{30}=0.38$) and for the reflection-symmetric case ($\lambda_{30}=0.0$). The unit is $\hbar\omega_0$.

this result for the simple Hamiltonian (1) agrees qualitatively with the result of realistic calculation by Höller and Åberg,[4] where the Nilsson potential is used.

From the shell-energy calculations presented above, we expect that the closed-shell configurations for the superdeformed oscillator potential are unstable against the doubly-stretched octupole deformation $(r^2 Y_{30})''$ when N_{sh}^F=even, whereas they are stable when N_{sh}^F=odd. This odd-even effect in N_{sh}^F may be intimately connected with the "supershell effect" (a modulation of the shell structure that arises from the interference between different periodic orbits) known in the semiclassical theory of shell structure.[10),15)~17)] In the case of the superdeformed oscillator potential, it arises from the interference between three-dimensional classical orbits with the period $2nT_0$ and the planar orbits in the (x, y) plane with the period $(2n-1)T_0$, T_0 being $2\pi/\omega_\perp$, $(n=1, 2, \cdots)$. Figure 6 shows the oscillating components of the single-particle level density calculated for the Hamiltonian (1) by using a smoothing method of Ref. 14). For $\lambda_{30}=0$, we can indeed see a beating pattern due to the interference between the oscillations with frequencies $\hbar\omega_z$ and $\hbar\omega_\perp=2\hbar\omega_z$, although it is rather weak. For the reflection-asymmetric case with $\lambda_{30}=0.38$, however, we find that the beating pattern becomes much more significant compared to the reflection-symmetric case ($\lambda_{30}=0$). Evidently, the deep minima at $N=62$ and 112 in the shell-energy diagram of Fig. 5 correspond to the pronounced minima at $e\approx 9$ and $11\hbar\omega_z$ of the oscillating level

density for $\lambda_{30}=0.38$. This result suggests that the octupole instability of the superdeformed shape is related with enhancement of the supershell effect associated with the breaking of reflection symmetry. It is an interesting open problem to clarify the origin of the supershell structure in reflection-asymmetric superdeformed potentials and to know how its effect varies with the magnitude of the octupole deformation. For this aim, we are currently investigating stabilities of the classical periodic orbits for the Hamiltonian (1),[18] and the result will be reported in future.

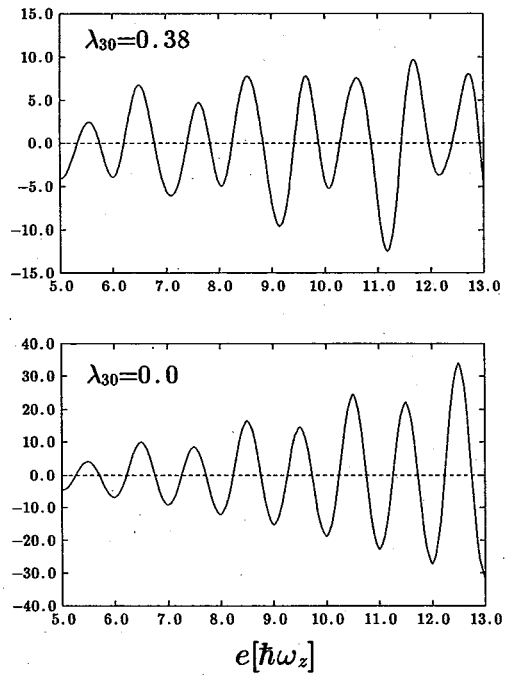

Fig. 6. Comparison between the oscillating components of the single-particle level density for the reflection-asymmetric case ($\lambda_{30}=0.38$) and for the reflection-symmetric case ($\lambda_{30}=0.0$). The smoothing width $\gamma=0.5\,\hbar\omega_{sh}$ is used.

References

1) J. Dudek, *The Variety of Nuclear Shapes*, ed. J. D. Garrett et al. (World Scientific, Singapore, 1987), p. 195.
2) S. Åberg, Nucl. Phys. **A520** (1990), 35c.
3) J. Dudek, T. R. Werner and Z. Szymanski, Phys. Lett. **B248** (1990), 235.
4) J. Höller and S. Åberg, Z. Phys. **A336** (1990), 363.
5) R. R. Chasman, Phys. Lett. **B266** (1991), 243.
6) J. Skalski, Phys. Lett. **B274** (1992), 1.
7) W. Nazarewicz and J. Dobaczewski, Phys. Rev. Lett. **68** (1992), 154.
8) W. Nazarewicz, J. Dobaczewski and P. Van Isacker, in *Proceedings of the Workshop-Symposium on Future Directions in Nuclear Physics with 4π Gamma Detection Systems of the New Generation*, Strasbourg, March 1991 (American Institute of Physics, New York, 1992), p. 30.
9) W. Nazarewicz, in *Proceedings of the International Conference on Nuclear Shapes and Nuclear Structure at Low Excitation Energies*, Cargèse, 1991 (Plenum, New York), (to be published).
10) A. Bohr and B. R. Mottelson, *Nuclear Structure* (Benjamin, New York, 1975), Vol. 2, p. 578.
11) T. Bengtsson, M. E. Faber, G. Leander, P. Möller, M. Ploszajczak, I. Ragnarsson and S. Åberg, Physica Scripta **24** (1981), 200.
12) H. Sakamoto and T. Kishimoto, Nucl. Phys. **A501** (1989), 205.
13) S. G. Nilsson, C. F. Tsang, A. Sobiczewski, Z. Szymanski, S. Wycech, C. Gustafson, I-L. Lamm, P. Möller and B. Nilsson, Nucl. Phys. **A131** (1969), 1.
14) M. Brack, J. Damgaard, A. S. Jensen, H. C. Pauli, V. M. Strutinsky and C. Y. Wong, Rev. Mod. Phys. **44** (1972), 320.
15) V. M. Strutinsky and A. G. Magner, Sov. J. Part. Nucl. **7** (1976), 138.
16) A. G. Magner, Sov. J. Nucl. Phys. **28** (1978), 759.
17) A. G. Magner, V. M. Kolomietz and V. M. Strutinsky, Sov. J. Nucl. Phys. **28** (1978), 764.
18) T. Nakatsukasa, K. Arita, K. Matsuyanagi, S. Mizutori and Y. R. Shimizu, in *Proceedings of the International Conference on Nuclear Structure at High Angular Momentum*, Ottawa, 1992, May, p. 166.

Progress of Theoretical Physics, Vol. 89, No. 4, April 1993

Effects of Octupole Vibrations on Quasiparticle Modes of Excitation in Superdeformed ^{193}Hg

Takashi NAKATSUKASA, Shoujirou MIZUTORI*
and Kenichi MATSUYANAGI

Department of Physics, Kyoto University, Kyoto 606-01
**Institute for Nuclear Study, University of Tokyo, Tanashi 188*

(Received October 16, 1992)

A particle-vibration coupling calculation based on the RPA and the cranked shell model has been carried out for superdeformed rotational bands in ^{193}Hg. The result suggests that properties of single-particle motions in superdeformed nuclei may be significantly affected by coupling effects with low-frequency octupole vibrational modes, especially by the lowest $K=2$ octupole mode.

Since the shell structure of superdeformed nuclei is drastically different from that of ordinary deformed nuclei, we expect that new kinds of nuclear surface vibrational mode emerge above the superdeformed yrast states. In fact, the RPA calculation in the uniformly rotating frame, with the use of the single-particle states obtained by the cranked Nilsson-Strutinsky-BCS procedure, has indicated that we can expect highly collective, low- frequency octupole vibrational modes (with $K=0$, 1, 2 and 3) about the superdeformed equilibrium shape.[1),2)] Importance of the octupole correlations in superdeformed high-spin states has been discussed also in Refs. 3)~13). The main reason why the octupole is more favorable than the quadrupole is that each major shell consists of about equal numbers of positive- and negative-parity single-particle levels which are approximately degenerate in energy at the superdeformed shape.

Existence of low-frequency octupole modes would imply that quasiparticle modes of motion in superdeformed nuclei might be significantly affected by the coupling effects with these vibrational modes. In this paper, we report some results of theoretical calculation which indicate the importance of such particle-vibration coupling effects to understand the properties of Landau-Zener band-crossing phenomena recently observed in ^{193}Hg.[14)]

We solve the RPA equations for the Hamiltonian

$$H=h'-\frac{1}{2}\sum_K \chi_{3K} Q''^{\dagger}_{3K} Q''_{3K}\,, \tag{1}$$

where h' is a cranked single-particle Hamiltonian of the Nilsson-plus-BCS type,

$$h'=h_{\text{Nilsson}}-\Delta\sum_i (c_i^{\dagger} c_{\bar{i}}^{\dagger}+c_{\bar{i}} c_i)-\lambda\hat{N}-\omega_{\text{rot}}\hat{J}_x\,, \tag{2}$$

and $Q''_{3K}=(r^3 Y_{3K})''$ are the doubly-stretched octupole operators.[15)] We determine the equilibrium quadrupole deformation by means of the Strutinsky method and use a large configuration space composed of 9 major shells (for both protons and neutrons) when solving the coupled RPA dispersion equations. The octupole-force strengths

χ_{3K} can be determined by the selfconsistency condition between the density distribution and the single-particle potential for the case of harmonic-oscillator potential.[15] However, the problem how to generalize this method to a more general single-particle potential like Eq. (2) is not solved. Therefore, in this paper, we put $\chi_{3K}=f\,\chi_{3K}^{\mathrm{HO}}$, where χ_{3K}^{HO} are the theoretical values[15] for the harmonic-oscillator potential, and regard f as a phenomenological parameter as well as the pairing gap Δ.

Figure 1 shows an example of the octupole strengths calculated at $\omega_{\mathrm{rot}}=0$ for the superdeformed ^{192}Hg. We see that the collectivity is highest for the $K=2$ octupole mode. Figure 2 represents how the octupole strength distribution changes at a finite value of the rotational frequency ω_{rot}. In this figure, we can clearly see the K-mixing effects due to the Coriolis force; for instance, considerable mixing among the $K=0$, 1 and 2 components is seen for the RPA eigenmode with excitation energy $\hbar\omega=1.04$ MeV.

Starting from the microscopic Hamiltonian (1) and using the standard procedure,[16] we can derive the following effective Hamiltonian describing systems composed of quasiparticle $a_\mu^\dagger$ and octupole vibrations $X_n^\dagger$,

$$\mathcal{H}=\sum_\mu E_\mu a_\mu^\dagger a_\mu+\sum_n \hbar\omega_n X_n^\dagger X_n+\sum_n\sum_{\mu\nu} f_n(\mu\nu)(X_n^\dagger+\tilde{X}_n)a_\mu^\dagger a_\nu \tag{3}$$

and we diagonalize it within the subspace $\{a_\mu^\dagger|0\rangle,\ a_\nu^\dagger X_n^\dagger|0\rangle\}$. The resulting state vectors can be written as

$$|\phi\rangle=\sum_\mu C_0(\mu)a_\mu^\dagger|0\rangle+\sum_n\sum_\nu C_1(\nu n)a_\nu^\dagger X_n^\dagger|0\rangle\,. \tag{4}$$

Recently, experimental data suggesting octupole correlations in superdeformed states have been reported by Cullen et al.[14] for ^{193}Hg. Figure 3 shows a result of

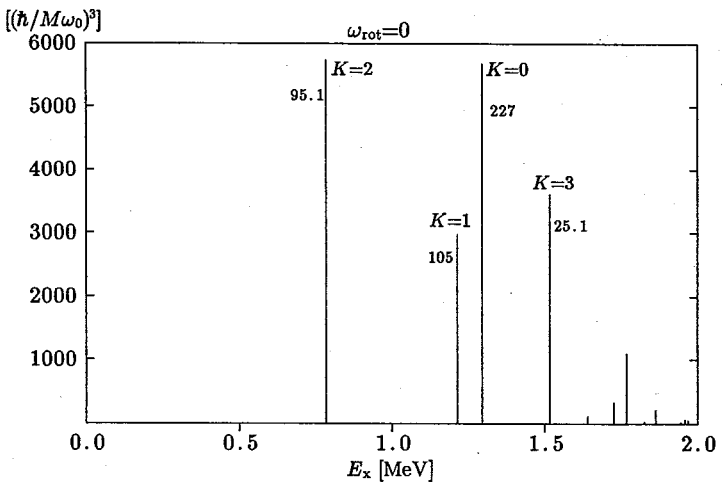

Fig. 1. Octupole strengths $|\langle n|(r^3Y_{3K})^{\nu}|0\rangle|^2$ calculated for the superdeformed states of ^{192}Hg at $\omega_{\mathrm{rot}}=0$. Note that positive- and negative-signature states are completely degenerate at $\omega_{\mathrm{rot}}=0$ (for peaks with $K=1$, 2 and 3). The deformation parameter $\delta_{\mathrm{osc}}=0.43$, the neutron gap $\Delta_n=0.7$ MeV, the proton gap $\Delta_p=0.7$ MeV and the doubly-stretched octupole interaction strengths $\chi_{3K}=1.08\,\chi_{3K}^{\mathrm{HO}}$, χ_{3K}^{HO} being the selfconsistent values for the harmonic-oscillator potential, are used. The numbers written beside the main peaks indicate the strengths for the $E3$ operators measured in Weisskopf units.

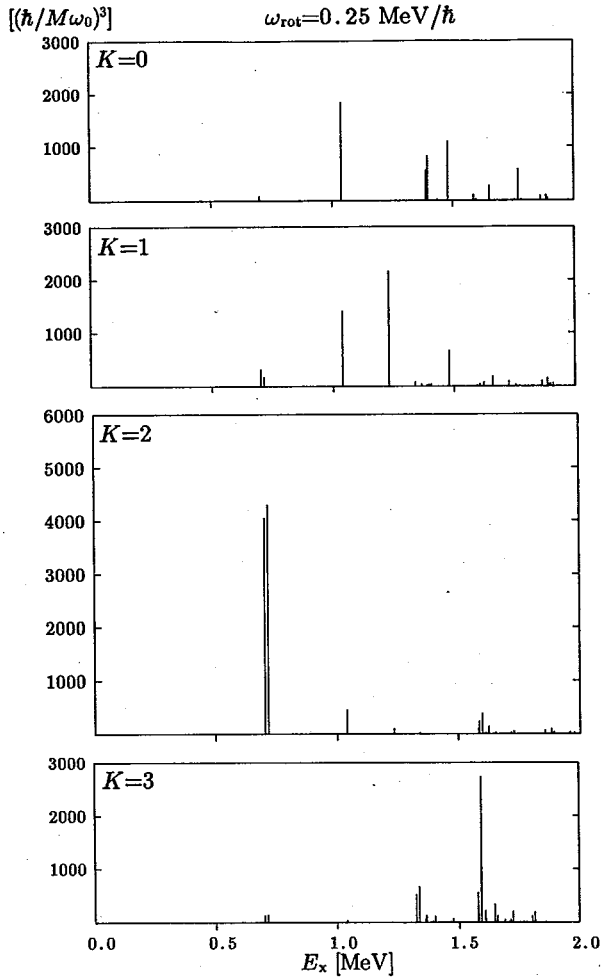

Fig. 2. The same as Fig. 1 but for $\omega_{rot}=0.25$ MeV/$\hbar$. Note that, for example, the RPA eigenstate at $E_x=1.04$ MeV has significant strengths for three components with $K=0$, 1 and 2.

calculation for excitation spectra in the rotating frame of this nucleus. By comparing the conventional quasiparticle energy diagram (Fig. 3(a)) with the result of diagonalization of $\mathcal{H}$ (Fig. 3(b)), we can clearly identify effects of the octupole vibrations: Energy shifts $\Delta e'_{vib}$ of 50~300 keV due to the coupling effects are seen. In particular, we note that the Landau-Zener crossing frequency ω_{cross} between band 1 (whose main component is the [512]5/2 quasiparticle state) and band 4 (associated with the [761]3/2 quasiparticle) is considerably delayed. Namely, we obtain $\omega_{cross}\approx 0.26$ MeV/$\hbar$ in agreement with the experimental value[14] $\omega_{cross}^{exp}\approx 0.27$ MeV/$\hbar$, whereas $\omega_{cross}\approx 0.17$ MeV/$\hbar$ if the octupole-vibrational effects are neglected. The reason for this delay is understood by examining the properties of the quasiparticle-vibration couplings in ^{193}Hg, which will be done below.

The amplitudes $C_0(\mu)$, $C_1(\nu n)$ obtained by diagonalizing the effective Hamiltonian $\mathcal{H}$ are displayed in Fig. 4 as functions of the rotational frequency ω_{rot}. Note that the K-quantum numbers used in this figure to label these amplitudes are valid only in the limit $\omega_{rot}\to 0$, because the K-mixing effects due to the Coriolis force

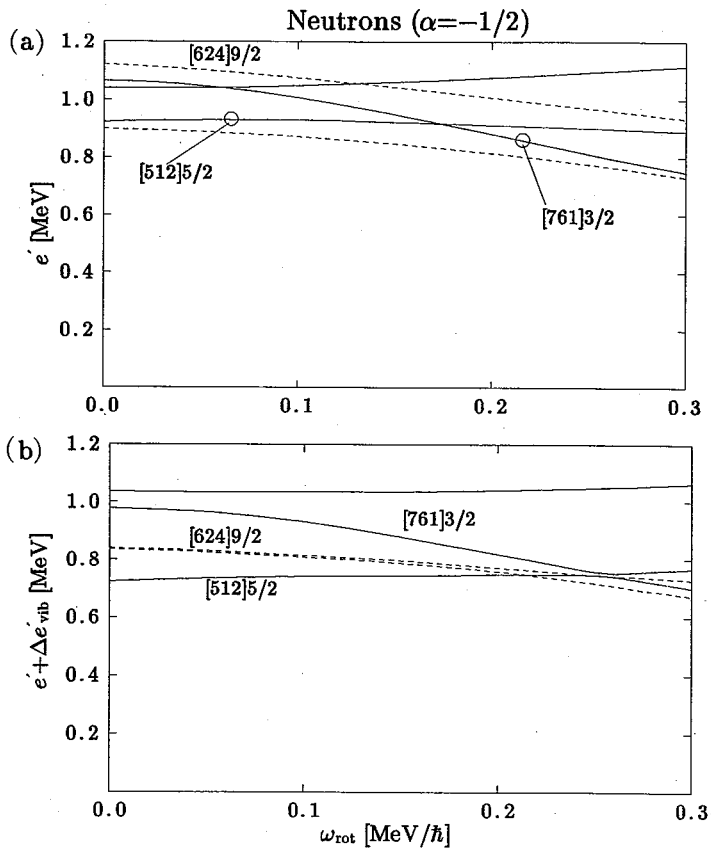

Fig. 3. (a) Quasiparticle energy diagram for neutrons with signature $\alpha=-1/2$ in ^{193}Hg, plotted as a function of $\omega_{\rm rot}$. (b) The same as (a) but the energy shifts $\Delta e'_{\rm vib}$ due to the coupling effects with the octupole vibrations are included. Parameters used in the calculation are the same as in Figs. 1 and 2. Notations like [512]5/2 indicate the main components of the wave functions.

are taken into account. It is seen that the main components of bands 1 and 4 are exchanged with each other at $\omega_{\rm rot}\approx 0.26$ MeV/$\hbar$ indicating the Landau-Zener crossing phenomena between the [512]5/2 and the [761]3/2 quasiparticle states. In this figure, we also see that the mixing of the states composed of the [624]9/2 quasiparticle and the $K=2$ octupole vibration is significant in band 1. Note that there are two such states; $|[624]9/2(\alpha=-1/2)\otimes\omega^{(+)}_{K=2}\rangle$ and $|[624]9/2[\alpha=1/2)\otimes\omega^{(-)}_{K=2}\rangle$ where α denotes the signature quantum number and $\omega^{(+)}_{K=2}$ and $\omega^{(-)}_{K=2}$ the octupole vibrations with positive and negative signatures, respectively, which reduce to the $K=2$ octupole vibration shown in Fig. 1 in the limit $\omega_{\rm rot}=0$.

It is worth emphasizing that the $K=2$ octupole matrix element between the [512]5/2 and the [624]9/2 Nilsson states is especially large since it satisfies one of the asymptotic selection rules ($\Delta N_{\rm sh}=1$, $\Delta n_3=1$, $\Delta\Lambda=2$) for the transitions associated with the $K=2$ octupole operator. ($N_{\rm sh}$ denotes the shell quantum number, defined by $N_{\rm sh}=2(n_1+n_2)+n_3$.[2]) Thus, these two Nilsson states are strongly coupled with each other due to the $K=2$ octupole correlation. This property is seen also in the single-neutron energy diagram plotted as a function of the $K=2$ octupole deformation

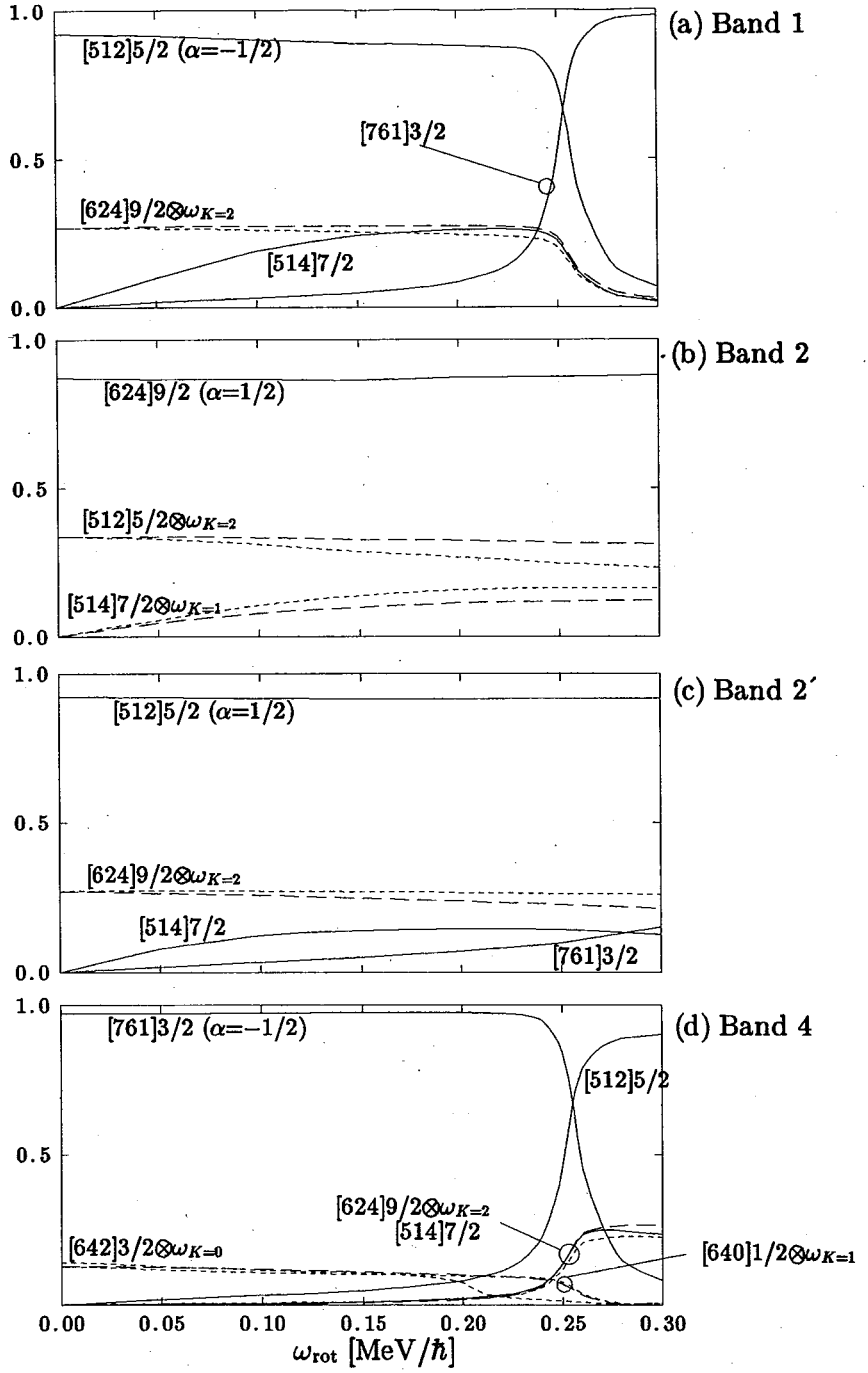

Fig. 4. Amplitudes $|C_0(\mu)|$ and $|C_1(\nu n)|$ in the wave function defined by Eq. (4), plotted as functions of $\omega_{\rm rot}$. The full lines are used for the one-quasiparticle amplitudes, while the broken (dotted) lines for the amplitudes involving the octupole vibrations with positive (negative) signature. (a), (b), (c) and (d) respectively show the results of calculation for bands 1, 2, 2′ and 4. The main component of band 2 is the [624]9/2(α=1/2) quasiparticle state. The observed band 2 was suggested in Ref. 14) that it could actually be two bands with identical γ-ray energies consisting of the [624]9/2(α=1/2) band and the [512]5/2(α=1/2) band. The latter band, which is the signature partner of band 1, is denoted here by band 2′. The parameters used in the calculation are the same as in Fig. 1.

parameter β_{32} in the paper by Skalski.[10] As a result of this property, we obtain a significant energy shift $\Delta e'_{\rm vib}$ for band 1. On the other hand, the octupole vibrational effect is rather weak for band 4. Thus, as shown in Fig. 3, the relative excitation energy between bands 1 and 4 increases, so that their crossing frequency also increases.

Next, let us discuss the alignment i of band 4 and the interaction matrix element $V_{\rm int}$ between bands 1 and 4, for which experimental data are available; $i^{\rm exp}_{\rm band4}\approx 1.3\,\hbar$ and $V^{\rm exp}_{\rm int}\approx 26$ keV.[14] We evaluate the alignment by $i=-\partial E'/\partial\omega_{\rm rot}$ using the eigenvalue E' of the effective Hamiltonian (3) and choosing the region of $\omega_{\rm rot}$ where E' linearly depends on $\omega_{\rm rot}$. The interaction $V_{\rm int}$ is evaluated, as usual, from the half of the shortest distance between the energy levels for bands 1 and 4 in the energy diagram like Fig. 3(b). The calculated value of the alignment for the [761]3/2 quasiparticle state (the main component of band 4) is $i^{\rm cal}\approx 1.8\,\hbar$. This value is reduced to $i^{\rm cal}\approx 1.2\,\hbar$ in good agreement with experiment, when the octupole-vibrational effects are taken into account. On the other hand, the interaction matrix element between the [761]3/2 quasiparticle state and the [512]5/2 quasiparticle (the main component of band 1) is almost zero and increases to about 5 keV due to the octupole-vibrational effects. This calculated value of $V_{\rm int}$ is, however, too small in comparison with the experimental data.

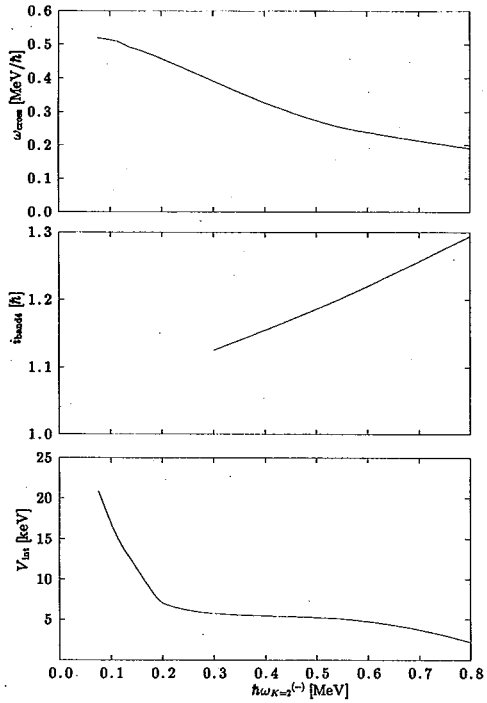

Fig. 5. Dependence of crossing frequency $\omega_{\rm cross}$ between bands 1 and 4, the aligned angular momentum of band 4 $i_{\rm band4}$, and the interaction matrix element $V_{\rm int}$ between bands 1 and 4, on the excitation energy $\hbar\omega^{(-)}_{K=2}$ of the lowest $K=2$ octupole vibration (with negative signature) calculated at $\omega_{\rm rot}=0.45$ MeV. The pairing gaps used are the same as in Fig. 1. The excitation energy $\hbar\omega^{(-)}_{K=2}=0.54$ MeV corresponds to the force-strengths $\chi_{3K}=1.08\,\chi^{\rm HO}_{3K}$.

Since we treat the doubly-stretched octupole force-strengths χ_{3K} as phenomenological parameters in this paper, it is necessary to examine the dependence on the force-strengths χ_{3K}, of the theoretical values for the crossing frequency $\omega_{\rm cross}$, the alignment $i_{\rm band4}$ and the interaction matrix element $V_{\rm int}$. This is done in Fig. 5. In this figure, the calculated values of $\omega_{\rm cross}$, $i_{\rm band4}$ and $V_{\rm int}$ are plotted as functions of the excitation energy $\hbar\omega^{(-)}_{K=2}$ of the lowest $K=2$ octupole vibration calculated at $\omega_{\rm rot}=0.45\,{\rm MeV}/\hbar$, instead of plotting directly as functions of χ_{3K}. We note that $\hbar\omega^{(-)}_{K=2}$ is a function of χ_{3K} and the force-strengths $\chi_{3K}=1.08\chi^{\rm HO}_{3K}$ adopted in the calculations of Figs. 1~4 correspond to the abscissa at $\hbar\omega^{(-)}_{K=2}\approx 0.5$ MeV in Fig. 5. It is seen from this figure that $\omega_{\rm cross}$ increases while $i_{\rm band4}$ decreases when $\hbar\omega^{(-)}_{K=2}$ decreases (i.e., when the octupole-vibrational effects become stronger), and we find that the experimental data for $\omega_{\rm cross}$ and $i_{\rm band4}$ are simultaneously reproduced at $\hbar\omega^{(-)}_{K=2}\approx 0.5$ MeV. On the other

hand, the calculated interaction matrix element $V_{\rm int}$ is too small within a reasonable range of $\hbar\omega^{(-)}_{K=2}$.

The main reason why the calculated value of $V_{\rm int}$ is small may be understood as follows: Generally speaking, we can expect that the band-band interactions increase due to the octupole-vibrational effects, because interactions between different quasiparticle states through intermediate configurations composed of one-quasiparticle and octupole vibrations become possible. However, in the specific case of band 4, as seen in Fig. 4, the octupole vibrational effects are rather weak because the octupole matrix element between the [761]3/2 Nilsson state and the neighboring Nilsson states are small. On the other hand, the octupole-vibrational effects are indeed strong in band 1 so that the considerable mixing of the states $|[624]9/2\ (\alpha=\mp 1/2)\otimes\omega^{(\pm)}_{K=2}\rangle$ occurs. This mixing does not, however, lead to a large interaction $V_{\rm int}$ between bands 1 and 4, because the octupole matrix element between the [624]9/2 and the [761]3/2 quasiparticle states remains small although the Coriolis K-mixing effects are taken into account in our calculation at finite rotational frequency.

The interaction $V_{\rm int}$ under consideration depends also on the pairing-gap parameter Δ as well as the force-strengths χ_{3K}. We have adopted $\Delta=0.7$ MeV in Fig. 5 (cf. we obtain $\Delta_p=0.72$ MeV and $\Delta_n=0.77$ MeV when the pairing gap is evaluated at $\omega_{\rm rot}=0$ by means of the conventional procedure of the Strutinsky method[17] with the pairing-force strengths G that gives the standard value of the smoothed pairing-gap parameter $\tilde{\Delta}=12.0\,A^{-1/2}$ MeV). The result of calculation using $\Delta=0.9$ MeV was reported in Ref. 18). In this case, we obtain $V_{\rm int}\approx 10$ keV keeping the agreement of $\omega_{\rm cross}$ and $i_{\rm band4}$ with experiment. This value of $V_{\rm int}$ is still too small compared with the experimental value $V_{\rm int}\approx 26$ keV. Thus, we conclude that the large value of $V_{\rm int}$ cannot be reproduced within the present framework of calculation by merely changing the pairing-gap parameter Δ within a reasonable range.

It is well known in the case of the crossing between the ground-band and the s-band that the interaction matrix element is an oscillating function of the degree of shell filling.[19),20)] Accordingly, its magnitude is quite sensitive to the single-particle level structure (used in the calculation) around the chemical potential. It is also known that the interaction matrix elements in the cranking model are considerably smaller than those evaluated by the particle-rotor model, mainly due to the absence of the contribution of the recoil term.[20)] It is not clear to us whether or not the above experience in the g-s crossing phenomena is applicable to the Landau-Zener crossing under consideration.

In summary, we have investigated the coupling effects between the quasiparticle and the octupole-vibrational modes of excitation in the superdeformed ^{193}Hg, by means of the particle-vibration coupling theory based on the cranking model. We have found that the inclusion of the octupole vibrational effects is important to reproduce the experimental data for the crossing frequency between bands 1 and 4, and for the aligned angular momentum of band 4. On the other hand, the calculated interaction matrix element between bands 1 and 4 is too small in comparison with the experimental data. To understand the spectrum of the superdeformed ^{193}Hg, there are several problems remaining for the future, e.g., improvement of the treatment of the pairing correlations, inclusion of the quadrupole-pairing, evaluation of the $E1$

transition probabilities, possibilities of other interpretation of the experimental data,[21] etc.

The computer calculation for this work has been financially supported in part by Research Center for Nuclear Physics, Osaka University and by Institute for Nuclear Study, University of Tokyo.

References

1) S. Mizutori, Y. R. Shimizu and K. Matsuyanagi, Prog. Theor. Phys. **83** (1990), 666; **85** (1991), 559; **86** (1991), 131; in *Proceedings of the Workshop-Symposium on Future Directions in Nuclear Physics with 4π Gamma Detection Systems of the New Generation, Strasbourg, March 1991* (American Institute of Physics, New York), p. 287.
2) T. Nakatsukasa, S. Mizutori and K. Matsuyanagi, Prog. Theor. Phys. **87** (1992), 607.
3) J. Dudek, T. R. Werner and Z. Szymanski, Phys. Lett. **B248** (1990), 235.
4) S. Åberg, Nucl. Phys. **A520** (1990), 35c.
5) J. Höller and Åberg, Z. Phys. **A336** (1990), 363.
6) R. R. Chasman, Phys. Lett. **B266** (1991), 243.
7) P. Bonche, S. J. Krieger, M. S. Weiss, J. Dobaczewski, H. Flocard and P.-H. Heenen, Phys. Rev. Lett. **66** (1991), 876.
8) Xunjun Li, J. Dudek and P. Romain, Phys. Lett. **B271** (1991), 281.
9) W. Nazarewicz and J. Dobaczewski, Phys. Rev. Lett. **68** (1992), 154.
10) J. Skalski, Phys. Lett. **B274** (1992), 1.
11) P. Piepenbring, Nucl. Phys. **A541** (1992), 148.
12) R. Nazmitdinov and S. Åberg, Phys. Lett. **B289** (1992), 238.
13) J. Skalski, P. -H. Heenen, P. Bonche, H. Flocard and J. Meyer, Preprint PNT/4192.
14) D. M. Cullen et al., Phys. Rev. Lett. **65** (1990), 1547.
15) H. Sakamoto and T. Kishimoto, Nucl. Phys. **A501** (1989), 205.
16) L. S. Kisslinger and R. A. Sorensen, Rev. Mod. Phys. **35** (1963), 853.
17) M. Brack, J. Damgaard, A. S. Jensen, H. C. Pauli, V. M. Strutinsky and C. Y. Wong, Rev. Mod. Phys. **44** (1972), 320.
18) T. Nakatsukasa, K. Arita, K. Matsuyanagi, S. Mizutori and Y. R. Shimizu, in *Proceedings of the International Conference on Nuclear Structure at High Angular Momentum, Ottawa, May 1992* (AECL-10613, Volume 2), p. 166.
19) I. Hamamoto, in *Nuclear Structure 1985,* ed. R. Broglia, G. B. Hagemann and B. Herskind (North-Holland, 1985), p. 129.
20) J. Almberger, I. Hamamoto and G. Leander, Phys. Lett. **B80** (1979), 153.
21) P. B. Semmes, I. Ragnarsson and S. Åberg, Phys. Rev. Lett. **68** (1992), 460.

ELSEVIER

Nuclear Physics A573 (1994) 333–355

NUCLEAR PHYSICS A

Low-energy M1 and E3 excitations in the proton-rich Kr–Zr region

T. Nakatsukasa [a], K. Matsuyanagi [a], I. Hamamoto [b,1], W. Nazarewicz [b,c,d,2]

[a] *Department of Physics, Kyoto University, Kyoto 606-01, Japan*
[b] *Joint Institute for Heavy-Ion Research, Oak Ridge National Laboratory, P.O. Box 2008, Oak Ridge, TN37831, USA*
[c] *Department of Physics, University of Tennessee, Knoxville, TN 37996, USA*
[d] *Physics Division, Oak Ridge National Laboratory, P.O. Box 2008, Oak Ridge, TN37831, USA*

Received 9 August 1993; revised 4 November 1993

Abstract

Low-energy intrinsic $K^\pi = 1^+$, 0^-, 1^-, 2^-, and 3^- states in the even–even proton-rich Sr, Kr, and Zr nuclei are investigated using the quasiparticle random-phase approximation. In the $Z \simeq N$ nuclei the lowest-lying 1^+ states are found to carry unusually large B(M1) strength. It is demonstrated that, unlike in the heavier nuclei, the octupole collectivity in the light zirconium region is small and, thus, is not directly correlated with the systematics of the lowest negative-parity states.

Key words: NUCLEAR STRUCTURE ^{76,78,80,82}Sr, ^{72,74,76,78,80}Kr, ^{80,82}Zr; calculated levels, $B(\lambda)$. Quasiparticle RPA.

1. Introduction

It has been shown experimentally [1–3] that shape coexistence, large deformations, the presence of well-deformed intruder orbitals, quenching of pairing correlations, low-lying octupole states, and dramatic shape changes induced by rotation are quite common phenomena in the zirconium region ($Z \simeq N \simeq 40$). The microscopic reason for such a strong variation of collective properties is the low

[1] On leave of absence from Department of Mathematic Physics, Lund Institute of Technology, Box 118, S-22100 Lund, Sweden.
[2] On leave of absence from Institute of Theoretical Physics, Warsaw University, ul. Hoza 69, P1-00689 Warsaw, Poland; Institute of Physics, Warsaw University of Technology, Warsaw, Poland.

SSDI 0375-9474(93)E0689-6

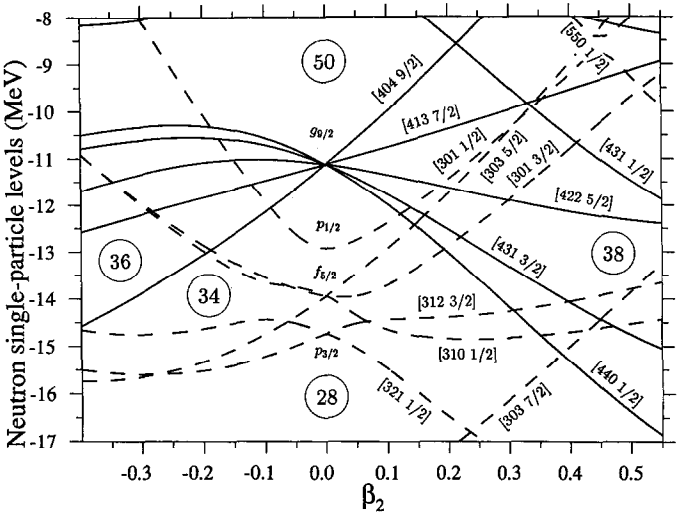

Fig. 1. Neutron single-particle levels in ^{78}Kr as functions of the quadrupole deformation β_2 ($\beta_4 = 0$). The Nilsson states are labelled by means of the asymptotic quantum numbers, $[Nn_z\Lambda\Omega]$.

single-particle level density in these medium-mass nuclei. Because of spectacular shape effects, relatively small size, and high collectivity, the nuclei from the $A \sim 80$ mass region have become favorite testing grounds for various theoretical approaches. Calculations based on the mean-field approach applied to nuclei in the light-Zr region suggest an interpretation of experimental data in terms of well-deformed prolate shapes, weakly-deformed oblate shapes, and spherical (shell-model) configurations [4–6].

There exist a number of mean-field calculations for the light-Zr region (for references, see review [3]). In most cases calculations give similar equilibrium deformations, but they differ in their predictions for excitation energies of shape-coexisting states. Best examples of the ground-state shape isomerism in nuclei in the light-Zr region are the Ge–Kr isotopes with $A \sim 70$. Calculations suggest the interpretation in terms of two competing configurations: one at an oblate shape, and the other at a prolate shape. Oblate ground states are predicted for Ge- and Se-isotopes and for most Kr-isotopes. For light Sr-isotopes the prolate configuration lies lower in energy. Because of the mutual interaction (of the order of a few hundred keV [1]) the prolate and oblate bands are strongly disturbed in the low-spin region.

The single-particle diagram representative of the discussed nuclei is shown in Fig. 1. In the $A \sim 80$ region both protons and neutrons lie in the same ($p_{1/2}$, $p_{3/2}$, $f_{5/2}$, $g_{9/2}$) shell. For $T_z \sim 0$ systems, the proton and neutron shell corrections add coherently and, consequently, dramatic shape effects are expected. A beautiful experimental signature of large prolate deformations in the $A \sim 80$ region, attributed to the large single-particle gaps at Z, $N = 38$ and 40, was observation of very collective rotational bands in neutron-deficient Sr and Zr isotopes [7–9].

The investigation of the medium-mass $N = Z$ nuclei has been the proprietary niche of groups who made investigations using the Daresbury Recoil Separator. Pioneering works from Daresbury include the spectroscopy of ^{64}Ge, ^{68}Se, ^{72}Kr, ^{76}Sr, ^{80}Zr, and ^{84}Mo (see ref. [10]). These studies confirmed earlier theoretical predictions of shape transition from strongly oblate shapes in ^{68}Se and ^{72}Kr to strongly prolate shapes in ^{76}Sr, and ^{80}Zr (actually, ^{76}Sr and ^{80}Zr are, according to calculations, very deformed, with the ground-state deformation around $\beta_2 = 0.4$). The nucleus ^{84}Mo is the heaviest $Z = N$ system known so far.

Spectroscopy in the light-Zr region will certainly become one of the main arenas of investigations around the proton drip line. The physics of exotic nuclei with $T_z \lesssim 0$ is one of the fastest developing subjects in nuclear physics, thanks to exotic (radioactive) ion beam (RIB) facilities currently under construction in Europe, USA, and Japan. In particular, the combination of RIB and the new-generation multidetector arrays should open up many new avenues of exploration [11].

The main motivation of this paper is to make predictions for low-energy collective M1 and E3 excitations around ^{76}Sr. Since the M1 collectivity of low-lying 1^+ states increases with deformation (though the energies of those states may increase), it is anticipated that in some well-deformed nuclei in the $A \sim 80$ mass region the strong magnetic dipole strength should lie low in energy. The existence of collective octupole states in this region is a long-standing question. The low-lying negative-parity states, often interpreted as octupole vibrations, can be of a single-particle character [12]. To shed some light on both issues we performed calculations based on the quasiparticle random phase approximation (QRPA). We hope, that those predictions will stimulate experimental investigations of medium-mass nuclei around the $N = Z$ line.

2. Deformations and pairing correlations in the $A \sim 80$ mass region

Calculations of equilibrium deformations of $A \sim 80$ isotopes were previously performed [4] within the Woods–Saxon–Strutinsky model [13]. In this work, new calculations have been carried out using the same single-particle model but the Yukawa-plus-exponential mass formula of ref. [14]. The particle–particle interaction was approximated by the state-independent monopole-pairing hamiltonian. The pairing energy was computed using the approximate particle-number projection in the Lipkin–Nogami version. The pairing strengths and the average pairing energy were taken according to ref. [15]. The calculated equilibrium deformations for selected Kr, Sr, and Zr isotopes are shown in Table 1. It is seen that the deformed → spherical shape transition is expected to occur around $N \sim 44$. Worth noting are very large equilibrium β_2 deformations (~ 0.4) of the lightest Kr, Sr, and Zr isotopes.

In several nuclei around ^{82}Sr highly-deformed and superdeformed bands ($\beta_2 > 0.4$) have been predicted to become yrast at high spin [4,5,16,17]. For example, in ^{82}Sr well-deformed nearly-prolate bands involving $h_{11/2}$ neutrons are expected to become yrast at $I > 32\hbar$. Experimentally, a weak ridge–valley structure with a

Table 1
Calculated equilibrium shape deformations β_2 and β_4, and proton and neutron pairing gaps, Δ_p and Δ_n (in MeV), at selected oblate and prolate configurations of Kr, Sr and Zr isotopes. According to calculations, the oblate $I=0$ minima lie lower in energy than the prolate $I=0$ minima in ^{72,74,78}Kr, ^{82}Sr, and ^{82}Zr. For ^{82}Sr the calculations were also performed at superdeformed configuration with $\beta_2 = 0.45$.

Nucleus		Oblate				Prolate			
Z	N	β_2	β_4	Δ_p	Δ_n	β_2	β_4	Δ_p	Δ_n
36	36	−0.31	−0.010	1.34	1.23	0.35	0.016	1.40	1.31
	38	−0.30	−0.016	1.26	1.46	0.37	0.0	1.31	1.12
	40	−0.25	−0.036	1.32	1.54	0.36	−0.016	1.24	1.25
	42	−0.24	−0.050	1.28	1.48	0.32	−0.023	1.18	1.46
	44	−0.23	−0.050	1.24	1.46				
38	38					0.39	−0.016	1.14	0.99
	40					0.39	−0.029	1.01	1.04
	42					0.37	−0.030	0.93	1.34
	44	−0.22	−0.065	1.35	1.37	0.28	−0.020	1.15	1.48
	44					0.45	0.0	0.83	1.45
40	40					0.40	−0.037	1.06	0.88
	42	−0.22	−0.078	1.39	1.31	0.39	−0.038	0.96	1.26

width of $\Delta E_\gamma \approx 150$ keV has been seen in the E_γ–E_γ correlation map [18]. This ridge corresponds to $\beta_2 \sim 0.5$ for a deformed rigid motor. However, no discrete band that could be associated with this ridge–valley was identified so far. Theoretically, the superdeformed band in ^{82}Sr is expected [4] to have deformation $\beta_2 \sim 0.45$, see Table 1.

The most important interaction, beyond the single-particle deformed mean field, is the short-ranged pairing interaction. This force is often approximated by means of a state-independent monopole pairing interaction. The general feature of the pairing interaction is that the pair correlation energy is anticorrelated with the shell correction. A smaller pairing gap results from a smaller density of single-particle levels around the Fermi level, which are available for pair correlation. For deformed $A \sim 80$ nuclei the weakest pairing is expected around the deformed gaps at N (or Z) = 38–42 [5]. A further reduction of pairing can occur in excited configurations, due to blocking.

In the $A \sim 80$ mass region are several good examples of very regular, rigid rotational bands. Among them there are negative-parity bands in ^{76}Kr and ^{78}Kr built upon the first $I^\pi = 3^-$ state at 2258 keV and 2399 keV, respectively. These bands are among the best *normally-deformed* rotors, with remarkably large and nearly constant moments of inertia, $\mathcal{J}^{(1)} \approx \mathcal{J}^{(2)}$ [19,20]. Theoretically, those bands are associated with two-quasiparticle excitations built upon the proton $[431\ \frac{3}{2}] \times [312\ \frac{3}{2}]$ Nilsson orbitals which happen to occur just below the strongly deformed subshell closure at $Z = 38$. (The proton character of those bands was recently confirmed by the g-factor measurement [21].) Another good example is the $[312\ \frac{3}{2}]$ band in ^{77}Rb [22] or the $[422\ \frac{5}{2}]$ band in ^{81}Y [23] having unusually large moments of

inertia. In all those cases the BCS calculations [5] suggest the dramatic reduction (or collapse) of the static pairing.

Weak pairing has important consequences for the low-energy electromagnetic transitions. Since the B(M1) values involving the ground state of even–even nuclei are proportional to the BCS factor $(u_\mu v_\nu - v_\mu u_\nu)^2$, weaker pair correlations enhance the low-lying M1 strength. For electric transitions, the related BCS factor is $(u_\mu v_\nu + v_\mu u_\nu)^2$. On the average, pairing correlations enhance the collectivity of the low-lying E3 transitions from/to the ground state in the Sr–Zr region (see sect. 4).

3. Magnetic dipole states

The deformation dependence of 1^+ states is a current subject of both experimental [24,25] and theoretical [26–29] studies. The low-energy B(M1) strength (defined as the summed strength over a given energy interval, e.g., 2–4 MeV in the rare-earth nuclei) increases with quadrupole deformation as, roughly, β_2^2. Recently, it was demonstrated in ref. [29] that the sum of B(M1) values in the region of $E_x < 10$ MeV at heavy superdeformed nuclei around ^{152}Dy and ^{192}Hg was several times larger than that at normal deformations. The reason for this enhancement is twofold. Firstly, the proton convection current contribution to B(M1) increases with deformation and at strongly deformed shapes becomes comparable to the spin-flip contribution in the low-energy region. Secondly, as discussed in sect. 2, the B(M1) strength increases if the pair correlations are weak, i.e., exactly what is expected at SD shapes [30].

Since some of the $A \sim 80$ nuclei are very well deformed in their ground states, their equilibrium deformations exhibit rapid isotopic and isotonic variations, and their pairing correlations are predicted to be weak due to deformed subshell closures (Table 1). Because the Kr, Sr, and Zr isotopes have these characteristics, they are ideally suited for investigations of the low-energy M1 strength and its deformation dependence. (The lighter and heavier systems, such as Ge, Se, and Mo, are less deformed and γ-soft.)

The properties of the $K^\pi = 1^+$ states have been investigated using the QRPA hamiltonian

$$H_{\mathrm{QRPA}} = h_{\mathrm{s.p.}} + V_{\mathrm{pair}} + V_{\mathrm{FF}} + V_{\sigma\sigma}, \tag{1}$$

where the single-particle hamiltonian,

$$h_{\mathrm{s.p.}} = \sum_i (\epsilon_i - \lambda) c_i^\dagger c_i \tag{2}$$

is an axially deformed Woods–Saxon hamiltonian of ref. [31] (see ref. [32] for parameters),

$$V_{\mathrm{pair}} = -\Delta \sum_i \left(c_i^\dagger c_{\bar{i}}^\dagger + c_{\bar{i}} c_i \right) \tag{3}$$

is the monopole-pairing field, $V_{\rm FF}$ is a long-ranged residual interaction (mainly of quadrupole–quadrupole type), and $V_{\sigma\sigma}$ is the spin–spin residual interaction. In Eq. (1)

$$V_{\rm FF} = -\tfrac{1}{2}\sum_{T=0,1} \kappa_T F_T^+ F_T, \tag{4}$$

where the isoscalar and isovector fields F are given by

$$F_{T=0} = F_n + F_p, \qquad F_{T=1} = F_{\rm n} - \xi F_{\rm p} \tag{5}$$

and

$$F_\tau = \frac{1}{i\hbar}\left[h^{(\tau)}_{\rm s.p.}, j^{(\tau)}_+\right], \qquad \tau = {\rm n}, {\rm p}, \tag{6}$$

while the residual spin–spin interaction is written as

$$V_{\sigma\sigma} = \tfrac{1}{2}\sum_{T=0,1} \chi_T S_T^+ S_T, \tag{7}$$

where

$$S_{T=0} = S_{\rm n} + S_{\rm p}, \qquad S_{T=1} = S_{\rm n} - S_{\rm p}. \tag{8}$$

The strength of $V_{\sigma\sigma}$ is taken [33] as $\chi_0 = \chi_1 = 100/A$ MeV.

The residual interaction $V_{\rm FF}$ gives rise to isoscalar and isovector shape oscillations. The isoscalar-coupling constant, κ_0, is determined by the condition [34] that the lowest RPA frequency for the isoscalar mode vanishes, since the lowest-lying mode with $K^\pi = 1^+$ is spurious and corresponds to a uniform rotation of the system. The value of ξ in (5) is determined by the requirement [35] that the spurious component should be absent in the RPA solutions with non-zero frequencies. We have numerically checked that the summed probability of the spurious component, $|S\rangle \propto j_+ |{\rm g.s.}\rangle$, remaining in the RPA solutions with non-zero frequency is less than 10^{-6}.

The isovector coupling constant, κ_1, is taken from the self-consistency condition for the harmonic-oscillator model [36], $\kappa_1 = -3.5\kappa_0$. In RPA calculations we take into account all two-quasiparticle configurations with excitation energies less than 26 MeV, and have checked that the configuration space is sufficiently large so as to include all M1 strengths.

The B(M1)-values have been calculated using the strong coupling scheme [36]. They are given by

$$B\left({\rm M1};\, 0^+_{\rm g.s.} \to 1^+;\, n\right) = 2\left|\langle 1^+;\, n \,|\, \hat{M}1 \,|\, 0^+_{\rm g.s.}\rangle\right|^2, \tag{9}$$

where $|1^+;\, n\rangle$ is the $K^\pi = 1^+$ QRPA phonon and $\hat{\rm M}1 = \sqrt{3/4\pi}\,\mu_{\rm N}\Sigma_{\tau={\rm n,p}}(g_{{\rm l},\tau}\boldsymbol{l}_\tau + g_{{\rm s},\tau}\boldsymbol{s}_\tau)$ is the usual magnetic-dipole operator. As a representative example, results of calculations for Sr isotopes are shown in Fig. 2, which shows the excitation energies of the low-lying $K^\pi = 1^+$ states. The values B(M1; g.s $\to 1^+$) (in $\mu_{\rm N}^2$) are indicated. The upper diagram was obtained by using the standard pairing gaps of Table 1. According to sect. 2, pairing correlations in the excited states of Sr–Zr are

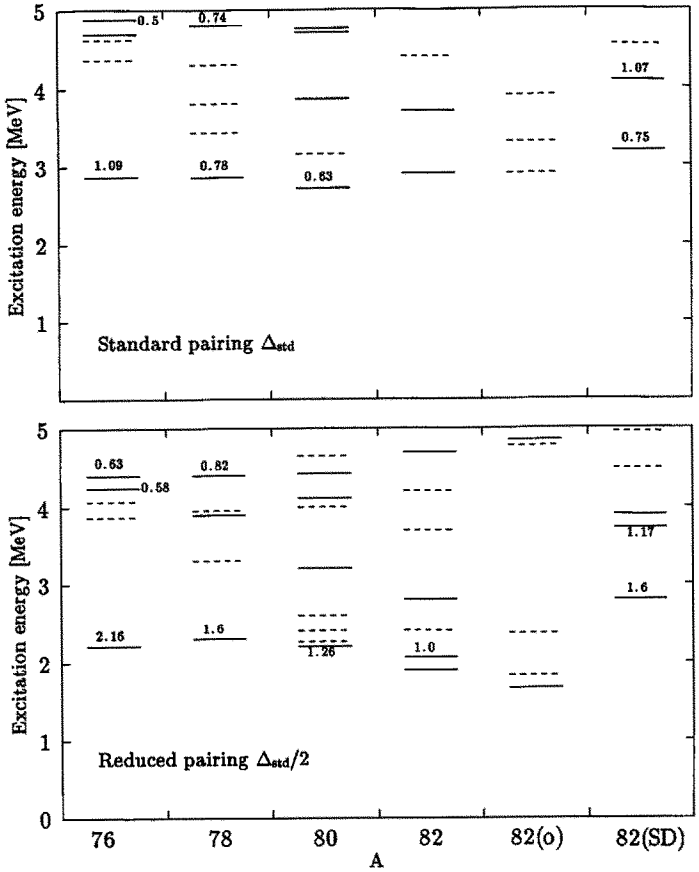

Fig. 2. Predicted excitation energies of low-lying 1^+ states of prolate configurations in ^{76,78,80,82}Sr, oblate minimum in ^{82}Sr [82(o)], and the superdeformed configuration in ^{82}Sr [82(SD)]. The numbers indicate the B(M1; g.s. $\rightarrow 1^+$) values (in μ_N^2) for transitions greater than 0.5 μ_N^2. Only states with B(M1; g.s. $\rightarrow 1^+$) > 0.1 μ_N^2 are shown (solid lines: B(M1) > 0.3 μ_N^2, dashed lines: B(M1) < 0.3 μ_N^2). The upper portion shows the results obtained with standard pairing, Δ_{std}, see Table 1. The results obtained with pairing reduced by 50% are displayed in the lower portion.

expected to be seriously quenched. Therefore, we performed a second set of calculations with Δ_p and Δ_n reduced by 50% with respect to the standard values. As discussed in refs. [27,29], reduced pairing leads to increased collectivity of the low-lying 1^+ states; as seen in Fig. 2 the B(M1) values calculated in the "weak pairing" variant are approximately twice as large as the M1 rates obtained in the "standard pairing" variant.

The best candidate for low-lying enhanced 1^+ states in the $A \sim 80$ mass region is the $N = Z$ nucleus ^{76}Sr. Its ground state is very well deformed due to the coherent superposition of proton and neutron shell effects associated with the deformed gap at the particle number 38. In Fig. 3 we show the B(M1; g.s. $\rightarrow 1^+$)

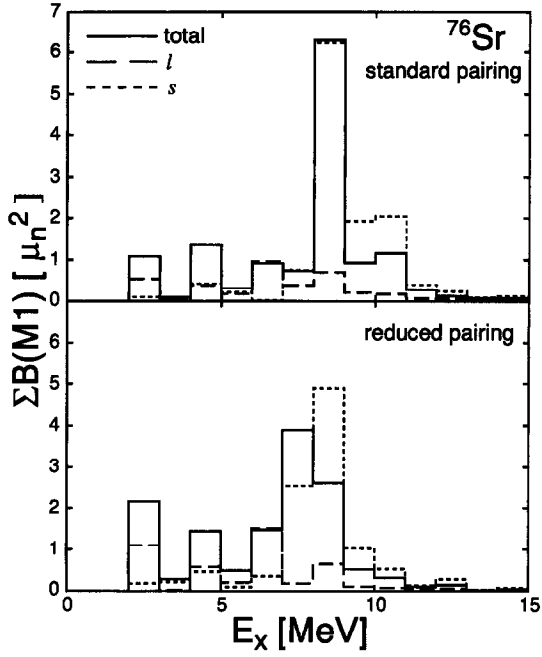

Fig. 3. B(M1; g.s., $K^\pi = 0^+ \rightarrow K^\pi = 1^+$) values for ^{76}Sr calculated in RPA as a function of the excitation energies of 1^+ states. The summed values per 1 MeV energy bin are plotted as a histogram (solid lines). For reference, the B(M1) values (9) associated with spin part only ($g_l = 0$, dotted line) or orbital part only ($g_s = 0$, dashed line) are also shown. The g-factors used are $g_l = g_l^{\rm free}$ and $g_s = (0.85)g_s^{\rm free}$. The upper (lower) diagram represents the "standard pairing" ("weak pairing") variant of the calculations.

strengths of the calculated $K^\pi = 1^+$ RPA excitation modes in ^{76}Sr (at the ground-state deformation), as a function of excitation energy. The upper (lower) diagram corresponds to the standard (weak) pairing variant. The M1 strength arising from only the proton convection current (i.e., $g_s = 0$) and the M1 strength from only the spin part (i.e., $g_l = 0$) are also plotted in Fig. 3. In both pairing variants of calculations, there appears only one low-lying 1^+ state which has unusually strong M1 collectivity. In the "weak pairing" variant this state is predicted at 2.2 MeV and the corresponding B(M1; g.s. $\rightarrow 1^+$) transition is 2.16 μ_N^2. The main components of the wave function of the 1^+ state in ^{76}Sr are the $\pi(g_{9/2})^2$ and $\nu(g_{9/2})^2$ excitations involving the two Nilsson orbitals [431 $\frac{3}{2}$] and [422 $\frac{5}{2}$]. The largest components of the low-lying 1^+ states in ^{76}Sr in the energy range of 4–5 MeV are the [431 $\frac{3}{2}$] $\times$ [431 $\frac{1}{2}$] (spin-flip) and [301 $\frac{3}{2}$] $\times$ [310 $\frac{1}{2}$] two-quasiparticle excitations. The main contribution to the peak in the M1 distribution seen in the energy range of 7–9 MeV in Fig. 3 comes almost exclusively from the spin-flip $f_{7/2} \rightarrow f_{5/2}$ and $g_{9/2} \rightarrow g_{7/2}$ transitions.

The contribution to the B(M1) strength coming from the unique-parity high-j excitations, such as $(h_{11/2})^2$ or $(g_{9/2})^2$, has a simple shell-model interpretation (in

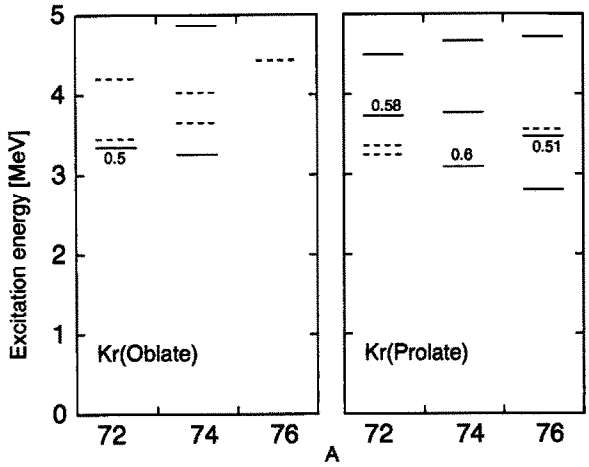

Fig. 4. Similar to Fig. 2 (standard pairing) but for the Kr isotopes.

terms of a single-j shell) and cannot be viewed as coming from a collective "scissors" mode (see discussion in ref. [33]). The synthetic orbital scissors state is defined as

$$|R\rangle = \mathcal{N}^{-1}\left(l_+^{(n)} - \alpha l_+^{(p)}\right)|\text{g.s.}\rangle, \tag{10}$$

where $\mathcal{N}$ is a normalization factor and the parameter α is determined by the requirement that the mode (10) is orthogonal to the spurious reorientation mode [29,37,38], i.e.,

$$\alpha = \langle \text{g.s.}|\, j_-^{(n)} l_+^{(n)}\,|\text{g.s.}\rangle / \langle \text{g.s.}|\, j_-^{(p)} l_+^{(p)}\,|\text{g.s}\rangle. \tag{11}$$

The calculations show that for the lowest 1^+ state in ^{76}Sr the overlap between its RPA wave function and the state (10) is only about 12%. Consequently, although this state is predicted to carry an unprecedented M1 strength, it cannot be given a geometric interpretation of the "scissors" mode. The $K^\pi = 1^+$ isovector giant quadrupole resonance in ^{76}Sr lying at $E_{ex} \sim 32$ MeV carries a significant M1 strength ($\sim 4\ \mu_N^2$) and contains a major component of the "scissors mode" (around 50%).

Figs. 4 and 5 show the calculated 1^+ states in Kr and Zr isotopes, respectively. As seen in Figs. 2, 4 and 5 when moving away from ^{76}Sr, the low-energy M1 strength becomes more fragmented. Good prospects where to find large M1 strength at low energies are the well-deformed prolate nuclei ^{78}Sr (where the 1^+ state is built mainly from the $\pi([431\ \frac{3}{2}] \otimes [422\ \frac{5}{2}])$ and $\nu([422\ \frac{5}{2}] \otimes [413\ \frac{7}{2}])$ two-quasiparticle excitations), ^{80}Sr, ^{80}Zr ($\pi([422\ \frac{5}{2}] \otimes [413\ \frac{7}{2}])$ and $\nu([422\ \frac{5}{2}] \otimes [413\ \frac{7}{2}])$), ^{82}Zr, and ^{74}Kr. The most promising oblate-shape candidate is the $N = Z$ nucleus ^{72}Kr. Similar to ^{76}Sr, the 1^+ state in ^{72}Kr has a $(g_{9/2})^2$ character. However, in this case the main contribution comes from the high-Ω substates, i.e., $\pi([413\ \frac{7}{2}] \otimes [404\ \frac{9}{2}])$ and $\nu([413\ \frac{7}{2}] \otimes [404\ \frac{9}{2}])$.

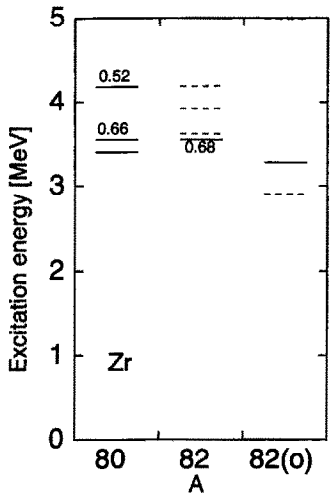

Fig. 5. Similar to Fig. 2 (standard pairing) but for the Zr isotopes.

As discussed in sect. 2, the best prospects for superdeformation in the $A \sim 80$ region are in the nuclei around ^{82}Sr. The calculations performed for superdeformed configuration of ^{82}Sr predict two states (around 3 MeV and 4 MeV) that carry a large M1 strength (see Fig. 2). They can be associated with the $\pi([431\ \frac{3}{2}] \otimes [422\ \frac{5}{2}])$, $\nu([422\ \frac{5}{2}] \otimes [413\ \frac{7}{2}])$ and $\nu([541\ \frac{3}{2}] \otimes [550\ \frac{1}{2}])$ two-quasiparticle excitations.

4. Octupole correlations

In the light zirconium region octupole correlations can be associated with the $g_{9/2}$ and $p_{3/2}$ subshells. Because of their rather large energy separation and a small number of coupling matrix elements, no pronounced octupole instability is expected. In addition, the small number of active subshells makes the octupole effect more sensitive to quadrupole distortion than in heavier nuclei around ^{146}Ba or ^{222}Th [39].

The systematics of the lowest 3^- excitations in the Zr-region is shown in Fig. 6. It is seen that E_{3^-} tends to decrease when approaching the nucleus ^{76}Sr. On the other hand, the shell correction calculations [12,40,41] predict octupole softness only in the transitional isotopes of Zn–Se with $N \leqslant 36$. Is the presence of low-lying negative-parity state always a good fingerprint of octupole collectivity? The answer to this question is negative. There are many nuclei that possess relatively high-lying negative-parity excitations but still are considered as good examples of systems with strong octupole correlations. In fact, the systematics of experimental B(E3) values in the light-Zr region [12,42] indicates that no correlation can be found between the behavior of the lowest negative-parity states shown in Fig. 6 and the B(E3; g.s. $\rightarrow 3^-$) strength.

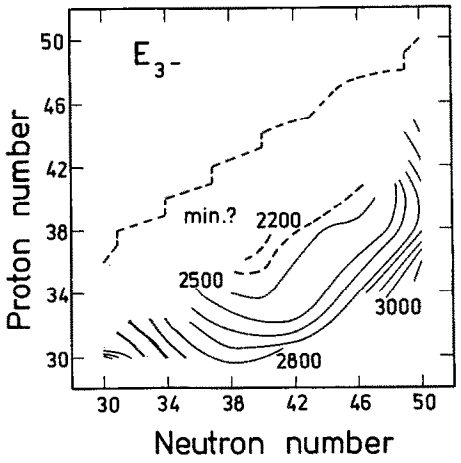

Fig. 6. The lowest 3^- energy level (in keV), observed experimentally for doubly even nuclei from the light zirconium region. The dashed contour lines represent the lowest contours, at 2.2 and 2.3 MeV. The upper dashed curve marks the proton-drip line.

According to the energy systematics presented in Fig. 6, the lowest negative-parity states are observed in strongly deformed nuclei with particle number (N or Z) close to 38. For example, in the nucleus ^{76}Kr two negative-parity rotational bands built upon the (3^-) (2258 keV) and (2^-) (2227 keV) band heads are known. However, the coexisting prolate and oblate minima in this nucleus are predicted [12] to be fairly rigid with respect to the reflection-asymmetric distortion. In ref. [43], based on energy systematics, it has been argued that some negative-parity bands in well-deformed nuclei from the $A \sim 80$ mass region can be interpreted as collective (aligned) octupole bands. However, it is not the excitation energy of the negative-parity band itself that determines the collective character of the underlying intrinsic configuration. In $\pi = -$ bands pairing correlations are usually reduced due to blocking and there is also significant Coriolis mixing. Consequently, these bands have usually larger moments of inertia than ground bands and, in some cases, can become yrast at high spins. In our opinion, the observed lowering of negative-parity states around the particle number 38 does not necessarily indicate strong octupole correlations as suggested in ref. [43] but rather has a non-collective origin, see below.

In order to clarify the issue of octupole collectivity around $Z = 38$, $N = 38$ we performed the RPA calculations with the hamiltonian

$$H_{\mathrm{QRPA}} = h_{\mathrm{s.p.}} + V_{\mathrm{pair}} - \tfrac{1}{2}\sum_K \chi_{3K}^{T=0} Q''^{\dagger}_{3K} Q''_{3K} - \tfrac{1}{2}\sum_K \chi_{3K}^{T=1} (\tau_3 Q_{3K})''^{\dagger} (\tau_3 Q_{3K})''$$
$$+ \tfrac{1}{2}\sum_K \chi_{1K}^{T=1} (\tau_3 D_{1K})''^{\dagger} (\tau_3 D_{1K})''. \qquad (12)$$

where $b_{\mathrm{s.p.}}$ is a single-particle Nilsson hamiltonian, V_{pair} is given by (3), and $Q''_{3K} = (r^3 Y_{3K})''$ [$D''_{1K} = (rY_{1K})''$] are the doubly-stretched octupole (dipole) opera-

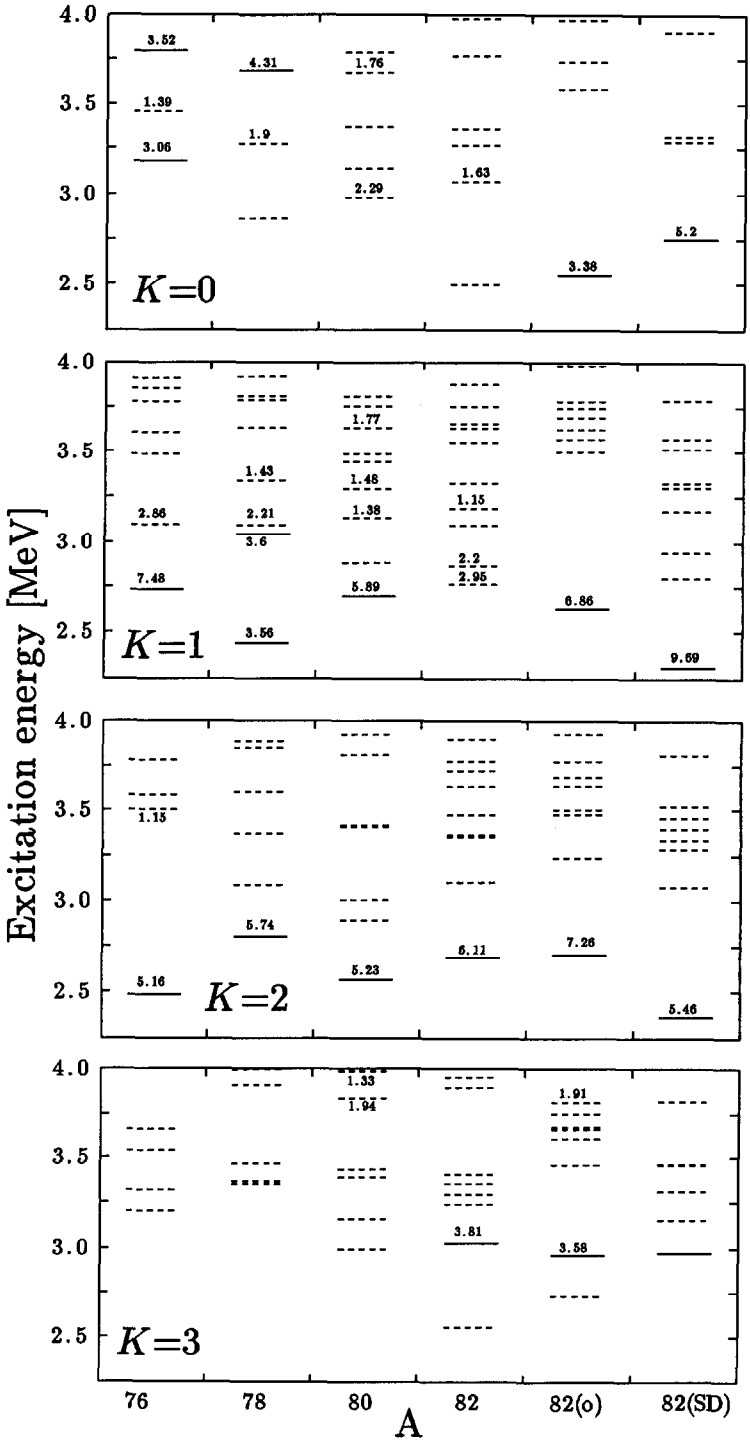
Excitation energy [MeV]
4.0
3.5
3.0
2.5
K=0
3.52
1.39
3.06
4.31
1.9
1.76
2.29
1.63
5.2
3.38
K=1
1.77
1.43
1.48
1.38
1.15
2.86
2.21
3.6
2.2
2.95
7.48
5.89
6.86
3.56
9.69
K=2
1.15
5.74
5.23
6.11
7.26
5.16
5.46
K=3
1.33
1.94
1.91
3.81
3.58
76
78
80
82
82(o)
82(SD)
A

tors [44]. A large configuration space composed of 7 major shells (for both protons and neutrons) was used when solving the coupled RPA equations. The octupole isoscalar coupling strengths, $\chi_{3K}^{T=0}$, were determined by the self-consistency condition for the harmonic-oscillator model [36,44],

$$\chi_{3K}^{T=0} = \tfrac{4}{7}\pi M\omega_0^2\Big\{\langle (r^4)'' \rangle_0 + \tfrac{2}{7}(4-K^2)\big\langle (r^4 P_2)'' \big\rangle_0 + \tfrac{1}{84}\big[K^2(7K^2-67)+72\big]\big\langle (r^4 P_4)'' \big\rangle_0\Big\}^{-1}. \tag{13}$$

The strength of the isovector octupole mode was taken from ref. [45]

$$\chi_{3K}^{T=1} = -0.5\chi_{3K}^{T=0}, \tag{14}$$

while for the isovector dipole mode we used the value [36,44],

$$\chi_{1K}^{T=1} = \frac{\pi V_1}{\langle (r^2)'' \rangle} M\omega_0^2 \tag{15}$$

with $V_1 = 140$ MeV. A similar model has been used recently [46,47] to discuss octupole excitations built upon superdeformed shapes. The doubly-stretched multipole interaction can be viewed as an improved version of the conventional multipole–multipole force. Namely, it has the following desirable properties in the limit of the harmonic-oscillator one-body potential. Firstly, it satisfies the nuclear self-consistency condition [36] rigorously even if the system is deformed. Secondly, it yields the zero-energy RPA spurious modes, i.e., it automatically separates the translational and reorientation modes. Last but not least, for the doubly-stretched multipole interaction the dipole-octupole coupling terms disappear [44].

The B(E3)-values have been calculated using the strong coupling scheme. They are given by

$$B(\mathrm{E3};\, 0^+_{\mathrm{g.s.}} \to I=3,\, K;\, n) = \frac{2}{1+\delta_{K0}} \big| \langle 3K;\, n | Q^c_{3K} | 0^+_{\mathrm{g.s.}} \rangle \big|^2, \tag{16}$$

where $|3K;\, n\rangle \equiv |n\rangle$ is the QRPA phonon and $Q^c_{3K} = (r^3 Y_{3K})_p$ is the charge (proton) octupole operator. It is worth noting that, because we use the doubly-stretched $Q''^{\dagger}_{3K} Q''_{3K}$ interactions, there is no simple correlation between the number of two-quasiparticle configurations contributing to an excited state and the corresponding B(E3) value. That is, an excitation which looks fairly collective in terms of the RPA amplitudes (i.e., appreciable size of backward-going amplitudes), it still can have a very small B(E3) value. Indeed, the ordinary octupole strengths $|\langle n | Q_{3K} | 0 \rangle|^2$ are quite different from the doubly-stretched octupole strengths $|\langle n | Q''_{3K} | 0 \rangle|^2$ in well-deformed nuclei. For example, in case of the prolate superdeformed harmonic-oscillator potential ($\omega_\perp = 2\omega_3$), ratios of the energy-

Fig. 7. Predicted excitation energies of low-lying intrinsic $K^\pi = 0^-, 1^-, 2^-$, and 3^- states in ^{76,78,80,82}Sr. The numbers indicate the B(E3; g.s. $\to K^-$) values in s.p.u. (1 s.p.u. = $0.416\times10^{-6}\ A^2e^2\mathrm{b}^3$, cf. ref. [42]). They are shown for the states with B(E3) > 1 s.p.u. Other states represent non-collective $\pi = -$ excitations. The solid lines correspond to states with B(E3) > 3 s.p.u. while the dashed lines correspond to states with B(E3) < 3 s.p.u. The results were obtained with standard pairing, Δ_{std}, see Table 1.

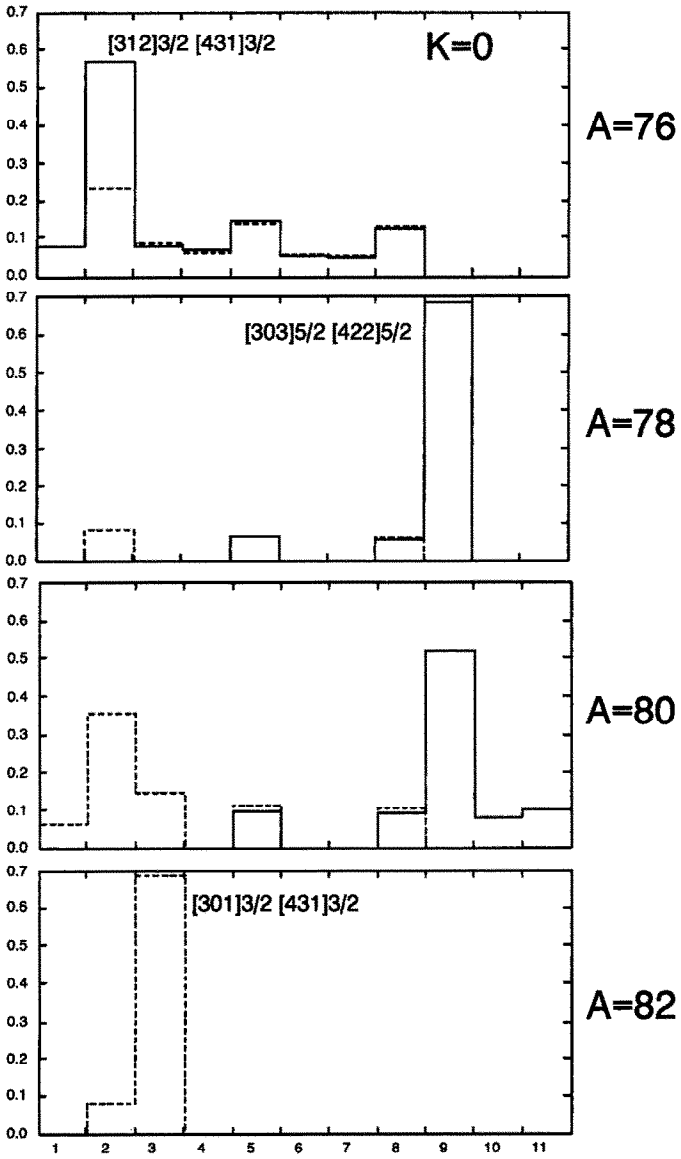

Fig. 8. Absolute values of forward RPA amplitudes of the lowest $K^{\pi} = 0^{-}$ states built upon prolate minima in the Sr isotopes versus the quasiparticle configuration (numbered according to their excitation energies) for neutrons (solid lines) and protons (dashed lines). All amplitudes whose absolute values greater than 5×10^{-2} are indicated. (Note that due to the time-reversal symmetry each amplitude contributes to the intrinsic wave function twice.) The results were obtained with standard pairing, Δ_{std}, see Table 1.

weighted sum rule values S_{3K} (for Q_{3K} operators) and S''_{3K} (for Q''_{3K} operators) are given by [48]

$$S_{3K} : S''_{3K} = \begin{cases} 50:11 & \text{for } K=0 \\ 13:4 & \text{for } K=1 \\ 1:1 & \text{for } K=2 \\ 1:4 & \text{for } K=3, \end{cases} \tag{17}$$

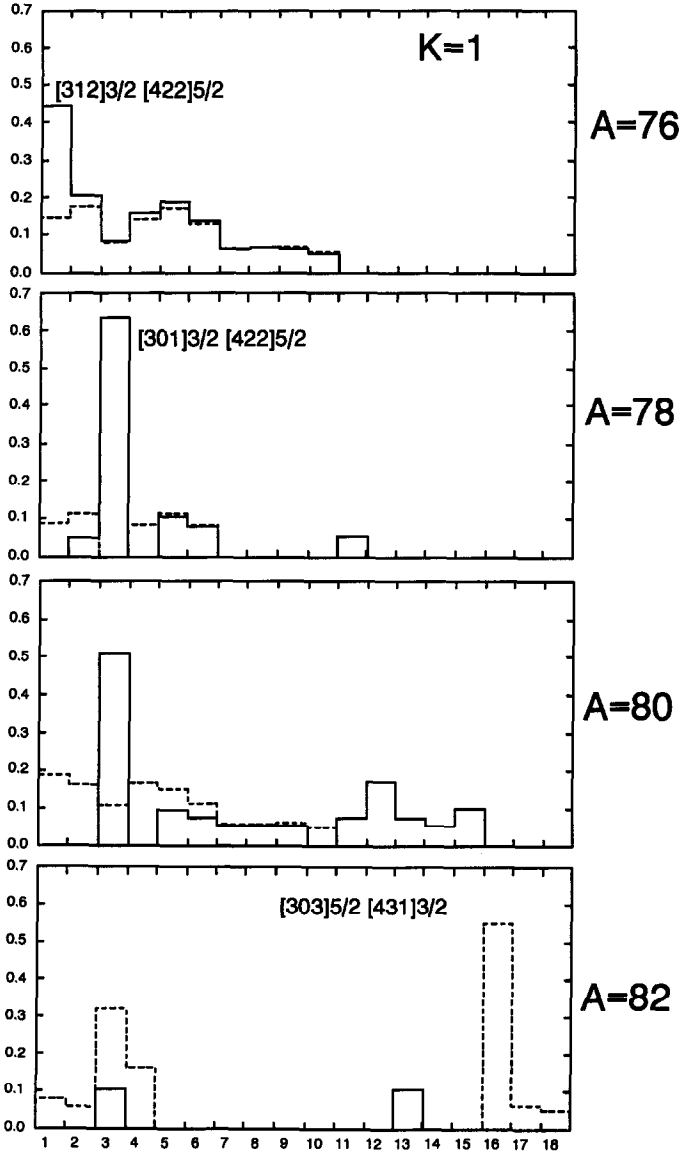

Fig. 9. Similar to Fig. 8 but for the lowest $K^\pi = 1^-$ states in the Sr isotopes.

while in the oblate superdeformed case ($\omega_3 = 2\omega_\perp$),

$$S_{3K} : S''_{3K} = \begin{cases} 5:8 & \text{for } K=0 \\ 17:26 & \text{for } K=1 \\ 1:1 & \text{for } K=2 \\ 4:1 & \text{for } K=3. \end{cases} \tag{18}$$

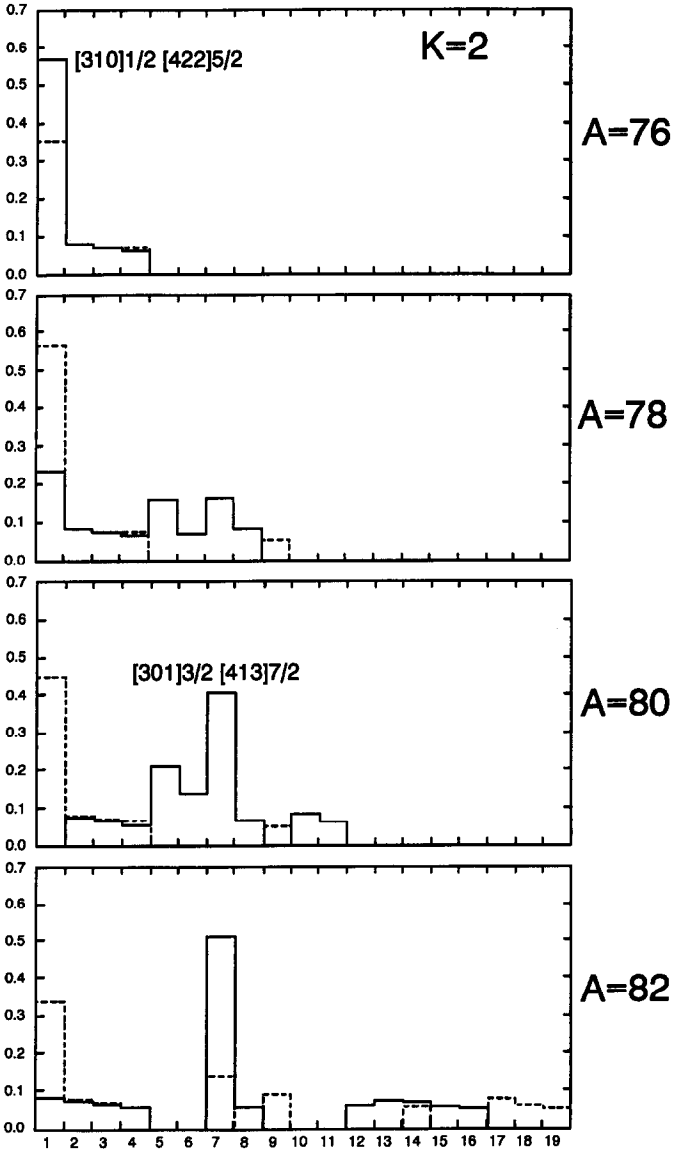

Fig. 10. Similar to Fig. 9 but for the lowest $K^\pi = 2^-$ states in the Sr isotopes.

Therefore, in the well-deformed prolate (oblate) configurations, B(E3) values overestimate (underestimate) the collectivity (in the sense of the RPA with doubly-stretched interaction) for the $K^\pi = 0^-$ and 1^- states, while they underestimate (overestimate) the "doubly-stretched" octupole collectivity of the $K^\pi = 3^-$ states.

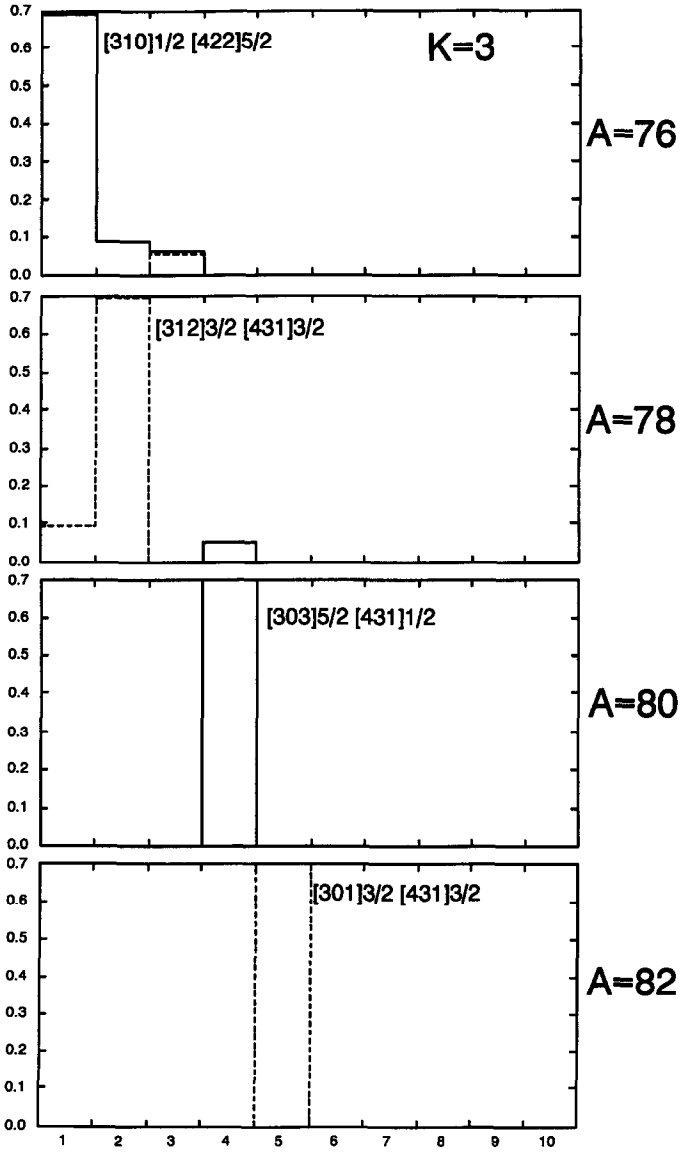

Fig. 11. Similar to Fig. 9 but for the lowest $K^\pi = 3^-$ states in the Sr isotopes.

The results of calculations for the Sr isotopes are shown in Fig. 7, which displays the predicted excitation energies of intrinsic $K^\pi = 0^-$, 1^-, 2^-, and 3^- states and the corresponding B(E3) values (in s.p.u.). The forward RPA amplitudes for the 0^-, 1^-, 2^-, and 3^- states built upon prolate configurations in ^{76,78,80,82}Sr are plotted in Figs. 8–11, respectively. In none of the nuclei considered, the low-lying negative-parity excitations can be considered as highly-collective states.

In the $N = Z$ nucleus ^{76}Sr the lowest negative-parity excitations with $K = 1$ and 2 can be considered as weakly collective. The $K = 1$ octupole phonon has a large component of the two-quasiparticle $[312\ \frac{3}{2}] \otimes [422\ \frac{5}{2}]$ neutron configuration, see Fig. 9. The $K^\pi = 2^-$ mode is less collective but it lies lower in energy. As seen in Fig. 10, the main contribution to its wave function comes from the $[310\ \frac{1}{2}] \otimes [422\ \frac{5}{2}]$ proton and neutron excitations. The lowest $K^\pi = 0^-$ excitation is mainly built upon the $[312\ \frac{3}{2}] \otimes [431\ \frac{3}{2}]$ excitations. The $K^\pi = 3^-$ state is predicted to be a non-collective $[310\ \frac{1}{2}] \otimes [422\ \frac{5}{2}]$ state, see Fig. 11. Of course, all those intrinsic

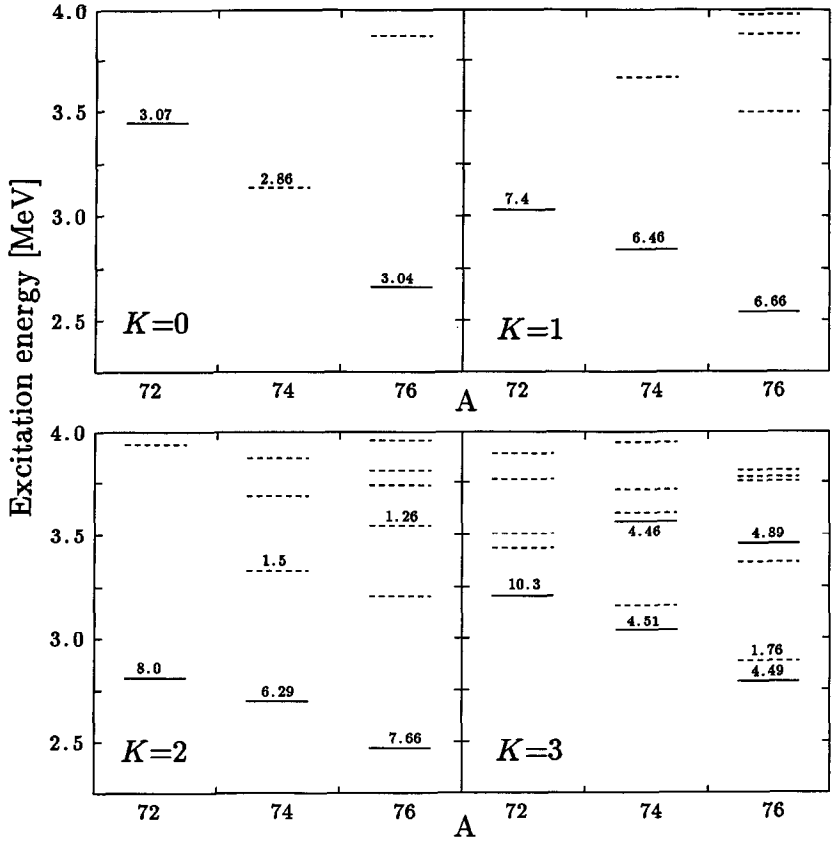

Fig. 12. Similar to Fig. 7 but for the lowest $\pi = -$ states in oblate configurations in the ^{72,74,76}Kr isotopes.

states are expected to be mixed through the Coriolis interaction [49]. In the "weaker pairing" variant of the calculations, the B(E3; g.s. $\rightarrow 1^-$) rate is reduced by a factor of ~ 3. This is because the "particle–particle" and "hole–hole" components such as $[301\ \frac{3}{2}] \otimes [422\ \frac{5}{2}]$ or $[310\ \frac{1}{2}] \otimes [431\ \frac{3}{2}]$ have much less effect. A similar quenching is calculated for the 0^- state, which becomes a pure particle–hole excitation if pairing is reduced. On the other hand, the characteristics of the 2^- state are only weakly influenced by pairing.

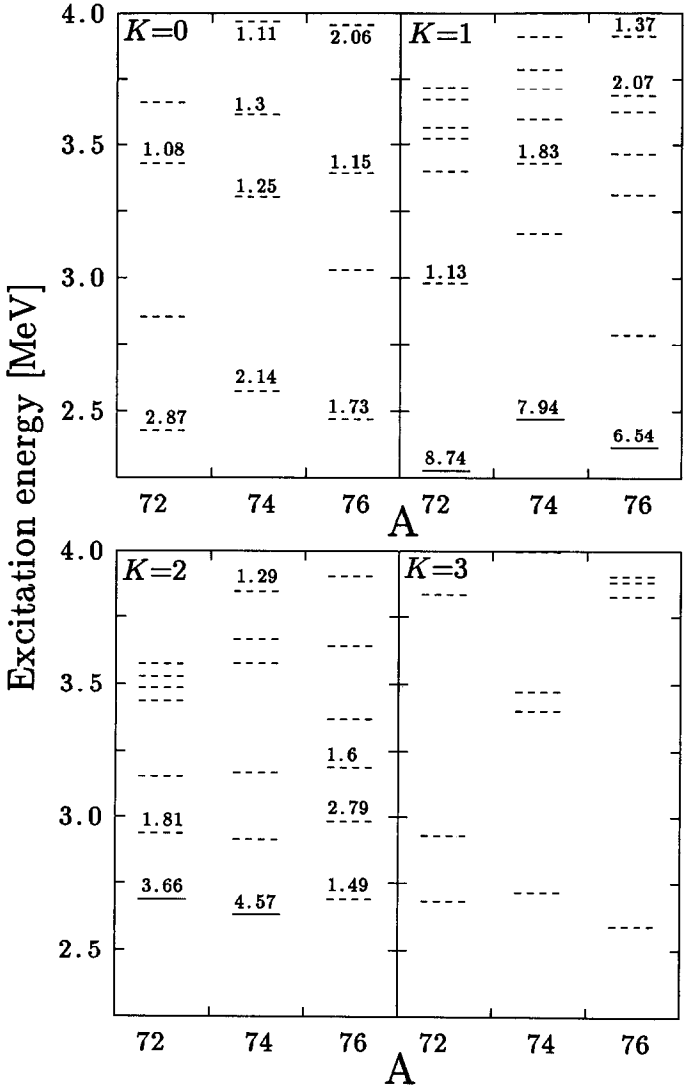

Fig. 13. Similar to Fig. 7 but for the lowest $\pi = -$ states in prolate configurations in the ^{72,74,76}Kr isotopes.

The lowest $K^\pi = 0^-$ excitations in prolate configurations of ^{78,80,82}Sr carry a rather weak collectivity. Like in ^{76}Sr, in the "weak pairing" variant those states become almost pure particle–hole excitations. A similar situation is predicted for the $K^\pi = 1^-$ and 3^-states. The $K^\pi = 2^-$ modes are found to be slightly more collective compared to other modes with $K = 0$, 1, and 3. They are expected to appear at about $E_{ex} = 2.7$ MeV and they carry E3 strength around 6 s.p.u. On the other hand, if pairing is reduced those states become less collective.

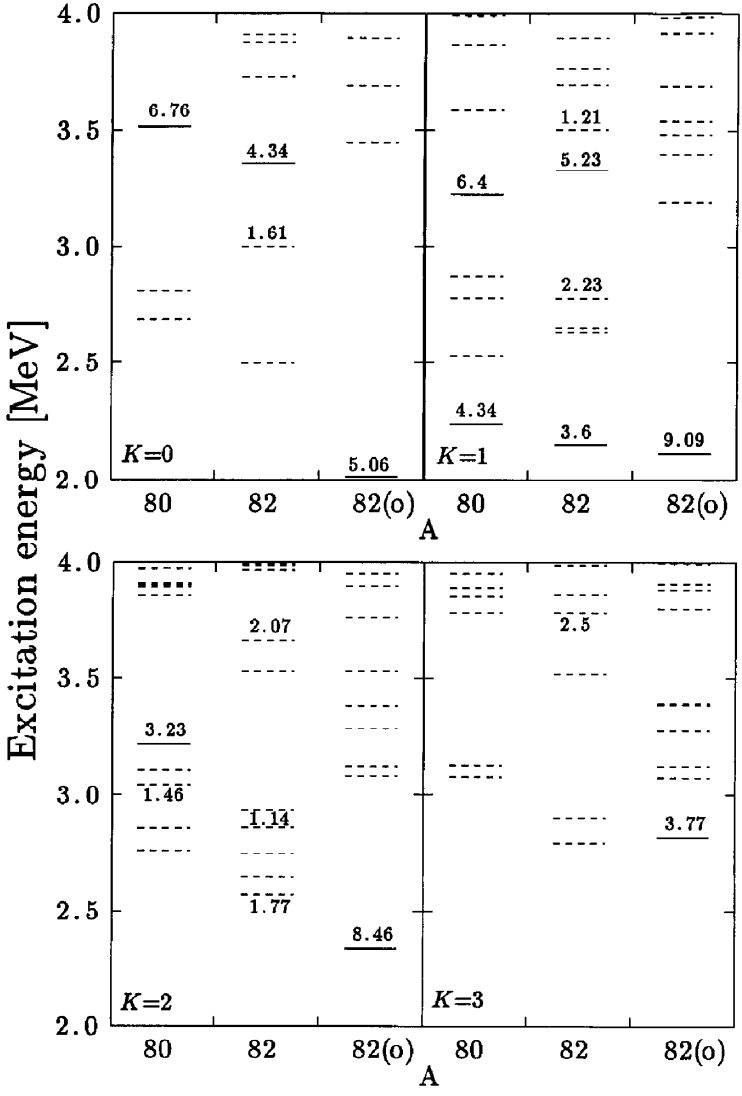

Fig. 14. Similar to Fig. 7 but for the lowest $\pi = -$ states in the ^{80,82}Zr isotopes.

The most collective octupole excitations in the oblate configuration of ^{82}Sr are the $K^\pi = 1^-$ and 2^- states [$E_{ex} \sim 2.7$ MeV, $B(E3) \sim 7$ s.p.u.]. The calculations also predict a low-lying weakly-collective $K^\pi = 1^-$ excitation in the superdeformed configuration of ^{82}Sr ($E_{ex} \sim 2.3$ MeV, $B(E3) \sim 10$ s.p.u.).

Figs. 12 and 13 display calculated low-lying negative-parity states built upon the oblate and prolate configurations in the Kr isotopes, respectively. On the average, negative-parity states in Kr's are slightly more collective than those in Sr's. The $K^\pi = 0^-$ prolate excitations are almost pure two-quasiparticle states. The $K^\pi = 1^-$ states and the $K^\pi = 2^-$ oblate states resemble octupole vibrations; they have $E_{ex} \sim 2.5$ MeV, $B(E3) \sim 7$ s.p.u. The most collective octupole state in the Kr isotopes is the $K^\pi = 3^-$ excitation ($E_{ex} \sim 3.2$ MeV, $B(E3) \sim 10$ s.p.u.) in ^{72}Kr built upon the oblate minimum. However, when pairing is reduced this state becomes almost a pure particle–hole excitation.

Finally, the results for the Zr isotopes are shown in Fig. 14. The lowest negative-parity excitations in ^{80}Zr and ^{82}Zr (prolate configuration) have a two-quasiparticle character. The $K^\pi = 0^-$, 1^-, and 2^- modes in the oblate minimum of ^{82}Zr are weakly collective, with $B(E3) \sim 5$–9 s.p.u. Interestingly, the $B(E3)$ rates for these states do not depend strongly on pairing. This is because their dominant two-quasiparticle components are the particle-like $(g_{9/2})_{1/2,3/2,5/2}$ orbitals and the hole-like negative-parity $p_{3/2} \oplus f_{5/2}$ levels with $\Omega = \frac{1}{2}$ and $\frac{3}{2}$.

5. Conclusions

In the light zirconium region there are many excellent candidates for the low-lying 1^+ states with unusually large $B(M1; 0^+ \to 1^+)$ rates, around 1–2 μ_N^2. The best prospects are the $Z = N$ nuclei, such as ^{76}Sr (prolate), ^{80}Zr (prolate), and ^{72}Kr (oblate), where protons and neutrons contribute equally strongly to the M1 collectivity. Interestingly, the unusually strong low-energy M1 strength in those nuclei has a simple interpretation in terms of $(g_{9/2})^2$ excitations, i.e., it does not result from a simplistic scissors mode. Also, it does not resemble the strong M1 transitions known in the light $Z = N$ nuclei [50], mainly of the spin-flip origin.

In ^{76}Sr and neighboring nuclei, the 1^+ excitations are predicted to appear just above the $\pi = -$ intrinsic states. Generally, the $K^\pi = 0^-$, 1^-, 2^-, and 3^- band heads are calculated to be very weakly collective in well-deformed proton-rich Kr, Sr, and Zr nuclei (except maybe ^{72}Kr). Namely, the low-lying negative-parity states have a dominant two-quasiparticle character when they are built on an intrinsic state with a large quadrupole deformation. There is no clear correlation between the excitation energy of the 3^- state and the magnitude of the $B(E3)\uparrow$ value in the nuclei from the proton-rich Sr–Zr region.

The results of our calculations are quite sensitive to the strength of pairing interaction. In general, the weaker the pairing correlations, the more (less) collective are the M1 (E3) excitations. There exists some indirect experimental evidence supported by calculations, see sect. 2, that pairing is seriously reduced in some excited states of well-deformed nuclei from the $A \sim 80$ mass region. We

hope that future measurements of excited states in the well-deformed nuclei around ^{76}Sr, especially their lifetimes, will shed new light on the collectivity of M1 and E3 states and, indirectly, on the magnitude of pairing correlations in this mass region.

The Joint Institute for Heavy Ion Research has as member institutions the University of Tennessee, Vanderbilt University, and the Oak Ridge National Laboratory; it is supported by the members and by the Department of Energy through Contract Number DE-FG05-87ER40361 with the University of Tennessee. Theoretical nuclear physics research at the University of Tennessee is supported by the U.S. Department of Energy through Contract Number DE-FG05-93ER40770. This work was also partly supported by the Yamada Science Foundation, Osaka, Japan, and the Swedish Natural Science Research Council. The calculations were supported in part by RCNP, Osaka University, as RCNP Computational Nuclear Physics Project (Project No. 93-B-02).

References

[1] J.H. Hamilton, in Lecture Notes in Physics 168, Heavy ion collision (Springer, Berlin, 1982) 631
[2] Nuclear structure of the zirconium region, ed. J. Eberth, R.A. Meyer and K. Sistemich (Springer, Berlin, 1988)
[3] J.L. Wood, K. Heyde, W. Nazarewicz, M. Huyse and P. van Duppen, Phys. Reports 215 (1992) 101
[4] W. Nazarewicz, J. Dudek, R. Bengtsson, T. Bengtsson and I. Ragnarsson, Nucl. Phys. A435 (1985) 397
[5] W. Nazarewicz and T. Werner, *in* Nuclear structure of the zirconium region, ed. by J. Eberth, R.A. Meyer and K. Sistemich (Springer, Berlin, 1988), p. 277
[6] R. Bengtsson, *in* Nuclear structure of the zirconium region, ed. J. Eberth, R.A. Meyer and K. Sistemich (Springer, Berlin, 1988) p. 371
[7] C.J. Lister, B.J. Varley, H.G. Price and J.W. Olness, Phys. Rev. Lett. 49 (1982) 308
[8] R.F. Davie, D. Sinclair, S.S.L. Ooi, A.E. Smith, H.G. Price, C.J. Lister, B.J. Varley and I.F. Wright, Nucl. Phys. A463 (1987) 683
[9] H.G. Price, C.J. Lister, B.J. Varley, W. Gelletly and J.W. Olness, Phys. Rev. Lett. 51 (1983) 1842
[10] C.J. Lister, P.J. Ennis, A.A. Chishti, B.J. Varley, W. Gelletly, H.G. Price and A.N. James, Phys. Rev. C42 (1990) R1191
[11] Physics and techniques of secondary nuclear beams, ed. J.F. Bruandet, B. Fernandez and M. Bex (Editions Frontières, Gif-sur-Yvette, 1992)
[12] P.J. Ennis, C.J. Lister, W. Gelletly, H.G. Price, B.J. Varley, P.A. Butler, T. Hoare, S. Ćwiok and W. Nazarewicz, Nucl. Phys. A535 (1992) 392
[13] S. Ćwiok, J. Dudek, W. Nazarewicz, J. Skalski and T. Werner, Comput. Phys. Commun. 46 (1987) 379
[14] P. Möller, and J.R. Nix, At. Data Nucl. Data Tables 39 (1988) 213
[15] P. Möller and J.R. Nix, Nucl. Phys. A536 (1992) 20
[16] I. Ragnarsson and T. Bengtsson, in Nuclear structure of the zirconium region, ed. J. Eberth, R.A. Meyer and K. Sistemich (Springer, Berlin, 1988), p. 193
[17] J. Dudek, W. Nazarewicz and N. Rowley, Phys. Rev. C35 (1987) 1489
[18] C. Baktash, G. Garcia-Bermudez, D.G. Sarantities, W. Nazarewicz, V. Abenante, J.R. Beene, H.C. Griffin, M.L. Halbert, D.C. Hensley, N.R. Johnson, I.Y. Lee, F.K. McGowan, M.A. Riley, D.W. Stracener, T.M. Semkow and A. Virtanen, Phys. Lett. B255 (1991) 174

[19] M.S. Kaplan, J.X. Saladin, L. Faro, D.F. Winchell, H. Takai and C.N. Knott, Phys. Lett. B215 (1988) 251
[20] C.J. Gross, J. Heese, K.P. Lieb, S. Ulbig, W. Nazarewicz, C.J. Lister, B.J. Varley, J. Billowes, A.A. Chishti, J.H. McNeill and W. Gelletly, Nucl. Phys. A501 (1989) 367
[21] J. Billowes, F. Cristancho, H. Grawe, C.J. Gross, J. Heese, A.W. Mountford and M. Weiszflog, Phys. Rev. C47 (1993) R917
[22] L. Lühmann, K.P. Lieb, C.J. Lister, B.J. Varley, H.G. Price and J.W. Olness, Europhys. Lett. 1 (1986) 623
[23] C.J. Lister, R. Moscrop, B.J. Varley, H.G. Price, E.K. Warburton, J.W. Olness and J.A. Becker, J. of Phys. G11 (1985) 969
[24] W. Ziegler, C. Rangacharyulu, A. Richter and C. Spieler, Phys. Rev. Lett. 65 (1990) 2515
[25] J. Margraf, R.D. Heil, U. Kneissl, U. Maier, H.H. Pitz, H. Friedrichs, S. Lindenstruth, B. Schlitt, C. Wesselborg, P. von Brentano, R.-D. Herzberg and A. Zilges, Phys. Rev. C47 (1993) 1474
[26] D.R. Bés and R.A. Broglia, Phys. Lett. B137 (1984) 141
[27] I. Hamamoto and C. Magnusson, Phys. Lett. B260 (1991) 6
[28] K. Heyde and C. de Coster, Phys. Rev. 44 (1991) R2262
[29] I. Hamamoto and W. Nazarewicz, Phys. Lett B297 (1993) 25
[30] W. Nazarewicz, *in* Recent advances in nuclear structure, ed. D. Bucurescu, G. Cata-Danil and N.V. Zamfir (World Scientific, Singapore, 1991), p. 175
[31] G. Ehrling and S. Wahlborn, Phys. Scripta 6 (1972) 94
[32] J. Dudek, Z. Szymański and T. Werner, Phys. Rev. C23 (1981) 920
[33] I. Hamamoto and S. Åberg, Phys. Lett. B145 (1984) 163; Phys. Scripta 34 (1986) 697
[34] I. Hamamoto, Nucl. Phys. A177 (1971) 484
[35] N.I. Pyatov and M.I. Cerney, Yad. Fiz. 16 (1972) 931
[36] A. Bohr and B.R. Mottelson, Nuclear structure, vol. 2 (Benjamin, New York, 1975)
[37] A. Faessler and R. Nojarov, Phys. Rev. C41 (1990) 1243
[38] D. Zawischa and J. Speth, Z. Phys. A339 (1991) 97
[39] W. Nazarewicz, Nucl. Phys. A520 (1990) 333c
[40] W. Nazarewicz, P. Olanders, I. Ragnarsson, J. Dudek, G.A. Leander, P. Möller and E. Ruchowska, Nucl. Phys. A429 (1984) 269
[41] J. Skalski, Phys. Rev. C43 (1991) 140
[42] R.H. Spear, At. Data Nucl. Data Tables 42 (1989) 55
[43] P.D. Cottle and O.N. Bignall, Phys. Rev. C39 (1989) 1158
[44] H. Sakamoto and T. Kishimoto, Nucl. Phys. A501 (1989) 205
[45] C.J. Veje, Mat.-fys. Medd. Dan. Vid. Selsk. 35 (1966)
[46] S. Mizutori, Y.R. Shimizu and K. Matsuyanagi, Prog. Theor. Phys. 83 (1990) 666
[47] S. Mizutori, Y.R. Shimizu and K. Matsuyanagi, Prog. Theor. Phys. 85 (1991) 559; Prog. Theor. Phys. 86 (1991) 131
[48] T. Nakatsukasa, S. Mizutori and K. Matsuyanagi, Prog. Theor. Phys. 87 (1992) 607
[49] K. Neergård and P. Vogel, Nucl. Phys. A149 (1970) 209; ibid., p. 217
[50] D. Kurath, Phys. Rev. 130 (1963) 1525

Progress of Theoretical Physics, Vol. 91, No. 4, April 1994

Semiclassical Analysis of the Supershell Effect in Reflection-Asymmetric Superdeformed Oscillator

Ken-ichiro ARITA and Kenichi MATSUYANAGI

Department of Physics, Kyoto University, Kyoto 606-01

(Received November 12, 1993)

An oscillatory pattern in the smoothed quantum spectrum, which is unique to single-particle motions in a reflection-asymmetric superdeformed oscillator potential, is investigated by means of the semiclassical theory of shell structure. Clear correspondence between the oscillating components of the smoothed level density and the classical periodic orbits is found. It is shown that an interference effect between two families of the short periodic orbits, called supershell effect, becomes more significant with increasing reflection-asymmetric deformations. Possible origins of this enhancement phenomena as well as quantum signatures of period-multipling bifurcations are discussed in connection with stabilities of the classical periodic orbits.

§ 1. Introduction

Possible occurrence of instability of superdeformed (SD) nuclei having the prolate shape with the axis ratio approximately 2:1 against the octupole-type reflection asymmetric deformation is one of the current topics of a growing interest in high-spin nuclear structure physics. Regions in the (N, Z) plane where we can expect the existence of reflection-asymmetric SD nuclei have been investigated[1)~5)] mainly by means of the Strutinsky-type calculations of the collective potential energy surface (see also Refs. 6) and 7) for other approaches). Concerning the physical condition for the occurrence of the octupole instability, Nazarewicz and Dobaczewski[8)] have recently discussed the connection between the dynamical symmetry of the anisotropic harmonic-oscillator with frequencies in rational ratio and the multi-cluster configurations. They have suggested that the closed-shell configurations in the prolate SD oscillator potential, defined as having the frequency ratio $\omega_\perp/\omega_z=2$, might be unstable (stable) against the octupole-type reflection asymmetric shapes when the single-particle levels are filled up to the major shells with $N_{\rm sh}$=even (odd), $N_{\rm sh}$ being the shell quantum number defined by $N_{\rm sh}=2n_\perp+n_z$ (see also the previous work, Ref. 9)). Their suggestion is in good qualitative agreement with the realistic shell-structure energy calculation by Höller and Åberg.[2)] We call the $N_{\rm sh}$-dependence of the octupole instability "odd-even effect in $N_{\rm sh}$".

We have suggested in Refs. 10) and 11) a possible relationship between the odd-even effect mentioned above and the "supershell effect" in reflection-asymmetric SD potentials. The general concept of supershell was originally introduced by Balian and Bloch[12)] in relation to the semi-classical theory of shell structure. Quite recently, the supershell effect has been observed, for the first time, in the mass abundance spectra of metal clusters. Theoretical analysis of this phenomenon has been made by Nishioka, Hansen and Mottelson.[13),14)]

As is well known, clustering of eigenvalues, that is, oscillating pattern in the energy-smoothed level density for single-particle motions in the mean field is called

shell structure.[15] In the semiclassical theory, classical periodic orbits having relatively short periods are responsible for the clustering of the levels; the frequencies in the level density oscillation are determined by the corresponding periods of classical motion.[16)~23)] When two families of short-period orbits interfere and produce an undulating pattern in the oscillating level density, this pattern is called supershell structure.[12),16)] In the case of the metal clusters, a beautiful beating pattern enveloping individual shell oscillations which is caused by the interference between the triangular and square orbits of an electron in a spherical Woods-Saxon potential has been demonstrated[13),14)] to nicely correspond to the experimental data.

In the case of the SD nuclei under consideration, an interference effect is expected to arise between the classical periodic orbits with period $T \approx 2\pi/\omega_\perp$ and those with $T \approx 2\pi/\omega_z$ of a nucleon in the reflection-asymmetric SD potential.[11] The main purpose of this paper is to show that the interference effect brings about another example of the supershell structure, which is intimately connected with the odd-even effect in $N_{\rm sh}$ mentioned above, and which is relevant to experimental investigations. It should be emphasized here that, contrary to the case of spherical potentials, the Hamiltonian describing the single-particle motions in a deformed mean field is non-integrable in general. Accordingly, our Hamiltonian system is a kind of mixed system whose phase space is composed both of regular and chaotic regions. As a consequence, properties of our phase space change in a quite sensitive manner when the shape of the nuclear surface is varied. In this paper, we shall show that the supershell effect becomes more significant with increasing octupole deformation. Possible origins of this enhancement of supershell pattern will be discussed in relation to the change in the properties of the classical periodic orbits as a function of the octupole deformation parameter.

After briefly reviewing the semiclassical theory of shell structure in § 2, we first apply in § 3 both the torus quantization method and the periodic-orbit quantization method to the case of the prolate SD oscillator potential. In this integrable limit, the supershell effect can be treated analytically. In § 4, a reflection-asymmetric SD potential model is introduced and the supershell pattern in the quantum level spectrum calculated for this potential is exhibited. In § 5, we investigate properties of classical motions in this potential, like stabilities and bifurcation phenomena of the periodic orbits. In § 6, we show that a nice correspondence holds between peak positions of the Fourier transform of quantum spectrum and periods of classical closed orbits; relative heights between peaks change as functions of the octupole-deformation parameter, providing us with a semiclassical interpretation of the origin and the octupole-deformation dependence of the supershell structure. Here, quantum signature of the bifurcations is also discussed. A summary of this work is given in § 7.

A preliminary version of this work was previously reported in this journal.[24)]

§ 2. Some elements of semiclassical theory of shell structure

In this section we briefly review some basic elements of the semiclassical theory of shell structure, which are necessary for later discussion.

2.1. *Torus quantization*

To begin with, let us consider the case of multi-dimensional, integrable Hamiltonian system, where the Hamiltonian can be written as a function of only action variables I_i, being independent of angle variables θ_i conjugate to them. Semiclassical quantization condition valid for such systems has been formulated by Einstein-Brillouin-Keller, and called torus quantization or the EBK quantization;

$$I_i(E_{n_1,\cdots,n_f})=\oint_i \boldsymbol{p}\cdot d\boldsymbol{q}=\hbar(n_i+\alpha_i/4)\,,\quad i=1,\cdots,f\,, \tag{2·1}$$

where indices i represent mutually independent paths on f-dimensional torus constructed by classical trajectories, α_i are Maslov indices related to the singularities of the Van Vleck determinant appearing in the semiclassical propagator along the path i. Thus, the semiclassical level density is given by

$$g(E)=\sum_{\{n\}}\delta(E-H(I_i=\hbar(n_i+\alpha_i/4)))\,. \tag{2·2}$$

The summation on the r.h.s. may be rewritten using the Poisson sum formula into the form of topological sum over periodic orbits.[25] In Ref. 25), spherical systems are analyzed and clear correspondence between the topological sum and the periodic orbits is shown. In the spherical case, periodic orbits generally satisfy the resonance condition, i.e., the frequency ratio of radial and angular motions are the same as that of topological indices. We shall apply this method to the SD harmonic oscillator potential in § 3, and discuss the correspondence between the topological indices and periodic orbits. There, it will be shown that some "partially-resonant" terms play an important role giving rise to the supershell effect.

2.2. *Periodic-orbit quantization*

Next, let us consider the case of multi-dimensional non-integrable Hamiltonian system. For such systems, as is well known, the periodic-orbit quantization method provides us with a useful base toward understanding the correspondence between classical periodic orbits and properties of quantum spectra.[22),26)] This theory is essentially based on the path integral formalism of quantum mechanics. The first step is to express the quantum level density $g(E)=\sum_n\delta(E-E_n)$ in terms of a trace of the energy-dependent Green function,

$$\begin{aligned} g(E)&=-\frac{1}{\pi}\mathrm{Im}\,\mathrm{Tr}\frac{1}{E+i\epsilon-\hat{H}} \\ &=-\frac{1}{\pi}\mathrm{Im}\int d\boldsymbol{q}G(\boldsymbol{q},\boldsymbol{q};E)\,. \end{aligned} \tag{2·3}$$

The Green function $G(\boldsymbol{q}'',\boldsymbol{q}';E)$ is a Fourier transform of the transition amplitude $K(\boldsymbol{q}'',t;\boldsymbol{q}',0)=\langle\boldsymbol{q}''|\exp(-it\hat{H}/\hbar)|\boldsymbol{q}'\rangle\cdot\theta(t)$, and we can express it in the path integral form. Evaluation of the path integral by the stationary phase approximation (SPA) extracts the classical trajectories. The Fourier transformation is also performed by means of the SPA. Finally, the trace integral appearing in Eq. (2·3) extracts the periodic orbits and one obtains the following expression called the Gutzwiller trace

formula:

$$g(E)\simeq \bar{g}(E)+\sum_{n,\gamma}A_{n\gamma}(E)\cos(nS_\gamma(E)/\hbar-(\pi/2)\mu_{n\gamma})\,, \tag{2·4}$$

where $\bar{g}(E)$ denotes the average level density and the second term on the r.h.s. represents the oscillating part. The summation is taken over all periodic orbits and their multiple traversals. S_γ is a classical action along the orbit γ, $S_\gamma=\oint_\gamma \boldsymbol{p}\cdot d\boldsymbol{q}$, and μ_γ is a Maslov phase. The amplitude factor $A_{n\gamma}$ depends on the phase space structure about the periodic orbit γ, as we shall discuss in § 2.4. For sufficiently isolated orbits, the trace integral is well approximated by the SPA and the amplitude factor for the n-fold traversal of orbit γ can be written as[26]

$$A_{n\gamma}=\frac{1}{\pi\hbar}\frac{T_\gamma}{\sqrt{|\det(1-M_\gamma^n)|}}\,, \tag{2·5}$$

where T_γ and M_γ represent the period and the monodromy matrix of the primitive orbit γ, respectively. This expression is known to work well for chaotic systems such as billiards.[21]

2.3. *Stability of classical trajectories*

The amplitude factor in the trace formula is related with the properties of phase space around the periodic orbits. Let us write the Hamilton equation in $2f$-dimensional phase space as

$$\frac{d}{dt}Z=\Lambda\nabla H \tag{2·6}$$

with

$$Z=\begin{pmatrix}\boldsymbol{p}\\ \boldsymbol{q}\end{pmatrix},\quad \nabla=\begin{pmatrix}\nabla_p\\ \nabla_q\end{pmatrix},\quad \Lambda=\begin{pmatrix}0 & -1\\ 1 & 0\end{pmatrix},$$

and consider the time evolution of the deviation $\delta Z(t)$ from the reference classical trajectory $Z_0(t)$. To the first order in δZ, we obtain

$$\frac{d}{dt}\delta Z=\Lambda\mathcal{H}\,\delta Z\,, \tag{2·7}$$

where $\mathcal{H}$ is the Hessian matrix defined by

$$\mathcal{H}=\begin{pmatrix}H_{pp} & H_{pq}\\ H_{qp} & H_{qq}\end{pmatrix}_{Z_0},\quad (H_{pq})_{ij}=\frac{\partial^2 H}{\partial p_i\partial q_j}\quad \text{etc}\,. \tag{2·8}$$

Knowing $\mathcal{H}(t)$, Eq. (2·7) can be easily integrated,

$$\delta Z(t)=\exp\Big[\Lambda\int_0^t dt'\mathcal{H}(Z_0(t'))\Big]\delta Z(0)\equiv\mathcal{M}(t)\delta Z(0)\,. \tag{2·9}$$

$\mathcal{M}$ is called the stability matrix. It is real and symplectic; $\Lambda\mathcal{M}^T\Lambda^{-1}=\mathcal{M}^{-1}$. When one takes a periodic orbit as the reference trajectory and the period T as time t, the stability matrix is particularly called monodromy matrix $M_\gamma\equiv\mathcal{M}(T_\gamma)$.[27] It is known

that the eigenvalues of M_γ are independent of the initial condition $Z(0)$ on the orbit. According to the symplectic property of the monodromy matrix, its eigenvalues appear in pairs $(+/-)(e^\alpha, e^{-\alpha})$, where α is real or pure imaginary. When α is pure imaginary ($\alpha=iw$), the orbit is stable and torus exists surrounding it. w is called a winding number of the torus. When α is real ($\alpha=\lambda T$), the orbit is unstable and λ is called the Lyapunov exponent which measures the degree of instability.

2.4. *Magnitudes of shell effects*

Strength of the shell effect depends mainly on three factors, to be discussed below, associated with the periodic orbits.[18]

The first factor is the degeneracy of the orbit. Here the term 'degeneracy' means the number of independent continuous parameters (additional to energy) that specify a certain orbit from a continuous family of orbits having the same action. For example, planar orbits in a spherical potential form a continuous family generated by rotation and the degeneracy is generally three, since a certain orbit belonging to this family is specified by three Euler angles. As illustrated by the above example, degeneracy is related to continuous symmetry of the system. These degeneracies correspond to the unit eigenvalues of M.

The second factor is the stability of the orbit. For non-integrable systems, evaluating the trace integral by the SPA, one sees that the amplitude behaves as

$$A_{n\gamma} \propto \frac{1}{\sqrt{|\det(\mathbf{1}-\tilde{M}_\gamma^n)|}}, \tag{2·10}$$

where $\tilde{M}$ is a reduced monodromy matrix in which degrees of freedom corresponding to the unit eigenvalues of M are excluded out. The more unstable is the orbit, the weaker is its contribution to the level density, because it has a large Lyapunov exponent and the denominator on the r.h.s. becomes large. The above proportionality is valid only when all the eigenvalues of $\tilde{M}$ are sufficiently distant from unity. However, one of the eigenvalues may happen to be very close to unity. This is called nonlinear resonance where two frequencies of the torus coincide with each other and gives rise to a periodic orbit bifurcation. Namely, the period n-upling bifurcation occurs when $\det(\mathbf{1}-\tilde{M}_\gamma^n)=0$. In this resonance region, one has to use a more sophisticated treatment than the SPA; for example, the uniform approximation using the resonant normal form. Such a procedure is formally discussed by Ozorio de Almeida and Hannay,[28] but, to the best of our knowledge, application of this theory to multi-dimensional, non-integrable Hamiltonian system has not been performed yet.

The third factor is the phase space volume occupied by an orbit. It is not important in our analysis because it is insensitive to the variation of potential parameters.

Let us examine how these three factors enter in the amplitude factors for different types of periodic orbits. First, consider a chaotic orbit, that is, a well-isolated orbit whose degeneracy equals zero. Its amplitude factor is given by Eq. (2·5). There appears the same stability factor as Eq. (2·10), and the period T measures the phase space volume of the orbit. Next, as an example of non-isolated orbits, let us consider orbits in axially symmetric deformed potentials, whose degeneracy equals one corre-

sponding to the rotation about the symmetry axis. It is convenient to use the cylindrical coordinates (ρ, φ, z). One should then perform the integral uniformly with respect to φ in the trace, because in this direction periodic orbits exist continuously. Thus we obtain the following expression of the amplitude factor for these orbits (see the Appendix):

$$A_{n\gamma}(E)=\frac{4\pi}{(2\pi\hbar)^{3/2}}\frac{B_\gamma}{\sqrt{|2-\mathrm{Tr}\tilde{M}_\gamma^{\,n}|}},$$

$$B_\gamma=\int_0^{T_\gamma}dt\left|\frac{\partial\varphi(t+T_\gamma)}{\partial p_\varphi(t)}\right|^{-1/2}. \tag{2·11}$$

Here, B_γ contains the first and the third factors mentioned above. The period n-upling bifurcation occurs when $\mathrm{Tr}\tilde{M}_\gamma^{\,n}=2$.

§ 3. Supershell effect in the SD oscillator

In this section we apply the semiclassical theories to the axially-symmetric 2:1 deformed harmonic oscillator Hamiltonian

$$H_0(\boldsymbol{p}, \boldsymbol{q})=\frac{\boldsymbol{p}^2}{2M}+\sum_{i=x,y,z}\frac{M\omega_i^{\,2}q_i^{\,2}}{2}, \tag{3·1}$$

where $\omega_x=\omega_y\equiv\omega_\perp=2\omega_z\equiv 2\omega_{\mathrm{sh}}$, and we discuss how the supershell structure emerges in this case. We compare the two semiclassical quantization methods summarized in the preceding section, and discuss their relations.

3.1. *The periodic orbit method*

In this subsection we analyze the supershell effect in the SD oscillator defined by (3·1) using the Gutzwiller trace formula. The trace formula can be derived also for such an integrable system if the degeneracy (mentioned below) is properly taken into account. According to Ref. 29), the semiclassical level density may be written as

$$g(E)\simeq\bar{g}(E)+g_{\mathrm{osc}}^{(\mathrm{IV})}(E)+g_{\mathrm{osc}}^{(\mathrm{II})}(E). \tag{3·2}$$

The first term on the r.h.s. represents the mean level density,

$$\bar{g}(E)=\frac{1}{(2\pi\hbar)^3}\int d\boldsymbol{p}d\boldsymbol{q}\delta(E-H(\boldsymbol{p}, \boldsymbol{q}))=\frac{E^2}{8(\hbar\omega_{\mathrm{sh}})^3}. \tag{3·3}$$

The second and the third terms are the oscillating parts representing the shell effects. The superscripts (II) and (IV) denote the degeneracies of the periodic orbits. $g_{\mathrm{osc}}^{(\mathrm{IV})}(E)$ is a contribution from four-hold degenerate orbits whose periods are multiples of $T^{(\mathrm{IV})}=2\pi/\omega_{\mathrm{sh}}$. The present model is very special in the sense that all trajectories are periodic, and one should explicitly perform four integrals (corresponding to the degeneracy) in evaluating the trace formula. Thus one obtains the following expression:

$$g_{\mathrm{osc}}^{(\mathrm{IV})}(E)=\sum_{m\neq 0}\frac{E^2}{8(\hbar\omega_{\mathrm{sh}})^3}\cos\left[m\left(\frac{S^{(\mathrm{IV})}}{\hbar}-(4+4+2)\frac{\pi}{2}\right)\right]$$

$$= \sum_{m=-\infty}^{\infty} \frac{E^2}{8(\hbar\omega_{sh})^3} \cos\left[m\left(\frac{ET^{(IV)}}{\hbar} - 5\pi\right)\right] - \bar{g}(E), \tag{3·4}$$

$$= \sum_{N} \frac{(N+5/2)^2}{8} \delta\left(E - \hbar\omega_{sh}\left(N+\frac{5}{2}\right)\right) - \bar{g}(E), \tag{3·5}$$

where $S^{(IV)}=ET^{(IV)}$ is the action integral along the primitive periodic orbit and the sum over m accounts for multiple traversals. The last expression is obtained by using the Poisson sum formula

$$\sum_{m=-\infty}^{\infty} \exp(2\pi i m A) = \sum_{N=-\infty}^{\infty} \delta(A-N). \tag{3·6}$$

In Eq. (3·2), $g_{osc}^{(II)}(E)$ is the contribution from two-fold degenerate orbits whose periods are odd integer times $T^{(II)}=T^{(IV)}/2$. It is obtained in a similar manner, except that the integrations with respect to the z direction may be performed by the SPA. The result is written as

$$g_{osc}^{(II)}(E) = \sum_{m'=\text{odd}} \frac{E}{8(\hbar\omega_{sh})^2 \sin(m'\pi/2)} \sin\left[m'\left(\frac{S^{(II)}}{\hbar} - (2+2)\frac{\pi}{2}\right)\right]$$

$$= \sum_{m=-\infty}^{\infty} \frac{E}{8(\hbar\omega_{sh})^2} \cos\left[(2m+1)\left(\frac{ET^{(II)}}{\hbar} - \frac{5\pi}{2}\right)\right], \tag{3·7}$$

$$= \sum_{N} (-)^N \frac{N+5/2}{8} \delta\left(E - \hbar\omega_{sh}\left(N+\frac{5}{2}\right)\right), \tag{3·8}$$

where the sum over m' accounts for multiple traversals of the primitive periodic orbit. The expressions (3·4) and (3·7) were first derived in Ref. 29).

Summing up the above three contributions, we obtain the degeneracy d_N of the N-th shell as

$$d_N = \frac{([N/2]+1)([N/2]+2)}{2} + \frac{3}{32}, \tag{3·9}$$

where $[*]$ is the Gauss symbol. The first term on the r.h.s. corresponds to the exact degeneracy of the quantum spectrum. We thus see that the result obtained by the trace formula is very accurate (the deviation from the exact quantum result is only 3/32).

Now let us focus our attention on a smoothed density of levels with finite energy resolution $\delta E=\hbar\omega_{sh}$. It is then sufficient to consider a finite number of periodic orbits of short periods satisfying the following uncertainty relation:

$$T \leq T_{max} = \frac{2\pi\hbar}{\delta E}. \tag{3·10}$$

As far as gross properties of the level density is concerned, therefore, the well-known problem of the long time propagation in the semiclassical approximation does not occur.

We show in Figs. 1(a) and (b) the contributions from the families of periodic orbits with periods $2\pi/\omega_{sh}$ and $2\pi/\omega_{\perp}$, respectively, and in Fig. 1(c) the sum of them. There appears an undulating pattern in the level density due to the interference of the

above two families of periodic orbits, which is just the supershell structure. Thus, one sees that the supershell structure emerges from this interference effect.

3.2. *The EBK method*

Defining the action-angle variables (I_i, θ_i) by

$$p_i=\sqrt{2M\omega_i I_i}\sin\theta_i\,,$$
$$q_i=\sqrt{2I_i/M\omega_i}\cos\theta_i\,, \qquad (3\cdot11)$$

we write the Hamiltonian (3·1) as a function of only action variables as $H_0(\boldsymbol{I})=\boldsymbol{\omega}\cdot\boldsymbol{I}$. The Maslov indices are 2 for all paths i, and therefore the EBK quantization condition becomes

$$I_i=\hbar(n_i+1/2)\,. \qquad (3\cdot12)$$

In the present case, this EBK quantization gives exact quantum eigenvalues: $E=\sum_i\hbar\omega_i(n_i+1/2)$. Now let us investigate the roles of classical periodic orbits in giving rise to the supershell structure in the quantum spectrum. For this purpose, we use the method of topological sum.[25] The semiclassical level density is written as

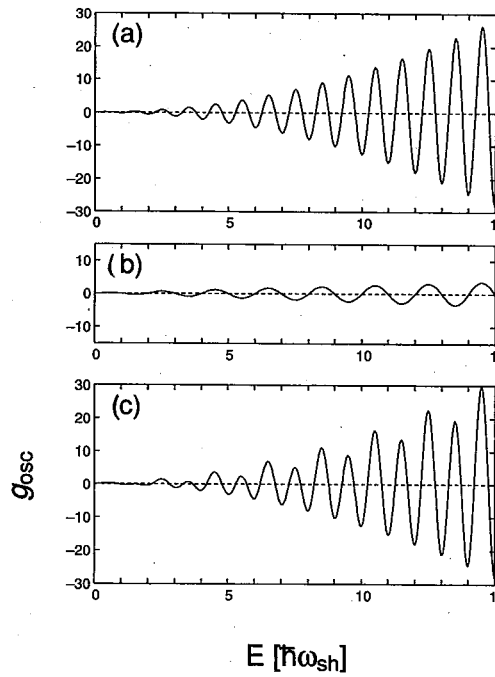

Fig. 1. Results of semiclassical calculation of the oscillating part of the level density for the SD oscillator model. (a) The contribution from orbits with $T=2\pi/\omega_z$, (b) the contribution from orbits with $T=2\pi/\omega_\perp$ and (c) the supershell structure caused by the interference between the above two families of orbits.

$$g(E)=\sum_{\{n\}}\delta(E-\sum_i\hbar\omega_i(n_i+\alpha_i/4))\,. \qquad (3\cdot13)$$

Using the Poisson sum formula (3·6), one can rewrite Eq. (3·13) as

$$g(E)=g_0(E)+\sum_{M\neq0}g_M(E)\,, \qquad (3\cdot14)$$

where

$$g_M(E)=\frac{1}{\hbar^3}\int_0^\infty d\boldsymbol{I}\delta(E-\boldsymbol{\omega}\cdot\boldsymbol{I})\exp(2\pi i\boldsymbol{M}\cdot(\boldsymbol{I}/\hbar-\boldsymbol{\alpha}/4))\,, \qquad (3\cdot15)$$

and the summation is taken over all the combinations of integers, $\boldsymbol{M}=(M_x, M_y, M_z)$. Here, $g_0(E)$ represents a mean level density corresponding to the Thomas-Fermi approximation,

$$g_0(E)=\frac{1}{\hbar^3}\int_0^\infty d\boldsymbol{I}\delta(E-\boldsymbol{\omega}\cdot\boldsymbol{I})=\frac{E^2}{8(\hbar\omega_{sh})^3}\,. \qquad (3\cdot16)$$

The remaining terms with non-zero $\boldsymbol{M}$ represent the oscillating part responsible for the shell structure. To simplify the expression, we introduce the notation $f_i = 2\pi M_i \omega_{\rm sh}/\omega_i$. The dominant contribution comes from terms satisfying the resonance condition $\boldsymbol{M} = \boldsymbol{M}^* \propto \boldsymbol{\omega}$, i.e., $f_x = f_y = f_z$ (in the present case, $\boldsymbol{M} = m(2, 2, 1)$). Carrying out the integration with respect to $\boldsymbol{I}$ and denoting the sum over such resonant terms as $g_{\rm osc}^{\rm (i)}$, we obtain

$$g_{\rm osc}^{\rm (i)}(E) = \frac{E^2}{8(\hbar\omega_{\rm sh})^3} \sum_{m\neq 0} e^{2\pi i m(E/\hbar\omega_{\rm sh} - 5/2)} . \tag{3·17}$$

Next, let us consider the 'partially resonant' terms which satisfy the condition $f_i = f_j \equiv f_\perp \neq f_k$. Carrying out the integration with respect to $\boldsymbol{I}$, they are evaluated as

$$\begin{aligned} & g_{M({\rm part.res.})}(E) \\ & = \frac{1}{4(\hbar\omega_{\rm sh})^2} \left(\frac{E}{i(f_\perp - f_k)} e^{if_\perp E/\hbar\omega_{\rm sh}} + \frac{\hbar\omega_{\rm sh}}{(f_\perp - f_k)^2} \left(e^{if_\perp E/\hbar\omega_{\rm sh}} - e^{if_k E/\hbar\omega_{\rm sh}} \right) \right) e^{i\pi M\cdot\alpha/2} \\ & \simeq \frac{1}{4(\hbar\omega_{\rm sh})^2} \frac{E}{i(f_\perp - f_k)} e^{if_\perp E/\hbar\omega_{\rm sh}} e^{i\pi M\cdot\alpha/2} , \end{aligned} \tag{3·18}$$

where the second term on the r.h.s. is neglected because it is higher-order in $\hbar$. Let us then take terms with $f_x = f_y \equiv f_\perp \neq f_z$, and write $\boldsymbol{M}$ as (m', m', l). Summing over terms with odd-m' and arbitrary integer l, we obtain

$$\begin{aligned} g_{\rm osc}^{\rm (ii)}(E) &= \sum_{m'={\rm odd}} \sum_{l=-\infty}^{\infty} \frac{1}{4(\hbar\omega_{\rm sh})^2} \frac{E}{2\pi i(m'/2 - l)} e^{2\pi i m' E/2\hbar\omega_{\rm sh}} \cdot e^{-2\pi i\{2m' + l\}/2} \\ &= \frac{E}{8(\hbar\omega_{\rm sh})^2} \sum_{m=-\infty}^{\infty} e^{i\pi(2m+1)(E/\hbar\omega_{\rm sh} - 5/2)} . \end{aligned} \tag{3·19}$$

The last expression is obtained using the expansion formula of cosecond in partial fractions:

$$\mathrm{cosec} z = \sum_{l=-\infty}^{\infty} \frac{(-)^l}{z - l\pi} . \tag{3·20}$$

It can be easily shown in a similar way that the sum of other terms which are the same order in $\hbar$ as (3·19) vanishes.

3.3. *Relation between the two methods*

Now, let us discuss the correspondence between the results obtained by the periodic-orbit method and the EBK method. It is evident that the two terms $g_{\rm osc}^{\rm (i)}(E)$ and $g_{\rm osc}^{\rm (ii)}(E)$ in the EBK treatment are identical with the contributions $g_{\rm osc}^{\rm (IV)}(E)$ and $g_{\rm osc}^{\rm (II)}(E)$ which are evaluated by the trace formula for the periodic orbits with periods $2\pi/\omega_{\rm sh}$ and $2\pi/\omega_\perp$, respectively. This result is very instructive to understand the physical meanings of the resummation with respect to the indices $\boldsymbol{M}$ by the use of the Poisson sum formula. The indices satisfying the resonance condition, $\boldsymbol{M} = m(2, 2, 1)$, correspond to a family of classical orbits with periods $2m\pi/\omega_{\rm sh}$. One can examine this by comparing Eqs. (3·4) and (3·17). On the other hand, for partially-resonant contributions, we find the correspondence in the following way. Comparing

Eqs. (3·7) and (3·19), we notice that the family of planar orbits in the (x, y) plane corresponds to the summation over indices $\boldsymbol{M}=(1, 1, l)$ with $-\infty<l<\infty$. Its m-fold traversals are related with $\boldsymbol{M}=(m, m, l)$. These partially-resonant terms play important roles in formation of the supershell structure in the present model.

§ 4. Reflection-asymmetric SD oscillator model

4.1. *Model Hamiltonian*

Let us consider a model Hamiltonian consisting of an axially-symmetric 2:1 deformed harmonic oscillator and a doubly-stretched octupole (Y_{30}) deformed potential,

$$H=\frac{\boldsymbol{p}^2}{2M}+M\omega_0{}^2\left(\frac{r^2}{2}-\lambda_{30}r^2Y_{30}(\theta)\right)'', \tag{4·1}$$

where double primes indicate that the variables in parenthesis are defined in terms of the doubly-stretched coordinates $q_i''=(\omega_i/\omega_0)q_i$ and $\omega_0=(\omega_x\omega_y\omega_z)^{1/3}$. As emphasized by Sakamoto and Kishimoto,[30] the doubly-stretched coordinates are suited to description of systems having quadrupole equilibrium deformations, and possess several advantages over the usual coordinates; for example, the center of mass motion is exactly decoupled from the octupole-type deformations described by the above Hamiltonian. Note that the doubly-stretched octupole operator is in fact a linear combination of the ordinary dipole and octupole operators, although we sometimes omit the adjective "doubly-stretched" for simplicity. In (4·1), we adopt the quadratic radial dependence for the octupole-deformed potential for the ease of taking into account the volume conservation condition. By requiring the volume surrounded by an equipotential surface to be independent of the octupole deformation parameter λ_{30}, the λ_{30}-dependence of ω_0 is determined as

$$\omega_0(\lambda_{30})=\omega_0(0)\left[\frac{1}{4\pi}\int d\Omega(1-2\lambda_{30}Y_{30}(\Omega))^{-3/2}\right]^{1/3}. \tag{4·2}$$

We note that the average level density $\bar{g}(E)$ is independent of λ_{30} when ω_0 satisfies Eq. (4·2). Let us define dimensionless variables as

$$\begin{cases} p_i\to\sqrt{M\hbar\omega_0}\,p_i, \\ q_i\to\sqrt{\hbar/M\omega_0}\,q_i, \\ H\to\hbar\omega_0 H. \end{cases} \tag{4·3}$$

Then the Hamiltonian (4·1) becomes

$$H=\frac{\boldsymbol{p}^2}{2}+\left(\frac{r^2}{2}-\lambda_{30}r^2Y_{30}(\theta)\right)''. \tag{4·4}$$

Since this potential is a homogeneous function of the second order in coordinates, the scaling relation

$$H(\alpha\boldsymbol{p}, \alpha\boldsymbol{q})=\alpha^2H(\boldsymbol{p}, \boldsymbol{q}) \tag{4·5}$$

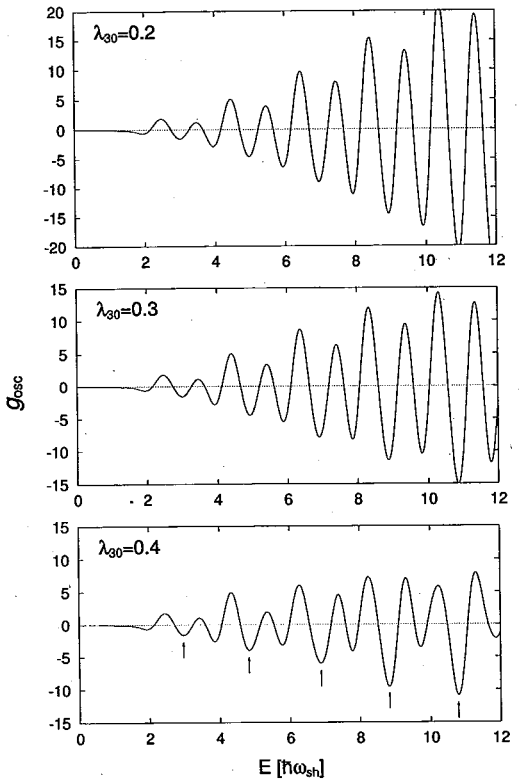

Fig. 2. Oscillating parts of the level density for the Hamiltonian (4·4) with $\lambda_{30}=0.2$, 0.3 and 0.4, calculated by means of the Strutinsky method with the smoothing width $\gamma=0.5\hbar\omega_{sh}$. The arrows indicate the minima associated with the even-N_{sh} closure.

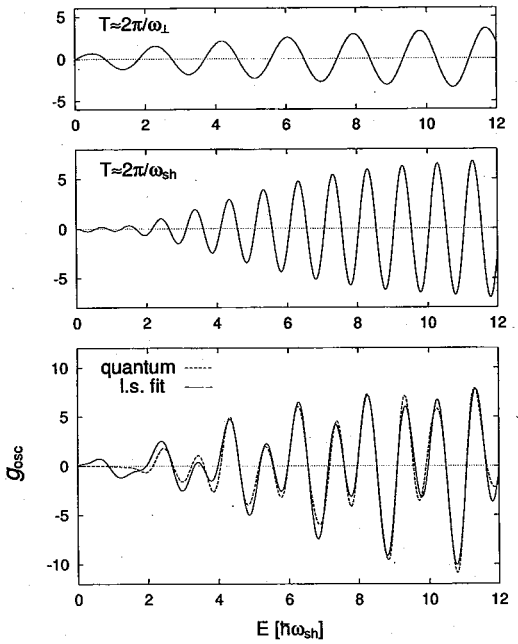

Fig. 3. The oscillating part of the level density at $\lambda_{30}=0.4$ obtained by the Strutinsky method (broken line) is compared with a superposition (solid line) of $\cos(ET_\gamma/\hbar)$ with the period T_γ evaluated for the classical orbit A ($T\approx 2\pi/\omega_\perp$) and that for orbits B, C, C', and 2A ($T\approx 2\pi/\omega_{sh}$) (see § 5 for the properties of these classical orbits). Amplitudes and phases of these cosine functions are determined so that the solid line best agrees with the broken line, except that the energy dependence of the amplitudes is assumed to fulfill the relation in Eq. (6·1) determined by the scaling property of the system under consideration (see § 6).

holds. Thus, if $(\boldsymbol{p}(t), \boldsymbol{q}(t))$ is a solution of the Hamilton equation with energy E, $(\alpha\boldsymbol{p}(t), \alpha\boldsymbol{q}(t))$ is also a solution but with energy $\alpha^2 E$. Namely, once the classical properties of the system are known on a certain energy surface E_0, properties on other energy surface E are obtained by scale-transforming the phase space variables $(\boldsymbol{p}, \boldsymbol{q})$ to $(\alpha\boldsymbol{p}, \alpha\boldsymbol{q})$ with $\alpha=\sqrt{E/E_0}$.

4.2. *Supershell structure*

Figure 2 shows the oscillating part of the level density for the Hamiltonian (4·4) calculated by means of the Strutinsky method. A characteristic property of the oscillating level density is that it exhibits the supershell pattern. Figure 3 gives a phenomenological illustration of the concept of the supershell. It is seen from this figure that the oscillating level density can be represented as a superposition of trigonometrical functions, $\cos(ET_\gamma/\hbar)$ with $T_\gamma\approx 2\pi/\omega_\perp$ and $2\pi/\omega_{sh}$, in a good approximation. We shall confirm in § 6 that this supershell pattern in fact arises from an interference effect between two families of classical periodic orbits with periods

$T_\gamma \approx 2\pi/\omega_{\rm sh}$ and $2\pi/\omega_\perp$.

It should be recalled here that the important factor from the point of view of gaining the shell-structure energy is not the heights of the maxima but the depths of the minima in the oscillating level density. Needless to say, the minima in Fig. 3 correspond to the closed-shell configurations with respect to the SD major shell quantum number $N_{\rm sh}$. Let us notice how the depths of the minima change as functions of λ_{30}. Then we find that the minima associated with the odd-$N_{\rm sh}$ closures become shallower as λ_{30} increases, whereas those at the even-$N_{\rm sh}$ closures are tough. Consequently, the odd-even staggering of the minima with respect to the $N_{\rm sh}$ quantum number develops with increasing λ_{30}. Possible mechanisms of the enhancement of the supershell structure will be discussed in § 6.

§ 5. Classical analysis

In this section, we discuss the classical-mechanical properties of the single-particle motion in the reflection-asymmetric SD potential defined in the preceding section.

5.1. *Poincaré map*

Let us examine classical phase space structure by plotting the Poincaré map.[21] Since our Hamiltonian is axially symmetric, it reduces to a two-dimensional one with the cylindrical coordinates (ρ, z) and with a definite angular momentum $p_\varphi = m$,

$$H = \frac{1}{2}(p_\rho^2 + p_z^2) + V_{\rm eff}(\rho, z; m), \tag{5·1}$$

where

$$V_{\rm eff}(z, \rho; p_\varphi) = \frac{p_\varphi^2}{2\rho^2} + \frac{4\rho^2 + z^2}{2} - \lambda_{30}\sqrt{\frac{7}{4\pi}}\frac{z^3 - 6z\rho^2}{\sqrt{4\rho^2 + z^2}}. \tag{5·2}$$

We can examine the Poincaré map for each value of m. It is convenient to choose the Poincaré section Σ as the surface with $p_\rho = 0$, which is intersected by any trajectory. Figure 4 shows calculated Poincaré maps (z, p_z) for the Hamiltonian (4·1) with various values of the octupole deformation parameter λ_{30}. We see that the system is quasi-integrable for small λ_{30} and almost all the phase space is foliated by KAM tori. With increasing λ_{30}, however, chaotic regions begin to spread out from the hyperbolic points. Figure 5 shows Poincaré maps for different values of p_φ. We note that the phase space volume corresponding to the (ρ, z) degrees of freedom contract and the system becomes more regular as p_φ increases.

Figure 6 shows Poincaré maps for the surface of section (ρ, p_ρ) with $z = 0$. The origin corresponds to the linear orbit along the z-axis and the structure around it is exhibited.

5.2. *Periodic orbits and their bifurcations*

While all trajectories are periodic when $\lambda_{30} = 0$, only very limited trajectories remain as periodic orbits when $\lambda_{30} \neq 0$. In the Poincaré section, centers of tori

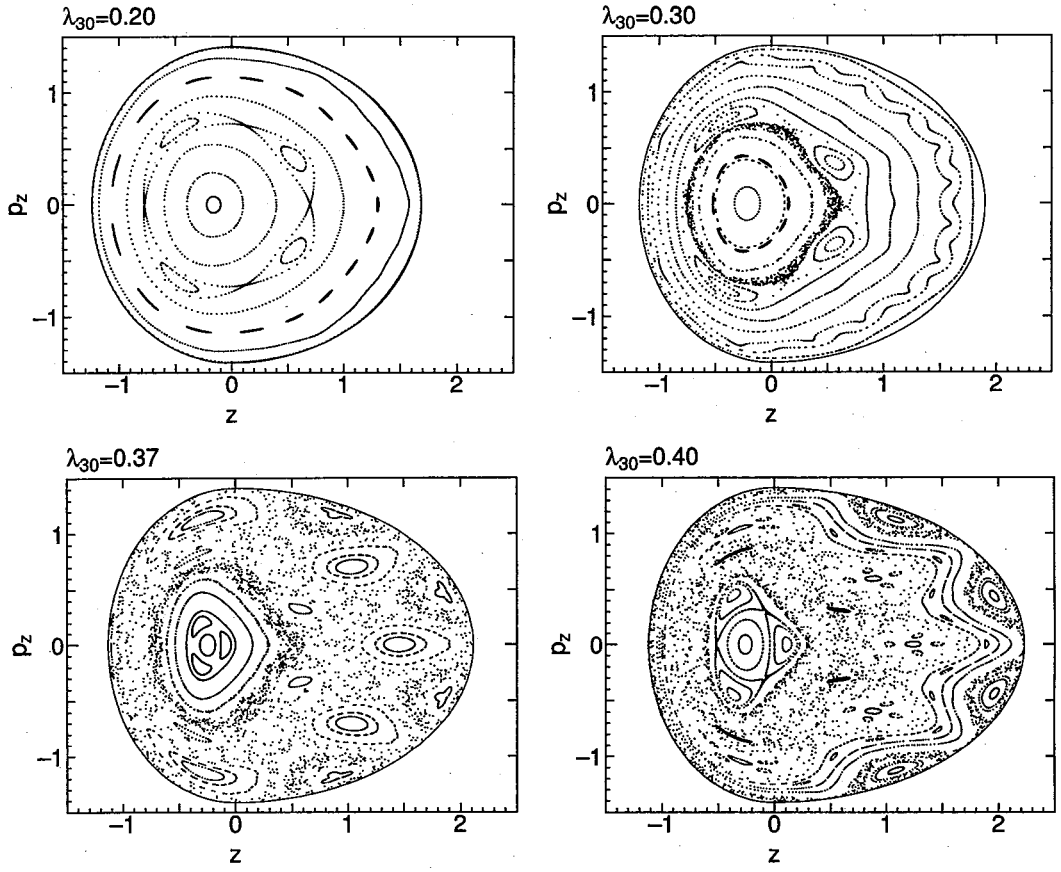

Fig. 4. Poincaré maps in the section (z, p_z) for the Hamiltonian (4·1) with $p_\varphi=0$ and with $\lambda_{30}=0.2 \sim 0.4$, defined by $p_\rho=0$ and $\dot{p}_\rho<0$.

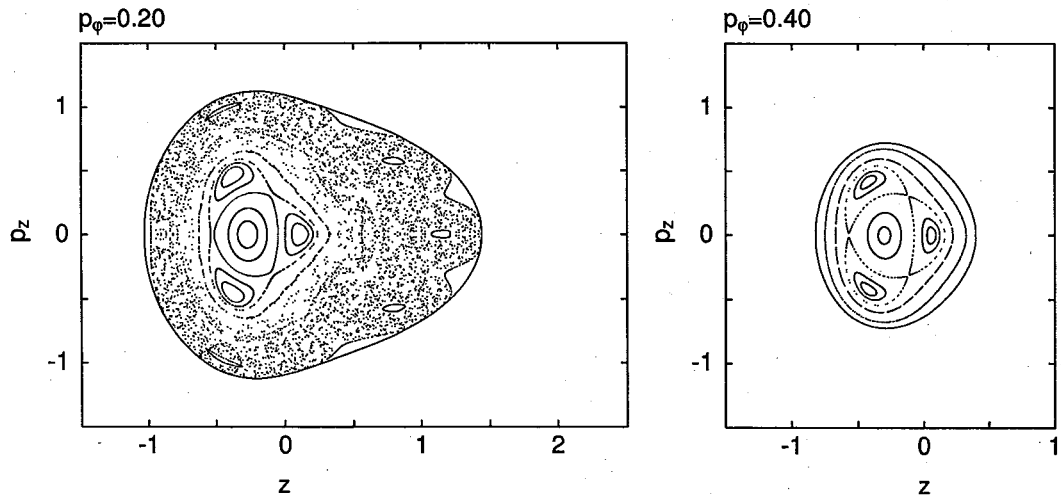

Fig. 5. Poincaré maps in the section (z, p_z) for the Hamiltonian (4·1) with $\lambda_{30}=0.4$ and with $p_\varphi/E=0.2$ and 0.4, defined by $p_\rho=0$ and $\dot{p}_\rho<0$.

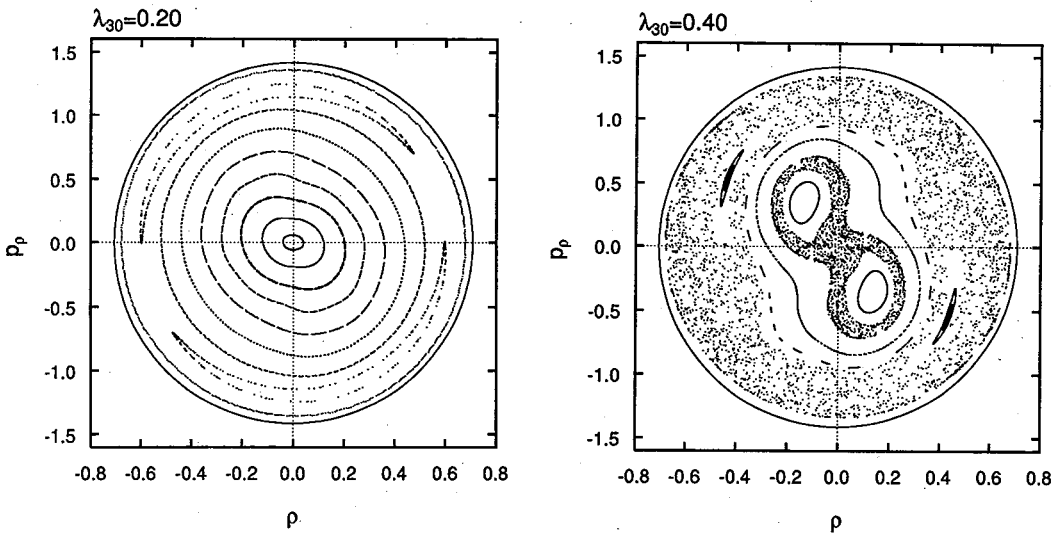

Fig. 6. Poincaré maps in the section (ρ, p_ρ) for the Hamiltonian (4·1) with $p_\varphi=0$ and with $\lambda_{30}=0.2$ and 0.4, defined by $z=0$ and $p_z>0$.

correspond to stable periodic orbits, while saddles to unstable ones. We calculate the periodic orbits by the monodromy method proposed by Baranger, Davies and Mahoney.[27] In this method, periodic orbits are found in an iterative manner starting with approximate closed curves. By gradually changing λ_{30}, we can use the periodic orbits found for a slightly smaller value of λ_{30} as inputs for this procedure. Figure 7 shows short periodic orbits for Hamiltonian (4·1) with $\lambda_{30}=0.4$ obtained in this way. Also shown in Fig. 8 are planar orbits for $\lambda_{30}=0.3\sim0.4$. As λ_{30} increases, the phase space structure becomes more complicated due to bifurcations of stable periodic orbits. For example, a period-tripling bifurcation of orbit A occurs at $\lambda_{30}\simeq0.36$. Thereafter, orbit A bifurcates into orbits 3A (triple traversal of orbit A), E and F. In the Poincaré map for $\lambda_{30}=0.37$ (see Fig. 4), we can see three resonant island chains surrounding the central KAM torus, which are associated with the newly-born periodic orbits E and F. Likewise, a period-doubling bifurcation of orbit B occurs at $\lambda_{30}\simeq0.4$, from where orbit B bifurcates into orbits 2B (double traversal of orbit B) and K. Many higher

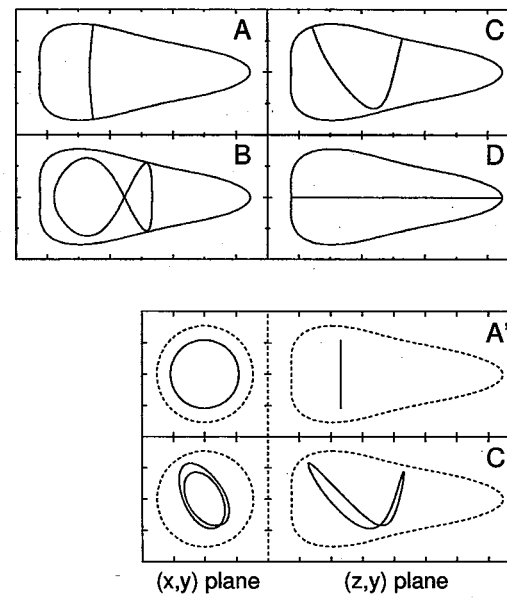

Fig. 7. Short periodic orbits for the Hamiltonian (4·1) with $\lambda_{30}=0.4$. Upper part: Planar orbits in the plane containing the symmetry axis z. Lower part: A circular orbit in the plane perpendicular to the symmetry axis (A') and a three-dimensional orbit (C'). Their projections on the (x, y) plane and on the (z, y) plane are shown.

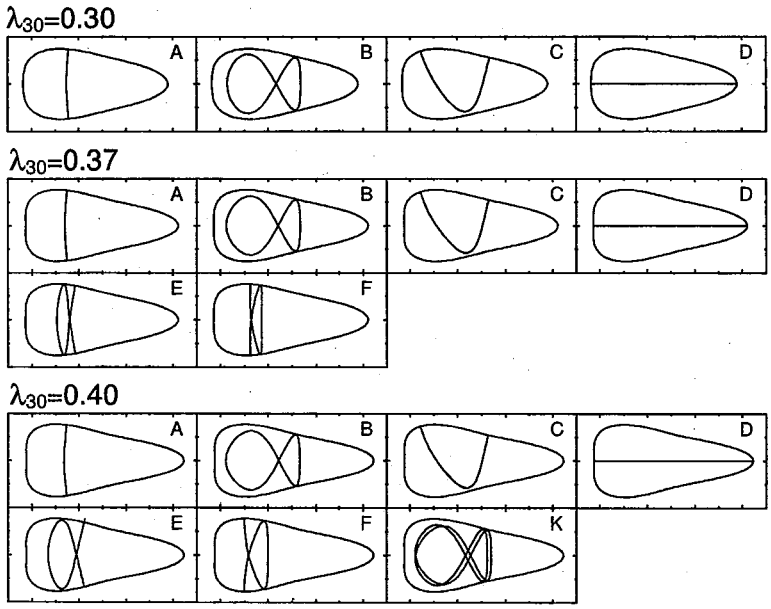

Fig. 8. Short planar orbits for the Hamiltonian (4·1) with $p_\varphi=0$ and $\lambda_{30}=0.3\sim0.4$.

Table I. Properties of the periodic orbits: periods T (in units of $1/\omega_{sh}(0)$) and traces of the reduced monodromy matrices TrM, evaluated for $\lambda_{30}=0$, 0.2, 0.3 and 0.4. Here, '$n\gamma$' denote the n-fold traversal of the primitive orbit γ. For the isolated orbit A' and D, the monodromy matrix M has two unit-eigenvalues and the remaining four eigenvalues appear in pairs $(e^{\alpha_a}, e^{-\alpha_a})$ and $(e^{\alpha_b}, e^{-\alpha_b})$. These pairs are identical ($\alpha_a=\alpha_b$) for orbit D, but they differ from each other for orbit A'. Traces of these pairs are given for orbit A'.

λ_{30}	0		0.2		0.3		0.4	
orbit	T/π	TrM	T/π	TrM	T/π	TrM	T/π	TrM
A	1	−2	1.018	−1.778	1.037	−1.362	1.062	−0.758
2A	2	2	2.036	1.161	2.075	−0.145	2.125	−1.426
3A	3	−2	3.054	−0.286	3.112	1.560	3.187	1.838
E	—	—	—	—	—	—	3.181	1.546
F	—	—	—	—	—	—	3.183	2.292
B	2	2	1.999	1.816	1.998	1.017	1.995	−2.054
2B	4	2	3.999	1.300	3.997	−0.966	3.989	2.221
K	—	—	—	—	—	—	3.989	1.572
C	2	2	2.001	2.030	2.004	2.383	2.009	4.277
D	2	2	2.072	1.845	2.177	3.498	2.367	−16.317
A'	1	−2, 2	1.024	−1.777, 1.992	1.050	−1.264, 1.960	1.086	−0.499, 1.869
C'	2	2	2.003	2.046	2.008	2.333	2.016	3.484

order bifurcations occur almost everywhere in regular regions of the phase space. Properties of the calculated periodic orbits are summarized in Table I for several values of λ_{30}.

§ 6. Semiclassical analysis

6.1. *The cause of the enhancement of the supershell effect*

As mentioned in § 2.4, strength of shell effect associated with a periodic orbit is mainly determined by degeneracy and stability of the orbit. Let us discuss how these properties change when the octupole deformation is added to the SD oscillator. When $\lambda_{30}=0$, orbits with the period $2\pi/\omega_{sh}$ and those with the period $2\pi/\omega_{\perp}$ have different degeneracies, 4 and 2, respectively. Therefore, the shell effect originating from the former families of orbits is much stronger than that from the latter. As a result, the interference effect between the two families of periodic orbit, i.e., the supershell effect, is rather weak. When $\lambda_{30}\neq 0$, in general, degeneracies of the orbits reduce to 1. (For orbits D and A' in Fig. 7 having special symmetry, the degeneracy is 0.) Thus, generally speaking, shell effects at $\lambda_{30}\neq 0$ are expected to become weaker in comparison with those in the $\lambda_{30}=0$ limit, and it seems hard to understand the enhancement mechanism of the supershell effect at $\lambda_{30}\neq 0$ in terms of the degeneracy property.

Next, let us consider the other factor, i.e., stability of periodic orbits. In Fig. 9 we show calculated values of TrM for relevant orbits as functions of λ_{30}. At $\lambda_{30}=0$, orbits with the period $2\pi/\omega_{sh}$ are resonant (Tr$M=2$), while orbits with the period $2\pi/\omega_{\perp}$ are non-resonant and take Tr$M=-2$. With increasing λ_{30}, TrM for orbits 2A (double traversal of orbit A) and B decrease and deviate from 2. At $\lambda_{30}\simeq 0.4$, a period-doubling bifurcation of orbit B occurs; a new stable orbit K is created and orbit B becomes unstable. Orbits C and C' are unstable for $\lambda_{30}>0$ and their values of TrM become larger as λ_{30} increases. According to the argument in § 2.4, we thus expect that the contributions of these orbits to the shell effect decrease with increasing λ_{30}. On the other hand, orbit A is stable and its TrM value approaches towards 2 as λ_{30} increases. This implies that the contribution of orbit A becomes more important. In this way, relative magnitude of the amplitude factors between the two families of orbits with the period $\approx 2\pi/\omega_{sh}$ and $\approx 2\pi/\omega_{\perp}$ changes so that the interference effect between them

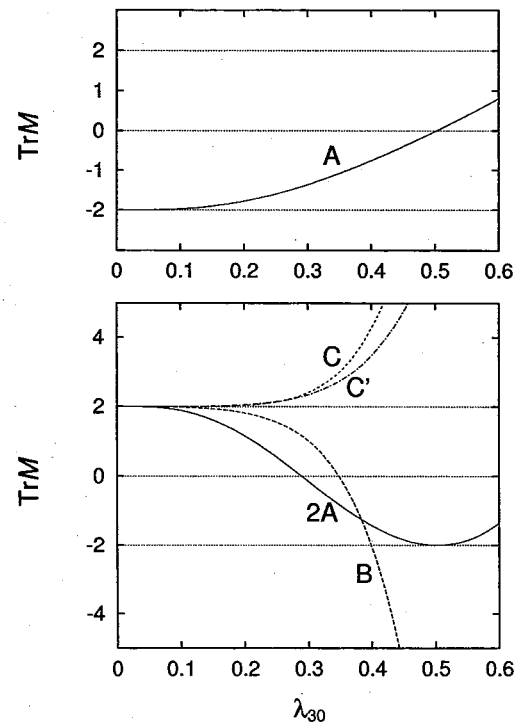

Fig. 9. Traces of the reduced monodromy matrices Tr$\tilde{M}$ for the non-isolated periodic orbits shown in Fig. 7 (see text for their definitions).

becomes stronger.

The above discussion is based on the expression (2·11) obtained by the SPA. We should note, however, that our classical phase space contains both regular and chaotic regions, i.e., our system is a mixed system. As is well known, such a system is abundant in the resonance regions where the SPA breaks down, so that the amplitude factors $A_{n\gamma}$ should be evaluated by means of a more sophisticated method beyond the SPA, e.g., the uniform approximation.[28] This is an interesting future subject, and we expect that the above consideration will remain valid, as long as a qualitative feature is concerned, even when nonlinear effects beyond the SPA are taken into account.

6.2. *Scaling properties and Fourier analysis*

By virtue of the scaling property, Eq. (4·5), the following scaling rules hold:

$$\begin{cases} S_\gamma(E)=ET_\gamma\,, \\ \bar{g}(E)=E^2\bar{g}(1)\,, \\ A_\gamma(E)=E^{d_\gamma/2}A_\gamma(1)\,; \end{cases} \tag{6·1}$$

where d_γ denotes the degeneracy of orbit γ; $d_\gamma=1$ for a general orbit and 0 for an isolated orbit like D or A' in Fig. 7.

Let us consider the Fourier transform

$$P(s)=\int dE e^{isE}E^{-d/2}g(E) \tag{6·2}$$

of the level density $g(E)$ multiplied by $E^{-d/2}$. (The factor $E^{-d/2}$ is attached here to compensate for the energy dependence of the amplitude factor A_γ; see below.) If one inserts the exact level density $g(E)=\sum_n\delta(E-E_n)$, it becomes

$$P^{(\mathrm{qm})}(s)=\sum_n E_n{}^{-d/2}e^{isE_n}\,. \tag{6·3}$$

This quantity can be evaluated with the use of the eigenvalues obtained by a quantum mechanical calculation. On the other hand, if we insert the semiclassical level density (2·4) in (6·2) and put $d=1$ appropriate to non-isolated orbits, then we obtain

$$P^{(\mathrm{cl})}(s)=\bar{P}(s)+\sum_{n,\gamma}A_{n\gamma}(1)e^{i\pi\mu_{n\gamma}/2}\delta(s-nT_\gamma)\,. \tag{6·4}$$

Here $\bar{P}(s)$ comes from $\bar{g}(E)$ and has a peak at $s=0$ associated with the orbits of zero length. On the other hand, the second term on the r.h.s. gives rise to sharp peaks at $s=nT_\gamma$ associated with the classical periodic orbits γ with periods T_γ (and their multiple traversals). Note that, owing to the scaling property (6·1), periods T_γ of the primitive orbits are equal to action $S_\gamma(1)$ calculated at $E=1$. If the trace formula is valid, one expect $P^{(\mathrm{cl})}\simeq P^{(\mathrm{qm})}$. Thus, we can extract information about classical periodic orbits by calculating $P^{(\mathrm{qm})}$. Namely, the amplitude factors and the Maslov phases of the periodic orbits may be obtained from absolute values and arguments of $P^{(\mathrm{qm})}(s)$, respectively.[12),31)]

Now, let us evaluate the Fourier transform (6·3). Since the summation is taken over a finite number of quantum levels in practice, we introduce the Gaussian cutoff and define a smoothed version of it;

$$P_{\Delta s}(s)=\int ds' P(s') f((s'-s)/\Delta s)\,, \tag{6·5}$$

where $f(x)$ is the Gaussian $f(x)=\exp(-x^2/2)$. For (6·3) and (6·4), we obtain

$$P_{\Delta s}^{(\mathrm{qm})}(s)=\sum_n E_n^{-d/2} e^{isE_n} f(E_n/E_{\max})\,, \tag{6·6}$$

$$P_{\Delta s}^{(\mathrm{cl})}(s)=\bar{P}_{\Delta s}(s)+\sum_{n,\gamma} A_{n\gamma}(1) e^{i\pi\mu_{n\gamma}} f((s-nT_\gamma)/\Delta s)\,, \tag{6·7}$$

where $E_{\max}=1/\Delta s$.

We calculate the eigenvalues by a matrix diagonalization method with the deformed oscillator bases, and use the lower part of the resulting spectrum. Figure 10 shows the absolute value of $P_{\Delta s}^{(\mathrm{qm})}(s)$ for $\lambda_{30}=0.2\sim0.4$ calculated with $E_{\max}=15\hbar\omega_{\mathrm{sh}}(\lambda_{30})$.

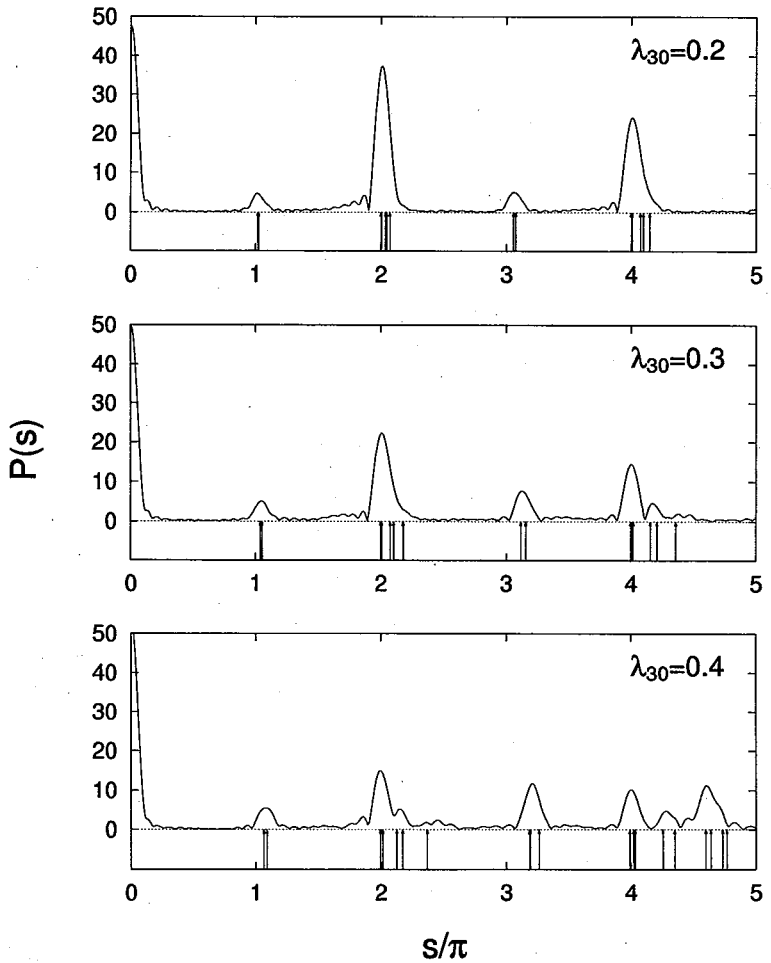

Fig. 10. Fourier transform $P_{\Delta s}^{(\mathrm{qm})}(s)$ of the level density $g(E)$ defined by Eq. (6·6), for $\lambda_{30}=0.2$, 0.3 and 0.4. $\omega_{\mathrm{sh}}(0)$ is put to 1. Gaussian cutoff is done with $E_{\max}=\hbar/\Delta s=15\hbar\omega_{\mathrm{sh}}(\lambda_{30})$. Arrows indicate periods of the classical periodic orbits (see Fig. 7) and of their repetitions. This figure is basically the same as Fig. 15 in our previous report;[11] but, accuracy of the numerical calculation is significantly improved so that the peak at $s/\pi\approx1$ is now clearly seen. This improvement greatly facilitates the discussion on the classical-quantum correspondence (see text).

The loci of the periods of classical periodic orbits and their multiple traversals are indicated by arrows in the figures. We see nice correspondence between the peaks of $P(s)$ and the periods of classical periodic orbits. Almost all peaks can be explained in terms of the classical orbits, indicating that the properties of quantum spectrum are characterized mostly by classical periodic orbits.

Next, let us notice the λ_{30} dependence of $P^{(\mathrm{qm})}(s)$. In Fig. 10 we see that the peak at $s\simeq 2\pi/\omega_{\mathrm{sh}}$ decreases, while the peak at $s\simeq\pi/\omega_{\mathrm{sh}}$ grows up with increasing λ_{30}. Since heights of the peaks in $P^{(\mathrm{qm})}(s)$ indicate intensities coming from the corresponding periodic orbits, this implies that the contributions from the orbits with the period $\approx\pi/\omega_{\mathrm{sh}}$ become increasingly important as λ_{30} increases. The change in relative intensity as a function of λ_{30} between the two families of periodic orbit seen in Fig. 10 may be responsible for the enhancement of the supershell effect in the reflection-asymmetric SD potential, in accordance with our discussion in the preceding subsection.

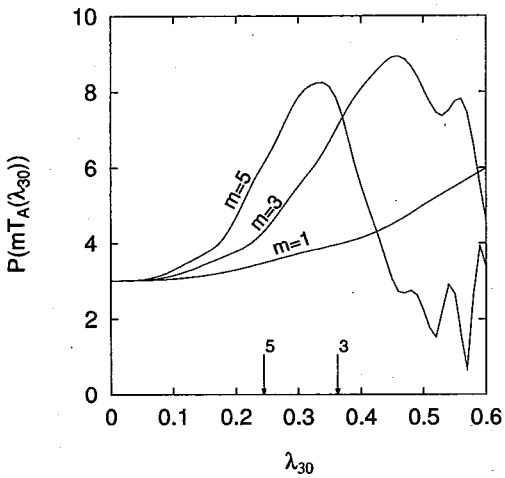

Fig. 11. Peak heights in the Fourier transform defined by Eq. (6·6) at the periods of classical periodic orbit A and of its multiple traversals (m=1, 3, 5), plotted as functions of λ_{30}. Gaussian cutoff is done with $E_{\max}=12\hbar\omega_{\mathrm{sh}}(\lambda_{30})$. Two arrows represent the period-tripling and period-5-upling bifurcation points.

6.3. *Quantum signature of bifurcations*

In order to see how the bifurcations (resonances) of periodic orbits affect the magnitudes of the Fourier amplitudes, let us evaluate the heights of the peak as functions of λ_{30} at the periods of the classical orbits. As examples, we take the period-tripling and the period-5-upling bifurcations of orbit A, which occur at $\lambda_{30}\simeq 0.36$ and 0.25, respectively. In Fig. 11 are plotted the calculated values of $P_{\Delta s}^{(\mathrm{qm})}(s)$ as functions of λ_{30} at specific values of s that correspond to the periods of single, three- and five-fold traversals of orbit A. In accordance with the argument given below Eq. (2·10), we find that the peak-heights indeed exhibit supremes about the bifurcation (resonance) points but with rather significant delays. To account for this delay, it may be necessary to go beyond the SPA.

6.4. *Angular momentum decomposition of the trace formula*

As our system is axially symmetric, the angular momentum about the symmetry axis p_φ is a good quantum number. Thus, the level density can be decomposed as $g(E)=\sum_m g(E;\, m)$ with m denoting the angular momentum quantum number. Let us derive a semiclassical expression of $g(E;\, m)$. Writing the three-dimensional coordinate vector as $\boldsymbol{q}=(\boldsymbol{Q}, \varphi)$ with $\boldsymbol{Q}=(\rho, z)$, the Green function may be decomposed as

$$G(\boldsymbol{q}'', \boldsymbol{q}'; E)=\sum_{n=-\infty}^{\infty} G((\boldsymbol{Q}'', \phi+2n\pi), (\boldsymbol{Q}', 0); E)$$

$$=\sum_n \int dM e^{i(\phi+2n\pi)M} \tilde{G}(\boldsymbol{Q}'', \boldsymbol{Q}'; E, M)$$

$$=\sum_{m=-\infty}^{\infty} e^{im\phi} \tilde{G}(\boldsymbol{Q}'', \boldsymbol{Q}'; E, m), \qquad (6\cdot8)$$

where $\tilde{G}$ denotes a Fourier transform of G with respect to $\phi=\varphi''-\varphi'$, and where the Poisson sum formula is used in obtaining the last expression. Taking the trace of Eq. (6·8), one can derive the trace formula for $g(E; m)$ in a way similar to (2·4),[32]

$$g(E; m)=-2\mathrm{Im}\int d\boldsymbol{Q}\rho\tilde{G}(\boldsymbol{Q}, \boldsymbol{Q}; E, m)$$

$$\simeq \bar{g}(E; m)+\frac{1}{\pi\hbar}\sum_{n,\alpha}\frac{\tau_\alpha}{\sqrt{|W_{n\alpha}|}}\cos(n\sigma_\alpha(E)/\hbar-(\pi/2)\mu_{n\alpha}), \qquad (6\cdot9)$$

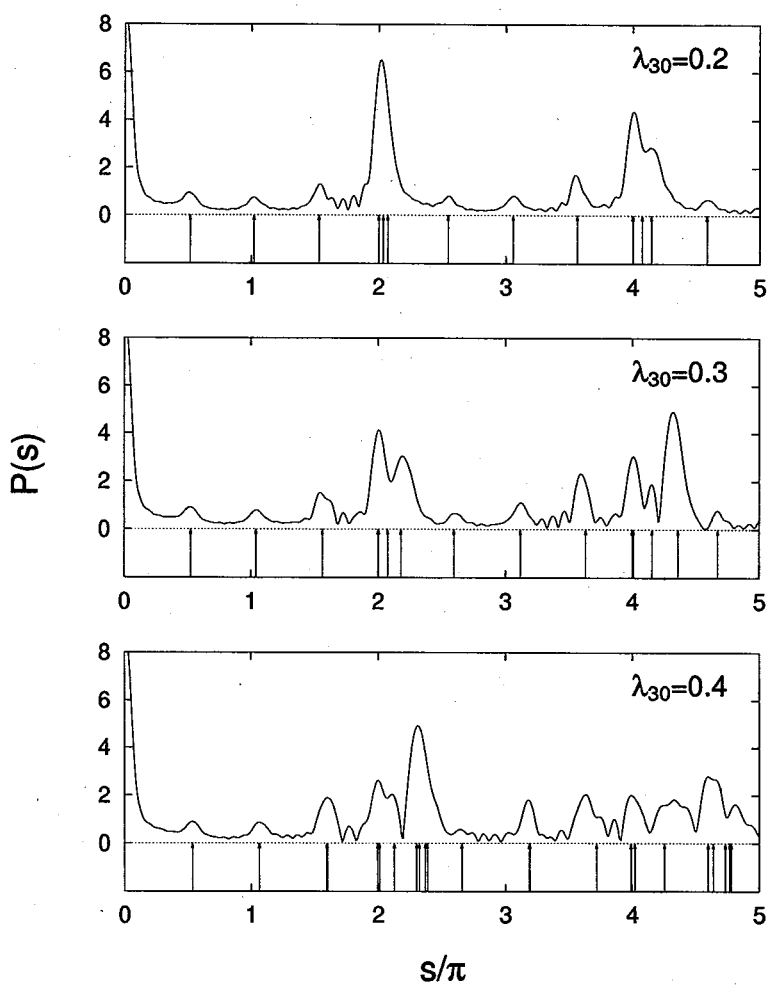

Fig. 12. Fourier transforms of the level density $g(E; m)$ in the $m=0$ subspace for $\lambda_{30}=0.2$, 0.3 and 0.4.

where σ_α denotes the action integrals along the two-dimensional closed orbits α in the (ρ, z) plane, τ_α the periods and μ_α the Maslov phases. Using the symplectic property of the monodromy matrix, $W_{n\alpha}$ can be written as

$$W_{n\alpha}=\det(\mathbf{1}-M_\alpha^n)=2-\mathrm{Tr}(M_\alpha^n)\,, \tag{6·10}$$

where M_α is a 2×2 monodromy matrix. Note that, for symmetric self-retracing orbits, M_α^n is different from $\tilde{M}_\alpha^n$ appearing in Eq. (2·11). It is easily seen that, due to the reflection symmetry with respect to the z-axis, these orbits in the (ρ, z) plane have periods half of those in the three-dimensional space.

Now, for $m=0$, a scaling property holds so that we can use the Fourier transformation technique. Since the degeneracy of the orbits is zero in the two-dimensional space, we put $d=0$ in Eq. (6·6). From the above consideration, one expect that the Fourier transform will exhibit peaks, in addition to those corresponding to the periods of closed orbits, also at half of the periods of the three-dimensional symmetric self-retracing orbits. The results of calculation is shown in Fig. 12. Again we find a clear correspondence between peaks of the Fourier transform and periods of classical orbits. As expected, peaks appear also at half integer times the period of orbit A.

§ 7. Concluding remarks

We have found a clear correspondence between the shell structure, i.e., the oscillatory structure in the smoothed level density, and the classical periodic orbits for single-particle motions in a reflection-asymmetric SD oscillator potential. We have then shown that the supershell effect, i.e., an interference effect between two families of the periodic orbits having periods approximately $2\pi/\omega_\perp$ and $2\pi/\omega_{\mathrm{sh}}$, becomes more significant when the reflection-asymmetric deformation increases. This supershell effect is in clear correspondence with the odd-even effect in N_{sh} pointed out in Refs. 8) and 10). Possible origins of this enhancement phenomena have been pointed out in connection with stabilities of the classical periodic orbits. Quantum signature of the period-tripling bifurcation of the shortest-period orbit is also pointed out.

It should be emphasized that our model Hamiltonian system is a mixed system where chaos and tori are intermixed; accordingly, period-multipling bifurcations occur, as we have seen, rather frequently when the reflection-asymmetric deformation parameter is varied. As is well known, the SPA breaks down at the bifurcation points so that we cannot use the Gutzwiller trace formula for the aim of calculating the smoothed level density. Instead, by virtue of the scaling property of our model Hamiltonian, we have been able to use the Fourier transformation technique to find the quantum-classical correspondence. Properties of the Gutzwiller amplitudes have been used only as a guide to qualitative discussions. It is an interesting future subject to investigate the problem discussed in this paper by using a more sophisticated method, like the uniform approximation, which goes beyond the SPA.

Acknowledgements

We thank W. Nazarewicz, M. Toda, Y. R. Shimizu, M. Matsuo, H. Aiba, S. Mizutori and T. Nakatsukasa for useful discussions.

Appendix

—— Derivation of Eq. (2·11) ——

The semiclassical expression of the Green function in an f-dimensional system is

$$G(\boldsymbol{q}'', \boldsymbol{q}'; E)=\sum \frac{2\pi}{(2\pi i\hbar)^{(f+1)/2}}\sqrt{|D_S|}\exp\left(\frac{i}{\hbar}S(\boldsymbol{q}'', \boldsymbol{q}'; E)-i\kappa\frac{\pi}{2}\right), \tag{A·1}$$

where $S(\boldsymbol{q}'', \boldsymbol{q}'; E)$ is the classical action $\int \boldsymbol{p}\cdot d\boldsymbol{q}$ along a trajectory connecting $\boldsymbol{q}'$ and $\boldsymbol{q}''$ with energy E. The determinant D_S in the amplitude factor is given by

$$D_S=\begin{vmatrix} \partial^2 S/\partial \boldsymbol{q}''\partial \boldsymbol{q}' & \partial^2 S/\partial E\partial \boldsymbol{q}' \\ \partial^2 S/\partial \boldsymbol{q}''\partial E & \partial^2 S/\partial E^2 \end{vmatrix}. \tag{A·2}$$

Let us consider a three-dimensional system ($f=3$) with axial symmetry, and define an orthogonal coordinate $\boldsymbol{q}=(\xi, \eta, \zeta)$ for each periodic orbit. We take ξ along the direction of the trajectory and η perpendicular to both ξ and the azimuthal direction φ. Differentiating the Hamilton-Jacobi equations

$$H(\boldsymbol{p}''=\partial S/\partial \boldsymbol{q}'', \boldsymbol{q}'')=E\,, \tag{A·3a}$$

$$H(\boldsymbol{p}'=-\partial S/\partial \boldsymbol{q}', \boldsymbol{q}')=E \tag{A·3b}$$

with respect to E and using $\dot{\eta}=\dot{\zeta}=0$, one obtains

$$1=\sum_i \frac{\partial H}{\partial p_i''}\frac{\partial^2 S}{\partial q_i''\partial E}=\dot{\xi}''S_{\xi''E}\,, \tag{A·4a}$$

$$1=-\sum_i \frac{\partial H}{\partial p_i'}\frac{\partial^2 S}{\partial E\partial q_i'}=-\dot{\xi}'S_{E\xi'}\,, \tag{A·4b}$$

where S_{xy} denotes $(\partial^2 S/\partial x\partial y)$. If one differentiates (A·3a) and (A·3b) with ξ' and ξ'', respectively, one obtains

$$S_{q_i'\xi'}=S_{\xi''q_i}=0\,. \tag{A·5}$$

Thus, the determinant (A·2) is written as

$$D_S=\begin{vmatrix} S_{EE} & S_{E\xi'} & S_{E\eta'} & S_{E\zeta'} \\ S_{\xi''E} & 0 & 0 & 0 \\ S_{\eta''E} & 0 & S_{\eta''\eta'} & S_{\eta''\zeta'} \\ S_{\zeta''E} & 0 & S_{\zeta''\eta'} & S_{\zeta''\zeta'} \end{vmatrix}=-\frac{1}{\dot{\xi}''}\frac{1}{\dot{\xi}'}\begin{vmatrix} S_{\eta''\eta'} & S_{\eta''\zeta'} \\ S_{\zeta''\eta'} & S_{\zeta''\zeta'} \end{vmatrix}. \tag{A·6}$$

If we use coordinates (ξ, η, φ) which are generally not orthogonal, then we obtain

$$D_S=\frac{1}{J''\dot{\xi}''}\frac{1}{J'\dot{\xi}'}\begin{vmatrix} S_{\eta''\eta'} & S_{\eta''\phi} \\ S_{\phi\eta'} & S_{\phi\phi} \end{vmatrix}, \tag{A·7}$$

where J is Jacobian of the coordinate transformation, J' and J'' denoting its value at $\boldsymbol{q}'$ and $\boldsymbol{q}''$, respectively, and $\phi=\varphi''-\varphi'$. Let us evaluate the trace of the Green function in the stationary phase approximation. As usual, the action integral along a closed path may be expanded about a stationary point $\bar{\boldsymbol{q}}$ as

$$S(\boldsymbol{q},\boldsymbol{q};E)=S(\bar{\boldsymbol{q}},\bar{\boldsymbol{q}};E)+(\boldsymbol{q}-\bar{\boldsymbol{q}})^T\left[\frac{\partial S}{\partial \boldsymbol{q}''}+\frac{\partial S}{\partial \boldsymbol{q}'}\right]_{q''=q'=\bar{q}}$$
$$+\frac{1}{2}(\boldsymbol{q}-\bar{\boldsymbol{q}})^T\left[\frac{\partial^2 S}{\partial \boldsymbol{q}''\partial \boldsymbol{q}''}+2\frac{\partial^2 S}{\partial \boldsymbol{q}''\partial \boldsymbol{q}'}+\frac{\partial^2 S}{\partial \boldsymbol{q}'\partial \boldsymbol{q}'}\right]_{q''=q'=\bar{q}}(\boldsymbol{q}-\bar{\boldsymbol{q}})+\cdots. \tag{A·8}$$

The stationary phase condition requires the second term on the r.h.s. to vanish. This is nothing but the condition for the trajectory to be periodic, i.e., $\boldsymbol{p}''=\boldsymbol{p}'$. Taking the axial symmetry into account, we can rewrite Eq. (A·8) as

$$S(\boldsymbol{q},\boldsymbol{q};E)=\bar{S}(E)+\frac{1}{2}W(\xi)\eta^2+\cdots, \tag{A·9}$$

where

$$W(\xi)=\det(\mathbf{1}-M)S_{\eta''\eta'}=(2-\mathrm{Tr}M)S_{\eta''\eta'}, \tag{A·10}$$

M being the (2×2) monodromy matrix for the periodic orbit (see § 2.2). Performing the Gauss-Fresnel integral with respect to η, we finally obtain the following result:

$$g_{\mathrm{osc}}(E)=\frac{1}{2\pi^2\hbar^2}\mathrm{Im}\sum\int d\varphi d\xi d\eta J\sqrt{|D_S|}\exp\left[\frac{i}{\hbar}\left(\bar{S}+\frac{1}{2}W(\xi)\eta^2\right)-i\kappa\frac{\pi}{2}\right]$$
$$=\frac{4\pi}{(2\pi\hbar)^{3/2}}\sum_\gamma\frac{B_\gamma}{\sqrt{|2-\mathrm{Tr}M_\gamma|}}\cos(S_\gamma/\hbar-\mu_\gamma\pi/2), \tag{A·11}$$

where $\mu_\gamma=\kappa_\gamma-\mathrm{sign}(W_\gamma)/2$ and

$$B_\gamma=\oint_\gamma\frac{d\xi}{|\dot{\xi}|}\left|\left(\begin{vmatrix} S_{\eta''\eta'} & S_{\eta''\phi} \\ S_{\phi\eta'} & S_{\phi\phi} \end{vmatrix}/S_{\eta''\eta'}\right)\right|^{1/2}=\int_\gamma dt\left|\frac{\partial p_\varphi}{\partial\varphi''}\right|^{1/2}=\int_\gamma dt\left|\frac{\partial\varphi(t+T_\gamma)}{\partial p_\varphi(t)}\right|^{-1/2}. \tag{A·12}$$

References

1) J. Dudek, T. T. Werner and Z. Szymanski, Phys. Lett. **B248** (1990), 235.
2) J. Höller and S. Åberg, Z. Phys. **A336** (1990), 363.
3) R. R. Chasman, Phys. Lett. **B266** (1991), 243.
4) Xunjun Li, J. Dudek and P. Romain, Phys. Lett. **B271** (1991), 281.
5) J. Skalski, Phys. Lett. **B274** (1992), 1.
6) P. Bonche, S. J. Krieger, M. S. Weiss, J. Dobaczewski, H. Flocard and P. -H. Heenen, Phys. Rev. Lett. **66** (1991), 876.
7) J. Skalski, P. -H. Heenen, P. Bonche, H. Flocard and J. Meyer, Nucl. Phys. **A551** (1993), 109.
8) W. Nazarewicz and J. Dobaczewski, Phys. Rev. Lett. **68** (1992), 154.
9) T. Bengtsson, M. E. Faber, G. Leander, P. Möller, M. Ploszajczak, I. Ragnarsson and S. Åberg, Physica Scripta **24** (1981), 200.

10) K. Arita and K. Matsuyanagi, Prog. Theor. Phys. **89** (1993), 389.
11) S. Mizutori, T. Nakatsukasa, K. Arita, Y. R. Shimizu and K. Matsuyanagi, Nucl. Phys. **A557** (1993), 125c.
12) R. Balian and C. Bloch, Ann. of Phys. **69** (1972), 76.
13) H. Nishioka, Klavs Hansen and B. R. Mottelson, Phys. Rev. **B42** (1990), 9377.
14) H. Nishioka, Z. Phys. **D19** (1991), 19.
15) M. Brack, J. Damgaard, A. S. Jensen, H. C. Pauli, V. M. Strutinsky and C. Y. Wong, Rev. Mod. Phys. **44** (1972), 320.
16) A. Bohr and B. R. Mottelson, *Nuclear Structure* (Benjamin, 1975), Vol. 2, p. 585.
17) V. M. Strutinsky and A. G. Magner, Sov. J. Part. Nucl. **7** (1976), 138.
18) V. M. Strutinsky, A. G. Magner, S. R. Ofengenden and T. Døssing, Z. Phys. **A283** (1977), 269.
19) H. Frisk, Nucl. Phys. **A511** (1990), 309.
20) C. P. Malta, M. A. M. de Aguiar and A. M. Ozorio de Almeida, Phys. Rev. **A47** (1993), 1625.
21) M. C. Gutzwiller, *Chaos in Quantum and Classical Mechanics* (Springer Verlag, 1990).
22) M. C. Gutzwiller, "The Semi-classical Quantization of Chaotic Hamiltonian Systems" in *Chaos and Quantum Physics, Proc. Les Houches Summer School, Session LII* (1989), p. 201.
23) A. M. Ozorio de Almeida, *Hamiltonian System, Chaos and Quantizaion* (Cambridge University Press, 1988).
24) K. Arita, Prog. Theor. Phys. **90** (1993), 747.
25) M. V. Berry and M. Tabor, Proc. R. Soc. London **A349** (1976), 101.
26) M. C. Gutzwiller, J. Math. Phys. 8 (1967), 1979; **12** (1971), 343.
27) M. Baranger, K. T. R. Davies and J. H. Mahoney, Ann. of Phys. **186** (1988), 95.
28) A. M. Ozorio de Almeida and J. H. Hannay, J. of Phys. **A20** (1987), 5873.
29) A. G. Magner, Sov. J. Nucl. Phys. **28** (1978), 759.
30) H. Sakamoto and T. Kishimoto, Nucl. Phys. **A501** (1989), 205.
31) D. Wintgen, Phys. Rev. Lett. **58** (1987), 1589; **61** (1988), 1803.
32) A. G. Magner, V. M. Kolomietz and V. M. Strutinsky, Sov. J. Nucl. Phys. **28** (1978), 764.

19 January 1995

PHYSICS LETTERS B

Physics Letters B 343 (1995) 19–24

Octupole correlations in excited bands of superdeformed ^{152}Dy

Takashi Nakatsukasa [a,1], Kenichi Matsuyanagi [b], Shoujirou Mizutori [c], Witold Nazarewicz [d,2]

[a] *Research Center for Nuclear Physics, Osaka University, Ibaraki 567, Osaka, Japan*

[b] *Department of Physics, Kyoto University, Kyoto 606-01, Japan*

[c] *Department of Mathematical Physics, Lund Institute of Technology, Box 118, S-22100 Lund, Sweden*

[d] *Joint Institute for Heavy-Ion Research, Physics Division, Oak Ridge National Laboratory, P.O. Box 2008, Oak Ridge, TN 37831, USA and Department of Physics, University of Tennessee, Knoxville, TN 37996, USA*

Received 7 September 1994; revised manuscript received 7 November 1994

Editor: G.F. Bertsch

Abstract

RPA calculations, based on the cranked shell model, are performed for superdeformed ^{152}Dy in which five excited bands have been found recently. We show that characteristic features of the observed dynamical moments of inertia are well accounted for by explicitly taking the octupole correlations into account. Importance of the interplay between rotation and octupole vibrations is stressed, and it is suggested that one of the observed excited bands might be a collective octupole vibration built on the superdeformed yrast band.

The discovery of superdeformed (SD) rotational bands has opened many new avenues in studies of nuclear structure at the extremes of rapid rotation and large deformation. Recent experimental developments, especially large γ-ray detector arrays (Eurogam, Gammasphere, Ga.Sp, etc.), have offered better observational limits which help in clarifying many aspects of high-spin nuclear structure.

Recently, five excited SD bands (Bands 2–6) have been observed in ^{152}Dy in a Eurogam experiment [1]. According to various theoretical calculations [2–4], ^{152}Dy has a SD doubly-closed-shell configuration corresponding to the large single-particle gaps at $Z = 66$ and $N = 86$. Since the pairing correlations in SD bands in the $A = 150$ region are expected to be seriously quenched due to the low level-density of single-particle states and rapid rotation, the angular momentum variations in the dynamical moments of inertia, $\mathcal{J}^{(2)} = dI/d\omega$, are mainly due to the intrinsic angular momentum alignment of single-particle orbitals, especially high-N intruder orbitals [2–4]. Consequently, the $\mathcal{J}^{(2)}$ moments of inertia carry important experimental information about single-particle configurations in SD bands.

The excited SD bands in ^{152}Dy, observed by Dagnall et al. [1], have a very low intensity relative to the yrast SD band. This might be related to the predicted SD magic structure in ^{152}Dy. Due to its magic structure, collective excitation modes are expected to influence the properties of near-yrast SD bands in ^{152}Dy. In this context, octupole vibrations play a very special role. According to the RPA calculations based on the cranked shell model [5,6], low-lying octupole vibra-

[1] Present address: AECL Research, Chalk River Laboratories, Chalk River, Ontario K0J 1J0, Canada.

[2] On leave of absence from Institute of Theoretical Physics, Warsaw University, Warsaw, Poland; Institute of Physics, Warsaw University of Technology, Warsaw, Poland.

SSDI 0370-2693(94)01484-1

tions are more important than low-lying quadrupole vibrations built on the SD shape. Strong octupole correlations in SD states have also been suggested theoretically in Refs. [7–15]. The calculations of Ref. [16] demonstrate that the inclusion of the coupling between quasiparticle and octupole vibrational modes is important for understanding the experimental data for SD ^{193}Hg [10].

In this Letter, we discuss octupole correlations in excited SD bands of ^{152}Dy. Comparing our results with the experimental data, we propose a plausible scenario for the microscopic structure of excited SD bands in ^{152}Dy. This scenario is compatible with the discussions by Dagnall et al. [1] but the influence of octupole correlations is explicitly considered. Indeed, one of the excited SD bands is suggested to have a collective octupole vibrational character. If this interpretation is correct, this is the first case in which the collective vibrational mode at SD states in the $A = 150$ region has been observed experimentally. [3]

In order to investigate the influence of octupole vibrations on the excitation spectrum of SD ^{152}Dy, the RPA treatment has been carried out. The model Hamiltonian has been assumed to be of the form:

$$H = h'_{\text{s.p.}} - \frac{1}{2}\sum_K \chi_{3K} Q''^{\dagger}_{3K} Q''_{3K} - \frac{1}{2}\sum_K \chi_{1K} (\tau_3 D_{1K})''^{\dagger} (\tau_3 D_{1K})'' , \qquad (1)$$

where $h'_{\text{s.p.}}$ is a cranked single-particle Nilsson Hamiltonian, $h'_{\text{s.p.}} = h_{\text{Nilsson}} - \omega_{\text{rot}} \hat{J}_x$, and $Q''_{3K} = (r^3 Y_{3K})''$ and $D''_{1K} = (rY_{1K})''$ are, respectively, the doubly stretched octupole and dipole operators defined by coordinates $x''_i = \frac{\omega_i}{\omega_0} x_i$ [18]. The equilibrium quadrupole deformations have been determined by means of the shell correction method. A large configuration space composed of nine major shells for both protons and neutrons has been used for solving the coupled RPA dispersion equations. The spurious velocity dependence associated with the l^2 and $\boldsymbol{l} \cdot \boldsymbol{s}$ terms in the Nilsson potential are removed by means of the method proposed in Ref. [19]. We note that the obtained single-particle routhians are similar to those for the Woods-Saxon potential [3]. The pairing gaps Δ_p and Δ_n are assumed to be zero: Although dynamical pairing fluctuations never vanish, *relative* energy spectra and *relative* alignments are known to be well described by the simple cranked shell-model routhians without pairing at $\omega_{\text{rot}} \geq 0.3$ MeV/$\hbar$, i.e., in the region where the experimental data are available [20,21]. In order to determine the isoscalar coupling strengths, χ_{3K}, we have carried out the systematic RPA calculations for the low-frequency $I^\pi = 3^-$ states in medium-heavy nuclei. Guided by these calculations, we use $\chi_{3K} = 1.05\chi^{\text{HO}}_{3K}$ where χ^{HO}_{3K} are the selfconsistent values for the harmonic oscillator potential [18]. For the isovector dipole coupling strengths we use $\chi_{1K} = -\pi V_1 / \langle (r^2)'' \rangle$ with $V_1 = 140$ MeV [22].

Fig. 1(a) shows the RPA eigenvalues as functions of rotational frequency ω_{rot}. The lowest excitation mode with signature $\alpha = 1$ (dotted line) can be associated with the collective octupole vibrational band. The band has $K = 0$ at $\omega_{\text{rot}} = 0$, but the K-mixing due to the Coriolis force is significant at high rotational frequencies. The B(E3)-values calculated at $\omega_{\text{rot}} = 0$ in the strong coupling scheme are around B(E3; $3^- \rightarrow 0^+$) $\approx$ 35 W.u. By comparing Fig. 1(b) and (c), we see that the octupole collectivity carried by the lowest $\alpha = 1$ band decreases gradually with ω_{rot}. On the other hand, collectivity of the lowest excitation mode with $\alpha = 0$ (solid line) is weak and this mode has a dominant 1p-1h configuration at high frequency. The excitation energy of this band drastically decreases in the high-frequency region and its alignment, $i = -dE_x/d\omega$, is evaluated to be about $5\hbar$. Since this band has much lower excitation energy at high frequency than the octupole vibrational $\alpha = 1$ band, it may be populated with higher intensity.

Calculations show that the neutron $N = 86$ single-particle shell gap persists at high frequencies, while the proton $Z = 66$ shell gap vanishes at high angular momenta where the proton $N = 7$ ($\alpha = -1/2$) orbital crosses the fourth $N = 6$ ($\alpha = -1/2$) orbital (see Fig. 2 and discussion in Ref. [1]). The 1p-1h excitation associated with these two orbitals gives rise to the lowest excited state with signature $\alpha = 0$. The alignment of this 1p-1h excitation is equal to $i_{\text{p}} - i_{\text{h}} \approx 4.5\hbar$; i.e., the large alignment of the band comes from the intrinsic angular momentum of the proton intruder $N = 7$ orbital. In contrast, the lowest 1p-1h excitation with $\alpha = 1$ is associated with the proton $N = 7$ ($\alpha =$

[3] An excited band in SD ^{190}Hg has been interpreted in terms of octupole vibrations [17].

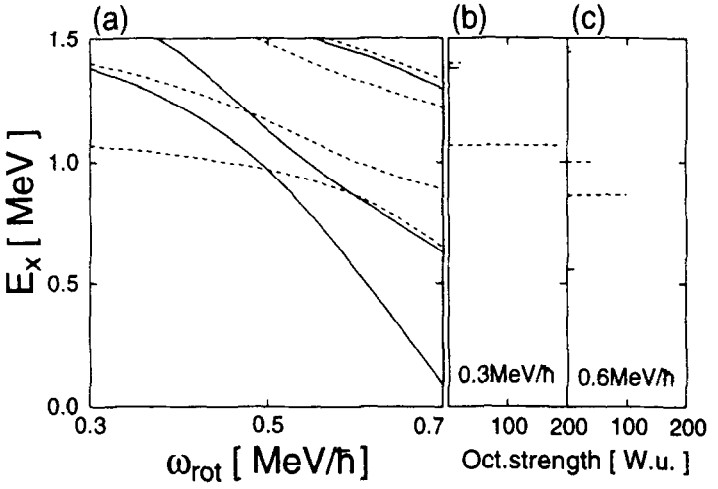

Fig. 1. Results of RPA calculations at quadrupole deformation $\delta_{osc} = 0.59$. (a) Calculated RPA eigenvalues (in MeV) for SD ^{152}Dy, plotted as functions of rotational frequency ω_{rot} (in MeV/$\hbar$). Solid (dotted) lines indicate negative-parity states with signature $\alpha = 0$ ($\alpha = 1$). The lowest $\alpha = 1$ state has $K = 0$ in the limit $\omega_{rot} = 0$. (b) Electric octupole strength $\sum_K |\langle n|\frac{1}{2}(1+\tau_3)Q_{3K}|0\rangle|^2$ at $\omega_{rot} = 0.3$ MeV/$\hbar$ in Weisskopf units ($|0\rangle$ and $|n\rangle$ denote the RPA ground state and excited states, respectively). Solid and dotted lines indicate the $\alpha = 0$ and $\alpha = 1$ states, respectively. The vertical axis represents the excitation energy as in (a). (c) The same as (b), except for $\omega_{rot} = 0.6$ MeV/$\hbar$.

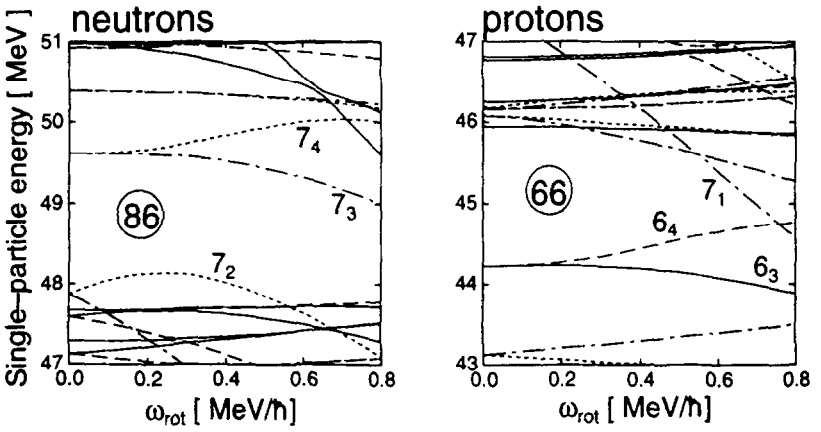

Fig. 2. Neutron and proton single-particle routhians as functions of rotational frequency ω_{rot}. The Nilsson parameters (κ, μ) are adopted from Ref. [23], and the spurious velocity dependence associated with l^2 and $\boldsymbol{l}\cdot\boldsymbol{s}$ terms are removed according to a prescription developed by Kinouchi and Kishimoto [19]. Orbitals having parity and signature, $(\pi, \alpha) = (+, 1/2)$, $(+, -1/2)$, $(-, 1/2)$, and $(-, -1/2)$ are shown by solid, dashed, dotted, and dash-dotted lines, respectively. The oscillator quantum number, N_{osc}, is indicated for "high-N" orbitals.

$-1/2)$ and the third $N = 6$ ($\alpha = 1/2$) orbital. Its excitation energy is about 1 MeV higher than that of the $\alpha = 0$ band in the highest frequency region. Because of this effective energy gap, the collective mode with $\alpha = 1$ survives up to rather high frequencies. Since the alignment of the collective octupole phonon is less than $3\hbar$, the lowest $\alpha = 0$ band carries a larger alignment and becomes lower at high frequency.

In the following, we discuss the dynamical moments of inertia of Bands 2, 3, and 6 for which octupole correlations are calculated to be important. Characteristic features of Bands 2, 3, and 6, determined in Ref. [1], can be summarized as follows: (i) $\mathcal{J}^{(2)}$ of Band 2 (Band 3) has a bump (dip) at $\omega_{rot} \approx 0.5$ MeV/$\hbar$; (ii) Bands 2 and 3 are populated with higher intensity compared to other excited bands (Bands 4–6); (iii) $\mathcal{J}^{(2)}$ of Band 6 is larger than that of the SD yrast band and is almost constant as a function of rotational fre-

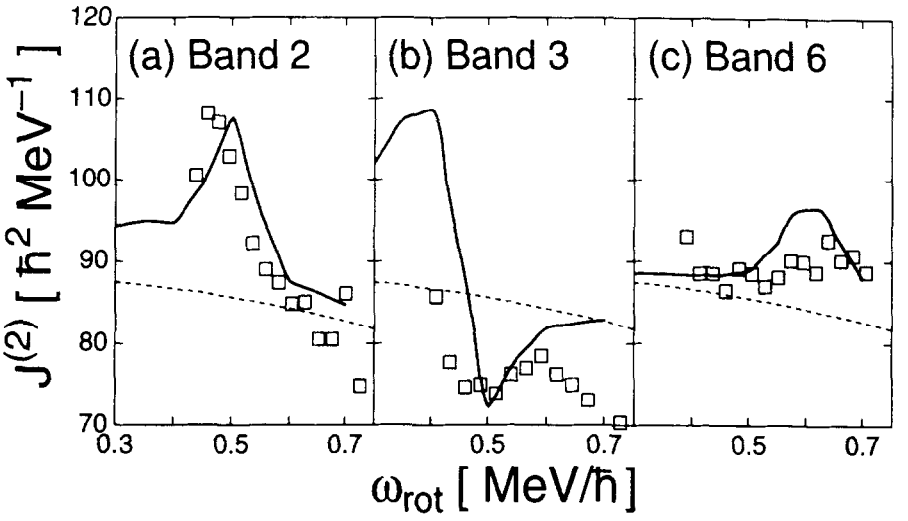

Fig. 3. Calculated (solid lines) and experimental (symbols) dynamical moments of inertia for excited SD bands (Bands 2, 3, and 6) in ^{152}Dy. Dotted lines indicate $\mathcal{J}^{(2)}$ for the yrast SD band, which is approximated by the Harris formula $\mathcal{J}_0^{(2)} = \alpha + \beta\omega^2$ with $\alpha = 88.5\hbar^2$ MeV^{-1} and $\beta = -11.9\hbar^4$ MeV^{-3}. See text for details.

quency; (iv) At low values of ω_{rot} Band 6 shows a decay branch into the yrast SD band.

On the basis of the above observations, we propose a scenario in which the lowest and the second lowest excited $\alpha = 0$ states (solid lines in Fig. 1), and the lowest $\alpha = 1$ state (dotted line) correspond to Bands 2, 3, and 6, respectively. Firstly, the $\mathcal{J}^{(2)}$ bump in Band 2 and the dip of Band 3 occurring at the same frequency can be associated with crossing between the two lowest $\alpha = 0$ states, see Fig. 1. Secondly, the high intensity of Bands 2 and 3 indicates that at high frequency these bands have lower excitation energy than the other bands. Our conjecture is consistent with the intensity data for Band 2.[4] Thirdly, weak ω_{rot}-dependence of $\mathcal{J}^{(2)}$ in Band 6 suggests an almost constant curvature $d^2E_x/d\omega^2$ of the routhian (see Eq. (2)). Finally, the partial decay of Band 6 into the yrast SD band indicates that Band 6 may be a collective band possessing significant (E1) transition matrix elements into the yrast SD band.

In order to make the comparison with experimental data quantitative, we calculate the dynamical moments of inertia $\mathcal{J}^{(2)}$. They can be decomposed as

$$\mathcal{J}^{(2)} = \mathcal{J}_0^{(2)} + \frac{di}{d\omega} = \mathcal{J}_0^{(2)} - \frac{d^2E_x}{d\omega^2}, \qquad (2)$$

where $\mathcal{J}_0^{(2)}$ denotes the dynamical moment of inertia of the yrast SD band of ^{152}Dy (RPA vacuum). We approximate the experimental $\mathcal{J}_0^{(2)}$ by the Harris expansion, $\mathcal{J}_0^{(2)} = \alpha + \beta\omega^2$, with $\alpha = 88.5\hbar^2$ MeV^{-1} and $\beta = -11.9\hbar^4$ MeV^{-3}. Calculated and experimental values of $\mathcal{J}^{(2)}$ are compared in Fig. 3; it is seen that the characteristic features of the experimental data are well reproduced. It is worth noting that the octupole correlations are also important for reproducing experimental $\mathcal{J}^{(2)}$ values for Bands 2 and 3.

In order to discuss the collectivity of octupole correlations, we show in Fig. 4 the forward RPA amplitudes[5] $\psi_n(\alpha\beta)$ for Bands 2, 3, and 6. We see that Bands 2 and 3 correspond to simple 1p-1h excitations at the highest frequency region; i.e., proton $N = 6 \rightarrow N = 7$ and proton $N = 6 \rightarrow N = 5$ excitations, respectively. Bands 2 and 3 cross at $\omega_{rot}^{(c)} \approx 0.5$ MeV/$\hbar$. For $\omega_{rot} < \omega_{rot}^{(c)}$, collective components in both bands are significant. In fact, the interaction matrix element between Bands 2 and 3 would be too small to reproduce the observed bumps and dips of $\mathcal{J}^{(2)}$ if octupole cor-

[4] On the other hand, calculations suggest that intensity of Band 3 should be weaker than that of Band 2 whereas experimentally it is similar; this weakens our interpretation of Band 3.

[5] Sums of the squared backward RPA amplitudes, $\sum_{\alpha\beta}|\varphi_n(\alpha\beta)|^2$, at $\omega_{rot} = 0.3$ MeV/$\hbar$ are 0.13, 0.11 and 0.48 for Bands 2, 3 and 6, respectively.

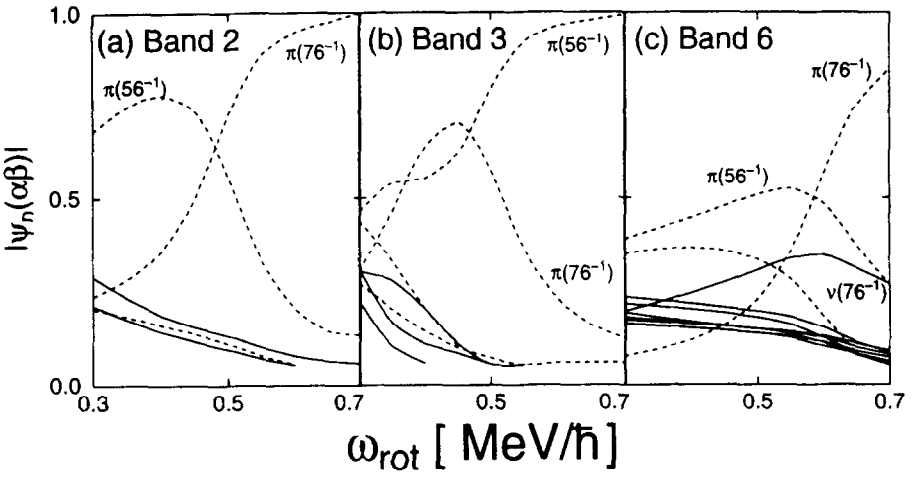

Fig. 4. Absolute values of the forward amplitudes, $|\psi_n(\alpha\beta)|$, of the lowest and the second lowest RPA solutions in the $\alpha = 0$ sector (portions a and b), and the lowest RPA solution in the $\alpha = 1$ sector (portion c), corresponding to Bands 2, 3, and 6, respectively. Solid (Dashed) lines indicate neutron (proton) amplitudes. All amplitudes whose absolute values are greater than 1.5×10^{-1} are displayed. The characteristic p-h excitations are indicated.

relations were turned off. On the other hand, Band 6 has vibrational character in the whole range of rotational frequency. The octupole collectivity of this band decreases with rotational frequency.

In summary, we have investigated the effects of octupole correlations in excited SD bands of ^{152}Dy by means of the RPA based on the cranked shell model. We found that a low-lying octupole vibrational band ($\alpha = 1$) appears near the yrast band ($E_x \approx 1$ MeV). According to our scenario, Bands 2, 3, and 6 have negative parity. Band 2 (3) is the lowest (second lowest) $\alpha = 0$ band. Band 6 is the octupole vibrational $\alpha = 1$ band. The collectivity of Band 6 is expected to gradually decrease with $\omega_{\rm rot}$, while Bands 2 and 3 cross each other at $\omega_{\rm rot} \approx 0.5$ MeV/$\hbar$. The calculated $\mathcal{J}^{(2)}$ values reflect the $\omega_{\rm rot}$-dependence of the internal structures of these bands, and seem to agree well with major characteristics found experimentally.

We would like to thank C.W. Beausang and P.J. Twin for valuable discussions. We are indebted to the ECT* for financial support which made possible our stay at the ECT* during the International Workshop on High Spins and Novel Deformations. Computational calculations were supported in part by the RCNP, Osaka University, as a RCNP Computational Nuclear Physics Project (Project No. 93-B-02). This work was also supported in part by the U.S. Department of Energy through Contract Numbers DE-AC05-840R21400, DE-FG07-87ER40361, and DE-FG05-93ER40770.

References

[1] P.J. Dagnall et al., Phys. Lett. B 335 (1994) 313.
[2] T. Bengtsson, S. Åberg and I. Ragnarsson, Phys. Lett. B 208 (1988) 39.
[3] W. Nazarewicz, R. Wyss and A. Johnson, Nucl. Phys. A 503 (1989) 285.
[4] Y.R. Shimizu, E. Vigezzi and R.A. Broglia, Nucl. Phys. A 509 (1990) 80.
[5] S. Mizutori, Y.R. Shimizu and K. Matsuyanagi, Prog. Theor. Phys. 83 (1990) 666; 85 (1991) 559; 86 (1991) 131.
[6] T. Nakatsukasa, S. Mizutori and K. Matsuyanagi, Prog. Theor. Phys. 87 (1992) 607.
[7] J. Dudek, T.R. Werner and Z. Szymański, Phys. Lett. B 248 (1990) 235.
[8] S. Åberg, Nucl. Phys. A 520 (1990) 35c.
[9] J. Höller and S. Åberg, Z. Phys. A 336 (1990) 363.
[10] D.M. Cullen et al., Phys. Rev. Lett. 65 (1990) 1547.
[11] P. Bonche, S.J. Krieger, M.S. Weiss, J. Dobaczewski, H. Flocard and P.-H. Heenen, Phys. Rev. Lett. 66 (1991) 876.
[12] Xunjun Li, J. Dudek and P. Romain, Phys. Lett. B 271 (1991) 281.
[13] W. Nazarewicz and J. Dobaczewski, Phys. Rev. Lett. 68 (1992) 154.
[14] J. Skalski, Phys. Lett. B 274 (1992) 1.
[15] J. Skalski, P.-H. Heenen, P. Bonche, H. Flocard and J. Meyer, Nucl. Phys. A 551 (1993) 109.

[16] T. Nakatsukasa, S. Mizutori and K. Matsuyanagi, Prog. Theor. Phys. 89 (1993) 847.
[17] B. Crowell et al., Phys. Lett. B 333 (1994) 320.
[18] H. Sakamoto and T. Kishimoto, Nucl. Phys. A 501 (1989) 205.
[19] S. Kinouchi, Ph.D. Thesis (1988), Univ. of Tsukuba.
[20] Y.R. Shimizu, Nucl. Phys. A 520 (1990) 477c.
[21] I. Ragnarsson, Nucl. Phys. A 557 (1993) 167c.
[22] A. Bohr and B.R. Mottelson, Nuclear Structure, Vol. 2 (W.A. Benjamin, New York, 1975).
[23] S.G. Nilsson et al., Nucl. Phys. A 131 (1969) 1.

Physica Scripta. Vol. T56, 276–279, 1995

Microscopic Structure of Octupole Correlations at High-Spin in Superdeformed Open-Shell Nuclei

S. Mizutori

Department of Mathematical Physics, Lund Institute of Technology, S221-00 Lund, Sweden

Y. R. Shimizu

Deparment of Physics, Kyushu University, Fukuoka 812, Japan

and

K. Matsuyanagi

Department of Physics, Kyoto University, Kyoto 606-01, Japan

Received October 4, 1994; accepted October 7, 1994

Abstract

We investigate microscopic structures of octupole correlations at high spin in superdeformed open-shell nuclei in the Gd-Dy region, using the random-phase approximation (RPA) based on the cranked shell model. The result of our calculation indicates that constructive interplay between rotation-aligned particle-hole (or two-quasiparticle) excitations and octupole vibrations is very important in determining octupole softness of superdeformed bands.

1. Introduction

Since the discovery in ^{152}Dy, the superdeformed bands are one of the focus in high spin nuclear physics. Many experimental and theoretical studies have been done on the nature of the yrast and excited superdeformed bands. Recently, some experimental data, suggesting the existence of octupole vibration built on superdeformed bands, have been reported both the $A \sim 150$ region [1, 2] and the $A \sim 180$ region [3]. The octupole degrees of freedom in the superdeformed region have been attracting theoretical attentions even before the appearance of any experimental information [4–17].

At the superdeformed shape, we have a new situation in shell structure. Namely, a major shell is composed of almost equal number of levels of both parities. This situation is in contrast to a major shell in spherical nuclei, which is composed of levels with specific parity except for the intruder levels. Therefore, it is expected that the negative parity excitations, such as octupole vibrations, play more important roles at low excitation energy in superdeformed nuclei than in spherical or normal deformed nuclei. Especially, in analogy with the well known shape transition from spherical to quadrupole deformed shapes due to the correlation between valence nucleons within a major shell, one might expect that, if nucleons are added to the superdeformed closed shell, octupole collectivity increases, and eventually the system acquires a stable octupole deformed shape.

In superdeformed high spin states, however, there are two important situations that would significantly affect the properties of the octupole vibrations and hence would affect the above scenario of shape transition. Firstly, due to the strong Coriolis mixing effect, the K-quantum number is not conserved. Therefore, there would be considerable differences between the structures of octupole vibrational states built on non-rotating states and those built on rapidly rotating states. Secondly, contrary to the spherical open shell nuclei at zero rotational frequency, which have considerable pairing gaps so that two-quasiparticle excitations have much larger excitation energies than collective vibrations, the pairing gaps are predicted to be zero or very small in the superdeformed bands. Furthermore, the excitation energies of some rotation-aligned quasiparticle states might become very small and appear in the same energy region where the low-lying octupole vibrational states exist. In this paper, we analyse the microscopic structure of octupole vibrations built on superdeformed open shell nuclei, directing our attention to the Coriolis alignment effects and the weak-pairing effects on them.

2. Rotating shell model + RPA

We have carried out the random phase approximation (RPA) calculation based on the cranked shell model with the use of the doubly stretched octupole-octupole interactions. The total Hamiltonian is written as

$$H = \sum_{\mu} E_{\mu} a_{\mu}^{\dagger} a_{\mu} - \frac{1}{2} \sum_{K} \kappa_K \hat{Q}_{3K}''^{\dagger} \hat{Q}_{3K}'', \tag{1}$$

where $a_\mu^\dagger$ and E_μ are respectively creation operators and energies of the quasiparticles, which are obtained from the cranked Nilsson-BCS Hamiltonian,

$$h_{sp} + h_{nils} - \Delta(\hat{P}^\dagger + \hat{P}) - \lambda\hat{N} - \hbar\omega_{rot}\hat{j}_x. \tag{2}$$

h_{nils}, $\hat{P}^\dagger$, and $\hat{N}$ denote the Nilsson Hamiltonian, the monopole pair-creation operator, and the number operator, respectively.

Doubly-stretched octupole operators, $\hat{Q}_{3K}^{\prime\prime(\pm)}$, are obtained from the usual octupole operators by the substitution, $x_i \to (\omega_i/\omega_0)x_i$. The interaction strength, κ_K, should be determined by fitting experimental data. However, we adopt the theoretical estimate by Sakamoto and Kishimoto [18] which is valid for the harmonic-oscillator potential, since such experimental data on superdeformed nuclei are not available. Octupole operators are classified according to the signature, the symmetry with respect to the rotation of π about the cranking axis (x-axis),

$$e^{-i\pi j_x} Q_{3K}^{\prime\prime(\pm)} e^{i\pi j_x} = \pm\hat{Q}_{3K}^{\prime\prime(\pm)}. \tag{3}$$

The angular momentum projection K on the symmetry axis runs from 0 to 3 (1 to 3) for the octupole operators with signature $-$ (+). Octupole operators can also be classified according to the angular momentum projections on the cranking axis, which we denote by ξ. ξ takes values $\{3, 1, -1, -3\}$ for negative signature and $\{2, 0, -2\}$ for positive signature.

The RPA equation is expressed as usual

$$[H, X_n^\dagger]_{RPA} = \hbar\Omega_n X_n^\dagger, \tag{4}$$

where $\hbar\Omega_n$ denote the excitation energies of the RPA phonons,

$$X_n^\dagger = \sum_{\mu\nu} \{\psi_n(\mu\nu)a_\mu^\dagger a_\mu^\dagger + \phi_n(\mu\nu)a_\mu a_\nu\}. \tag{5}$$

The forward and backward amplitudes, $\psi(\mu\nu)$ and $\phi(\mu\nu)$, are normalized as

$$\sum_{\mu\nu} \{\psi_n(\mu\nu)^2 - \phi_n(\mu\nu)^2\} = 1. \tag{6}$$

3. Results

In the following, we present the result of the calculation on some isotones of $N = 86$, including nuclei in which superdeformed bands have not been found yet. The rotational frequency is fixed to 0.7 MeV, which corresponds to the high end of the observed superdeformed bands in this mass region. The equilibrium shapes are determined for each nuclei by the minimization of the total Routhian surface calculated with the Strutinsky method, therefore slightly differ for each nuclei. The pairing gaps are calculated selfconsistently, with the interaction strength determined from the average-gap method given in [19].

Figure 1 shows the octupole strength functions. All RPA solutions lower than 3.5 MeV are shown in the figure. Figure 1(a) is for the signature (−) excitations while Fig. 1(b) is for the signature (+) operators. The strengths are drawn for each isotone and are classified according to the angular momentum projection on the cranking axis, ξ. As ξ

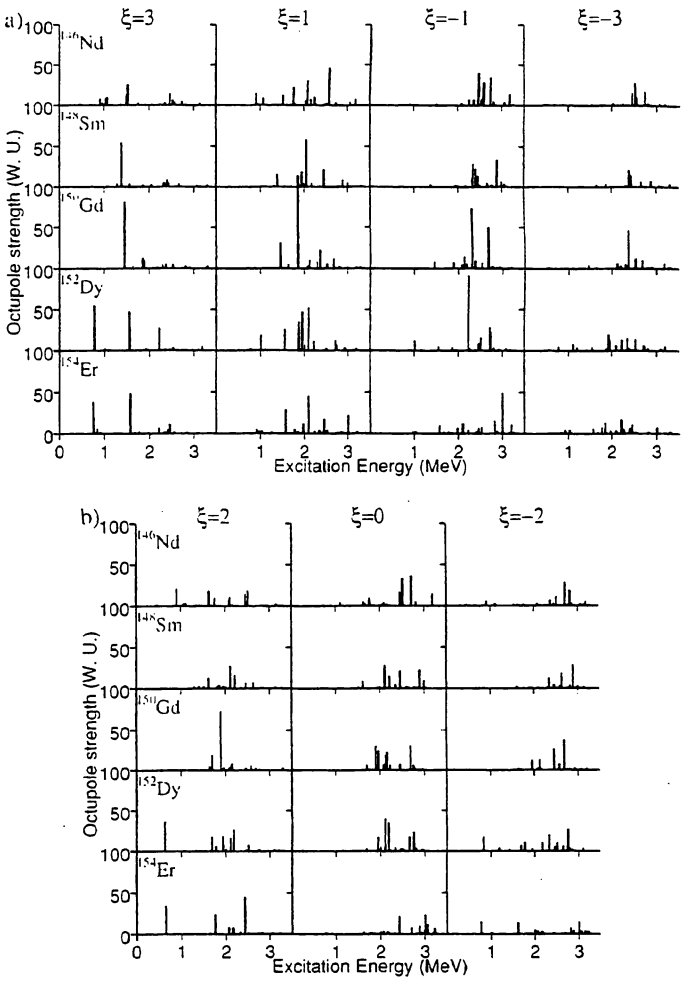

Fig. 1. Octupole strength functions calculated at the rotational frequency 0.7 MeV for the isotones of ^{150}Gd. The negative and positive signature sectors are shown in panels (a) and (b), respectively. All RPA solutions below 3.5 MeV are shown. The horizontal axis indicates the excitation energy in MeV, while the vertical axis the intrinsic mass octupole strength in the Weisskopf unit. The strengths are drawn for each ξ component. For every nuclei, the equilibrium deformations are calculated in terms of the Strutinsky method and the pairing gaps are calculated selfconsistently.

is not a good quantum number, each RPA solution has strengths for all values of ξ available for a given signature. An interesting observation in Fig. 1 is that the octupole operator with larger ξ tends to have more strength in the lower excitation energy region on the average. (It does not mean that the low-lying levels always have largest strength for largest ξ, however.) Another observation is that, the octupole strength is concentrated in a narrow region for ^{150}Gd, while it is more spread in other nuclei. This is because there are more proton particle-hole excitations carrying octupole strengths in other nuclei, while those excitations are mostly blocked in ^{150}Gd and there are only a smaller number of low-lying unperturbed particle-hole excitations carrying octupole strength.

It is remarkable that for ^{152}Dy and ^{154}Er, there are low-lying solutions with considerable octupole strengths for $\xi = 3$ [signature (−)] and $\xi = 2$ [signature (+)]. One might call these nuclei "octupole soft" because of the existence of low-lying octupole strengths. It should be noted, however, that the octupole strengths of these lowest RPA solutions are not necessarily largest, nor larger than the octupole vibrational state in ^{150}Gd. Therefore, the collectivity of

these states might not be very large, unlike the collectivity of the quadrupole vibrations in spherical open shell nuclei.

In order to get a better understanding on this point, we show in Table I and II the microscopic structure of the lowest excited states. Here, we have listed the energy of the RPA solutions, the largest two-quasiparticle (2qp) components of the RPA phonons, the squared forward amplitudes $\psi_n(\mu\nu)^2$, the sums of the squared forward amplitudes for protons $\Psi_n(\pi) = \sum_{\mu\nu} \psi_n(\mu\nu)^2$, the sums of the squared forward amplitude $\Psi_n = \sum_{\mu\nu} \psi_n(\mu\nu)^2$, unperturbed excitation energies and unperturbed octupole strengths carried by the largest 2qp components. We also list, for reference sake, these quantities for ^{150}Gd zero rotational frequency.

It is seen that the lowest excited state of ^{152}Dy is composed mainly of a single proton 2qp excitation, whose unperturbed energy is not much larger than the excitation energy of the RPA phonon. In the case of ^{154}Er, the lowest RPA phonon is composed not of a single but of a few proton 2qp excitations. Namely these states are composed mainly of valence proton excitations. On the other hand, in the excitation energy region about 1.5 MeV [for signature $(-)$] and 2 MeV [for signature $(+)$], proton excitations and neutron excitations contributes more or less equally to the RPA phonons.

It should be stressed that the magnitudes of the octupole strengths of low-lying RPA modes cannot be explained in terms of only the main 2qp components. In fact, the octupole strengths are carried by a huge number of small components. Namely, the octupole softness in open shell nuclei emerges as a result of the constructive interplay between very low lying particle-hole (or two-quasiparticle) excitations and coherent contributions from numerous two-quasiparticle (or particle-hole) excitations of small amplitudes.

4. Conclusion

We have investigated the microscopic structure of octupole vibrations built on superdeformed open shell nuclei at high spin. We obtained low lying solutions with large octupole strengths in the $N = 86$ isotones heavier than $Z = 64$. Those strengths are mainly carried by the octupole operators with large angular momentum projections on the cranking axis. We have found that, in some cases, the RPA phonons are dominated by one or a few components of the proton particle-hole (or two-quasiparticle) excitation(s). However, they have significant octupole collectivities which arise from

Table I. *Microscopic structures of some of the RPA phonons with negative signature appeared in Fig. 1(a). Listed are the excitation energies of the RPA phonons $\Omega_n(MeV)$, mass octupole strengths $|\langle n|Q_3''|0\rangle|^2$ (w.u.), the largest two-quasiparticle components of the RPA phonons, the squared forward amplitudes $\psi_n(\mu\nu)^2$, sums of the squared forward amplitudes for protons $\Psi_n(\pi)$, sums of the squared forward amplitudes Ψ_n, unperturbed energies $E_{\mu\nu}(MeV)$ and unperturbed octupole strengths $|\langle\mu\nu|Q_3''|0\rangle|^2$ (w.u.) of the largest two-quasiparticle components. For reference sake, the results for ^{150}Gd at zero rotational frequency are also shown in the lowest rows, denoted as (^{150}Gd)*

nuclei	Ω_n	$\lvert\langle n\rvert Q_3''\rvert 0\rangle\rvert^2$	main configuration	$\psi_n(\mu\nu)^2$	$\Psi_n(\pi)$	Ψ_n	$E_{\mu\nu}$	$\lvert\langle\mu\nu\rvert Q_3''\rvert 0\rangle^2$
^{146}Nd	0.92	27	$\pi(532)5/2(-i) - [420]1/2(-i)$	0.65	0.99	1.03	0.99	0.48
	1.52	42	$\nu(761)3/2(i) - [642]5/2(i)$	0.23	0.60	1.04	1.85	0.91
^{148}Sm	1.38	74	$\pi[651]3/2(-i) - [532]5/2(-i)$	0.17	0.71	1.06	1.75	0.75
^{150}Gd	1.45	115	$\pi[651]3/2(-i) - [532]5/2(-i)$	0.33	0.60	1.12	1.80	0.79
^{152}Dy	0.77	58	$\pi[770]1/2(i) - [651]3/2(i)$	0.87	0.96	1.06	0.98	1.20
	1.55	82	$\nu[761]5/2(i) - [642]5/2(i)$	0.40	0.32	1.08	1.85	0.91
^{154}Er	0.75	41	$\pi[532]3/2(i) - [404]9/2(i)$	0.50	0.98	1.03	0.98	1.20
	1.58	95	$\nu[761]3/2(i) - [642]5/2(i)$	0.31	0.44	1.09	1.85	0.91
(^{150}Gd)	2.01	300	$\nu[880]1/2(i) - [770]1/2(i)$	0.07	0.59	1.27	6.14	4.65
	2.14	143	$\nu[770]1/2(i) - [660]1/2(i)$	0.11	0.39	1.11	2.35	0.05
	2.33	100	$\pi[532]3/2(i) - [404]9/2(i)$	0.23	0.60	1.07	2.69	0.51

Table II. *Same as Table I but for some of the RPA phonons with negative signature appeared in Fig. 1(b)*

nuclei	Ω_n	$\lvert\langle n\rvert Q_3''\rvert 0\rangle\rvert^2$	main configuration	$\psi_n(\mu\nu)^2$	$\Psi_n(\pi)$	Ψ_n	$\Sigma_{\mu\nu}$	$\lvert\langle\mu\nu\rvert Q_3''\rvert 0\rangle\rvert^2$
^{146}Nd	0.91	27	$\pi[532]5/2(i) - [420]1/2(-i)$	0.79	0.99	1.03	1.00	0.46
	2.52	63	$\nu[642]5/2(i) - [521]3/2(-i)$	0.34	0.40	1.04	2.54	0.91
^{148}Sm	1.58	25	$\pi[532]5/2(i) - [641]3/2(-i)$	0.43	0.77	1.02	1.73	0.46
	2.11	58	$\pi[422]3/2(i) - [532]5/2(-i)$	0.40	0.78	1.04	2.16	0.05
^{150}Gd	1.89	103	$\nu[761]3/2(i) - [642]5/2(-i)$	0.22	0.54	1.07	2.06	0.60
^{152}Dy	0.63	37	$\pi[770]1/2(i) - [660]1/2(-i)$	0.95	1.00	1.04	0.76	0.95
	0.82	19	$\pi[532]3/2(i) - [660]1/2(-i)$	0.95	1.00	1.02	0.90	0.49
	2.11	73	$\nu[413]5/2(i) - [301]1/2(-i)$	0.40	0.85	1.04	2.04	0.19
^{154}Er	0.65	36	$\pi[770]1/2(i) - [660]1/2(-i)$	0.89	1.00	1.04	0.79	0.83
	0.77	18	$\pi[532]3/2(i) - [404]9/2(-i)$	0.67	1.00	1.02	0.84	0.38
	2.42	69	$\pi[413]5/2(i) - [301]1/2(-i)$	0.10	0.56	1.04	2.24	0.15
(^{150}Gd)	2.13	143	$\nu[770]1/2(i) - [660]1/2(-i)$	0.11	0.39	1.11	2.35	0.05
	2.33	100	$\pi[532]3/2(i) - [404]9/2(-i)$	0.23	0.60	1.07	2.69	0.51

coherent contributions of a huge number of small components. Thus, the constructive interplay of a few lowest-lying particle-hole (or two-quasiparticle) excitations and octupole vibrations is very important in determining the octupole softness of superdeformed bands.

Acknowledgements

S.M. and K.M. are indebted to the ECT* for financial supports which made possible our stay in the ECT* and the attendance to the International Workshop on High Spins and Novel Deformation.

References

1. Dagnall, P. J. *et al.*, Phys. Lett. **B335**, 313 (1994).
2. Nakatsukasa, T., Matsuyanagi, K., Mizutori, S. and Nazarewicz, W., to be published.
3. Crowell. B. *et al.*, Phys. Lett. **B333**, 320 (1994).
4. Mizutori, S., Shimizu, Y. R. and Matsuyanagi, K., Prog. Theor. Phys. **83**, 666 (1990); *ibid*, **85**, 559 (1991); *ibid*, **86**, 131 (1991).
5. Nakatsukasa, T., Mizutori, S. and Matsuyanagi, K., Prog. Theor. Phys. **87**, 607 (1992); *ibid*, **89**, 847 (1993).
6. Mizutori, S., Nakatsukasa, T., Arita, K., Shimizu, Y. R. and Matsuyanagi, K., Nucl. Phys. **A557**, 125c (1993).
7. Dudek, J., Werner, T. R. and Szymański, Z., Phys. Lett. **B248**, 235 (1990).
8. Höller, J. and Åberg, S., Z. Phys. **336**, 363 (1990).
9. Li, X., Dudek, J. and Romain, P., Phys. Lett. **B271**, 281 (1991).
10. Chaseman, R. .R., Phys. Lett. **B266**, 243 (1991).
11. Bonche, P., Krieger, S. J. and Weiss, M. S., Phys. Rev. Lett. **66**, 876 (1991).
12. Nazarewicz, W. and Dobaczewski, J., Phys. Rev. Lett. **68**, 154 (1992).
13. Skalski, J., Phys. Lett. **B274**, 1 (1992).
14. Piepenbring, P., Nucl. Phys. **A541**, 148 (1992).
15. Nazmitdinov, R. and Åberg, S., Phys. Lett. **B289**, 238 (1992).
16. Skalski, J., Heenen, P.-H., Bonche, P., Flocard, H. and Meyer, J., Nucl. Phys. **A551** 109 (1993).
17. Arita, K. and Matsuyanagi, K., Prog. Theor. Phys. **89**, 389 (1993), *ibid*, **91**, 723 (1994).
18. Sakamoto, H. and Kishimoto, T., Nucl. Phys. **A501**, 250 (1989).
19. Brack, M. *et al.*, Rev. Mod. Phys. **44**, 320 (1972).

ELSEVIER

Nuclear Physics A 592 (1995) 9–32

NUCLEAR PHYSICS A

Classical bifurcation and enhancement of quantum shells: Systematic analysis of reflection-asymmetric deformed oscillator

Ken-ichiro Arita[1], Kenichi Matsuyanagi

Department of Physics, Kyoto University, Kyoto 606-01, Japan

Received 1 May 1995

Abstract

The correspondence between classical periodic orbits and quantum shell structure is investigated for a reflection-asymmetric deformed oscillator model as a function of quadrupole and octupole deformation parameters. The periodic orbit theory reveals several aspects of quantum level structure for this non-integrable system. Good classical-quantum correspondence is obtained in the Fourier transform of the quantum level density, and the importance of periodic orbit bifurcation is demonstrated. A systematic survey of the local minima of shell energies in the two-dimensional deformation parameter space shows that prominent shell structures do emerge at finite values of the octupole parameter. Correspondences between the regions exhibiting strong shell effects and the classical bifurcation lines are investigated, and the significance of these bifurcations is indicated.

1. Introduction

Shell structure is one of the important aspects of finite quantum many-body systems. In the single-particle level density, one may generally find some regular patterns like shells consisting of dense and thin regions. This pattern changes with deformation, and the system favors the shape which makes the level density at the Fermi surface lower. Predictions of the superdeformed (extremely large quadrupole deformations with axis ratio about 2:1) and the hyperdeformed (the axis ratio about 3:1) nuclear states, which are hot current topics of high-spin nuclear structure physics, had been based on the

[1] Present address: Yukawa Institute for Theoretical Physics, Kyoto University, Kyoto 606-01, Japan.

SSDI 0375-9474(95)00219-7

above kind of consideration. Strong shell effects which appear at ellipsoidal shapes with the axis ratios about 2:1 and 3:1 play essential roles in stabilizing such exotic shapes. Reflection-asymmetric degrees of freedom are also one of the most exciting subjects in the current high-spin physics. Superdeformed potentials possess remarkable single-particle level structures where levels with different parities approximately (exactly in the harmonic oscillator limit) degenerate in the same major shell, which may bring about strong octupole correlations [1–3]. The recent remarkable development of large γ-ray detector arrays encourages us to find such exotic shapes like reflection-asymmetric superdeformations, and to investigate the mechanism of producing them. Recently micro-cluster physics has also attracted much attention, and many nuclear physicists have been contributing to this new field. Shell structures and deformations of clusters are very interesting subjects – their shapes can actually be seen with an electron microscope – and one can apply almost the same theoretical framework to both nuclei and micro-clusters [4–6].

A clear understanding of the origin of shell structure may be obtained by the use of semiclassical theory. Correspondences between quantum spectra and classical dynamical properties of Hamiltonian systems have been extensively investigated for two limiting cases, namely, for integrable and strongly chaotic situations. Most physical systems are situated in the midst of these limits, however, and belong to what we call "mixed" systems. The semiclassical theory for mixed systems is difficult and only a few aspects have been clarified up to now. This difficulty is associated with the periodic-orbit bifurcations (characteristic to the mixed systems) where the stationary phase approximation (SPA) and the conventional trace formula for representing the quantum spectrum in terms of classical periodic orbits breaks down. Fortunately, however, an approach in the inverse direction sometimes works and one can extract the periodic orbit information from the quantum spectrum by means of the Fourier transformations. This approach is very useful to understand the shell structure of the quantum spectrum. We take this approach and clarify some aspects of a mixed system, directing our attention to the influence of the bifurcations of short periodic orbits on the gross structure of the quantum spectrum.

In this paper, we investigate the classical-quantum correspondence for an axially-symmetric deformed oscillator model with reflection-asymmetric terms. This is a non-integrable model and chaotic behavior gradually emerges in the dynamics as the octupole deformation becomes large. The role of periodic orbit bifurcations will be emphasized. In Section 2, basic elements of the semiclassical theory relevant to our analysis are briefly reviewed. Special attention will be paid to the classical bifurcation phenomena and their effects on the quantum spectra. In Section 3 our model is introduced and several aspects of it are summarized. In Sections 4–7, we will present numerical results of the semiclassical analysis and discuss their implications. It will be shown that prominent shell structures emerge for finite octupole deformations superposed on the prolate shapes. Origins of such new shell structures will be clarified. Section 8 is devoted to summary and conclusion.

2. Basic formulae

2.1. Classical Hamiltonian system

Let us consider a Hamiltonian system with f degrees of freedom. The equation of motion (EOM) for a $2f$-dimensional phase space vector $Z = (\boldsymbol{p}, \boldsymbol{q})$ is expressed as

$$\frac{\mathrm{d}}{\mathrm{d}t} Z = \Lambda \frac{\partial H}{\partial Z}, \qquad \Lambda = \begin{pmatrix} O & -I \\ I & O \end{pmatrix}, \tag{1}$$

where O and I denote the f-dimensional zero and identical matrices, respectively. Now consider a bundle of trajectories around a certain solution $Z_\alpha(t)$ and write them as $Z(t) = Z_\alpha(t) + \delta Z(t)$. Then the EOM for $\delta Z(t)$ is given by

$$\frac{\mathrm{d}}{\mathrm{d}t} \delta Z = \Lambda \mathcal{H}(Z_\alpha(t))\, \delta Z, \qquad \mathcal{H}(Z)_{ij} = \frac{\partial^2 H(Z)}{\partial Z_i \partial Z_j} \tag{2}$$

up to the first order in δZ. $\mathcal{H}$ is called Hessian matrix. One can easily integrate the above differential equation and obtain the following solution:

$$\delta Z(t) = \mathcal{T}_\tau \exp\left[\int_{t_0}^{t} \mathrm{d}\tau\, \Lambda \mathcal{H}(\tau)\right] \delta Z(t_0) \equiv \mathcal{S}_\alpha(t - t_0)\, \delta Z(t_0), \tag{3}$$

where $\mathcal{T}_\tau$ denotes that the exponential is defined by time-ordered product. $\mathcal{S}_\alpha$ is called the stability matrix of the trajectory α, whose eigenvalues determine its stability.

Let Σ denote a $(2f-2)$ dimensional hypersurface in the phase space with fixed energy E. It defines a time-discretized mapping $\mathcal{M} : \Sigma \mapsto \Sigma$ with classical trajectories, which is called the Poincaré map. Periodic orbits $\bar{Z}$ are defined as the fixed points of $\mathcal{M}$, namely, by $\mathcal{M}(\bar{Z}) = \bar{Z}$. The linear part M_r (with respect to δZ) of $\mathcal{M}$ about a periodic orbit $\bar{Z}_r$ is called "monodromy matrix" and describes the stability of the orbit:

$$\mathcal{M}(\bar{Z}_r + \delta Z) = \bar{Z}_r + M_r\, \delta Z + \mathrm{O}(\delta Z^2). \tag{4}$$

The monodromy matrix is a symplectic matrix satisfying

$$\Lambda M_r{}^T \Lambda^{-1} = M_r{}^{-1}, \tag{5}$$

and this property restricts its eigenvalues as follows. Let λ be one of the eigenvalues of M_r. Relation (5) guarantees that the reciprocal of λ is another eigenvalue of M_r. Furthermore, M_r is a real matrix so that the complex conjugates of these eigenvalues are also eigenvalues. Thus the eigenvalues of the monodromy matrix generally appear in quartets ($\mathrm{e}^{\pm\alpha \pm i\beta}$). In the two-dimensional case, they appear in a pair.

Let us now proceed to a discussion on bifurcations of stable periodic orbits. Consider a trajectory that emerges at $\boldsymbol{q}$ with energy E and returns to the initial point, $\boldsymbol{q}' = \boldsymbol{q}$. This kind of trajectory certainly exists for any $\boldsymbol{q}$. The condition for this trajectory to

be periodic is that the initial and final momenta coincide; namely, $\boldsymbol{p}' = \boldsymbol{p}$. Using the Hamilton–Jacobi equation, this condition can be rewritten as

$$0 = \boldsymbol{p}' - \boldsymbol{p} = \frac{\partial S(\boldsymbol{q}', \boldsymbol{q}; E)}{\partial \boldsymbol{q}'} - \left(- \frac{\partial S(\boldsymbol{q}', \boldsymbol{q}; E)}{\partial \boldsymbol{q}} \right) = \frac{\partial S(\boldsymbol{q})}{\partial \boldsymbol{q}}, \tag{6}$$

where $S(\boldsymbol{q})$ denotes the action integral along the closed path under consideration. Thus, the periodic orbit is the stationary point of this action integral. Let us expand $S(\boldsymbol{q})$ about the periodic point $\bar{\boldsymbol{q}}$:

$$\begin{aligned} S(\bar{\boldsymbol{q}} + \delta\boldsymbol{q}) &= S(\bar{\boldsymbol{q}}) + \tfrac{1}{2}\, \delta\boldsymbol{q}^T \frac{\partial^2 S(\boldsymbol{q}, \boldsymbol{q})}{\partial \boldsymbol{q} \partial \boldsymbol{q}}\, \delta\boldsymbol{q} + \cdots \\ &\equiv \bar{S} + \tfrac{1}{2}\, \delta\boldsymbol{q}^T \mathcal{B}\, \delta\boldsymbol{q} + \cdots . \end{aligned} \tag{7}$$

After some simple matrix rearrangements, one can express $\mathcal{B}$ in terms of the quadrants of the monodromy matrix as

$$\mathcal{B} = B - (I - A) C^{-1} (I - D), \qquad M \equiv \begin{pmatrix} A & B \\ C & D \end{pmatrix}. \tag{8}$$

Note that

$$\det(\mathbf{1} - M) = - \det[C] \det[\mathcal{B}]. \tag{9}$$

The above relations provide us with a clear understanding of the connection between eigenvalues of the monodromy matrix and the bifurcation of periodic orbits. Suppose that one of the eigenvalues of M becomes unity. Then the curvature tensor $\mathcal{B}$ for the action S has a zero eigenvalue. This means that the stationary points of S (periodic orbits) locally form a continuous set and a bifurcation can occur hereafter; namely a (few) new stationary point(s) can emerge.

2.2. *Trace formula*

By means of the semiclassical theory, we can relate properties of the quantum spectrum with those of the corresponding classical system. For non-integrable Hamiltonian systems, Gutzwiller's trace formula [7–9] represents the quantum level density $g(E) = \sum_i \delta(E - E_i)$ as a sum over classical periodic orbits:

$$g^{(\mathrm{sc})}(E) = \bar{g}(E) + \sum_{r,n} A_{nr}(E) \cos\left(\frac{n S_r(E)}{\hbar} - \frac{\pi}{2} \mu_{nr} \right). \tag{10}$$

$\bar{g}(E)$ is called Weyl term (or Thomas–Fermi approximation), which is a monotonic function of energy. The sum is taken over all primitive periodic orbits r and their multiple traversals. $S_r = \oint_r \boldsymbol{p} \cdot \mathrm{d}\boldsymbol{q}$ is the action integral along the orbit r, and μ_r denotes the Maslov phase. Several numerical application of this formula to strongly chaotic systems have shown its effectiveness. As is well known, however, exact reproduction of a quantum spectrum is not an easy task, because one has to treat a huge number

of periodic orbits which show exponential proliferation as a function of energy. On the other hand, since our purpose is to understand the gross structure of the spectrum we need only a finite number of periodic orbits which have rather short periods. If one is interested in the gross structure with energy resolution δE, the change of the phase in Eq. (10) must be less than 2π for the change of energy by δE. Namely,

$$nS_r(E+\delta E) - nS_r(E) \simeq n\frac{\partial S_r(E)}{\partial E}\delta E = nT_r\delta E \lesssim 2\pi\hbar, \tag{11}$$

which leads to the relation

$$nT_r \lesssim T_{\max} \equiv \frac{2\pi\hbar}{\delta E}. \tag{12}$$

Thus, we need only short periodic orbits whose periods are less than $T_{\max}$ defined above. Although much efforts have been devoted to reproduce individual eigenenergies by calculating millions of periodic orbits, gross structures of the level spectra have rarely been discussed in connection with periodic orbits for non-integrable systems. (For integrable systems, there are several works; see for instance, Refs. [4,10–13].)

2.3. *Bifurcations*

Let us next discuss the condition for the amplitude factor A_{nr} in the trace formula (10) to take a large value. In the stationary phase approximation, the amplitude factor is expressed for isolated orbits as

$$A_{nr} = \frac{1}{\pi\hbar}\frac{T_r}{\sqrt{|\det(\mathbf{1} - M_r{}^n)|}}. \tag{13}$$

For degenerate orbits with degeneracy 1, it is represented by

$$A_{nr} = \frac{4\pi}{(2\pi\hbar)^{3/2}}\frac{B_r}{\sqrt{|\det(\mathbf{1} - M_r{}^n)|}}, \qquad B_r = \int_0^{T_r} \mathrm{d}t \left[\frac{\partial\varphi(t+T_r)}{\partial p_\varphi(t)}\right]^{-1/2}, \tag{14}$$

where φ and p_φ denote an ignorable variable in the Hamiltonian and its canonically conjugate momentum, respectively (see the appendix in Ref. [14]). From the difference in order of $\hbar$, one sees that the contribution of degenerate orbits is more important than that of isolated ones.

Another important factor, which plays an essential role in our analysis below, is the stability factor $\det(\mathbf{1} - M_r{}^n)$. Its value is independent of the point chosen on the periodic orbit. As discussed above, eigenvalues of the monodromy matrix M_r appear in pairs $(+/-)(\mathrm{e}^{\lambda}, \mathrm{e}^{-\lambda})$, λ being real or pure imaginary, or in quartets $(\mathrm{e}^{\pm\alpha\pm i\beta})$. One should note that the periodic orbit generally appears in at least one parameter family, so that the monodromy matrix always has two unit eigenvalues. Other pairs of unit eigenvalues correspond to the global continuous symmetries which the Hamiltonian possesses but the orbit itself does not. These degrees of freedom are responsible for the degeneracy and, as seen in Eq. (14), can be separated out from the definition of

M_r appearing in the stability factor. In the case of three-dimensional systems with axial symmetry, the monodromy matrix has (except for isolated non-degenerate orbits) four unit eigenvalues, and the remaining two appear in a pair $(+/-)(e^{\lambda}, e^{-\lambda})$. Thus, M_r may be reduced to a (2×2) matrix for most orbits. λ is purely imaginary for stable orbits, and real for unstable ones. The stability factor for each case becomes

$$\det(\mathbf{1} - M_r) = 2 - \mathrm{Tr}\, M_r$$

with

$$\mathrm{Tr}\, M_r = \begin{cases} 2\cos(\beta) & \text{stable,} \quad \lambda = i\beta, \\ \pm 2\cosh(\alpha) & \text{unstable,} \quad \lambda = \alpha. \end{cases} \tag{15}$$

Thus, the stability of orbit is determined by the value of $\mathrm{Tr}\, M$.

If a parameter in the Hamiltonian is continuously varied, the periodic orbits change their shapes and the values of λ also change continuously. It may occur that the β for a certain stable orbit becomes a fraction of 2π, namely, $\beta = 2\pi m/n$ with n and m being relatively prime integers. At this point $\mathrm{Tr}\, M_r^n$ becomes 2, and the amplitude factor A_{nr} suffers divergence. This singularity corresponds to the period n-upling bifurcation of the orbit r. Near the bifurcation point, the stationary phase approximation breaks down. It is then necessary to take into account higher-order fluctuations about the classical orbit to extract a finite value of A_{nr} [15]. Although we leave this task as a challenging future subject, we expect that the amplitude factor takes a large value in the bifurcation region. It will result in a large-amplitude oscillation in the level density, leading to an enhancement of the shell effect.

3. The model and its scaling properties

3.1. The model

We adopt a model Hamiltonian consisting of an axially deformed harmonic oscillator and a reflection asymmetric octupole deformed potential:

$$H = \frac{p^2}{2M} + \sum_i \frac{M\omega_i^2 x_i^2}{2} - \lambda_{30} M\omega_0^2 \left[r^2 Y_{30}(\Omega)\right]'' . \tag{16}$$

Here, the double primes denote that the variables in square brackets are defined in terms of the doubly-stretched coordinates $x_i'' = (\omega_i/\omega_0)x_i$, where $\omega_0 \equiv (\omega_x\omega_y\omega_z)^{1/3}$ being determined so that the volume conservation condition is satisfied [16]. For simplicity, we define dimensionless variables as follows:

$$\begin{cases} p_i \longrightarrow \sqrt{M\hbar\omega_0}\, p_i, \\ q_i \longrightarrow \sqrt{\hbar/M\omega_0}\, q_i, \\ H \longrightarrow \hbar\omega_0 H. \end{cases} \tag{17}$$

Then, the Hamiltonian is written as

$$H = \tfrac{1}{2}p^2 + \tfrac{1}{2}[r^2(1 - 2\lambda_{30}Y_{30}(\Omega))]''. \tag{18}$$

Since the radial dependence of the octupole potential is quadratic, the Hamiltonian obeys the following scaling rule:

$$H(\alpha \boldsymbol{p}, \alpha \boldsymbol{q}) = \alpha^2 H(\boldsymbol{p}, \boldsymbol{q}). \tag{19}$$

Thanks to this property, if one solves the Hamilton equations of motion at a certain energy E_0, the solution at any energy E is obtained by just scale transforming the solution at E_0 as $Z(t; E) = \sqrt{E/E_0}\, Z(t; E_0)$, Z denoting a phase space vector $(\boldsymbol{p}, \boldsymbol{q})$.

In the cylindrical coordinates (ρ, z, φ), the above Hamiltonian (18) is written as

$$H = \tfrac{1}{2}(p_\rho^2 + p_z^2) + V(\rho, z; p_\varphi),$$

$$V(\rho, z; p_\varphi) = \frac{p_\varphi^2}{2\rho^2} + \left[\frac{\rho^2 + z^2}{2} - \lambda_{30}\sqrt{\frac{7}{16\pi}}\frac{2z^3 - 3z\rho^2}{\sqrt{\rho^2 + z^2}}\right]''. \tag{20}$$

Thus, we can treat the system as a two-dimensional one with fixed angular momentum p_φ. This reduction enables us to make use of the Poincaré surface of section in order to survey the classical phase space profile. Note that $\chi \equiv p_\varphi/E$ is a scaling-invariant parameter and, therefore, classical properties are the same for the same χ.

In the following sections, we shall investigate how the properties of the quantum spectrum for the Hamiltonian (16) changes as the two deformation parameters, $\delta_{\rm osc} = (\omega_\perp - \omega_z)/\bar{\omega}$ and λ_{30}, are varied. We shall then discuss the physical origins of these changes by means of the periodic orbit theory reviewed in Section 2.

3.2. *Fourier transformation of quantum level density*

As we will see in the following numerical analyses, the Hamiltonian above becomes chaotic with increasing octupole deformation parameter λ_{30}. But considerable parts of the phase space remain regular and the system is considered as a so-called "mixed system". The trace formula based on the stationary phase approximation (SPA) does not work well in such situations. The amplitude factors suffer divergences at the bifurcation points of stable periodic orbits because of the breakdown of SPA. Consequently, we cannot directly use the conventional semiclassical expression to analyze the quantum spectrum. Fortunately, we can avoid the above difficulty by using the Fourier transformation technique for the quantum level density. Suppose that the level density is characterized by the classical periodic orbits and is expressed as

$$g_{\rm osc}^{\rm (sc)}(E) = \sum_{n=1}^{\infty}\sum_{r} A_{nr}(E)\cos\left(\frac{nS_r(E)}{\hbar} - \frac{\pi}{2}\mu_{nr}\right), \tag{21}$$

without specifying the concrete expression of the amplitude factor $A_{nr}(E)$ which may be obtained by going beyond the SPA. Since our model obeys the scaling rule (19), energy dependence of the classical variables entering Eq. (21) is factored out as follows:

$$S_r(E) = ET_r,$$
$$A_{nr}(E) = E^{d_r/2} A_{nr}^{(0)}, \tag{22}$$

where d_r is the effective degeneracy of the orbit, and equal to 1 for most orbits due to the axial symmetry. For isolated orbits, $d_r = 0$ and we expect that their contributions to the level density may be small. The degeneracies are integers in the classical dynamics, but in the quantum mechanics this restriction is relaxed and d_r changes continuously in the bifurcation regions [15,9]. Using the above relations, Eq. (22) is expressed as

$$g^{(\mathrm{sc})}(E) = \bar{g}(E) + \sum_{r,n} E^{d_r/2} A_{nr}^{(0)} \cos\left(\frac{nET_r}{\hbar} - \frac{\pi}{2}\mu_{nr}\right). \tag{23}$$

Now let us consider the Fourier transformation of the level density, defined by

$$F(s) = \frac{1}{2\pi\hbar} \int \mathrm{d}E\, \mathrm{e}^{isE/\hbar} E^{-d/2} g(E) \exp\left[-\frac{1}{2}\left(\frac{E}{E_{\max}}\right)^2\right]. \tag{24}$$

Here the Gaussian damping factor is used for energy cut-off, and we shall put $d = 1$ in order to cancel the energy dependence of the amplitude factors for most orbits. Inserting the quantum level density $g(E) = \sum_i \delta(E - E_i)$ and the semiclassical one (23) into Eq. (24), we obtain quantum mechanical and semiclassical expressions for $F(s)$:

$$F^{(\mathrm{qm})}(s) = \frac{1}{2\pi\hbar} \sum_i \frac{1}{\sqrt{E_i}} \mathrm{e}^{isE_i/\hbar} \exp\left[-\frac{1}{2}\left(\frac{E_i}{E_{\max}}\right)^2\right],$$
$$F^{(\mathrm{sc})}(s) \simeq \bar{F}(s) + \sum_{r,n} A_{nr}^{(0)} \frac{1}{\sqrt{2\pi}\Delta s} \exp\left[-\frac{1}{2}\left(\frac{s - nT_r}{\Delta s}\right)^2\right], \tag{25}$$

respectively, where $\Delta s = \hbar/E_{\max}$. $F^{(\mathrm{qm})}$ is calculated from the single-particle spectrum obtained by diagonalizing the Hamiltonian with deformed oscillator basis. The result is compared with the semiclassical expression $F^{(\mathrm{sc})}$. In Eq. (25), $\bar{F}(s)$ corresponds to the Weyl term which is regarded as a contribution from orbit of zero-length, and it has peak at $s = 0$. The remaining part has a functional form exhibiting successive peaks at the periods of classical periodic orbits and their heights are proportional to the amplitude factors of the corresponding orbits. By comparing the calculated $F^{(\mathrm{qm})}(s)$ with $F^{(\mathrm{sc})}(s)$, we can thus extract information about periodic orbits from the quantum spectrum.

4. Shell structure energy calculation

A useful quantitative measure of shell structure is the shell structure energy which is defined as the fluctuation part of the sum of single-particle energies, i.e.,

$$\mathcal{E}_{\mathrm{sh}}(N) = \sum_{k=1}^{N} E_k - \tilde{\mathcal{E}}(N), \tag{26}$$

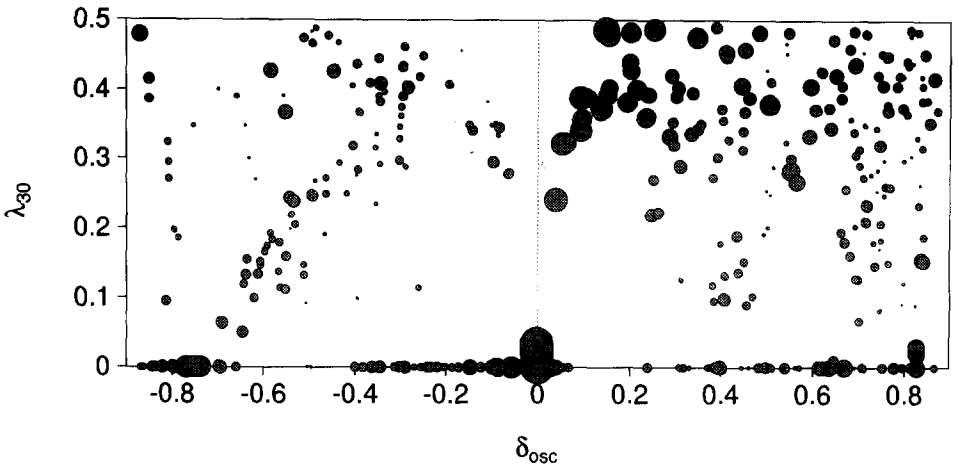

Fig. 1. Local minima of shell structure energy in the two-dimensional deformation parameter space (δ_{osc}, λ_{30}). The size of each disc represents the absolute value of the shell structure energy normalized as $\mathcal{E}_{sh}/N^{1/3}$. Plotted data are for even N in the range $16 \leqslant N \leqslant 160$.

where E_k's represent eigenvalues of the single-particle Hamiltonian. The second term $\tilde{\mathcal{E}}(N)$ is obtained by smoothing the first term by means of the Strutinsky method; it is a smooth function of particle number N and of other potential parameters. The shell structure energy takes a large negative value when the single-particle level density at the Fermi surface is low.

We have carried out a systematic calculation of the shell structure energy for the Hamiltonian (16) as a function of the deformation parameters δ_{osc} (quadrupole deformation), λ_{30} (octupole deformation) and of the particle number N. Fig. 1 shows a map of the local minima of shell structure energies in the two-dimensional deformation parameter space calculated for particle numbers in the range $16 \leqslant N \leqslant 160$. The centers of discs show the loci of local minima (corresponding to different values of N) and the sizes of the discs represent the absolute values of shell structure energies. As the order of magnitude of the shell structure energy is roughly proportional to $N^{1/3}$ in the harmonic oscillator case [19], we normalize them by multiplying $N^{-1/3}$ in order to compare system with different values of N.

For $\lambda_{30} = 0$, it is well known that strong shell structure exists at $\delta_{osc} = 0$ (spherical), 3/5 (prolate superdeformed), 6/7 (prolate hyperdeformed), $-3/4$ (oblate superdeformed) and so on. The distribution of discs is actually dense around such points. We find in Fig. 1 that, in addition to such known cases, prominent shell structure emerges also at finite values of octupole deformation. Their shell-structure energies are comparable, in magnitude, to (sometimes larger than) those for the purely quadrupole shapes. The most remarkable region is that of $\lambda_{30} = 0.3 \sim 0.4$ and $\delta_{osc} \simeq 0.1$. Using the semiclassical theory, let us analyze in the following sections the mechanism which creates the above new shell structures for the combination of the quadrupole and octupole deformations.

5. Semiclassical analyses

In this section, we investigate how the structure of the quantum spectrum changes as the octupole deformation parameter λ_{30} is increased, fixing quadrupole deformation parameter $\delta_{\rm osc}$ at several positive values (between the spherical and the prolate superdeformed shapes). Fig. 2 shows the single-particle spectra as functions of λ_{30} for the Hamiltonian (16) with $\delta_{\rm osc} = 0.1$, 0.3 and 0.5. The corresponding axis ratios $\omega_\perp/\omega_z$ are 31/28, 11/8 and 7/4, respectively. They are not in simple ratios so that there is no prominent shell structure at $\lambda_{30} = 0$. However, new shell structures emerge at finite values of λ_{30}. To see features of these spectra, we show in Fig. 3 the Fourier transforms of the level density defined by (25). As discussed in Section 3.2, one sees prominent Fourier peaks at the periods of classical periodic orbits. It means that the fluctuation of the spectrum is characterized by the periodic orbits, demonstrating a beautiful applicability to our model of the semiclassical method in Section 2.2. For elucidating the features of shell structure, it is essential to understand the behavior of these Fourier peaks with respect to the deformation parameters. As discussed in the previous sections, short periodic orbits play important roles for the formation of gross structure of quantum spectrum. There are various periodic orbits of various topologies in each part of the deformation parameter space and the same type of orbits change their characters as the parameters change. This fact is clearly seen in the Fourier transforms where peaks corresponding to certain orbits change their heights. The heights of the peaks represent nothing but the strengths of the shell structures. Let us discuss in the following what kind of periodic orbits exist and how they determine the features of quantum spectra in several regions on the $(\delta_{\rm osc}, \lambda_{30})$ plane.

5.1. The case of δ_{osc}=0.1

Let us first take up the case of $\delta_{\rm osc} = 0.1$, where we obtain especially strong shell structures at finite λ_{30} values in the shell structure energy calculation (see Fig. 1), and let us discuss which orbits are responsible for these shell structures. Fig. 4 shows, for several values of λ_{30}, some planar periodic orbits in the plane including the symmetry axis. We use the Monodromy Method developed by Baranger et al. [17] to calculate periodic orbits and their monodromy matrices. At $\lambda_{30} = 0$, the most important orbit family is the ellipse-shaped one in the (x, y) plane. The next orbit family is 31:28 Lissageous. They are very long orbits and unimportant for the gross shell structure. Adding the octupole deformation, new types of orbits are born. Orbit PR appears at $\lambda_{30} = 0.12$ by the isochronous bifurcation of the orbit PA, and PA becomes unstable after this bifurcation. At $\lambda_{30} = 0.24$, the orbit PA becomes stable again and a new orbit PM appears.

To see these bifurcations, the Poincaré map is a very convenient implement. As our Hamiltonian has axial symmetry, we can treat it as a two-dimensional system with fixed angular momentum p_φ. Fig. 5 is the Poincaré map (z, p_z) for the "projected" Hamiltonian (20) with $p_\varphi = 0$. Here the surface is defined by $p_\rho = 0$ and $\dot{p}_\rho < 0$. In

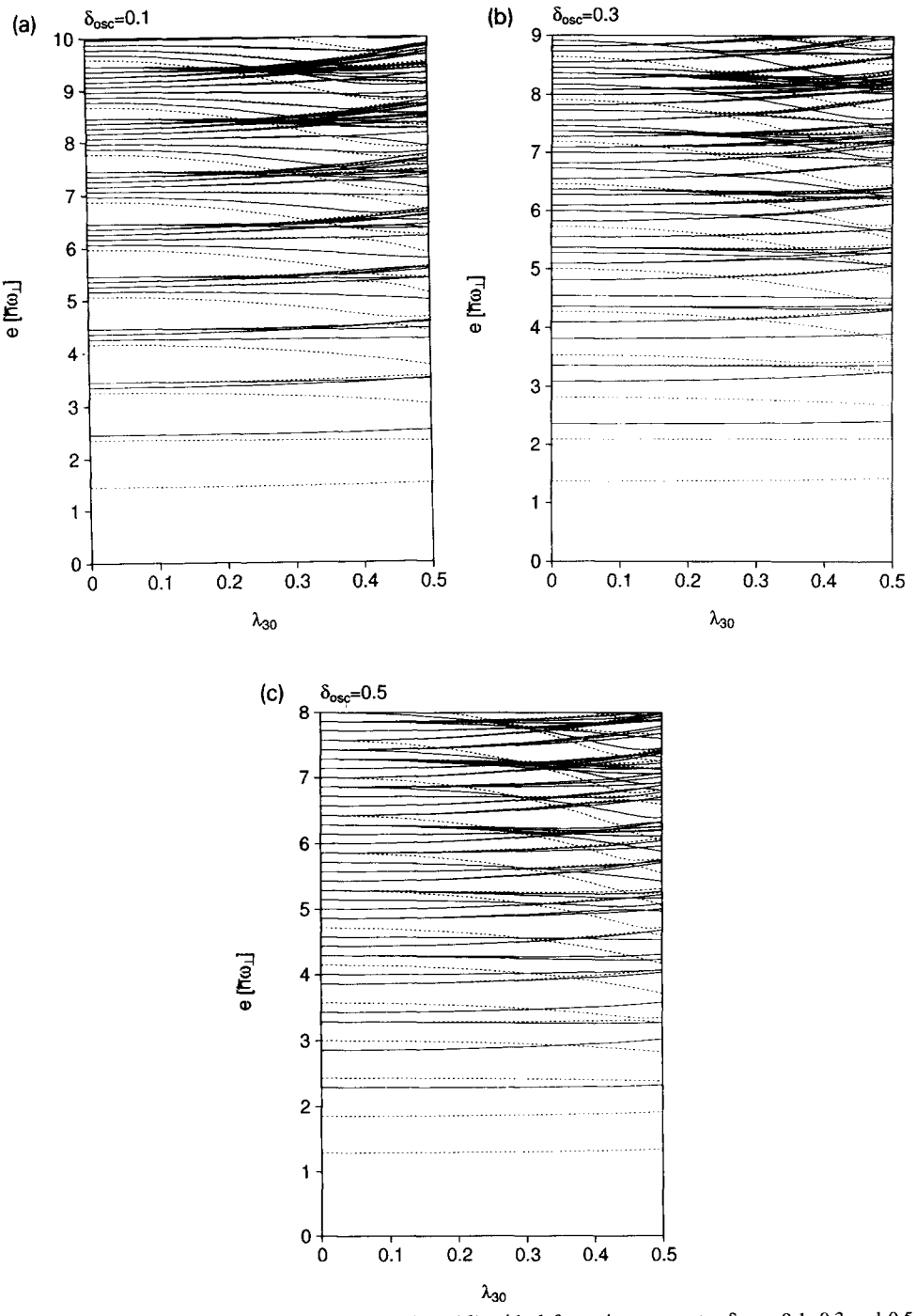

Fig. 2. Single-particle spectrum of the Hamiltonian (16) with deformation parameter $\delta_{\rm osc} = 0.1$, 0.3 and 0.5 as functions of the octupole parameter λ_{30}. Dashed and solid curves represent the levels whose K quantum numbers are zero and nonzero, and the latter degenerate in two due to the time-reversal symmetry.

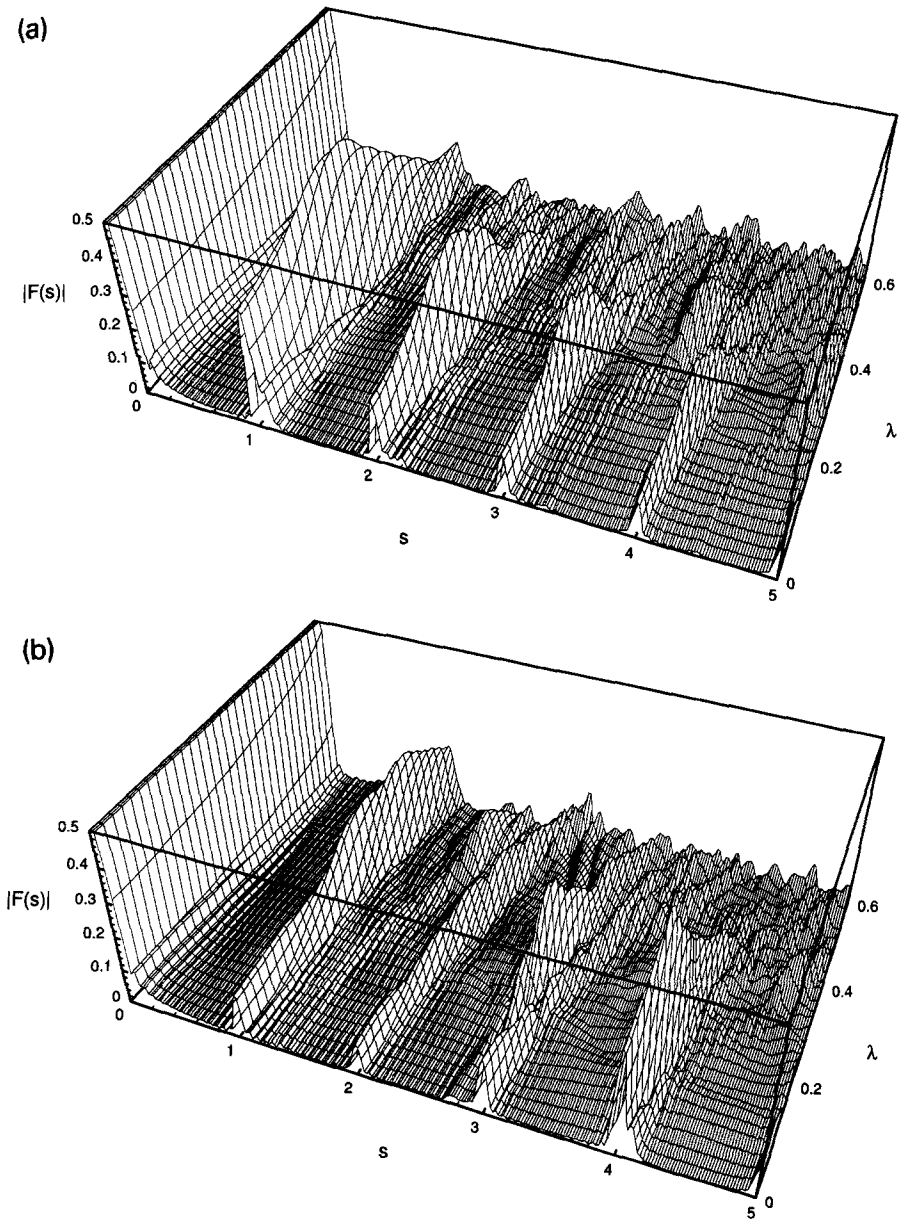

Fig. 3. Fourier transforms $|F(s)|$ of the level densities for the Hamiltonian (16) with $\delta_{\rm osc} = 0.1$, 0.3 and 0.5, plotted as functions of the action s and the octupole parameter λ_{30}.

the top panel, the center of the main torus corresponds to the orbit PA. In the middle panel, the orbit PA becomes an unstable saddle and a new pair of island is created. These islands correspond to the orbit PR. In the bottom panel the orbit PA comes back to a stable one and creates a new pair of saddles confronting horizontally. These saddles

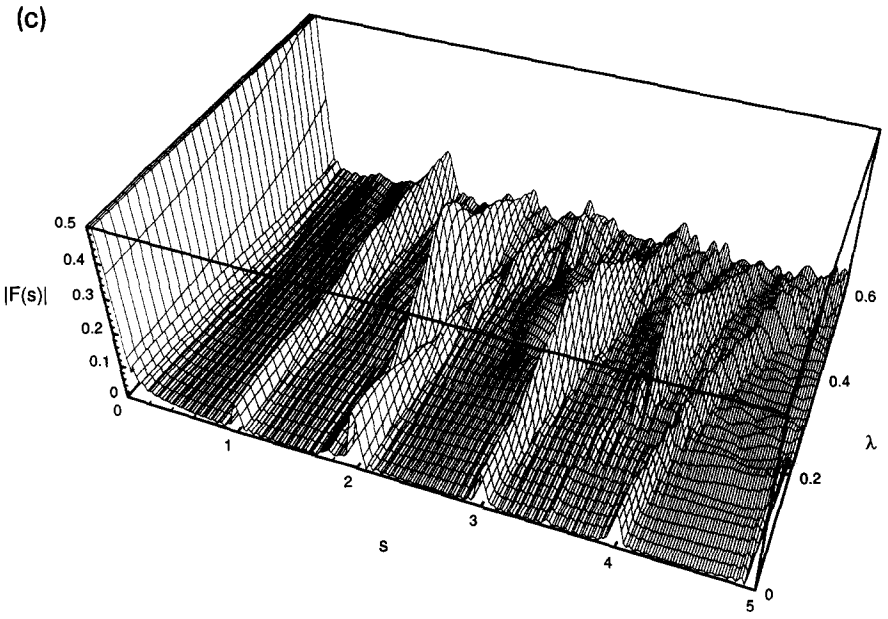

Fig. 3 — continued.

correspond to the orbit PM.

As is well known, stabilities of periodic orbits are determined by the monodromy matrices. Fig. 6 shows the traces of the two-dimensional monodromy matrices for orbits associated with the above bifurcations. The bifurcation occurs at $\mathrm{Tr}\, M = 2$ where the monodromy matrix has the unit eigenvalues $(1, 1)$. Period n-upling bifurcations occur at $\mathrm{Tr}\, M^n = 2$. Higher order (large n) resonances occur at every points of the torus and new orbits bifurcate from them, but they are of rather long periods and are related with more detailed structure of the spectrum. In the Fourier transform Fig. 3a, the peak corresponding to the orbit PA with period $T \simeq 2\pi/\omega_\perp$ strongly enhances at $\lambda_{30} \simeq 0.2$. It mainly characterizes the shell structure seen in the spectrum Fig. 2a at $\lambda_{30} = 0.2 \sim 0.3$.

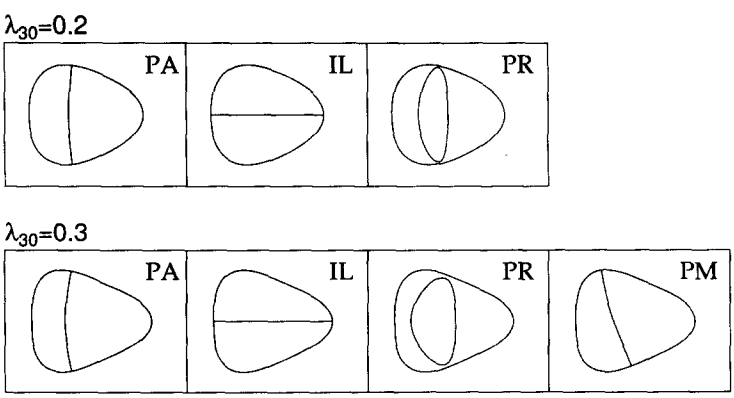

Fig. 4. Some short planar periodic orbits of the Hamiltonian (16) with $\delta_{\mathrm{osc}} = 0.1$.

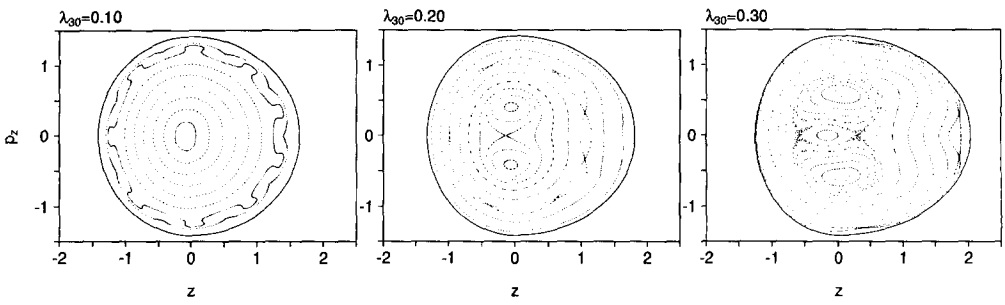

Fig. 5. The Poincaré surface of section (z, p_z) for the Hamiltonian (20) with $p_\varphi = 0$. The surface is defined by $p_\rho = 0$ and $\dot{p}_\rho < 0$.

This enhancement is related with the above bifurcations of PA at $\lambda_{30} = 0.128$ and 0.227.

5.2. *The case of δ_{osc}=0.3*

Next let us discuss the case of $\delta_{\rm osc} = 0.3$. Some important classical orbits are drawn in Fig. 7. Orbit PO is born out of the period-doubling bifurcation of the orbit IL at $\lambda_{30} = 0.215$. Orbits PP and PQ are created by the saddle-node bifurcation (pair creation of stable and unstable orbits from nothing) at $\lambda_{30} = 0.221$. Orbit PR emerges from the isochronous bifurcation of the orbit PA at $\lambda_{30} = 0.338$. In the Fourier transform Fig. 3b, the enhancement of the peak with $s \simeq 1$ is related with the isochronous bifurcation. The orbits associated with the period-doubling and saddle-node bifurcations mentioned above are of similar periods and contribute to the same peak with $s \simeq 2.75$ in the Fourier transform. It also shows strong enhancement in the bifurcation region.

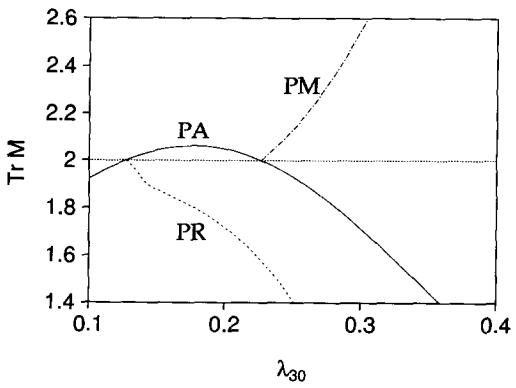

Fig. 6. Traces of the monodromy matrices at $\delta_{\rm osc} = 0.1$ for some short periodic orbits plotted as functions of the octupole deformation parameter λ_{30}.

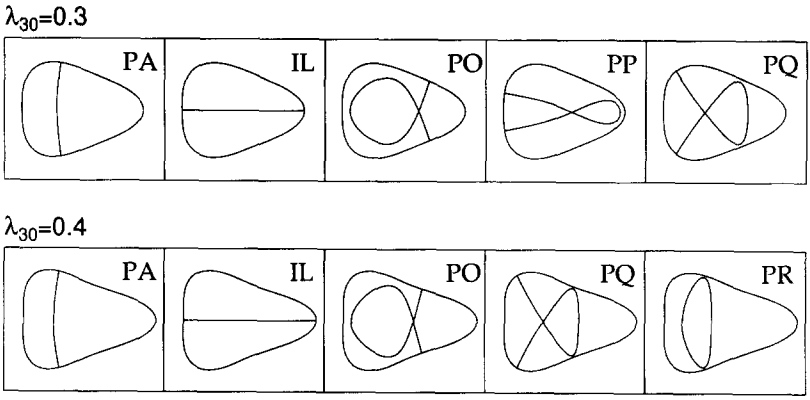

Fig. 7. Some short planar periodic orbits for the Hamiltonian (16) with $\delta_{osc} = 0.3$.

5.3. The case of $\delta_{osc}=0.5$

Lastly, let us consider the case of $\delta_{osc} = 0.5$. This quadrupole deformation is almost equivalent to the case of axis ratio $\sqrt{3} : 1$ treated in Ref. [18]. The feature of the shell is rather weak at $\lambda_{30} = 0$. However, one may notice in Fig. 2 that a remarkable shell structure emerges at $\lambda_{30} \simeq 0.3$. In the Fourier transform Fig. 3c, a significant enhancement of the peak with $s \simeq 1.75$ is observed. It seems that this is the most typical example in our model, which clearly exhibits a new shell structure emerging at finite octupole deformation.

Some short periodic orbits are illustrated in Fig. 8. At $\lambda_{30} = 0$, the ellipse-shaped family in the (x, y) plane characterize the structure of the spectrum. Orbit PB is born out of the isochronous bifurcation of the orbit IL at $\lambda_{30} = 0.276$, orbits PC and PD are created by the saddle-node bifurcation at $\lambda_{30} = 0.274$. The Poincaré maps and the traces of the monodromy matrices are displayed in Figs. 9 and 10, respectively. The strong enhancement of the peak with $s \simeq 1.85$ at $\lambda_{30} \simeq 0.4$ are related with the bifurcations mentioned above. Orbits associated with these bifurcations are of similar periods and thus contribute to the same peak in the Fourier transform Fig. 3c. These bifurcations may be regarded as the mechanism which creates the prominent shell structure at finite octupole deformation.

Orbits PE and PF are born associated with the period-tripling bifurcation of the orbit PA at $\lambda_{30} = 0.376$. A quantum signature of this bifurcation is also seen in the Fourier peak with $s \simeq 3$. Thus, we can conclude that the enhancement of the Fourier peak in the bifurcation region is a general phenomenon.

6. Bifurcation lines in the two-dimensional parameter space

In the preceding section, we presented several examples where bifurcations of short periodic orbits play important roles in forming shell structures. In this section, let us dis-

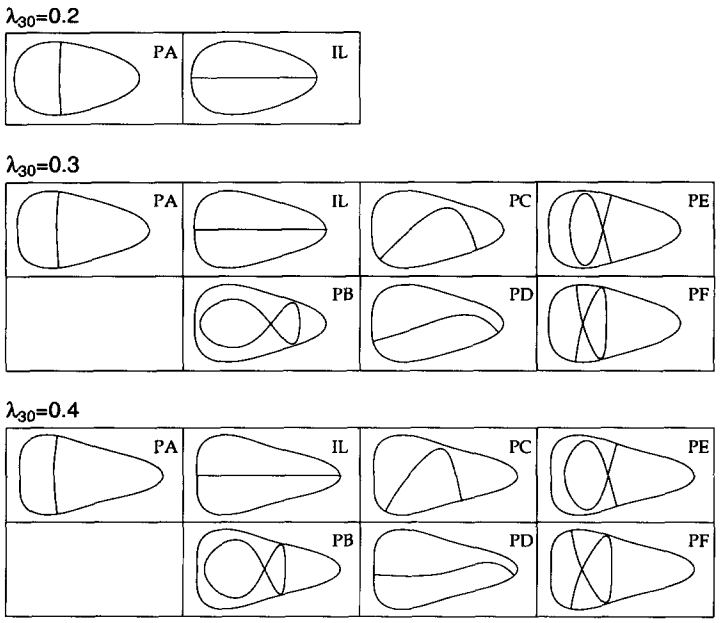

Fig. 8. Some short planar periodic orbits for the Hamiltonian (16) with $\delta_{\rm osc} = 0.5$.

cuss roles of the bifurcations varying two deformation parameters systematically. In the n-dimensional parameter space, bifurcation points generally form $(n-1)$-dimensional manifolds; they are 1-dimensional curves in the present case. We have evaluated these bifurcation lines for some short periodic orbits. The result of the calculation is presented in Fig. 11. These bifurcation lines always emerge at the points where the ratios $\omega_\perp/\omega_z$ are rational and $\lambda_{30} = 0$. Note that $\delta_{\rm osc}$=0, 3/5, 6/7 and $-3/4$ correspond to the spherical, prolate superdeformed, prolate hyperdeformed and oblate superdeformed shapes, respectively. The orbit PA causes isochronous bifurcations across the lines i and ii (in

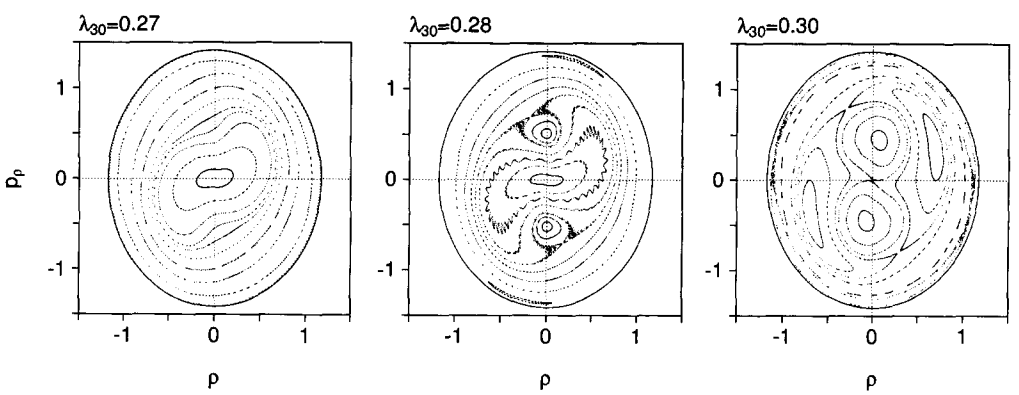

Fig. 9. Poincaré surfaces of section for $\delta_{\rm osc} = 0.5$ in the bifurcation region of short periodic orbits. The surface (ρ, p_ρ) is defined by $z = 0$ and $p_z > 0$.

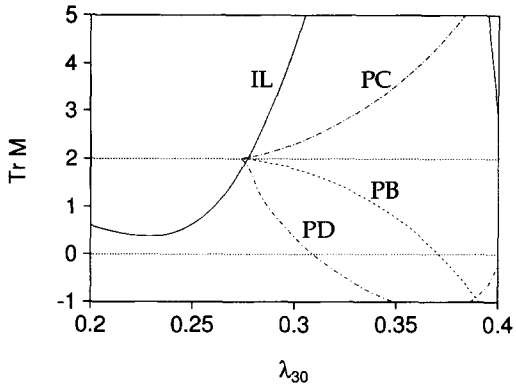

Fig. 10. Same as Fig. 6 but $\delta_{osc} = 0.5$.

direction from the right to the left). As discussed in the case $\delta_{osc} = 0.1$, new orbits PM and PR are born after the bifurcations i and ii, respectively. On the other hand, as discussed in the case $\delta_{osc} = 0.5$, the lines iii∼vi are related with the orbits PB, PC, PD, IL and 2PA (double traversals of the orbit PA). The orbit IL causes isochronous bifurcation (from the left to the right) and produces the orbit PB (stable) across the line iii, while the orbit PC (unstable) and PD (stable) are born out of the saddle-node bifurcation across the line iv in the region $\delta_{osc} \lesssim 0.5$. As δ_{osc} increases, orbit PB becomes unstable while orbit PC becomes stable across the line v and they annihilate into 2PA across the line vi. Across the line vii, the orbit PA causes period-tripling bifurcation (from the right to the left) and produces orbits PE and PF.

According to the discussions in the preceding sections, we expect strong shell effects along these bifurcation lines. Prominent shell structures are known to exist for the spherical and superdeformed shapes (the end points of the bifurcation lines) where periodic orbit conditions for the harmonic oscillator potential are satisfied. Conditions

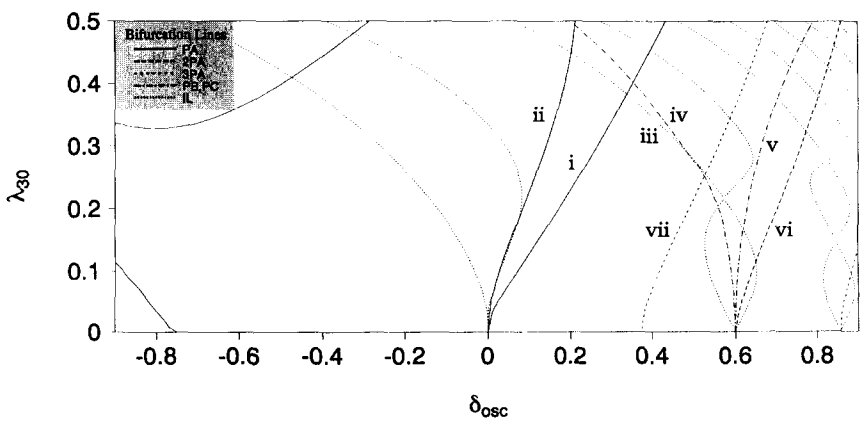

Fig. 11. Bifurcation lines for some short periodic orbits in the two-dimensional deformation parameter space $(\delta_{osc}, \lambda_{30})$.

for the emergence of pronounced shell structure in non-integrable systems are not well known, however. As is indicated in Fig. 1, shell structure energies at equilibrium shapes with finite λ_{30} are comparable in magnitude to those of spherical and superdeformed shapes. The most remarkable one is the region with $\delta_{\rm osc} \simeq 0.1$ and $\lambda_{30} = 0.3 \sim 0.4$. The bifurcation map of Fig. 11 suggests that the strong shell effect in this region may be connected with the bifurcation of orbit PA (the lines `i` and `ii`). In fact, we saw in the preceding section that the Fourier peak corresponding to the orbit PA is strongly enhanced by the bifurcation phenomena. It is worth emphasizing that such a strong shell effect can arise associated with classical orbit bifurcations in non-integrable systems.

One should also note that most of the large discs in Fig. 1 at finite λ_{30} locate in the prolate side ($\delta_{\rm osc} > 0$). This is related with the property of the shortest periodic orbit: For prolate shapes, the shortest orbit is of the type-PA. It is degenerate and stable, so its contribution to the level density is important. On the other hand, the shortest orbit for oblate shapes is of the type-IL, which is isolated and, accordingly, its contribution to the level density is rather small. The orbit of type-PA, the second shortest orbit, is unstable against the octupole deformation, and less important in comparison with the prolate case. A more detailed discussion on the difference in stability between the oblate and prolate superdeformed shapes against octupole deformations will be given in the next section. The same problem was discussed also in [20,21] from a somewhat different point of view.

7. Octupole deformation superposed on the prolate and oblate superdeformations

Let us discuss the origin of the difference in octupole stability between the prolate and oblate superdeformed states. In Refs. [16,14] we have shown that the supershell effect in the prolate superdeformed states increases with increasing octupole deformation. As an underlying mechanism of that enhancement, we emphasized the importance of stability properties of two kinds of periodic orbit family and of their interference effect. The oblate case is similar to the prolate case in that there are two kinds of periodic orbit family whose periods are in the ratio 2:1. But the structure of the quantum spectrum is quite different for each of them. In Fig. 12 are compared the single-particle spectra for the prolate ($\omega_\perp/\omega_z = 2$) and oblate ($\omega_\perp/\omega_z = 1/2$) superdeformed oscillators as functions of the octupole deformation parameter λ_{30}. The way the degeneracy is solved is different between the two. The octupole operator Y_{30} has matrix elements between states in the same major shell in the oblate case and, therefore, it affects the spectrum in the first order perturbation, while it affects only in the second order in the prolate case. Let us discuss below how this difference be explained in terms of the classical dynamics point of view. For this purpose, representative periodic orbits with short periods are displayed in Fig. 14 for several octupole deformation parameters λ_{30}.

We first compare the features of the two spectra without the octupole term. Fig. 13 shows the oscillating level density smoothed to an energy width $\delta E = \omega_{\rm sh}/2$ ($\omega_{\rm sh}$ being the energy spacing between adjacent major shells). A characteristic feature is that the

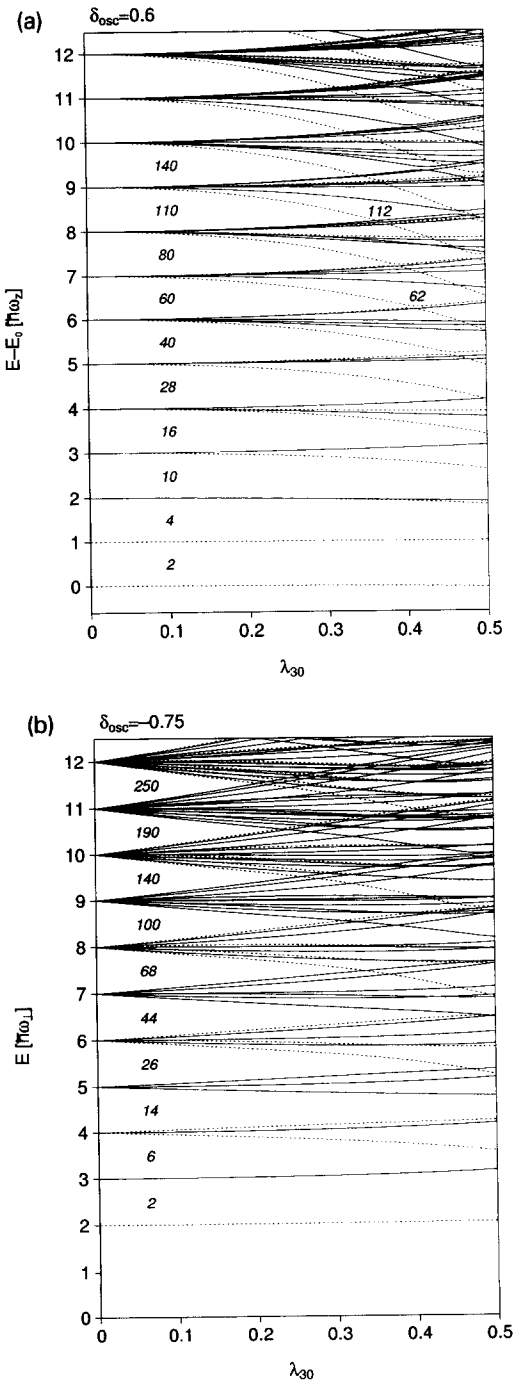

Fig. 12. Single-particle spectra for (a) prolate and (b) oblate superdeformed oscillators plotted as functions of the octupole deformation parameter λ_{30}.

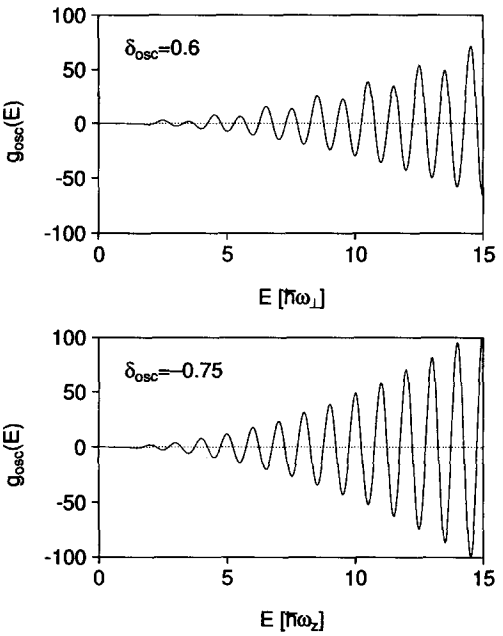

Fig. 13. Oscillating level density of prolate and oblate superdeformed oscillators, which are smoothed to an energy width $\delta E = \hbar\omega_{sh}/2$.

prolate superdeformed spectrum has an undulating pattern (supershell structure) while the oblate one does not. This is due to the difference in degeneracies of contributing periodic orbits. As discussed in Ref. [14], two orbit families (corresponding to orbits (PB, PC) and orbit PA in the upper panel of Fig. 14, respectively) in the prolate superdeformed states have degeneracies 4 and 2. In the oblate case, the orbit family with period $2\pi/\omega_\perp$ (corresponding to orbits (PA, PL) in the lower panel of Fig. 14 has the maximal degeneracy 4, but the shortest orbit (the linear orbit IL along the z-axis) is isolated and has degeneracy 0. Thus the interference effect between these two families is so small that one cannot see the supershell effect in the spectrum.

Fig. 15 compares the Fourier transforms of the level density for the prolate and oblate cases. One can hardly see the component at $s = 1$ in the oblate case and the oscillating pattern of the spectrum is determined by the $s = 2$ component almost exclusively. Comparing the two figures, one notices that the reduction rate of the peak-height due to the octupole deformation is much greater in the oblate case. This rapid decline clearly corresponds to the rapid disappearance of the shell effect in the oblate case.

The main reason for reduction of the shell effect with increasing octupole deformation is two-fold: The first is the reduction of degeneracy of the periodic orbit families, and the second is the change of stabilities. As the degeneracies are the same for the major orbit families in both cases (orbits PB, PC, ... in the prolate case and orbits PA, PL, ... in the oblate case), we expect that the differences are associated mainly with the stability properties. In Fig. 16 we show the stability factors $X \equiv \sqrt{|\det(1 - M_r)|}$ calculated as

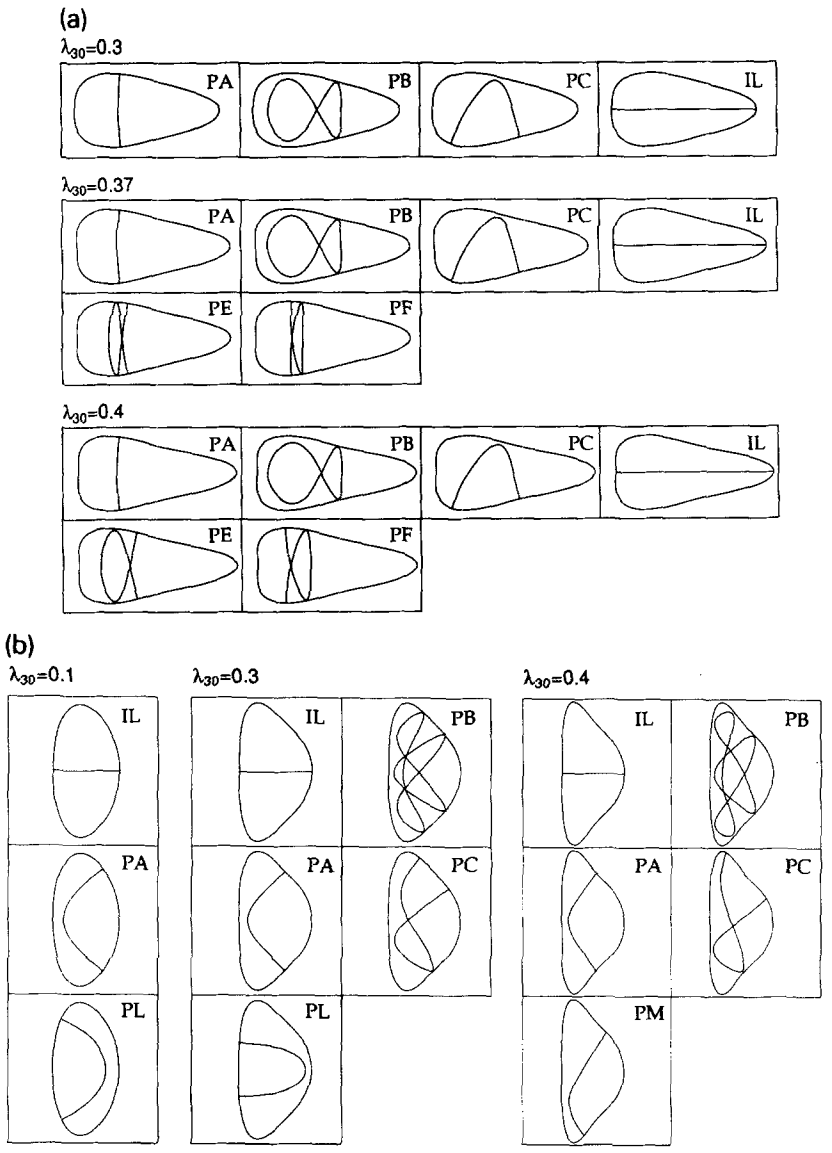

Fig. 14. Some short periodic orbits in the prolate (upper panel) and the oblate (lower panel) superdeformed potentials with octupole deformations.

function of λ_{30}. The stability factors for orbits in the oblate potential depend linearly on λ_{30} for $\lambda_{30} \simeq 0$ while they depend quadratically in the prolate case. Consequently the amplitude factors reduce much faster in the former case. This seems to be the main cause of the rapid reduction of shells with octupole deformation in the oblate potential.

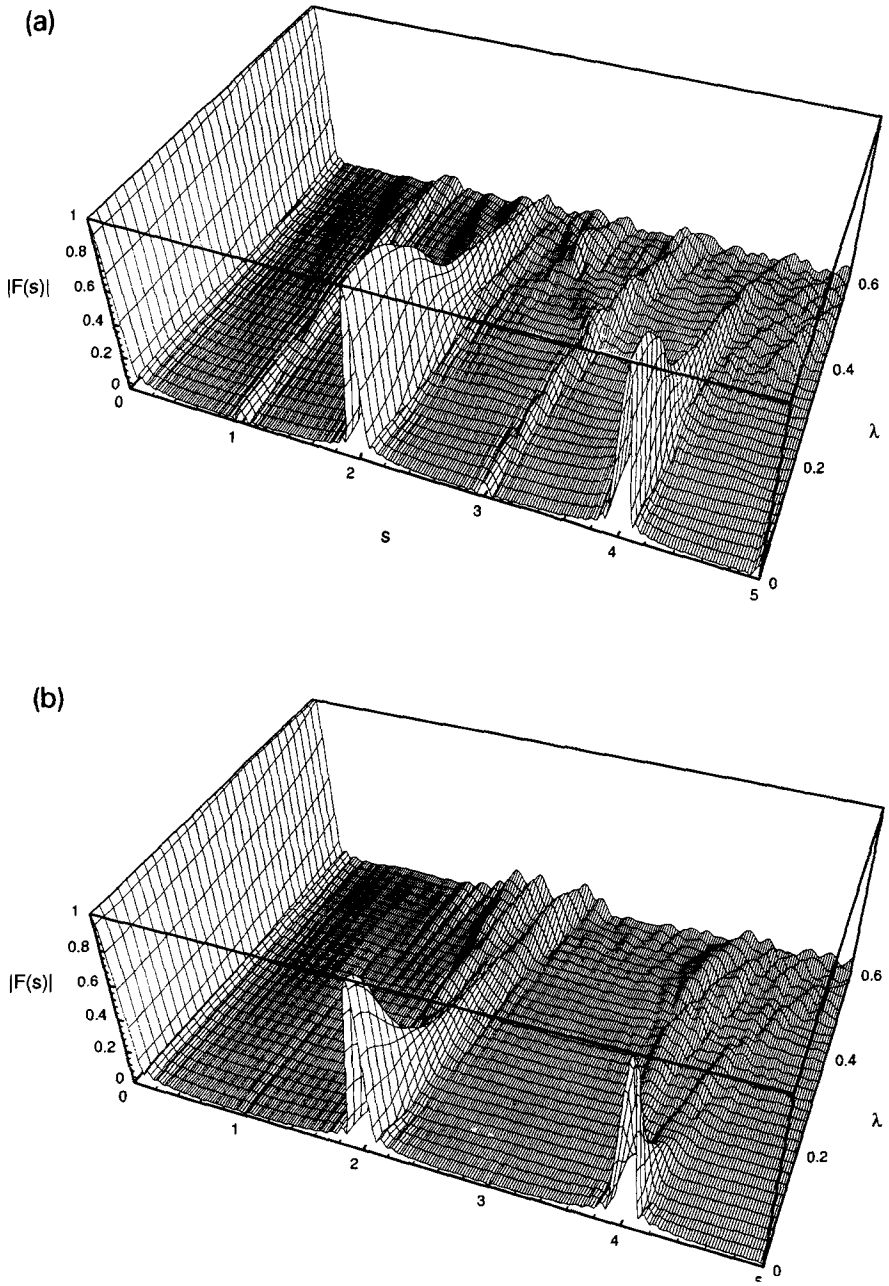

Fig. 15. Fourier transforms of the quantum level densities for the prolate (upper panel) and the oblate (lower panel) superdeformed oscillators with octupole deformations.

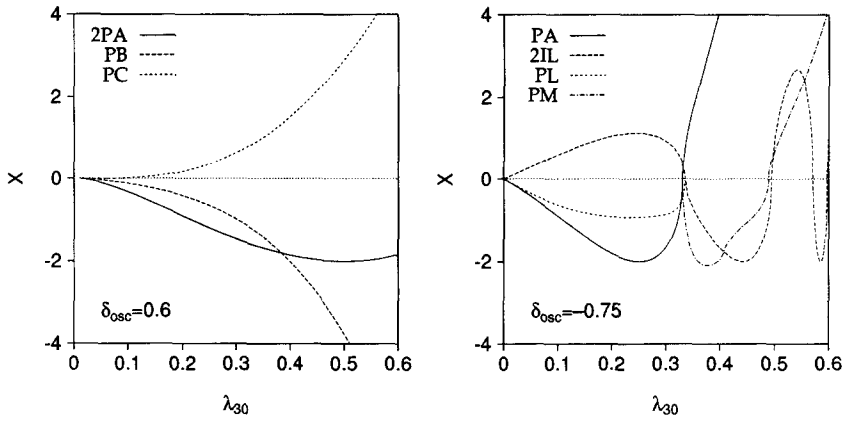

Fig. 16. Stability factors $X = \sqrt{|\det(1 - M_r)|}$ of the short periodic orbits for the prolate (left) and the oblate (right) superdeformed potentials plotted as functions of the octupole deformation parameter λ_{30}. The sign of X is that of $\det(M_r - 1) = \mathrm{Tr}\, M_r - 2$. Namely, $-2 < X \leqslant 0$ for stable orbits and otherwise for unstable ones.

8. Summary and conclusion

We have analyzed the gross structure of single-particle spectra in reflection-asymmetric deformed oscillator potentials using the semiclassical method. Our model is nonintegrable and is regarded as a mixed system where regular and chaotic dynamics coexist. The periodic orbit theory, which is well established for regular and strongly chaotic limits, seems to be also applicable to such a situation. Fourier transforms of the quantum level density reveal almost perfect correspondences with classical periodic orbits. The importance of classical orbit bifurcations has been demonstrated in our model. Strong shell effects arise also for rather chaotic regions, and their strengths are comparable in magnitude to those of regular regions. We obtain an interesting result which indicates that classical bifurcations may be responsible for the emergence of shell structure in the mixed system. Applications of the semiclassical theory of shell structure to more realistic mean-field potential models and identifications of classical orbits which play decisive roles in determining exotic shapes of nuclei or micro-clusters remain as exciting future subjects.

Acknowledgements

The authors thank Dr. M. Matsuo (Yukawa Institute for Theoretical Physics) and Dr. H. Aiba (Koka Women's College) for fruitful discussions.

References

[1] S. Åberg, H. Flocard and W. Nazarewicz, Ann. Rev. Nucl. Part. Sci. 40 (1990) 439.

[2] W. Nazarewicz, P. Olanders, I. Ragnarsson, J. Dudek, G.A. Leander, P. Möller and E. Ruchowska, Nucl. Phys. A 429 (1984) 269.
[3] S. Mizutori, T. Nakatsukasa, K. Arita, Y.R. Shimizu and K. Matsuyanagi, Nucl. Phys. A 557 (1993) 125c.
[4] H. Nishioka, Klavs Hansen and B.R. Mottelson, Phys. Rev. B 42 (1990) 9377.
[5] S. Frauendorf and V.V. Pashkevich, Rossendorf preprint FZR-37 (1993).
[6] D. Heiss and R.G. Nazmitdinov, preprint (1994), to appear in Phys. Rev. Lett.
[7] M.C. Gutzwiller, J. Math. Phys. 8 (1967) 1979; 12 (1971) 343.
[8] M.C. Gutzwiller, Chaos in quantum and classical mechanics (Springer, Berlin, 1990).
[9] A.M. Ozorio de Almeida, Hamiltonian system: chaos and quantization (Cambridge Univ. Press, Cambridge, 1988).
[10] R. Balian and C. Bloch, Ann. Phys. 69 (1972) 76.
[11] M.V. Berry and M. Tabor, Proc. Roy. Soc. Lond. A 349 (1976) 101.
[12] A.G. Magner, V.M. Kolomietz and V.M. Strutinsky, Sov. J. Nucl. Phys. 28 (1978) 764.
[13] H. Frisk, Nucl. Phys. A 511 (1990) 309.
[14] K. Arita, Prog. Theor. Phys. 90 (1993) 747;
K. Arita and K. Matsuyanagi, Prog. Theor. Phys. 91 (1994) 723.
[15] A.M. Ozorio de Almeida and J.H. Hannay, J. Phys. A 20 (1987) 5873.
[16] K. Arita and K. Matsuyanagi, Prog. Theor. Phys. 89 (1993) 389.
[17] M. Baranger, K.T.R. Davies and J.H. Mahoney, Ann. Phys. 186 (1988) 95.
[18] K. Arita, Phys. Lett. B 336 (1994) 279.
[19] A. Bohr and B.R. Mottelson, Nuclear structure, vol. 2 (Benjamin, New York, 1975) p. 585.
[20] W.D. Heiss, R.G. Nazmitdinov and S. Radu, Phys. Rev. Lett. 72 (1994) 2351.
[21] W.D. Heiss, R.G. Nazmitdinov and S. Radu, Phys. Rev. B 51 (1995-I) 1874.